An investigation into the drying of thin films of ink, using infra-red dryness measurement.

Hardisty, Hylton

Award date:
1980

Awarding institution:
University of Bath

AN INVESTIGATION INTO THE DRYING OF THIN FILMS OF INK, USING INFRA-RED DRYNESS MEASUREMENT

Submitted

by

Hylton Hardisty

for the degree of PhD

of the University of Bath

1980

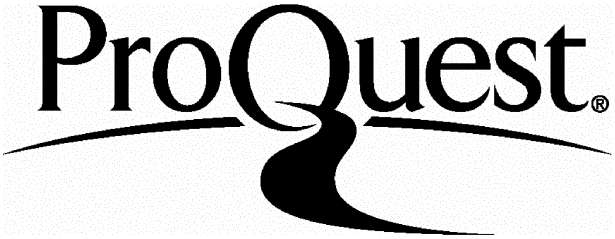

ACKNOWLEDGEMENTS

The author would like to place on record his sincere gratitude to the following people, for the help he has received from them during the period of this research.

Professor Joseph Black, the senior member of the research group, for his continued encouragement, advice and help throughout the programme.

Mr. I. Miller who, as research technician, ably carried out a variety of modifications and constructions, and operated the printing press during the drying tests.

Mr. R. Godoy, who, as a Research Officer, was responsible for the later heat transfer investigations.

Miss Trisha Sherrin, who remained cheerful throughout the depressing task of typing this manuscript.

The author would also like to thank the Department of Industry who supported this program of research.

To Jennifer, Claire and Michael

whose support and forbearance made this possible.

SUMMARY

An experimental and theoretical investigation has been carried out into the evaporation of organic solvents (drying) from thin films of ink. By means of the infra-red technique, experimental drying curves have been recorded from stationary inked specimens during various conditions of forced convective drying. In the constant-rate period, the effect on the drying time of changes in air velocity, air temperature, coating thickness and percentage solvent in the ink, have been measured. Heat and mass transfer theory has been used to develop a criterion for the relative rate of drying of a range of solvents. Theoretical predictions of constant-rate drying time show good agreement with experimental measurements.

In the falling-rate period, both the theoretical and experimental evidence appears to show that the rate of drying is limited by the rate at which solvent can diffuse through the polymer residue to the free surface. Analysis of experimental drying curves indicates that the diffusion coefficient is concentration dependent. To provide a theoretical solution of this process, numerical methods were used to solve the diffusion equation, with the diffusion coefficient exponentially dependent upon solvent concentration. The concept of the characteristic drying curve has been successfully used to correlate experimental drying rates in the falling-rate region. Non-dimensional results from the numerical solution of the diffusion equation have also been expressed in the form of a characteristic drying curve. Qualitative agreement between theory and experiment is good.

CONTENTS page no

Page no.

Chapter 9 - Falling Rate Drying - The Diffusion Equation

Chapter 10 - Development Of A Computer Program To Solve The Diffusion Equation With A Concentration Dependent Diffusion Coefficient

Chapter 11 - Analysis Of IR-Curves In The Falling-Rate Period

Page no.

Chapter 12 - Summary, Discussion and Conclusions

APPENDICES

NOTATION

A	Surface area	m^2
B	Width of slot nozzle	m
B	Measure of molecular hole size, equn 8.62	
Bi	Biot number for heat transfer (hL/k)	
Bi_1	Biot number of mass transfer ($k_\rho L/D$)	
Bi_2	Biot parameter ($k_\rho L/D_o$) equn 10.2.1	
C	Dimensionless concentration (c/c_o)	
c	Concentration	kg/m^3, mol/m^3
c_p	Specific heat at constant pressure	J/kg K
D	Diffusion coefficient	m^2/s
D_{AB}	Binary diffusion coefficient, A thro' B	m^2/s
D_T	Thermodynamic diffusion coefficient, equn 8.4.24	m^2/s
D_o	Diffusion coefficient at zero concentration	m^2/s
D^*	Dimensionless diffusion coefficient (D/D_o)	
D_1^*	Maximum value of D^*, when C = 1, equn 9.5.5	
E	Dimensionless concentration, equn 9.3.6	
E	Electric field strength	N/Coulomb
e	Charge on electron	Coulomb
F	Correction factor, equn 5.4.10	
F	Force	N
F'	Force per particle	N
f	Free volume, fractional, equn 8.5.4	
f	Relative drying rate, equn 11.4.1	

f	Friction factor $(2\tau_w/\rho V^2)$	
	Molar friction factor, equn 8.4.16	Ns/m
f'	Molecular friction factor, equn 8.4.14	Ns/m
H	Thickness	m
h	Heat transfer coefficient	W/m^2 K
h_o	h at stagnation point	W/m^2 K
h_{fg}	Enthalpy of evaporation	J/kg
Δh_v	Molar enthalpy of evaporation	J/mol
J	Molar diffusion flux, equn 3.2.2	mol/m^2 s
J'	Molecular flux, equn 8.4.11	molecules/m^2 s
K	Exponential constant, equn 9.5.4	
k_c	Mass transfer coefficient	mol/m^2 s(mol/m^3)
k_ρ	Mass transfer coefficient	kg/m^2 s
k^o	Mass transfer coefficient, independent of bulk flow	kg/m^2 s
k	Thermal conductivity	W/m K
k	Boltzmann constant	$1.38 \cdot 10^{-23}$ J/K
L	Characteristic length in Re, Bi etc	m
L	Avogadro's constant	$6.02 \cdot 10^{23}$ molecules/mole
Le	Lewis number $(\alpha/D \equiv Sc/Pr)$	
M	Molecular weight	
m	mass	kg
m	mass flux	kg/m^2 s
m	mobility	
m_c	relative evaporation rate	

Nu	Nusselt number (hL/k)	
P	Permeability	mol/m s (N/m^2)
Pr	Prandtl number ($\mu C_p/k$)	
p	Pressure	N/m^2
Q	Energy	J
Q	Heat transfer rate	W
q	Heat flux	W/m^2
R	Molar gas constant	8.31 J/mol K
Re	Reynolds number ($VL\mu/\rho$)	
r	Evaporative index, equn 5.4.8	
S	Dimensionless transformation variable, equn 9.5.3	
S	Solubility coefficient	
Sc	Schmidt number ($\mu/\rho D$)	
Sh	Sherwood number ($k_c L/D$)	
T	Temperature	K
T_A	Air temperature at nozzle outlet	K
T	Dimensionless time	
t	Time	s
t_c	Hypothetical constant-rate drying time, equn 5.6.10	s
1^{t_c}		
u	Velocity in the x-direction	m/s
V	Infragauge output signal	Volt
V	Velocity	m/s
V_E	Air velocity at nozzle outlet	m/s
ν	Drift velocity	m/s
ν	Specific volume	m^3/kg, m^3/mol

ν_f	Free volume	m^3/mol
ν_g	Specific volume saturated vapour	m^3/kg
X	Dimensionless distance (x/L)	
X	Mass of solvent on web	kg/m^2
x	Distance (parallel to surface)	m
x_n	Nozzle pitch	m
y	Distance normal to surface	m
Z	Normal distance from nozzle exist to surface	m

Subscripts

c	Critical point
o	Zero time (except where denoted otherwise)
s	Surface

Greek symbols

α	Thermal diffusivity, k/ C_p	
δ	Thickness of hypothetical stagnant film	m
θ	Temperature difference	K
	Wet bulb depression	K
μ	Absolute viscosity	kg/m s
ν	Kinematic viscosity	m^2/s

ρ	Mass concentration, density	kg/m^3
τ	Shear stress	N/m^2
ϕ	Relative solvent content	
ω	Mass fraction	

LIST OF FIGURES

1. INTRODUCTION

1.1 Background

The drying of solids is an operation of widespread importance in the chemical process, pharmaceutical and food industries; also in the manufacture of paper, plastics and textiles. The effective drying of thin films is becoming increasingly important in the rapidly growing printing, packaging and coating industries. These latter industries, when taken together, presently constitute an important sector of the British economy. The increasing importance of drying was recently recognised when the First International Symposium on Drying was held in Montreal in 1978. In a paper presented at this symposium, Keey (1) stated that in the UK 13.10^6 ton of moisture must be evaporated annually and that this represented 7% of the total UK industrial energy expenditure. A comparable estimate for the USSR is 10%.

The research described in this thesis is an investigation into the evaporative drying of ink coatings by means of impinging air jets. This type of drying is commonly employed on the large rotary printing presses used in the converting industry (the collective name for the packaging, coating and allied industries). Rotary presses are used to deposit a coating of "ink" onto a thin moving web or substrate, which may be paper, plastic or metal. In practice the ink coating may be applied by a variety of methods such as flexography, rotogravure, lithography, etc. The basic components of an ink are a finely ground pigment and a polymer resin mixed in a blend of solvents to a suitable viscosity for printing.

Printing inks may "dry" by a variety of physical and chemical processes such as penetration into the substrate, oxidation, thermal setting, etc.

However inks which become dry by the physical evaporation of solvents are widely used on the large high speed presses in the packaging and converting industry and this is the only type of drying to be considered in this investigation. It should also be mentioned, that in this research the ink was deposited onto a plastic substrate which, tests showed, was largely impervious to solvent penetration.

In the evolution of the modern rotary press Harrison (2) describes the period from theyear 1945 as one of progressive and rapid increase in both printing speed and web width. An important objective of the modern press designer is to combine a number of disparate processes into a single unified system. It is essential that the output of this costly system is not limited by an ineffective dryer.

1.2 Ink Drying Research - Infra-Red Drying Curves

Outside the converting industry, drying technology is usally concerned with the evaporation of water from porous solids. For this type of system, research has established that early drying proceeds at a virtually constant rate which is controlled by the external conditions, and that later the drying rate falls with time, Sherwood (3). At the inception of the research reported here it was beginning to be recognised by researchers, that the characteristics of ink drying were probably similar to those described above. However there appeared to be little published data to back up these assumptions for the evaporation of organic solvents from thin films, under air flow conditions relevant to practical dryers.

The various factors which have made the application of theory to dryer design such an intractable problem in all branches of the technology

are discussed in the next chapter, but one fundamental problem must be commented upon here. This is the difficulty of obtaining reliable and accurate experimental data, under realistic conditions, on the drying process itself. It is now becoming to be generally recognised that this data is most conveniently expressed either in a drying curve (which shows the moisture or solvent content of the material as a function of time) or in a rate of drying curve. For large size solids, drying data has in the past been obtained by weighing, but it is difficult to apply this method to the drying of paint films whose thickness lies in the range, 2 - 15 μm.

For ink drying research, the author overcame the difficulties associated with solvent measurement by the introduction of a novel non-contact method based on the principle of selective absorption of infra-red radiation by the solvent, Black and Hardisty (4). By directing a weak beam of IR radiation of a precise frequency onto the ink, the solvent content is continuously monitored throughout the drying process and a drying curve is recorded. Detailed descriptions of the IR instrument, its associated electronic processing systems and the characteristics of its operation are given in Hardisty (5).

In the research reported in this thesis the IR technique is used to record ink drying curves for a wide variety of experimental conditions. For the research ink, these curves show that approximately 80% of the solvent is removed in the early period of drying and that during this period drying does in fact occur at constant-rate, Hardisty (6). It is believed that these curves constitute the first records of ink films drying under realistic air-flow conditions. It was also demonstrated that empirical heat transfer data, coupled with heat and

mass transfer theory, can be used to predict solvent evaporation rates in this important constant-rate period, Hardisty (7).

In the later falling-rate period, it appears that drying is limited by the rate at which solvent can diffuse through the ink residue to the free surface. In the more recent research an attempt has been made to analyse this complex, solvent-through-polymer diffusion, process by means of a computer model. In parallel with this theoretical analysis an attempt has been made to use the concept of the characteristic drying curve to correlate the IR drying curves in the falling-rate period, Hardisty (8).

2. INDUSTRIAL DRYING - BACKGROUND TO THEORY AND PRACTICE

2.1 Introduction

Although the research described in this thesis is entirely concerned with film drying, an attempt has been made to relate it to the wider field of general industrial drying. Experience and inquiry have shown that the sort of difficulties encountered when trying to apply basic theory to the design of a film dryer are also encountered in other fields of drying. Because of their importance and because of their wider significance, a brief account of the nature of these difficulties will now be given.

In contemporary chemical engineering, drying is classified as one of the unit operations and in textbooks the subject and its practice are often presented as straightforward. In fact, until quite recently, the design of industrial dryers was based largely on experience and empiricism, with little reliance being placed on heat and mass transfer theory. This situation has largely arisen because, historically, drying is one of the oldest operations in technology. A wide variety of dryer types has evolved, each to perform a specialised task and each with its established code of practice.

In practice, drying effectiveness must be demonstrated to the customer on a pilot rig or on the plant itself. Because of the diversity of dryer types, generalised theories of drying have not been developed to a point where they can replace empirical data. Indeed, in the recent opinion of van Brakel (9), a gulf has opened between design practice and the generalised theories of drying published by researchers.

In contrast to this view, the way forward may lie in seeking a basic methodology which can be applied to all drying research. It would

appear that drying problems can be divided into two fundamental categories:-

a) Individual materials differ widely in their physical and chemical structure and this dictates the manner and the rate at which they may be dried. At the molecular level the transfer processes within the material are immensely difficult to analyse, but because they exert a profound effect on the rate of drying, these details cannot be omitted if the theory is to have practical relevance. A pertinent example of this type of difficulty, is that though the drying of both paper pulp and paint films can be broadly classified as the drying of continuous sheets, the technology of paper drying has, so far, proved of little use in the present investigation.

b) Individual materials differ widely in their handling characteristics. In practice, the basic design problem of introducing the wet feed stock into the dryer, and then transporting it through the plant, may present even greater problems than the drying process itself. The solution of the handling problem may dictate not only the manner in which heat is supplied to the material, but the configuration of the dryer itself.

It would appear necessary to divide drying research into two separate, but complementary fields of enquiry*

i) The drying characteristics of the material itself.

ii) The external drying environment which is imposed on the material by the dryer.

* It was recently learned by the author that such a subdivision of effort is made in the drying research carried out at SPP, Harwell, Reay (10).

It was possible, and convenient, to sub-divide the ink-drying research in this way. One field of enquiry was into the heat transfer characteristics of impinging air jets, while the other was to record IR drying curves to yield the drying characteristics of the ink-film. Heat and mass transfer theory was later applied to unite the two lines of research.

2.2 The Process of Drying

Drying is a simultaneous heat and mass transfer operation, in which the enthalpy to evaporate a liquid from a solid is provided in the drying air. The historical origins of drying technology appear to lie in the paper making industry.

The drying characteristics of different materials are most conveniently compared by plotting drying rate against either time or moisture content. During the early stages of drying, moisture can reach the free surface sufficiently rapidly to maintain this surface in a saturated condition. In this period the drying rate depends only on the velocity and the thermodynamic state of the drying air and when these external conditions do not vary this period is characterised as "constant-rate". Although the analysis of this period appears straightforward, confusion still persisted between such fundamental concepts as wet-bulb temperature and adiabatic saturation temperature as recently as 1933, Sherwood (11).

When moisture can no longer reach the free surface at a rate sufficient to keep it saturated, the drying rate will begin to fall. Drying will cease when the moisture content of the solid falls to the equilibrium value corresponding to the temperature, pressure and

humidity of the drying air. An end state of complete dryness is possible only in a non-hygroscopic material.

The constant-rate and falling-rate periods are separated by the critical point. The critical moisture content is usually defined as

$$\frac{\text{average moisture content at critical point}}{\text{initial moisture content}}$$

Experiments appear to indicate that the critical moisture content is not a physical constant for a particular substance, but depends upon the size and shape of the body and its previous drying history.

The critical point is a significant design parameter since at this point the drying mechanism changes from one controlled externally to one controlled internally. It is unfortunate that theoretical methods of predicting the critical moisture content are by no means highly developed.

Theories of falling rate drying appear to have originated rather independently in two different fields. For homogeneous materials such as clay and gels, Sherwood (3) postulated that moisture was transferred internally by diffusion and obtained excellent agreement between theory and experiment.

Beginning with the work of Buckingham in 1907, moisture flow in porous bodies had been investigated by soil scientists who postulated that flow is caused by capillary suction. Discrepancies which arose due to the uncritical use of the diffusion equation to predict movement of moisture in granular materials were pointed out by Hougan et al (12).

At this time it appears to have been agreed that the movement of liquid water by diffusion is restricted to the equilibrium moisture content below the point of atmospheric saturation and to single phase solid systems in which the water and solid are mutually soluble (ibid). The dispute between diffusion and capillary theory appears to have been resolved in contemporary publications as follows. The basic partial differential equation has the form of the diffusion equation, but the physical variables in it may have been obtained from capillary theory.

Recent, more detailed, investigations have revealed that pressure gradients which cause moisture flow may be generated by shrinkage and by high temperatures. Evidently, in general, internal moisture transfer may be brought about by several mechanisms and the heat and mass transfer processes may be coupled. Luikov (13) has attempted a general treatment of this problem using the method of irreversible thermodynamics, indeed this approach is often referred to as the most fundamental. However, great physical insight is required to formulate the desired coupled linear equations and empirical data is still required for their solution. For these reasons the method of irreversible thermodynamics has not proved to be attractive to the engineer and it was not used in this research.

2.3 Drying Practice in the Packaging and Converting Industry

Modern rotary presses must be capable of printing in full colour and this is achieved by passing the web through a series of separate printing units each of which applies a primary colour. Inter-colour dryers ensure that each colour is ostensibly dry before the succeeding colour is printed on top of it. The printed coating is brought to the

specified degree of final dryness in a dryer situated between the last colour unit and the reeling or folding device.

Historically, early rotary presses printing on an absorbent substrate, such as paper, did not require a dryer as such. Later, when drying units were added to the press, they were usually in the form of drying tunnels which utilised low velocity warm air. Drying rates were low in long tunnels because boundary layer build-up caused a progressive lowering of heat and mass transfer coefficients. The desire for higher press speeds and throughputs led in turn to a demand for more effective dryers. In the late 1950's high velocity and high temperature impinging air jets were introduced to accelerate the drying process. This is brought about by the extremely high heat transfer rates which occur in the impingement zone. It should be noted that this research is concerned only with heat and mass transfer under impinging jets and not with other "direct" methods where the energy for drying is supplied by infra-red or ultra-violet radiators.

It should be apparent from even these brief remarks, that the primary problem of handling the fragile web on a higher-speed press severely constrains the dryer design. In addition special problems arise when the liquid evaporated is an organic solvent. Questions such as the quantity of solvent retained in the final dried product, the necessity to prevent explosions, solvent recovery from the dryer exhaust, pollution, etc., all require detailed design consideration, but these important topics lie outside the scope of this thesis.

2.4 Review of Previous Research into Ink Drying

The need for research appears to have been emphasised by the introduction of the impinging jet dryer in the late 1950's. Outside

the field of ink drying a number of experimental investigations into jet heat transfer were carried out. However, because of the complex nature of the turbulent flow, a fluid dynamic theory of the impingement region has proved to be difficult. The published information on the fluid dynamic and heat transfer characteristic of jets was reviewed by the author (14).

Quantitative data on the ink drying process itself is sparse. Tests carried out on operating presses are usually inadequately documented and tests carried out in the laboratory are frequently unrealistic. In addition film-drying does not readily fit into any of the classical unit operations of the chemical engineer and is usually dealt with by industrial chemists. Indeed, an early suggestion by Bennett and Wright (15) was that the early stage of ink drying should be treated as a distillation process.

The three articles by Graf (16) constitute a useful review of drying problems in rotogravure, but only semi-quantitative data from press operation are reported. Krizek and Korger (17) report data on the constant-rate period of film drying, but give no details of how their experimental drying curves were obtained. Wilhoit (18) describes an interesting laboratory investigation into the drying of PVDC aqueous coatings, but due to difficulties with the experimental technique reproducibility appears to be marginal. Scheuter and Dosdogru (19) outline the print drying research carried out at the Institute for Printing Machines and Printing Processes at Darmstadt. After the research at Bath based on the IR technique had begun, it was learned that Scheuter and Dosdogru (20) also proposed to use this principal to measure solvent content in their work. However after this description of preliminary tests nothing further has been heard of this research.

2.5 Presentation of Drying Theory in this Thesis

The basic theme which runs through the account of drying theory presented here, is that of diffusion in the important constant-rate period the rate of drying is limited by the rate at which solvent vapour can diffuse through the air-side boundary layer. In the falling-rate period, where some of the most intractable problems occur, it appears that the rate of drying is limited by the rate at which solvent molecules can diffuse through the solidifying polymer resin.

In spite of this underlying connection, it will be convenient to treat the two periods of drying separately. Investigation has shown that diffusion of solvents in polymers requires a markedly different treatment from that of the more straightforward process of gaseous diffusion.

Aspects of the theory of diffusion and mass transfer in gaseous systems are set out in Chapter 3, to form a basis for the theory of constant-rate drying which follows in Chapter 5. The theory of diffusion in liquids and polymers is given in Chapter 8. The presentation of the diffusion equation itself is delayed until Chapter 9, where the appropriate form of a solution to it are discussed. This is an essential preliminary to the computer solution of diffusion equation which is presented in Chapter 10.

3. BASIC MASS TRANSFER THEORY

3.1 General

In the early sections of this chapter the fundamental equations used to define the diffusion coefficient are presented and some basic mass transfer situations are considered. This provides a theoretical basis for the following two aspects of this research:-

i) Vapour evaporating from the free surface is transferred across the outer region of the boundary layer by turbulent eddies. However, the rate of evaporation is usually limited by the rate at which solvent vapour can diffuse through the viscous region of the boundary layer adjacent to the wall.

ii) The basic definitions of diffusion coefficients are required in Chapter 8 where diffusion of solvents through polymers is discussed in greater detail.

It is appreciated that the basic material described in these early sections will be familiar to the chemical engineer, but the material is much less familiar to the mechanical engineer and to the industrial chemist. In addition, definitions of the diffusion coefficient and the mass transfer coefficient require much greater care than the analogous definitions in heat transfer.

3.2 Fick's Law of Diffusion

The fundamental law expressing the rate of diffusion of a dissolved substance in a solvent was first proposed by Adolf Fick in 1855.* Fick first attempted to establish this basic law by an analysis of

* Earlier pioneering experiments on diffusion, effusion and transpiration had been carried out by Thomas Graham in 1850.

molecular motion, Tyrrell (21). When these attempts failed, Fick postulated the law which bears his name by invoking the similarity between the processes of the spreading of a dissolved substance in a solvent, the spreading of heat in a thermal conductor and the spreading of electricity in an electrical conductor. Nothing was more probable, he stated, than that all these processes "takes place according to the same law which Fourier has suggested".

Fick's first law is the hypothesis that the rate of transfer of matter by diffusion is directly proportional to the concentration gradient

$$j = - D \frac{\partial c}{\partial y} \qquad 3.2.1$$

where

j = diffusion flux

D = diffusion coefficient or diffusivity

$\partial c/\partial y$ = concentration gradient in the y direction

Data on diffusion may be presented in various systems of units, but provided that j and c are both expressed in forms of the same quantity of matter, eg. kg or kg-mole, then the diffusion coefficient D will have the dimensions of $(\text{length})^2/\text{time}$ and the units of m^2/s. Fick's Law is phenomenological in character. The final justification for the manner in which it is expressed should be that the diffusion coefficient which it defines is independent of the concentration gradient.

Of necessity, discussion will be limited to isothermal, isobaric systems with no external force fields. Thus, temperature diffusion, pressure diffusion and forced diffusion will not be considered. For an isothermal, isobaric, binary mixture of two components A and B

Fick's Law may be written in molar units as

$$J_A = - D_{AB} \frac{\partial c_A}{\partial y} \qquad 3.2.2$$

J_A = flux of A relative to molar average velocity, mole/m^2s

c_A = molar concentration of A, mole/m^3

D_{AB} = binary diffusion coefficient, m^2/s

Equation 3.2.2 is applicable when there is no volume change in mixing ie. to ideal gases and to ideal solutions. For this case the plane of zero net volume flow and the plane of zero net molar flow, coincide.

To deal with situations in which the overall concentration changes in the y-direction, a more rigorous definition of Fick's Law is

$$J_A = - c D_{AB} \frac{dx_A}{dy} \qquad 3.2.3$$

where

c = concentration of mixture, mol/m^3

x_A = mole fraction of A

For a binary mixture, the diffusion of component B can also be expressed in terms of equation

$$J_B = - c D_{BA} \frac{dx_B}{dy}$$

By definition, equal amounts of the two components are transferred in opposite direction across the plane of zero molar diffusion

$$J_A = - J_B \qquad 3.2.4$$

noting that $dx_A/dy = - dx_B/dy$

$$D_{AB} = D_{BA} \qquad 3.2.5$$

The diffusion coefficient in a binary mixture is termed the mutual-diffusion coefficient and is a function of composition. Diffusion in a homogeneous mixture can be measured if one of the components is labelled by means of a radioactive tracer (isotope). In this case, the tracer-diffusion coefficient is also a function of the composition. As the mole fraction of the labelled component approaches unity then the value of the tracer diffusion-coefficient approaches that of the self-diffusion coefficient D_{AA}. The smaller the difference in properties between labelled and unlabelled species the closer will this approach be.

The implication of equation 3.2.3, that diffusion will cease when the concentration is everywhere the same is true within a single phase. However in multi-phase systems spontaneous movements towards equilibrium only stop when the chemical potential or activity is the same in each phase. Thus the true driving force of diffusion is not concentration but chemical potential. This further elaboration will be taken up later.

3.3 Diffusion in Binary Mixtures

A rigorous statement of Fick's requires specification of the reference frame with respect to which the diffusion takes place, Bird et al (22). True diffusion occurs when the velocity of a component in a mixture differs from the average velocity of the mixture. This average

velocity may be expressed either on a molar basis (V) or on a mass basis (V^1).

For a binary system with constant average velocity and considering the y direction only, the molar flux relative to the molar average velocity is

$$J_A = c_A (V_A - V) \qquad 3.3.1$$

V_A = velocity of component A, relative to stationary co-ordinates

V = molar average velocity of mixture relative to stationary co-ordinates.

The two expressions for the diffusion flux from equations 3.2.3 and 3.3.1 may be set equal to each other, to give

$$c_A V_A = c_A V - c\, D_{AB} \frac{dx_A}{dy}$$

and denoted a molar flux relative to stationary co-ordinates by the symbol N

$$N_A = x_A (N_A + N_B) - c\, D_{AB} \frac{dx_A}{dy} \qquad 3.3.2$$

Equation 3.3.2 shows that the molar flux N_A is the vector resultant of a flux due to the bulk motion of the mixture added to a diffusive flux due to the concentration gradient.

The equivalent expression for the mass flux m_A relative to stationary co-ordinates is

$$m_A = \omega_A (m_A + m_B) - \rho D_{AB} \frac{d\omega_A}{dy} \qquad 3.3.3$$

Because mass transfer phenomena may be described in terms of different frames of reference, care is required when comparing or converting data. In experimental work the most convenient reference frame is one fixed to the apparatus, which is usually stationary. In this type of situation, mass transfer by pure diffusion may be accompanied by mass transfer by bulk movement of the fluid or solid. Even in ostensibly stationary systems, detailed analysis based on equations 3.3.2 and 3.3.3 may reveal bulk movement of the system. To evaluate the true diffusion coefficient from experimental mass transfer data the effect of bulk transport must either be eliminated or be shown to be negligible.

One-Dimensional, Steady-State Diffusion

To solve equation 3.3.2 for a particular physical situation the boundary-conditions appropriate to that situation must first be stated.

For the steady-state both N_A and N_B are constants.
Assume that the diffusion coefficient is constant.

a) Equimolar counter-diffusion

For this case

$$N_A = - N_B$$

Using this condition in equation 3.3.2 and integrating

$$N_A = - \frac{c\, D_{AB} (x_{A2} - x_{A1})}{(y_2 - y_1)} \qquad 3.3.4$$

b) Diffusion of A through a layer of stagnant gas B

This physical situation occurs when steady-state evaporation takes place from a free liquid surface. The evaporating vapour may be regarded as component A and the boundary layer formed by the air blowing over the surface may be regarded as component B.

Making use of the fact that for a stagnant gas N_B is zero, equation 3.3.2 may be integrated

$$N_A = - \frac{c\, D_{AB}\, (x_{A2} - x_{A1})}{\bar{x}_B\, (y_2 - y_1)} \qquad 3.3.5$$

where $\bar{x}_B$ = log mean value of the mole fraction of B

$$= \frac{x_{B2} - x_{B1}}{\ln\, (x_{B2}/x_{B1})} \qquad 3.3.6$$

Equation 3.3.5 is required in section 3.7.

3.4 Diffusivity in Gases

An expression for the binary diffusion coefficient D_{AB} for two gases A and B may be derived from kinetic theory. Making the assumptions that the molecules of both species are elastic spheres having the same diameter d and mass m, then from simple kinetic theory (23)

$$\text{Mean molecular velocity} = \bar{V} = \sqrt{\frac{8kT}{\pi\, m}}$$

$$\text{Mean free path} = \lambda = \frac{1}{\sqrt{2}\, \pi\, d^2\, n}$$

where

n = number density of all molecules

k = Boltzmann's constant

T = Thermodynamic temperature

A determination of the flux of species A which arises from random molecular movements and a comparison of this flux with Fick's Law, leads to

$$D_{AB} = \frac{1}{3} \bar{V} \lambda$$

Noting that $n = \frac{p}{Tk}$, then

$$D_{AB} = \frac{2}{3} \frac{T^{3/2}}{\sigma p} \left(\frac{k^3}{M_A \pi} \right)^{\frac{1}{2}} \qquad 3.4.1$$

where

σ = collision cross-section πd_A^2

For binary diffusion in gases of two different molecular sizes, more advanced kinetic theory yields the following formula for the diffusion coefficient (23)

$$D_{AB} = \frac{3 T^{3/2}}{32 p \sigma_{AB}^2} \left[\frac{8k^3}{\pi} \left(\frac{1}{m_A} + \frac{1}{m_B} \right) \right]^{\frac{1}{2}} \qquad 3.4.2$$

m_A, m_B = molecular mass, gm

$\sigma_{AB} = \frac{1}{2} (\sigma_A + \sigma_B)$

This theory was further developed by Chapman and Enskog using the postulate that the manner in which molecules attract or repel one

another may be analysed by means of an intermolecular potential function.

An alternative to a purely theoretical approach is to preserve the form of the above equation, but to evaluate the constants in it from experimental data. Various attempts have been made to correlate experimental values of diffusion coefficients in this semi-empirical manner. One of the most successful of these is due to Fuller et al (24) who carried out a least squares analysis of 340 data points obtained from the work of 15 other investigations:-

$$D_{AB} = \frac{0.001\ T^{1.75}\left(\frac{1}{M_A} + \frac{1}{M_B}\right)^{\frac{1}{2}}}{p\{(\Sigma v_A)^{1/3} + (\Sigma v_B)^{1/3}\}^2} \qquad 3.4.3$$

M = relative molecular mass

Σv = molecular diffusion volumes

Σv are obtained by the summation of "special atomic diffusion volumes" which are tabulated in Fuller et al.

Equation 3.4.3 was used in this research to calculate the diffusivity of solvent vapour through air for the constant-rate period of drying. For this purpose the parameters in equation 3.4.3 had the following numerical values:-

4 methyl 2 pentanol

$M_A = 102.0$

$\Sigma v_A = 132.2$

For Air

$M_B = 28.96$

$\Sigma v_B = 20.1$

3.5 Convective Mass Transfer

The speed of constant-rate drying clearly depends upon the rate at which heat and vapour can be transferred, simultaneously and in opposite directions, across the fluid dynamic boundary layer next to the free surface of evaporation. It is assumed that the energy to vapourise the liquid is supplied entirely by convection and that the mainstream state of the drying air is constant.

In practice the boundary layer is almost always turbulent in character and usually no exact theoretical solutions are available. In this situation it is customary to express the convective transfer of heat and mass in terms of empirical rate equations. The heat flux q, from the drying air to free surface, is given by

$$q = h(T_G - T_s) \qquad 3.5.1$$

h = heat transfer coefficient, $W/m^2\ K$

T_G = mainstream air temperature, C

T_s = surface temperature, C

The analogous convective rate equation for the mass flux from the surface is

$$N_A = k_c(c_s - c_G) \qquad 3.5.2$$

N_A = mass flux, mol/m^2s

k_c = mass transfer coefficient, $mol/m^2s(mol/m^3)$

c_s = saturated vapour concentration corresponding to T_s, mol/m^3

c_G = vapour concentration in mainstream, mol/m^3

During the constant rate period a condition of dynamic equilibrium is established when the heat transferred to the surface is just sufficient to increase the enthalpy of the liquid to be vapourised. This dynamic balance is represented by the following equation

$$h(T_G - T_s) = k_c(c_s - c_G)h^l_{fg} \qquad 3.5.3$$

h^l_{fg} = latent heat of vapourisation, J/mol

One of the difficulties of mass transfer theory is that the driving force in equation 3.3.2 can be expressed in other units than molar concentration. For example in theory developed later the following form of the rate equation is used

$$m_A = k_\rho(\rho_s - \rho_G) \qquad 3.5.4$$

m_A = mass transfer flux, kg/m^2s

k_ρ = mass transfer coefficient, m/s

ρ = mass concentration (density) kg/m^3

Of course the various forms of the mass transfer coefficient are related. For example, inspection will show that k_c and k_ρ are dimensionally and numerically identical

$$k_\rho \equiv k_c \qquad 3.5.5$$

3.6 Film Theory of the Turbulent Boundary Layer

The concept that in convection a heated body is separated from the main bulk of the fluid by a thin layer of stationary fluid across which heat is transferred by pure conduction, was first suggested by Nernst in 1904. This hypothesis was further developed by Langmuir. The concept was used on a heuristic basis by Lewis and Whitman in their pioneering work on mass transfer.

More recent fluid dynamic research has shown that the turbulent boundary which forms next to a drying surface is a flow field of great complexity. Numerical solutions of the boundary layer equations are possible on a high speed computer, but there was insufficient time in which to attempt such a solution. Faced with this situation, it was necessary to have a physical model on which to base theoretical analysis and to guide physical thinking. The stagnant film hypothesis was adopted for this purpose because of its simplicity and because it still retains its conceptual usefulness. A change to a more complex model of the boundary layer would be straight forward if this was later felt to be desirable.

To demonstrate the connection between the processes of heat, mass and momentum transfer, the stagnant film hypothesis is presented in its simplest form. Heat transfer across the film is analysed first, then, by analogy, the treatment is extended to cover momentum and mass transfer.

Secondary effects, such as the effect of bulk-flow and the effect of the mass transfer on the heat transfer coefficient, are dealt with later in Section 3.7.

Heat Transfer

The effective thickness δ_T of the hypothetical stagnant film is such that it offers the same resistance to heat transfer (by conduction) as the real boundary layer

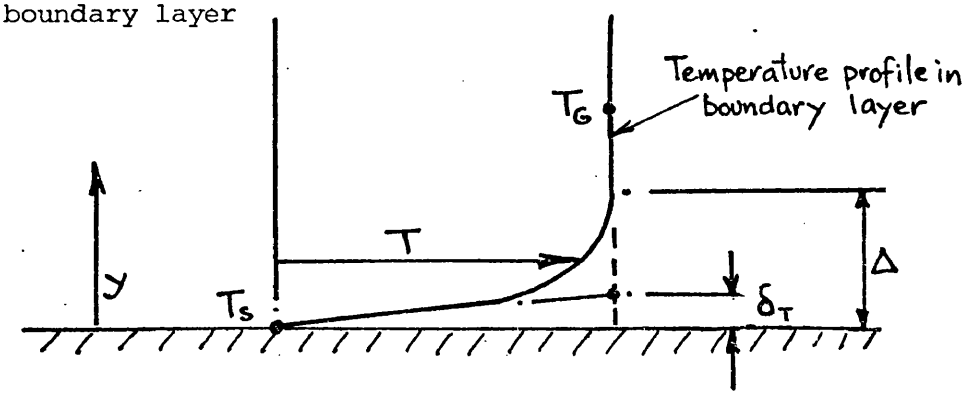

Δ = thickness of real boundary layer

The following identity must be satisfied at the boundary surface

$$h(T_G - T_s) = k(dT/dy)_s$$

$$\text{but } (dT/dy)_s = \frac{T_G - T_s}{\delta_T}$$

$$h = k/\delta_T \qquad 3.6.1$$

A comparison of this expression with the expression defining the Nusselt number

$$Nu = hL/k$$

yields

$$Nu = L/\delta_T \qquad 3.6.2$$

L = characteristic scale dimension

Theory and dimensional analysis shows that heat transfer data may be correlated by a non-dimensional expression of the form

$$Nu = C\ Re^{a}\ Pr^{b} \qquad 3.6.3$$

where C, a and b are constant to be determined by experiment. Reasoning from the results of boundary layer theory, Colburn (34) suggested that the unknown index b had the value of 1/3.

Momentum Transfer

Assume that next to the wall there exists a thin layer of thickness δ_v across which the shear stress τ is transferred entirely by the action of molecular viscosity. The following identity must be satisfied at the boundary surface

$$f\,\frac{\rho V^2}{2} = \mu\,(dV/dy)_s$$

by definition

f = friction factor = $2\tau_w/\rho V^2$

V = main stream velocity

but $(dV/dy)_s = V/\delta_v$

$$f = \frac{2\mu}{\rho\ V\ \delta_v} = \frac{2}{Re}\,\frac{L}{\delta_v} \qquad 3.6.4$$

Re = Reynolds number = $VL\rho/\mu$

Heat and momentum are transferred by the same fluid dynamic mechanism. This underlying similarity finds expression in the various forms of

the analogy between the processes heat and momentum transfer which have been developed. More will be said on this subject in Section 5.2, but it is a consequence of the Chilton-Colburn analogy that

$$f = 2C\ Re^{a-1} \qquad 3.6.5$$

Equating 3.6.4 and 3.6.5 gives

$$\frac{L}{\delta_v} = C\ Re^{a} \qquad 3.6.6$$

These relations may be used to interpret the heat transfer correlation equation 3.6.3

$$Nu = C\ Re^{a}\ Pr^{b}$$

$$L/\delta_T = C\ Re^{a}\ Pr^{1/3} \qquad 3.6.7$$

$$\delta_v/\delta_T = Pr^{1/3} \qquad 3.6.8$$

The Reynolds number controls the thickness of the momentum layer. It is apparent that the role of the Prandtl number

$$Pr = \nu/\alpha = \frac{\text{momentum diffusivity}}{\text{thermal diffusivity}}$$

is to relate the thicknesses of thermal and momentum layers.

Mass Transfer

Because of the similarity between the physical processes of heat and mass transfer, the stagnant film hypothesis may also be applied to the concentration boundary layer.

Let

δ_M = thickness of stagnant film for mass transfer

The following identity is satisfied at the bounding surface

$$k_c(c_s - c_G) = D(dC/dy)_s$$

$$\text{but } (dc/dy)_s = \frac{c_s - c_G}{\delta_M}$$

$$k_c = D/\delta_M \qquad 3.6.9$$

The mass transfer analogue of the Nusselt number is the Sherwood number

$$Sh = k_c L/D$$

From which it follows that

$$Sh = L/\delta_M \qquad 3.6.10$$

The Schmidt number

$$Sc = \nu/D = \frac{\text{momentum diffusivity}}{\text{mass diffusivity}}$$

has the same form as the Prandtl number

3.7 Transfer Coefficients - Secondary Effects

In forced convective heat transfer (in the absence of mass transfer) the concept of the heat transfer coefficient is a powerful one for two reasons. Firstly, experimental determination of h is apparently straightforward. Secondly, h is a unique function of flow conditions and fluid properties, in particular it is independent of the heat flux.

However, a closer analysis shows that, even in simple situations, a rigorous definition of the mass transfer coefficient in terms of the rate equation is not necessarily straightforward. There are two principal reasons for this. Firstly, when vapour diffuses from the surface of liquid through the stagnant film, a bulk flow is induced in the air which constitutes the film (Section 3.3). For the transfer coefficient to be independent of mass flux this effect must be eliminated. Secondly it can be shown, both experimentally and theoretically, that the effect of a mass flux normal to the boundary is to distort the boundary layer velocity profile. At high mass flow rates this distortion is sufficient to effect the magnitude of the mass transfer coefficient.

In cases of combined heat and mass transfer, distortion of the velocity profile by the mass flux may in turn affect the heat transfer coefficient.

These effects will now be examined. In spite of its approximate nature the stagnant film hypothesis should be adequate for this purpose as the effects themselves are of the second order of magnitude.

The Effect of Bulk Flow on the Mass Transfer Coefficient

The rate equation 3.5.2

$$N_A = -k_c(c_{A2} - c_{A1})$$

may be regarded as an integration and replacement of equation 3.3.2

$$N_A = x_A(N_A + N_B) - c\, D_{AB}\, dx_A/dy$$

in which the bulk flow term has been neglected in the transformation. Thus rate equations such as equation 3.5.2 are strictly valid only in the following two situations:-

i) Equi-molar counter-diffusion, where by definition bulk flow is zero.

ii) At low mass transfer rates, where bulk flow may be considered negligibly small.

For equi-molar counter-diffusion across a stagnant film of thickness δ, equation 3.3.4 gives

$$N_A = -\frac{D_{AB}\,(c_{A2} - c_{A1})}{\delta} \qquad 3.7.1$$

The mass transfer coefficient k_c^1 for equi-molar counter diffusion is defined in terms of the rate equation

$$N_A = -k_c^1\,(c_{A2} - c_{A1}) \qquad 3.7.2$$

Comparison of equations 3.7.1 and 3.72 shows that

$$k_c^1 = D_{AB}/\delta \qquad 3.7.3$$

The mass transfer coefficient k^0 is defined as being independent of bulk flow

$$k_c^0 = k_c^1 = D_{AB}/\delta \qquad 3.7.4$$

Consider next, the mass transfer process relevant to evaporation from a free surface, i.e. diffusion of A through stagnant B. Adopting equation 3.3.5

$$N_A = - \frac{D_{AB}\, c}{\delta} \frac{(c_{A2} - c_{A1})}{\bar{c}_B} \qquad 3.7.5$$

where $\bar{c}_B$ = log mean value of c_B.

The mass transfer coefficient for this process is defined in terms of the rate equation

$$N_A = - k_c (c_{A2} - c_{A1}) \qquad 3.7.6$$

It follows from a comparison of equations 3.7.5 and 3.7.6 that

$$k_c = \frac{D_{AB}\, c}{\delta\, \bar{c}_B} \qquad 3.7.7$$

and using equation 3.7.4

$$k_c = k_c^0\, c/\bar{c}_B \qquad 3.7.8$$

Measurements of mass transfer rates from a solid surface entail that the mass transfer coefficient actually determined is k_c. This

coefficient must be corrected for bulk flow before it is included in the Sherwood number

$$Sh = L/\delta_M = k_c^0 L/D_{AB} = \frac{k_c \bar{c}_B L}{D_{AB} C} \qquad 3.7.9$$

Equation 3.7.8 may be rewritten in terms of pressure as

$$k_G = k_G^0 P/\bar{P}_B$$

The Effect of Mass Transfer on the Heat Transfer Coefficient

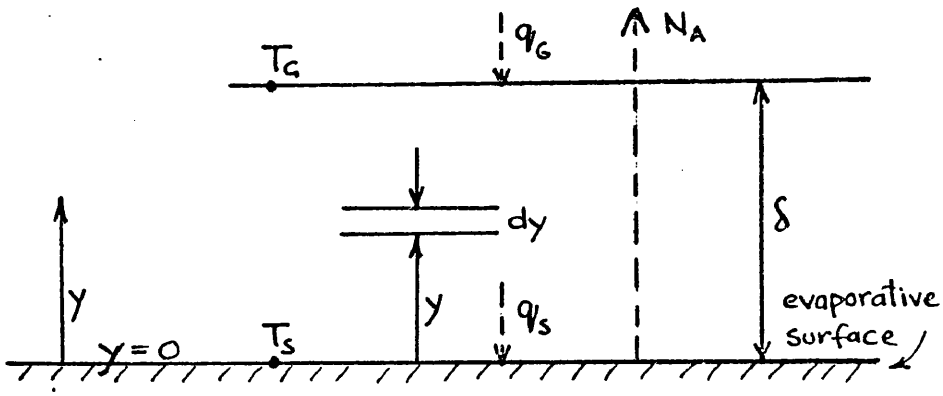

Assume

$T_G > T_S$

Consider any plane normal to the y-direction.

Energy must be conducted downwards to supply the latent heat of vapourisation h_{fg} and to increase the temperature of the vapour above T_S

$$k_d T/dy = m_A h_{fg} + m_A C_p (T - T_S)$$

m_A = mass transfer rate, kg/s

Cp = specific heat, J/kg K

rearranging and writing $q_s = m_A h_{fg}$

$$\frac{q_s \, dy}{k} = \frac{dT}{1 + C_p(T - T_s)/h_{fg}}$$

integrating between the limits of y = 0 and y = δ

$$\frac{q_s \delta}{k} = \frac{h_{fg}}{C_p} \ln(1 + R)$$

where

$$R = C_p(T_G - T_s)/h_{fg}$$

Now conventionally the heat transfer coefficient is defined by the rate equation

$$h(T_G - T_s) = q_s$$

$$h = \frac{k}{\delta R} \ln (1 + R) \qquad 3.7.10$$

Also by definition when there is no mass transfer

$$h^0 = k/\delta$$

The effect of mass transfer on the heat transfer coefficient may now be expressed in terms of the ratio

$$\gamma = h/h_o \qquad 3.7.11$$

and finally using equation 3.7.10

$$\gamma = \frac{\ln (1 + R)}{R} \qquad 3.7.12$$

4. DRYING CURVES USING INFRA RED

4.1 General

Over a three year period of research and development, a large number of IR drying curves have been recorded, of which the curves presented in this thesis are a selection. The early experiments were concerned with the influence of external air on the constant-rate period and later the falling-rate period was investigated. To help in their assimilation, the curves are presented in sets. The sequence of presentation roughly follows the chronological order in which the tests were carried out.

In this chapter the research rig and the experimental technique are described and the first set of drying curves is presented. Because the curves in this first set are generally representative of the others, they provide a background against which the theory of both constant-rate and falling-rate theory can then be developed.

In the early research, Hardisty (5), great difficulty was experienced when attempting to devise laboratory methods for laying down ink films in an accurate and repeatable form. For the present research ink is applied by means of a gravure printing press and the results will demonstrate that the early difficulties have been overcome.

4.2 Experimental Technique

Description of Drying Research Rig

The research rig is shown in Figures 4.1 and 4.2.a. The ink coating was printed onto the plastic substrate by means of a small rotary gravure press. The gravure cylinder was etched with four separate bands each approximately 4 cm wide and of increasing depth of etch,

Figure 4.2.b. By this means four inked strips of increasing thickness (No. 1 - thinnest; No. 4 - thickest) were printed onto the polypropylene substrate. This allowed the influence of coating thickness on the drying characteristics of the ink to be studied. The uncontrollable variation in thickness of the ink coatings produced by the gravure printer is extremely small. This is demonstrated by the close agreement achieved between two drying curves when a test is repeated.

Commercial inks usually consist of a blend of solvents but for research purposes the following single solvent ink was formulated

Pigment	Isol pthalo blue	7%
Resin	Versamid 930	16%
Solvent	4 methyl pentan-2-ol	77%

The solvent was selected because its low volatility allowed sufficient time for its drying characteristics to be studied.

During operation of the press, the gravure cylinder is driven at constant speed by an electric motor and revolves continuously. The underside of the cylinder dips into the ink reservoir. Surplus ink is scraped from the surface of the cylinder by the doctor blade, but ink is retained in the tiny etched pores in the surface. Before printing is started the impression roller is held clear of the gravure roller and the plastic web is stationary. When required, fresh plastic may be drawn from the "unwind" reel, which is prevented from turning freely by a light friction brake. A torque is continuously applied to the "wind" reel by means of a slipping belt drive. By this means printed and dried plastic is accepted and reeled up at the speed which it is produced.

To print, the pneumatic cylinder is activated and the impression roller is pulled down. This roller, which is manufactured from a relatively flexible material, forces the web into the etched cells on the gravure cylinder, and ink transfer takes place. The web is gripped tightly in the "nip" between the two rollers, and pulled from the unwind reel. It was soon realised that for research, continuous operation of the press would be both costly and undesirable. Instead short lengths of web (approximately 2m) were printed and then brought to rest for drying beneath scanning head of the IR instrument. Approximately one metre of plastic was left uncoated between printed sections.

The ink was dried by a single air jet, issuing from a slot nozzle of width B, 3 mm, and directed vertically downwards onto the web. Air was supplied by a constant speed centrifugal fan and the air flow was regulated by means of a damper at fan discharge. Jet efflux velocity was calculated from the manometric head measured at the plenum chamber immediately upstream of the nozzle, the loss coefficient of the slot nozzle was negligible. The air was heated by means of a small electric heater positioned in the fan delivery duct. Air temperature was regulated by varying the electrical power to the heater. Heat transfer research has shown, Hardisty (6), that the maximum value of stagnation point heat transfer coefficient occurs when the nozzle is positioned at a distance of eight slot widths from the surface. Accordingly the slot nozzle was positioned at a height (Z) of 24 mm above the web.

For each test, a section of the web was dried while stationary in the wall jet formed at the side of the slot nozzle, Figure 4.3. In this way the quantity of solvent in the ink could be continuously monitored during drying in a controlled environment.

IR Drying Curves

The solvent content of the ink (dryness) was detected and measured with a commercial IR instrument, the SM2 Infragauge (25), which operates on the principle of selective absorption of IR. Details of this instrument have been given elsewhere, Hardisty (4) and (5), but for an understanding of the present work, it will be necessary to describe briefly its salient operating characteristics.

A beam of radiation at a precise wavelength of 2.95 μm is directed onto a horizontal inked specimen situated above a reflecting aluminium plate. At this wavelength the solvent absorbs IR strongly while the remaining constituents of the ink and the plastic substrate absorb IR only weakly. After interaction with the solvent radiation is back-scattered from the aluminium plate to a photo-conducting IR detector situated in the measuring head. The electrical output of the measuring head is electronically processed so that, over the linear portion of its range the output voltage V of the Infragauge is directly proportional to the quantity of solvent in the IR beam. For almost all of the research the IR measuring head was positioned on the press side of the drying jet so that virtually no drying occurred before the freshly printed ink was brought to rest in the measuring beam, Figure 4.3. The centre of the IR beam was 10 cm from the nozzle centre line.

The following method was evolved to obtain a continuous record of solvent content during drying - an experimental drying curve. The Infragauge output was connected to the Y-axis of an X-Y recorder. By starting and stopping the press a short length of freshly coated plastic was brought to rest in the IR beam. The time base on the X-Y recorder was started at the instant the freshly coated plastic came

to rest, and a continuous drying curve was subsequently recorded from the stationary specimen.

Experimental Drying Curves

Before the IR drying curves can be fully understood the operating characteristics of the Infragauge must be appreciated. These can most readily be explained with reference to a typical curve shown in Figure 4.4.

At zero time, the true origin of the drying curve should be V_o, the voltage directly proportional to the quantity of solvent in the freshly applied ink. The discrepancy between the Infragauge signal and the true drying curve which occurs at small values of time arises from two practical limitations of the instrument.

i) A relatively slow response from the instrument when fresh ink is sudden introduced into the measuring beam. This response is an inherent characteristic of the electronic processing circuits within the Infragauge and is discussed in greater detail in Section 6.5.

ii) For large solvent quantities, the relation between solvent in the measuring beam and output voltage becomes non-linear.

This second characteristic is a fundamental consequence of the manner in which radiation is absorbed by matter. The ability of the layer of solvent to absorb radiation increases exponentially with the thickness of the layer (Beer's Law). For moderate ink thicknesses electronic systems within the Infragauge are designed to compensate for this exponential characteristic. Thus, in the range 0 - 8 volt, the

Infragauge output voltage is directly proportional to the quantity of solvent present in the IR beam. As the ink thickness is further increased, the electronic systems are no longer capable of linearising the output. Eventually, excessively thick solvent layers possess sufficient absorptivity to extinguish the IR beam entirely. When this occurs the sensitivity of the instrument is saturated. In practice, at the beginning of drying, ink layers from gravure bands 2, 3 and 4 contained sufficient solvent to saturate instrument sensitivity. Tests showed that the early portions of drying curves from band No. 4, the thickest band, were so affected by this phenomena, as to significantly reduce the validity of data taken from them. Drying curves from band No. 1, were the least subject to these unwanted, non-linear effects. However, the thinnest layer has the shortest drying time, and this reduced the time available in which to carry out the experiment. Band No. 3 offered a practical compromise between these two effects, and it was the one most frequently selected for test work.

The early portion of a drying curve, shown as a straight line in Figure 4.4, is usually referred to as the "constant-rate" region but such a designation requires qualification. The period of the constant-rate drying is in general preceded by a period of initial adjustment, during which the system is brought to its equilibrium, wet-bulb temperature. When the temperature of the drying air is low this initial period is short enough to be neglected. However this is not true at high temperatures when the initial adjustment period takes up a significant fraction of the total drying time.

On this same point, any change in the state of the external environment during drying will be accompanied by a corresponding change in

surface temperature. In an industrial air jet dryer, this will occur each time the printed web passes underneath an air nozzle. For reasons such as these, the so-called constant-rate period should more properly be referred to as the period of externally-controlled drying or as the initial drying period.

4.3 Ink Viscosity and Thickness of Ink Coating

When delivered the research ink was in the form of a gel. For test purposes it was necessary to add sufficient solvent to produce an ink viscosity suitable for gravure printing. The empirical method in use throughout the printing industry to estimate ink viscosity, is by means of a "Zahn Cup". This is a small stainless steel cup 3.25 cm in diameter and 5.8 cm in length in the bottom of which is a small hole of precise diameter. By means of a handle the cup is dipped into the ink, filled and then at given time lifted out again. The ink drains out of the cup through the small hole and the time in seconds for the cup to empty is a measure of ink viscosity. Numbered cups, with drainholes of different diameter, allow inks with a range of viscosities to be dealt with. In practical roto-gravure printing ink viscosity is usually maintained in the range 20 - 30 s, determined on a No. 2 Zahn cup.

To convert drying times into drying rates the amount of solvent, kg/m , deposited on the web by the gravure cylinder must be known. The first step was to relate ink viscosity to solvent content and this was determined as follows. A sequence of weighings, on a chemical balance, showed that the ink gel as delivered consisted of 50% solvent. Next, measured quantities of solvent were added to, and mixed with, a known mass of gel and after each addition the ink

viscosity was measured using a No. 2 Zahn cup. The relationship between the percentage solvent in the ink and the time to empty the Zahn cup is shown graphically in Figure 4.5.

The mass of a dry ink on the plastic, kg/m^2, was estimated by weighing on a chemical balance, Hardisty (5). This data together with appropriate specific gravity data and the percentage of solvent in the ink, allowed the thickness of ink deposited by each gravure band to be estimated as follows:-

Band Number	1	2	3	4
Ink Thickness, μm	6.6	9.4	11.3	13.8

specific gravity of solvent 0.808

specific gravity of dry ink (pigment + resin) = 1.1

4.4 Constant-Rate Drying: The Effect of Ink Thickness and Solvent Content

The drying curves shown in Figures 4.6a - 4.6d are the results of a series of tests to determine the effect on the constant-rate region of changes in both ink layer thickness and percentage solvent in the ink. The air velocity and temperature at the drying nozzle were maintained constant for all tests. For the first tests, Figure 4.6a, the ink viscosity was the highest possible, consistent with practical printing. For the tests at lower viscosity, pure solvent was added to the ink reservoir. The ink viscosity for last test, Figure 4.6d, corresponds to standard rotogravure practice.

As a check, at least three drying curves were recorded at each test condition and it can be seen that repeatability was excellent. This repeatability is a visible confirmation that by changing to a gravure printing press, earlier difficulties of applying thin ink layers had been overcome. The curves also demonstrate the ability of the IR instrument to discriminate between minute differences in ink thickness.

The Infragauge beam monitored only one of the four printed strips. To obtain curves from other strips of different thickness it was necessary to move the measuring head parallel to the slot nozzle in bearings provided for this purpose, Figure 4.2. In practice this was a tedious adjustment to make since even a small change in the angular orientation of the IR beam causes an unwanted change in the output voltage of the instrument. An attempt was made to record curves from gravure band No. 4, but the thick ink layer saturated the sensitivity of the Infragauge (see Section 4.2). Curves from this band were difficult to interpret and little reliability could be placed in results extracted from them. For this reason, no drying curves were recorded from band No. 4 in this series of tests.

It is apparent, and this is true of all IR drying curves recorded from the research ink, that the early portion of each curve in Figures 4.6a - 4.6d is in fact linear. It is also apparent that the gradients of these linear portions are approximately the same and largely independent of ink thickness and solvent content. To quantify this point, the gradients (volt/s) of the linear portions of the curves are set out in the Table 4.4.1

	Fig 5.3a	Fig 5.3b	Fig 5.3c	Fig 5.3d
Band 1: ink thickness, 6.6 μm	0.5	0.49	0.52	0.54
Band 2: ink thickness, 9.4 μm	0.48	0.45	0.45	0.55
Band 3: ink thickness, 11.3 μm	0.43	0.41	0.41	0.52

TABLE 4.4.1

Although there is some evidence of systematic variation (discussed further below) all gradients are within ±15% of the average, 0.48 V/s.

It should be noted that, although all drying curves clearly show a linear (constant-rate) section, this is somewhat surprising. True constant-rate drying only occurs when free liquid evaporates from a solid, such that the surface vapour pressure remains constant. This boundary condition does not necessarily hold for evaporation from a solution, where, in general, the vapour pressure of the solvent at the surface will change as the concentration of the solvent in the solution changes. This point is discussed in greater detail in Section 6.6 and in Appendix 2. However the large number of drying curves recorded throughout this research show that, for the research ink, the early stages of drying take place at constant-rate.

V_o, the virtual voltage at zero time, was determined for each of the drying curves in this test series, by extrapolating the linear portions of the curves backwards to cut the voltage axis. The quantity of solvent deposit m_o corresponding to each value of V_o was estimated from

$$m_o = \Delta . F_s . SG$$

Δ = Thickness of initial ink deposit, μm

F_s = Fraction solvent in ink

SG = Specific gravity solvent

To check both the consistency of the test results and the linearity of the Infragauge, corresponding values of V_o and m_o were plotted against each other in Figure 4.7. The graph is reasonable confirmation of the consistency of the experimental data. Table 4.4.1 shows that thicker ink layers dry more slowly than thin, i.e. they have smaller gradients. If this effect was not a real one, but arose from some inconsistency of technique, then the most likely cause of it is that the estimated value of V_o is low. Figure 4.7 indicates that this conjecture could be true.

The drying curves from this test series showed, that in the constant-rate period, the rate of drying was largely independent of the percentage solvent in the ink. Because of this, the solvent content of the ink was maintained constant for all subsequent constant-rate tests. An ink viscosity of 30 sec on a No. 2 Zahn cup (77% solvent) was selected as standard, this value being in accordance with good gravure practice.

4.5 Externally Controlled Drying - The Effect of Air Velocity and Air Temperature

Figure 4.8 shows the effect on the IR drying curves of systematically varying air jet velocity whilst maintaining all other parameters constant. All tests were carried out on gravure band 3 to ensure drying times of sufficient length to allow an accurate comparison with theory. The air velocity V_E, measured at nozzle outlet, was varied by adjusting the air pressure in the nozzle box. Because the jet

entrained ambient air, its temperature at the IR measuring point was lower than at the nozzle outlet. The air temperature T_A was measured by a glass stem thermometer placed in the wall jet boundary layer at the IR measuring point. Thermocouple traverses showed that this thermometer sensed the maximum in the wall jet temperature profile. To confirm repeatability two drying curves were recorded at each test condition.

Figure 4.9 shows the effect on the IR drying curves of systematically varying air temperature whilst maintaining all other parameters constant. To check repeatability three drying curves were recorded at each test condition. Inspection of Figures 4.8 and 4.9 shows that repeatability is excellent.

The calibration of the Infragauge (proportionally between V_o and solvent deposit m_o) will change with time if there is a change in instrumental gain. It is useful therefore to have a parameter with which to characterise constant rate drying that is independent of uncontrollable electronic changes such as amplifier drift. Such a parameter is, t_c defined as the hypothetical time for the solvent content of the ink to fall to zero, the drying rate being maintained as its constant-rate value (see Section 6.7). Provided that the mass of solvent deposited on the web at the beginning of each test is a constant, then, t_c depends only upon the velocity and temperature of the drying air, t_c may be estimated graphically by extrapolating the linear portion of the drying curve to the point where it cuts the time axis, Figure 4.4. Values of, t_c were estimated for all drying curves in Figures 4.8 and 4.9.

Based on the mass transfer theory described in Chapter 5 and on the thermodynamic properties of the ink system a computer program was written to predict t_c. The development of this program and the comparison of predictions from it with experimentally determined values of t_c are described in Chapter 6, Section 6.

4.6 The Critical Point

The drying curves of this chapter may also be examined to assess the effect of the physical variables on the critical point. Before making this assessment, the following two points should be noted,

i) A detailed discussion of the phenomenon of the critical point is inappropriate at this stage. Rather, this will come later, in Section 9.3, after the constant-rate period has been dealt with.

ii) It is difficult to locate by inspection of the smooth drying curve, the exact position of the critical point. This point is best located by constructing a rate of drying curve and this technique is used in Chapter 11.

In spite of what has been said, it is worthwhile to gauge, in a preliminary manner, the effect of the main experimental variables on the critical point. The ink solvent content at the critical point will be identified with the voltage ratio.

$$\frac{V_c}{V_o}$$

V_c = Infragauge voltage at the critical point

V_o = Infragauge voltage at time zero (estimated)

a) Air Velocity

From Figure 4.8, it appears that the ratio (V_c/V_o) remains essentially unaffected by significant changes in the rate of drying brought about by variations in the velocity of the drying air. From this figure it was estimated that

V_c = 2.75 volt = constant

V_o = 17.8 volt = constant

$$\frac{V_c}{V_o} = \frac{2.75}{17.8} = .154 = \text{constant}$$

b) Air Temperature

Similarly Figure 4.9, shows that (V_c/V_o) is unaffected by the changes in the rate of drying brough about by variations in the temperature of the drying air. From Figure 4.9 it was estimated that

V_c = 3.0 volt = constant

V_o = 18.6 volt = constant

$$\frac{V_c}{V_o} = \frac{3.0}{18.6} = .16 = \text{constant}$$

c) Ink Thickness

The four Figures 4.6a - d, each exhibit the same characteristic. On each figure, the critical points could be approximately located on straight line which passes through the origin of the co-ordinate system. Thus the ratio (V_c/V_o) is dependent upon the ink viscosity and is independent of the ink thickness.

d) Ink Viscosity - Solvent Content

It follows from c) above that on each of the Figures 4.6a - d the ratio (V_c/V_o) is a constant. The value of these four constants were estimated and are listed in Table 4.6.1 below for comparison with the non-volatile content of the ink. The percentage of non-volatiles were estimated from the constitution of the ink gel given in Section 4.1 and the proportion of solvent in ink given on Figure 4.7.

Table 4.6.1

Figure	Ink Constituent (as applied) %			$\frac{V_c}{V_o}$ %
	Solvent	Total non-volatile	Resin only	
4.6a	50	50	35	27
4.6b	57	43	30	22
4.6c	70	30	21	17
4.6d	77	23	16	13

It appears that the ratio (V_c/V_o) is related to the percentage of non-volatiles in the ink. However, whether it is the pigment alone, the resin alone or the sum of the two which is the influential variable is not clear.

Interim remarks on the critical point in this research

This preliminary analysis has indicated that the fraction of the applied solvent remaining at the critical point is largely a function of the percentage of non-volatiles in the ink. This fraction appears to be independent of the rate of drying and of the ink thickness. This

behaviour was broadly typical, and was encountered throughout later test work.

One final point on this topic is worth making. Because the ratio (V_c/V_o) did not vary widely with drying rate, investigation of the behaviour of the critical was not taken up until a relatively late stage in the research. In fact the so called "preliminary analysis" described above was carried out some considerable time after the tests themselves.

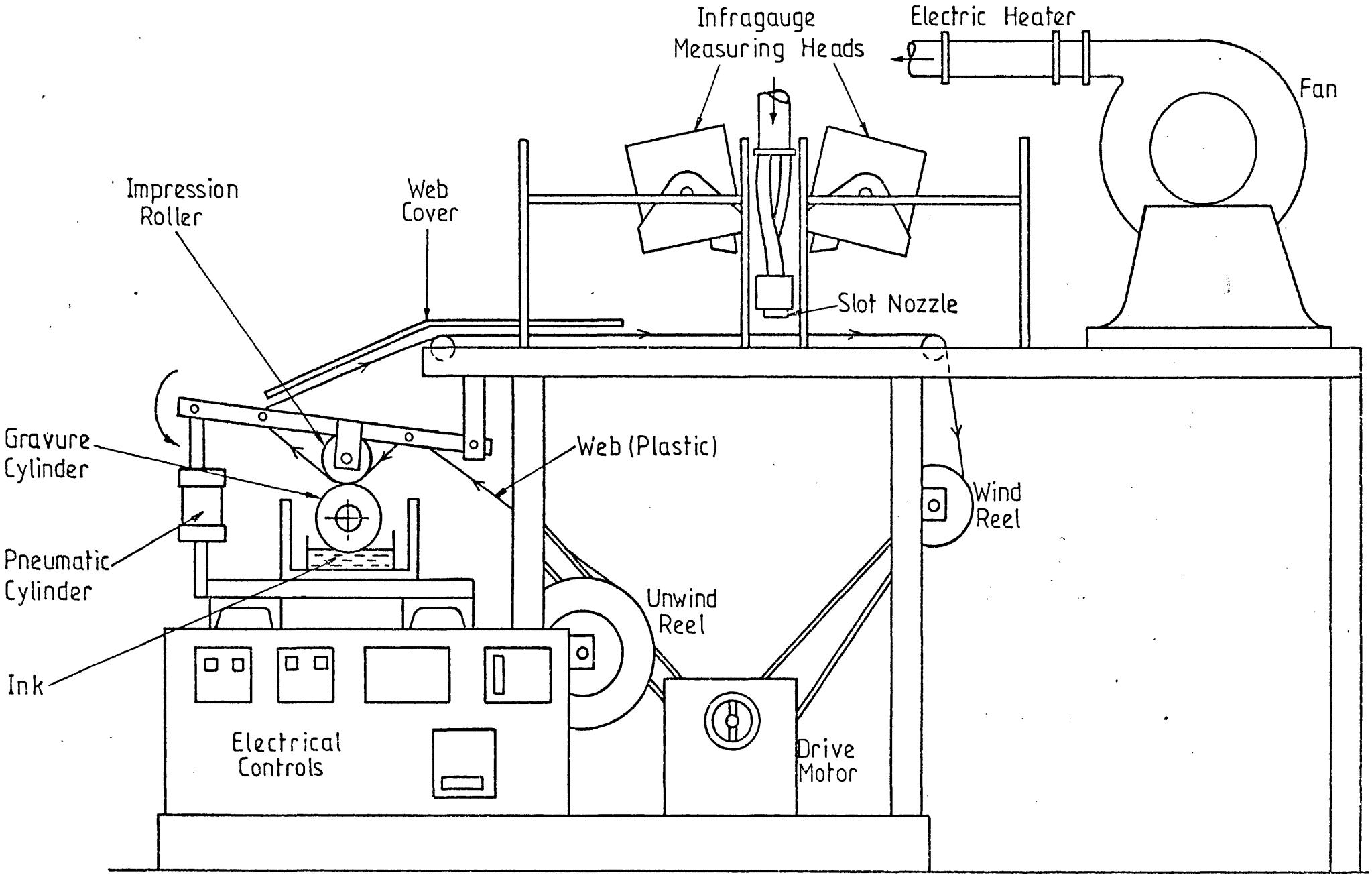

FIGURE 4.1. DRYING RESEARCH RIG

FIGURE 4.2.

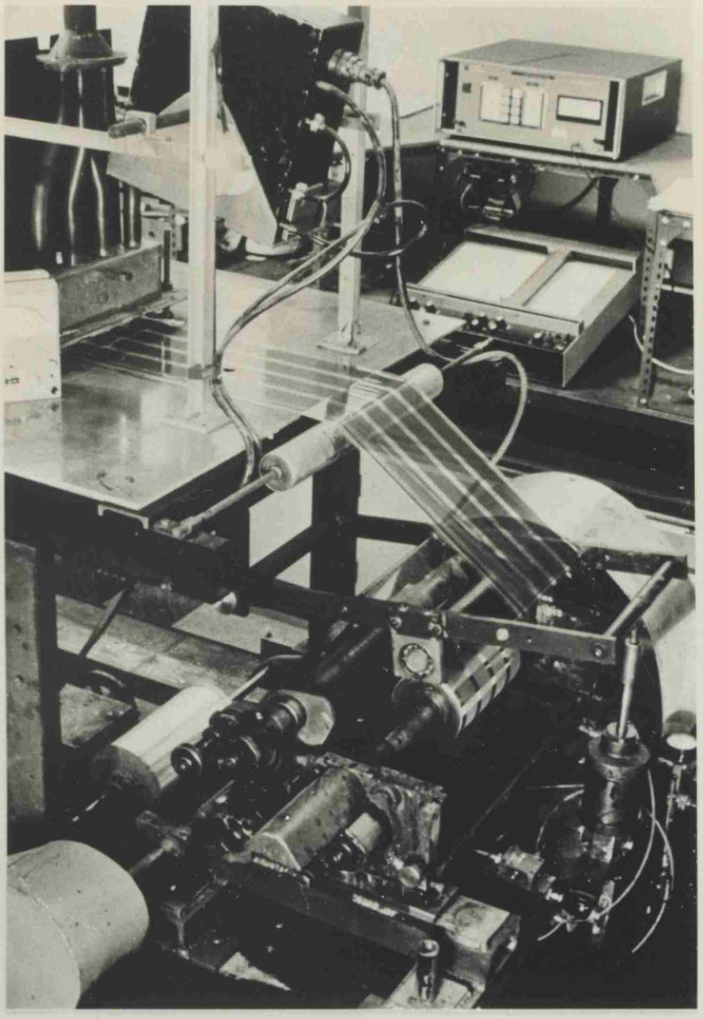

(a) DRYING RESEARCH RIG

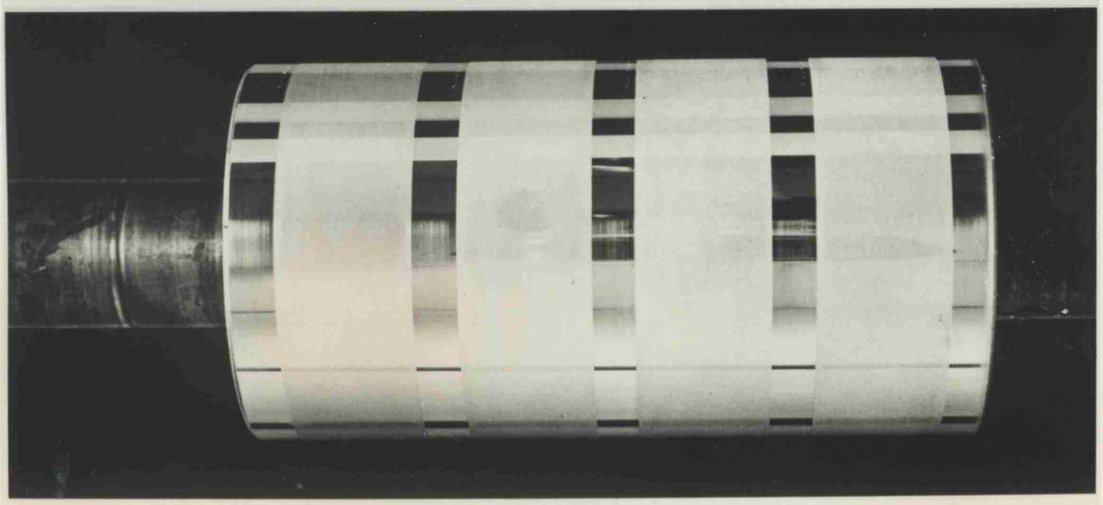

(b) GRAVURE CYLINDER

FIGURE 4.3

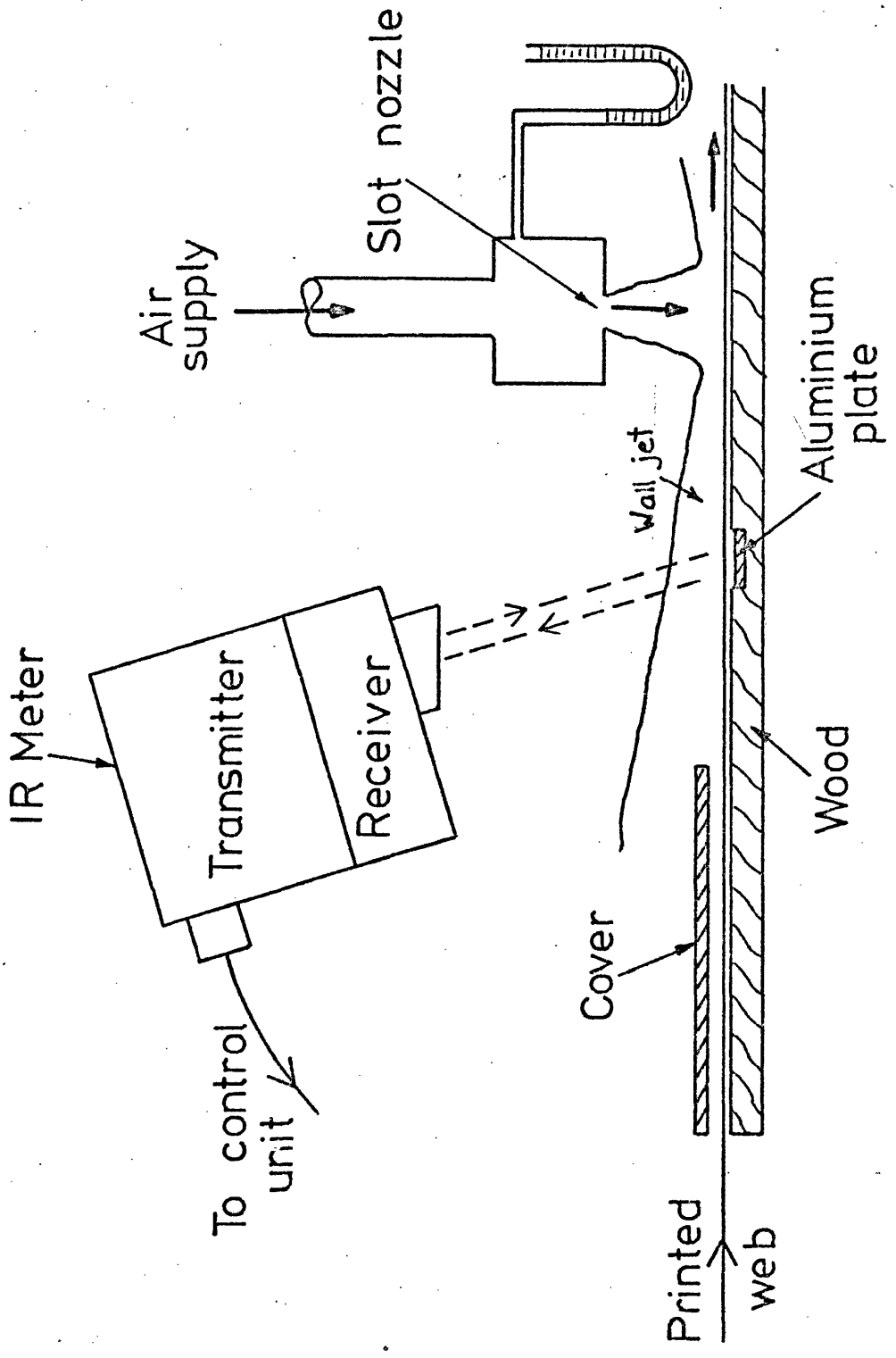
Air supply
Slot nozzle
Wall jet
Aluminium plate
IR Meter
Transmitter
Receiver
To control unit
Cover
Wood
Printed web

FIGURE 4.4

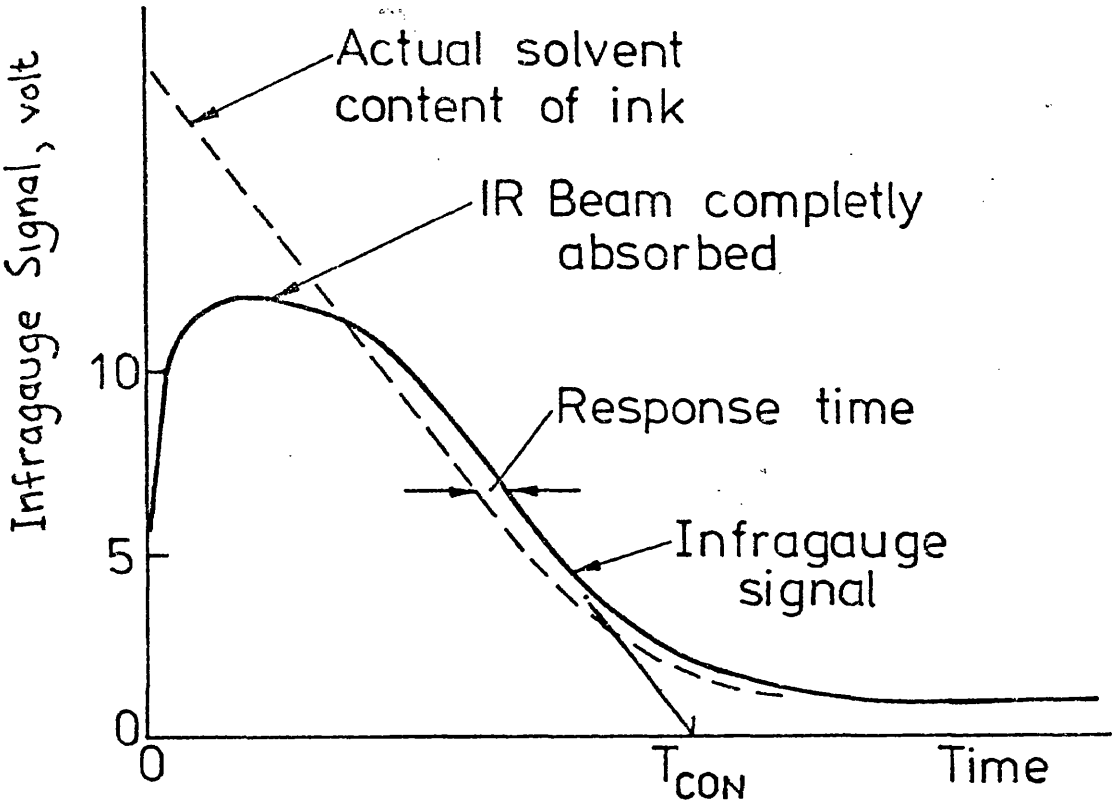
Infragauge Signal, volt
Actual solvent content of ink
IR Beam completly absorbed
Response time
Infragauge signal
10
5
0
0
T_{CON}
Time

FIGURE 4.5

MEASUREMENT OF INK SOLVENT CONTENT BY ZAHN CUP

Relation between Percentage Solvent in Ink and Time to Empty a No. 2 Zahn Cup

Solvent - 4 methyl 2 pentanol

Temperature 23 C

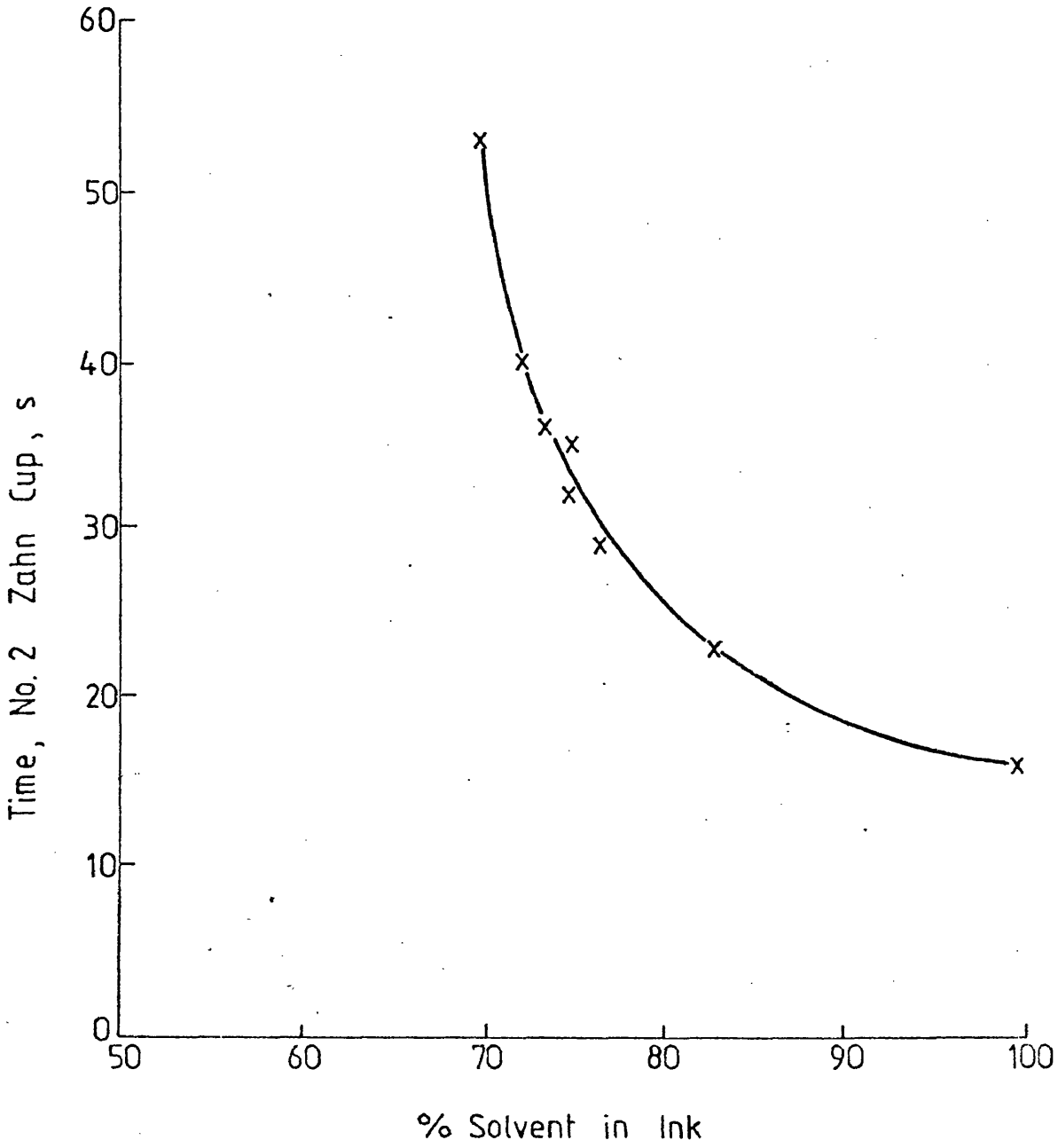

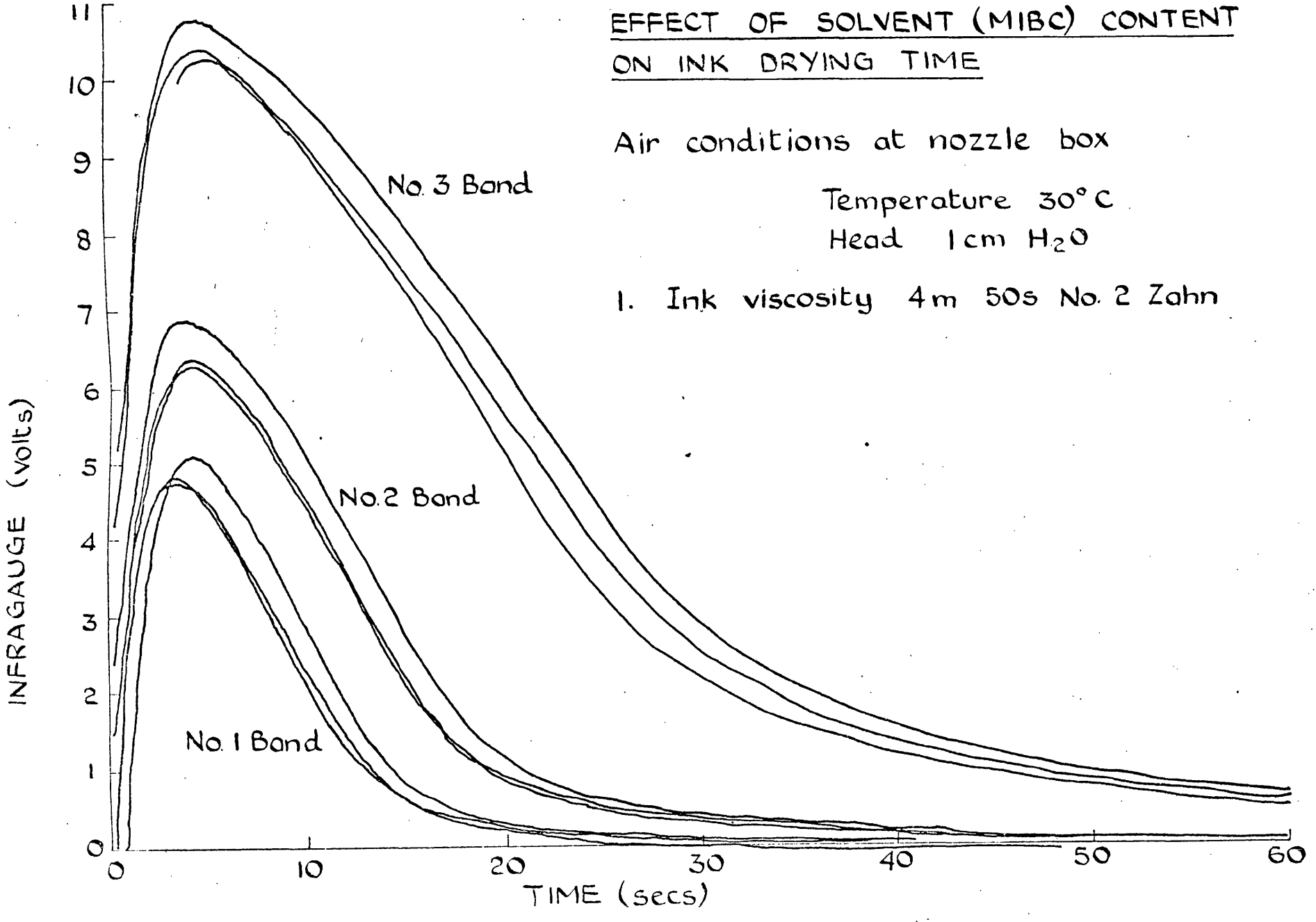
EFFECT OF SOLVENT (MIBC) CONTENT
ON INK DRYING TIME
Air conditions at nozzle box
Temperature 30° C
Head 1 cm H_2O
1. Ink viscosity 4m 50s No. 2 Zahn
No. 3 Band
No. 2 Band
No. 1 Band
INFRAGAUGE (volts)
TIME (secs)
0
1
2
3
4
5
6
7
8
9
10
11
0
10
20
30
40
50
60

FIGURE 4.6a

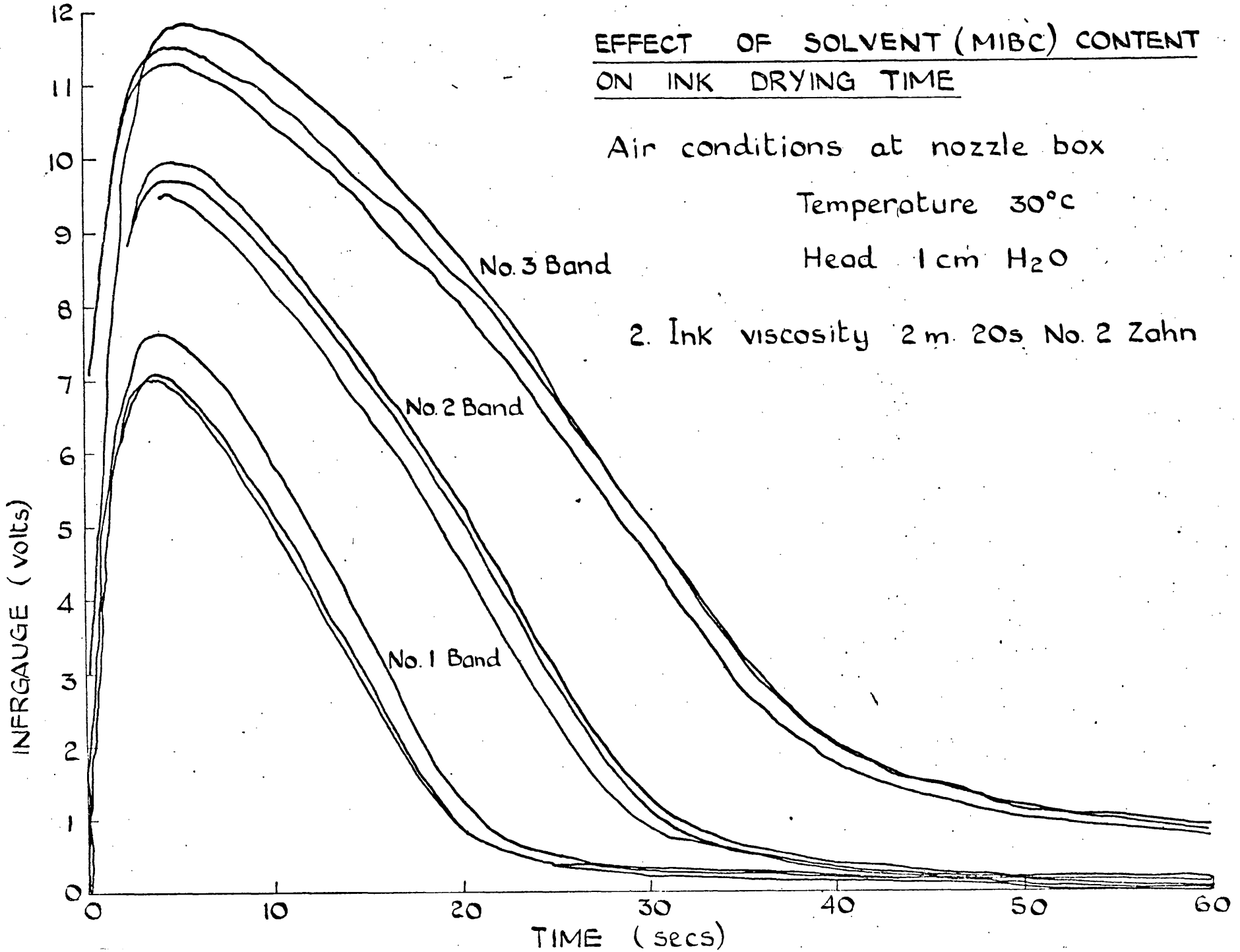
EFFECT OF SOLVENT (MIBC) CONTENT
ON INK DRYING TIME
Air conditions at nozzle box
Temperature 30°c
Head 1 cm H_2O
2. Ink viscosity 2 m. 20s No. 2 Zahn
No. 3 Band
No. 2 Band
No. 1 Band
INFRGAUGE (volts)
TIME (secs)
0
1
2
3
4
5
6
7
8
9
10
11
12
0
10
20
30
40
50
60

FIGURE 4.6b

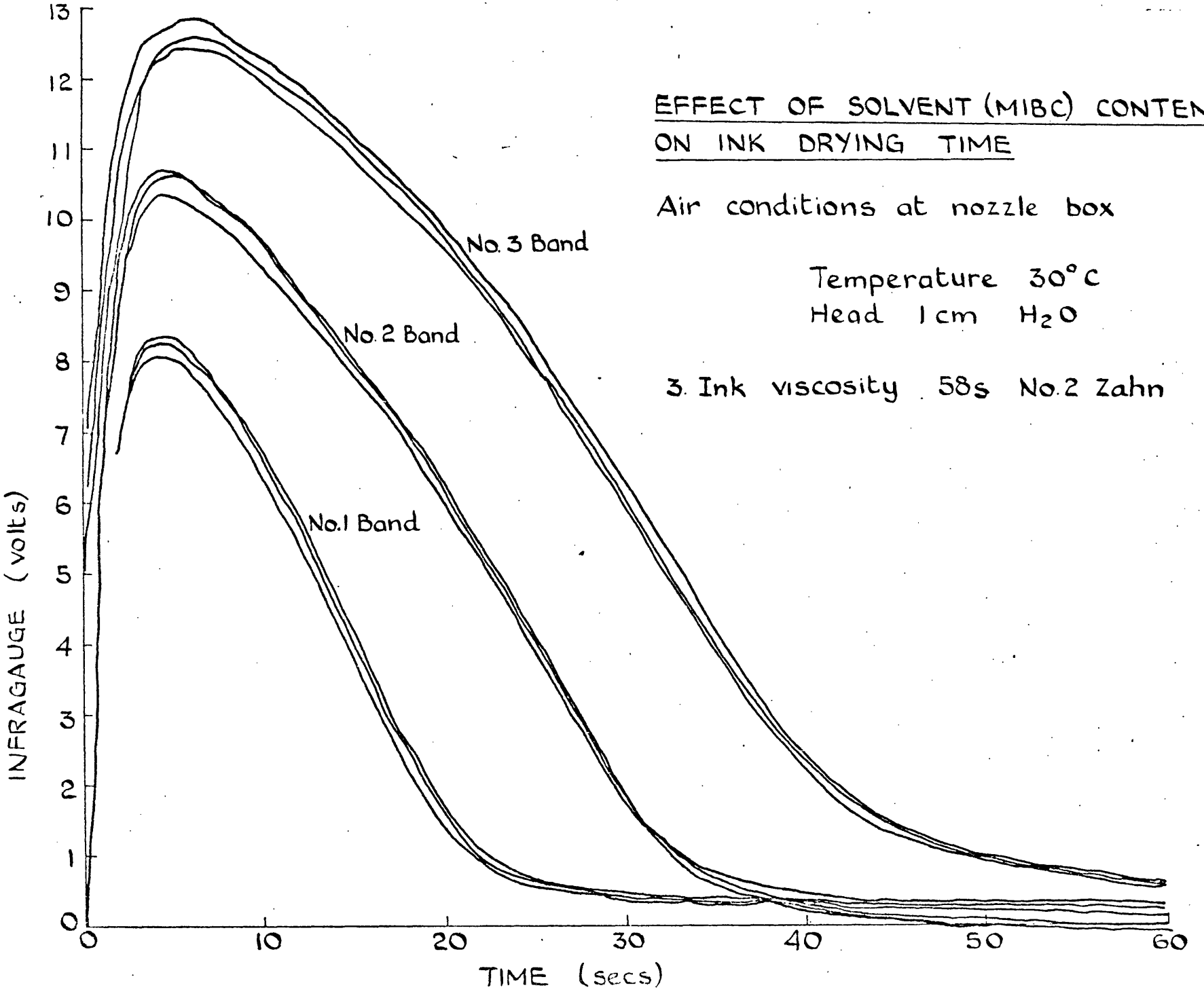
EFFECT OF SOLVENT (MIBC) CONTENT ON INK DRYING TIME
Air conditions at nozzle box
Temperature 30°C
Head 1 cm H_2O
3. Ink viscosity 58s No.2 Zahn
No. 3 Band
No. 2 Band
No. 1 Band
INFRAGAUGE (volts)
TIME (secs)
0
1
2
3
4
5
6
7
8
9
10
11
12
13
0
10
20
30
40
50
60

FIGURE 4.6c

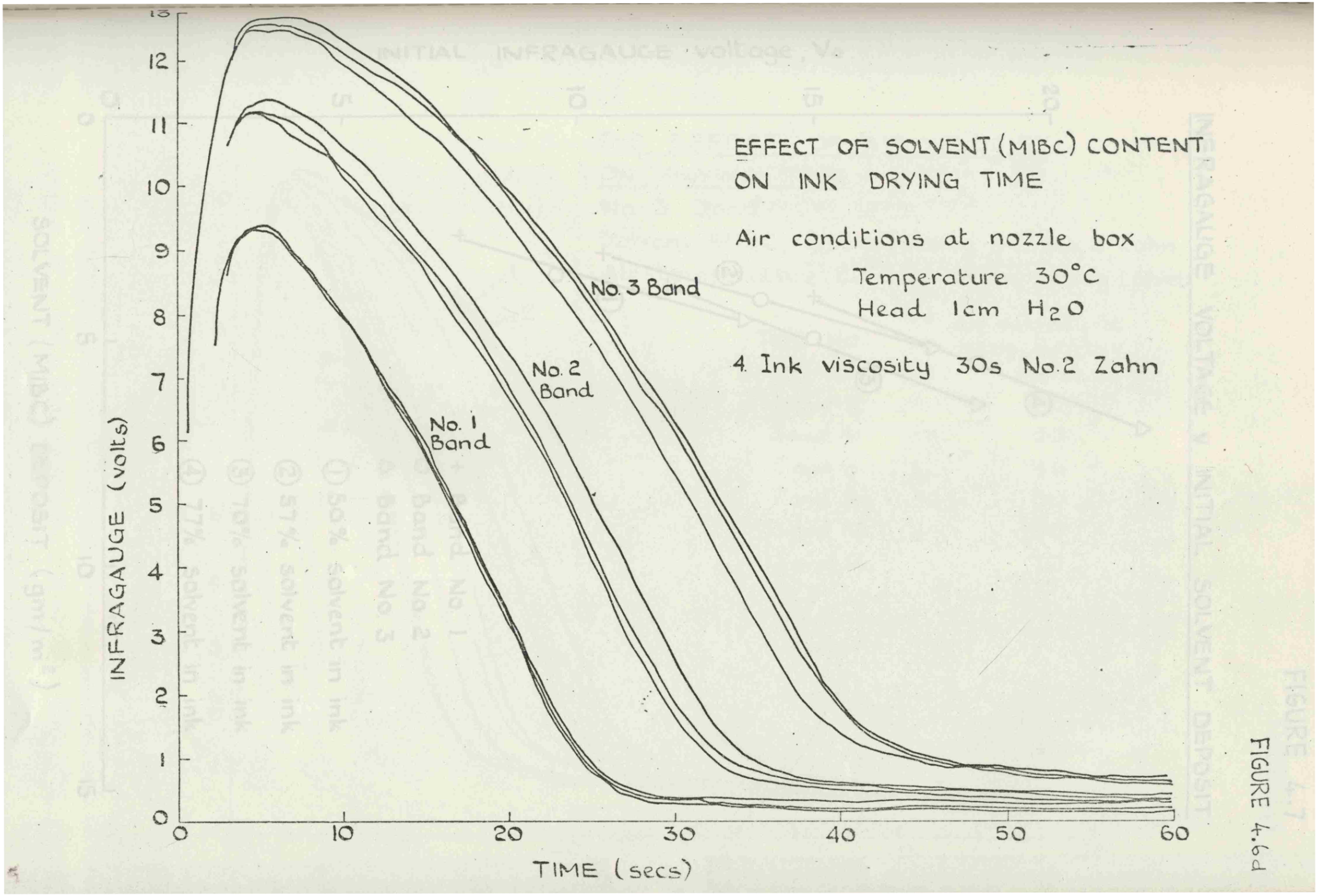
EFFECT OF SOLVENT (MIBC) CONTENT
ON INK DRYING TIME
Air conditions at nozzle box
Temperature 30°C
Head 1cm H_2O
4. Ink viscosity 30s No.2 Zahn
No. 3 Band
No. 2 Band
No. 1 Band
INFRAGAUGE (volts)
TIME (secs)
0
1
2
3
4
5
6
7
8
9
10
11
12
13
0
10
20
30
40
50
60

FIGURE 4.6d

FIGURE 4.7

INFRAGAUGE VOLTAGE v INITIAL SOLVENT DEPOSIT

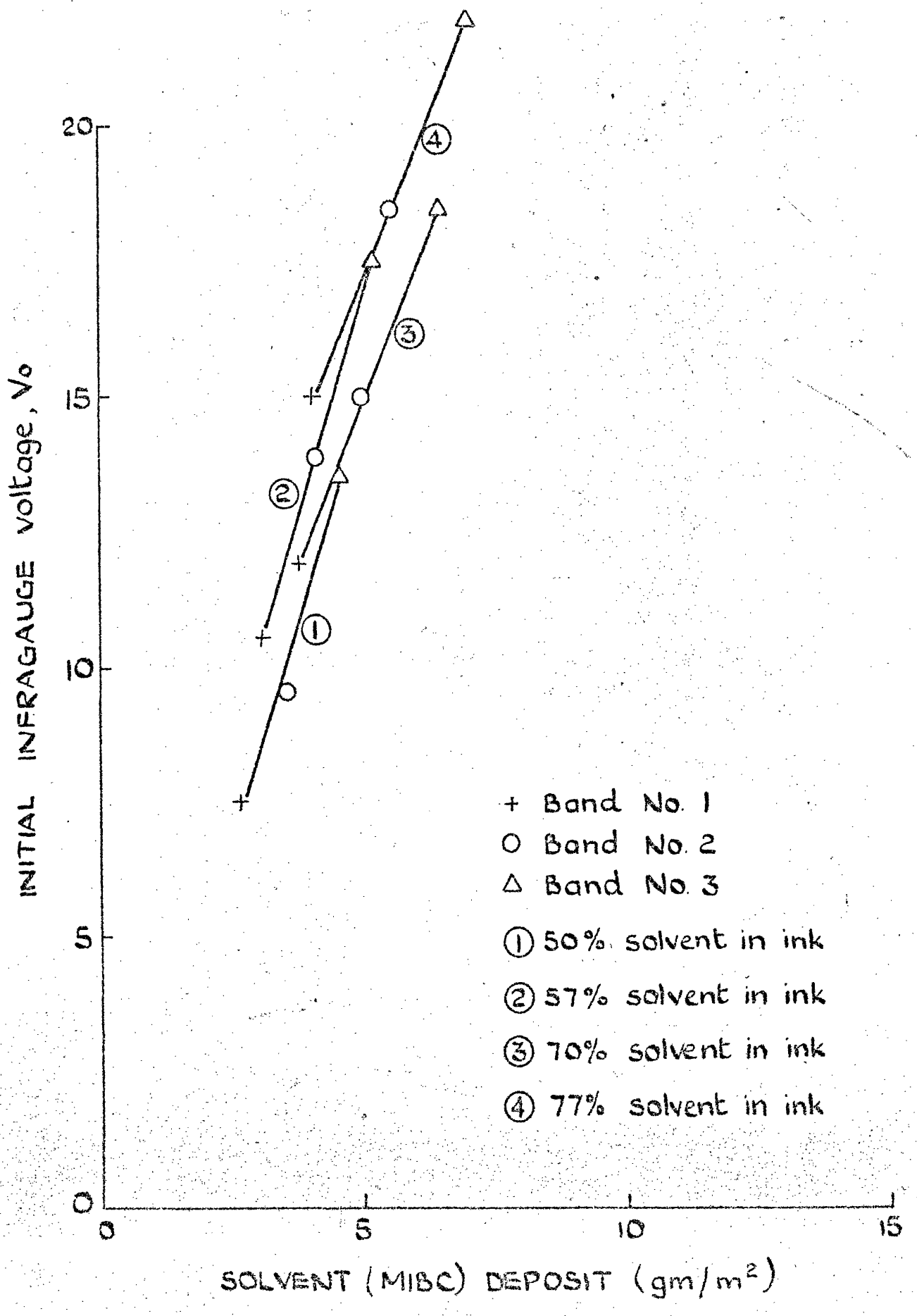

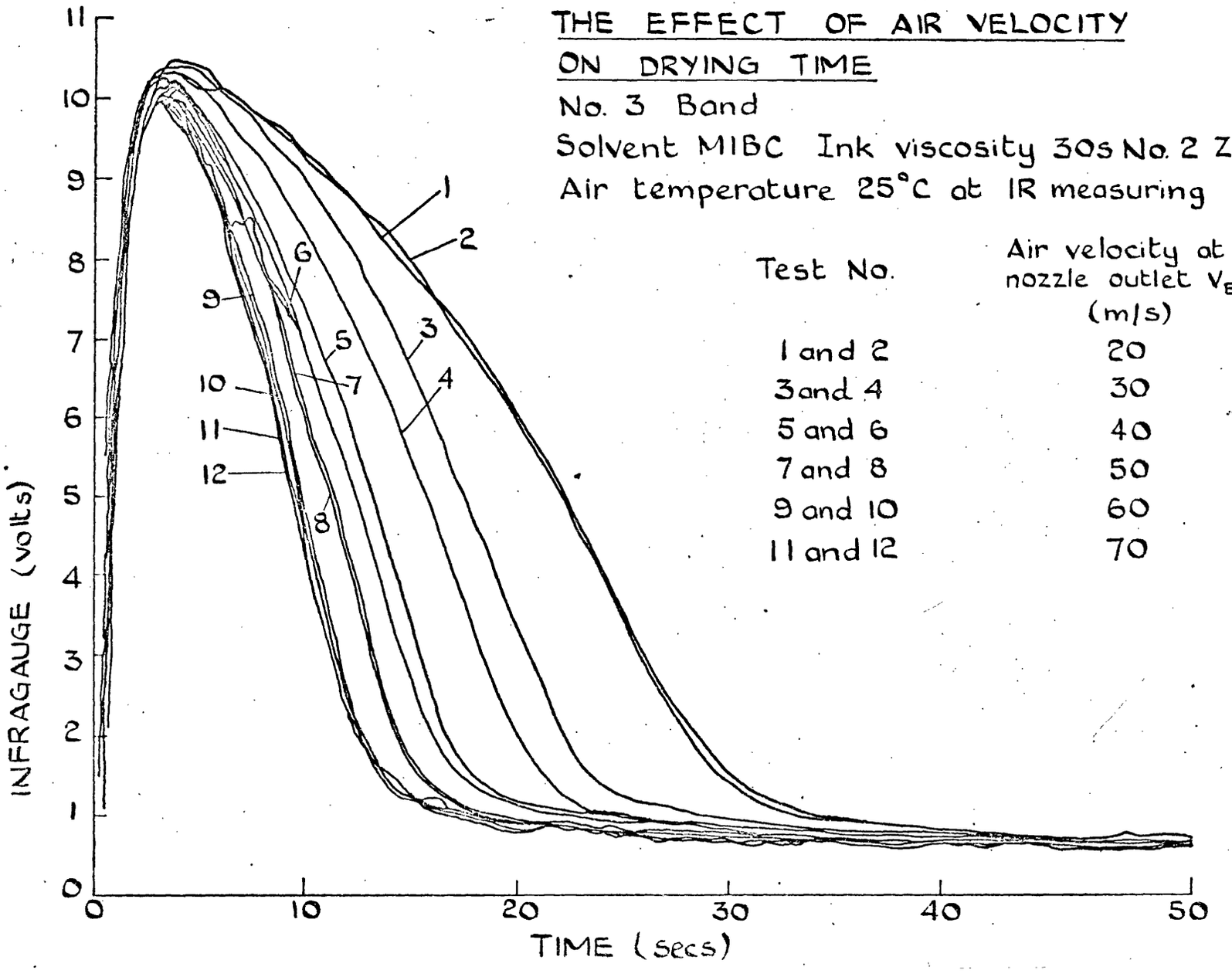

THE EFFECT OF AIR VELOCITY ON DRYING TIME

No. 3 Band

Solvent MIBC Ink viscosity 30s No. 2 Zahn

Air temperature 25°C at IR measuring point

Test No.	Air velocity at nozzle outlet V_E (m/s)
1 and 2	20
3 and 4	30
5 and 6	40
7 and 8	50
9 and 10	60
11 and 12	70

FIGURE 4.8

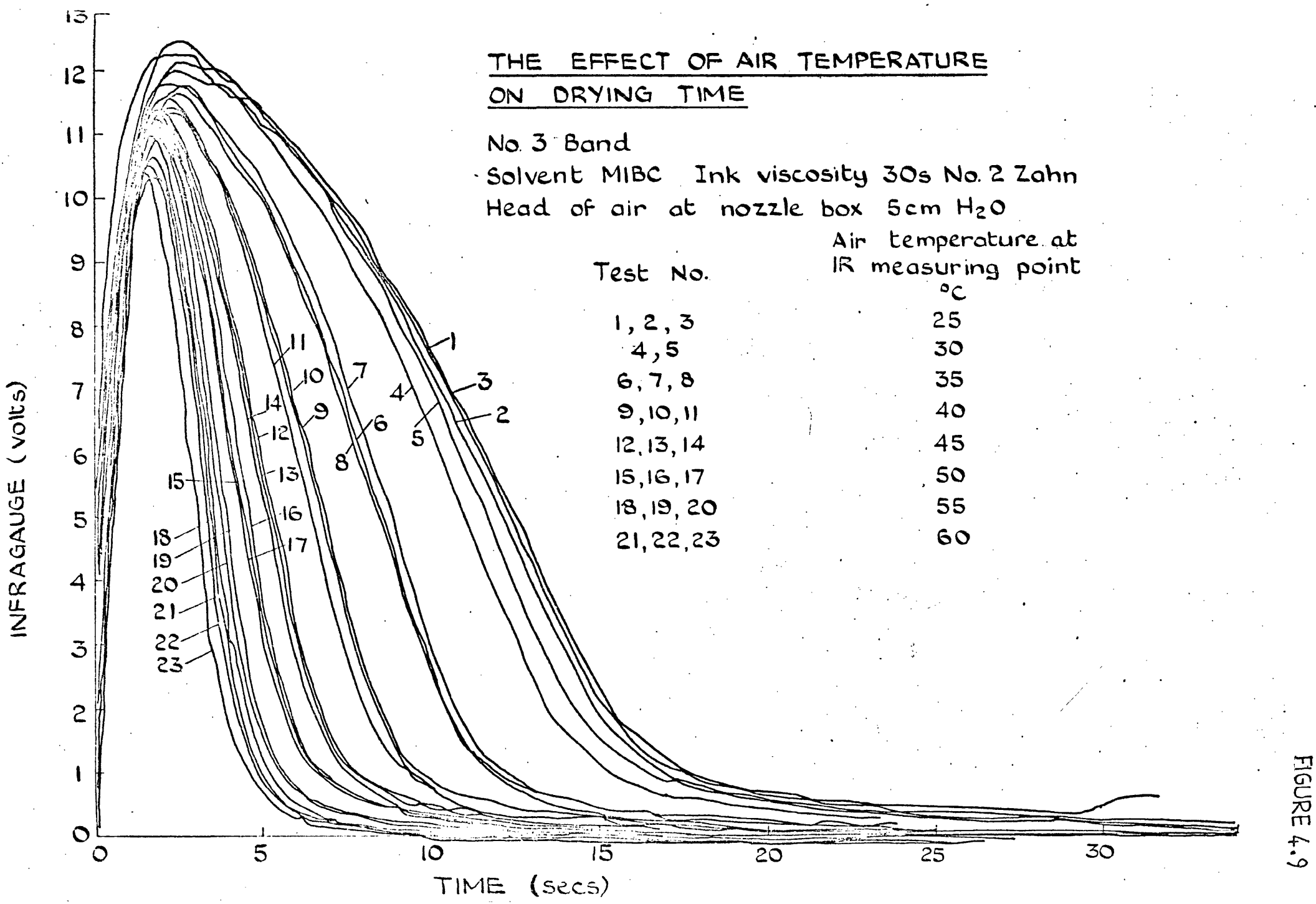
THE EFFECT OF AIR TEMPERATURE ON DRYING TIME
No. 3 Band
Solvent MIBC Ink viscosity 30s No. 2 Zahn
Head of air at nozzle box 5cm H_2O
Test No. | Air temperature at IR measuring point °C
1, 2, 3 | 25
4, 5 | 30
6, 7, 8 | 35
9, 10, 11 | 40
12, 13, 14 | 45
15, 16, 17 | 50
18, 19, 20 | 55
21, 22, 23 | 60
INFRAGAUGE (volts)
TIME (secs)
0
1
2
3
4
5
6
7
8
9
10
11
12
13
0
5
10
15
20
25
30

FIGURE 4.9

5. THEORY OF CONSTANT RATE PERIOD OF INK DRYING

5.1 Review of Previous Research

A number of investigators have attempted to categorise those physical properties which influence the relative evaporation rate of pure solvents and of solvent blends. Most of their research has been devoted to devising a convenient method of measuring the rate at which a solvent evaporates under standard conditions. The apparatus can then be used to determine comparative evaporation rates of different solvents.

The theory of the relative evaporation rate is an example of the difficulty of obtaining agreement even on the mechanism of evaporation. If evaporation is regarded as a distillation process then, starting from the Langmuir-Knudson equation, which gives the number of molecules escaping from a surface, Reynolds (26), it can be shown that the evaporative mass flux, m, is given by

$$m = p\left(\frac{M}{2\pi RT}\right)^{\frac{1}{2}} \qquad 5.1.1a$$

p = saturated vapour pressure of solvent at temperature T

M = molecular weight of solvent

$$\text{or } m \propto p M^{\frac{1}{2}} \qquad 5.1.1b$$

Alternatively Gardner (27) regarded the rate of evaporation as limited by diffusion across a stagnant air film. Writing equation 3.5.2 in terms of partial vapour pressure, his equation for the rate of evaporation was

$$m = C(D\ M\ p) \qquad 5.1.2$$

C = constant

D = diffusion coefficient of solvent

The controversy between these different viewpoints appears never to have been resolved. Perhaps for evaporation in a closed laboratory vessel equation 5.1.1 is appropriate while for evaporation through a boundary layer equation 5.1.2 should be used. The present position is that most commentators on the ink drying process state that, in the early stages, the rate of drying is externally controlled. However, at the time when this research was started, there appeared to be little or no data on the drying of thin films under realistic air-flow conditions, with which to quantify these statements.

The starting point for experiments to determine evaporation rate is usually from a pool of pure solvent in an open pan. Although simple to perform, data from such experiments are frequently of doubtful validity. This is because controlled air conditions are extremely difficult to achieve and heat transfer from the apparatus to a relatively small sample will be significant. The quantity of solvent present, at a particular time is usually determined by weighing. It will be appreciated that if weighing is carried out in a standard laboratory cabinet, then controlled and realistic air conditions are precluded.

A number of workers have attempted refinements of the simple weighing technique, usually by attempting to standardise the environment. A number of these are described by Billmeier and Ritterhausen (28). Possibly the most successful of these devices is the Shell Liquid Film

Evaporometer (29). This instrument produces a graphical record of solvent mass against time obtained by weighing solvent in a pan under standardised air flow conditions. By means of the Shell Evaporometer, ranges of solvents have been tested and their evaporation rates, relative to n-butyl acetate, are given in Ref. (29). Although this data is of great practical value the following reservations regarding it should be noted:-

a) The solvent is present under conditions which only approximate to those of the real film. Tysall (30) has drawn attention to the anomalies which can arise between measurements of evaporation rates from thin films, thick films and filter paper.

b) No variation in the standardised air conditions appears possible. All weighing techniques have the disadvantage that it would be extremely difficult to use them with impinging air jets.

c) Some statement on the magnitude of the heat conducted from the apparatus to the solvent is required. If the solvent receives a fraction of its enthalpy of evaporation by heat leakage from the apparatus, it will not attain the wet-bulb temperature. The cooling effects, produced by the evaporation of volatile solvents, are significant.

d) The instrument appears unsuitable for measurements in the falling rate period, because such measurements should, if possible, be performed on the actual paint film itself. Also to measure the extremely small changes in mass, a balance of extremely high accuracy is required.

A difficulty encountered in this type of research into the evaporation of solvents, is that it is usually necessary to incorporate a secondary substance to act as a "film former". Such a substance should, if this is possible, be miscible with all solvents and be free from special retention effects shown by resins. In the constant-rate period the effect of a dissolved solute is to modify the vapour pressure, and hence the evaporation rate, of the solvent. Because of the complexity of ink systems such effects are usually estimated empirically. The manner in which this was done for this research, for the constant-rate period, is described in Section 6.6. For the falling-rate region it seems essential to simulate the physical characteristics of the real material to be dried as closely as possible.

5.2 The Psychrometric Ratio

When a pure liquid evaporates from an inert solid, sufficiently slowly so that the secondary effects of Section 3.7 are negligible, then the dynamic energy balance is given by equation 3.5.3. Transforming from molar to mass units this energy balance may be written

$$h(T_G - T_s) = k_\rho (\rho_s - \rho_G) h_{fg} \qquad 5.2.1$$

k_ρ = mass transfer coefficeint, kg/m^2s

ρ = mass concentration, kg/m^3

h_{fg} = enthalpy of evaporation, J/kg

This theory is identical with the theory of the wet-bulb thermometer and the surface temperature T_s is equal to the wet-bulb temperature.

Rearrangement of equation 3.6.3 gives the value of the "wet bulb depression"

$$T_G - T_s = \frac{(\rho_s - \rho_G)\, h_{fg}}{h/k_\rho} \qquad 5.2.2$$

h/k_ρ = psychrometric ratio (Treybal (77) p 193)

Before the wet bulb depression and the evaporation rate can be evaluated the psychrometric ratio must be known. In the present research, surface heat flux meters have been used to measure the heat transfer coefficient h under impinging jets. Some of these results are reported in Hardisty (5). To develop a theory of constant-rate drying a value of k_ρ is required. This allows theoretical predictions of drying times which may then be compared with times measured from the IR drying curves. To predict k_ρ a suitable form of the heat-mass transfer analogy is required.

The analogy between momentum, heat and mass transfer in turbulent flow has been used by several investigators to analyse their psychrometric data. The analogy finds expression in various analytical forms, depending on the particular boundary layer model which is selected, and the particular assumptions which are made to integrate it. A detailed review of the historical development of the important analogies is given by Sherwood (31). Based on a 3-layer model of the boundary layer von Karman (32) derived the following expression for the heat transfer Stanton number, St_x

$$St_x = \frac{f_x/2}{1 + 5\sqrt{f_x/2}\ \{Pr - 1 + \ln\ (\frac{1}{6} - \frac{5Pr}{6})\}} \qquad 5.2.3$$

It can be seen that the effect of Prandtl number on the simple Reynolds analogy resides in the function of Prandtl number contained in the denominator on the r.h.s. The corresponding expression for the mass transfer Stanton number St_M is obtained by substituting the Schmidt number for the Prandtl number in the above expression. Lewis (33) has pointed out that, when either Prandtl number or Schmidt number differ appreciably from unity, the psychrometric ratio obtained by dividing equation 5.2.3 by its mass transfer analogue, depends upon Reynolds number.

Colburn (34) suggested that in turbulent shear flow, the effect of Prandtl number on heat transfer could be simply expressed in the form

$$j_H = St\ Pr^{2/3} = 0.023\ Re^{-0.2} \qquad 5.2.4$$

It can be seen that $Pr^{2/3}$ is much simpler than the Prandtl number fuction appearing in equation 5.2.3. Equation 5.2.4 has been widely accepted. Chilton and Colburn (35) proposed that an analogous equation should hold for mass transfer

$$j_D = St_M\ Sc^{2/3} = 0.023\ Re^{-0.2} \qquad 5.2.5$$

There is less detailed confirmation of this equation. For example Gilliland (36) correlated his experimental data from wetted-wall towers by the equation

$$Sh = 0.023\ Re^{0.83}\ Sc^{0.46} \qquad 5.2.6$$

Sherwood and Pigford (37) later pointed out that, because of the

narrow range of Gillilands data, it could also be correlated by means of the Colburn analogy, equation 5.2.5.

A great deal of test data appears to confirm the close similarity between the processes of heat and mass transfer. This is true, even when the wider analogy with momentum transfer breaks down. This usually occurs in separated flows, when fluid dynamic drag does not arise purely from surface friction.

The psychrometric ratio can be readily calculated from accurate wet and dry bulb data, but these results are strictly applicable only to other situations with similar geometry. The data of several investigators is critically examined by Bedingfield and Drew (38) who proposed that for various liquids evaporating into air

$$\frac{h}{k_Y} = 0.294\ Sc^{0.56} \qquad 5.2.7a$$

which may be transformed to

$$\frac{h}{k_\rho} = \rho\ C_p \left(\frac{Sc}{Pr}\right)^{0.56} \qquad 5.2.7b$$

A later attempt to correlate experimental data on psychrometric ratio was carried out by Wilke and Wassan (39). It can be inferred from their graphs that the exponent of the Schmidt number lies in the range 0.62 - 0.74. In almost all of the investigations reviewed in references (38) and (39), no appreciable variation of the psychrometric ratio with gas velocity was reported.

For purposes of this research, it was decided to base the equation for the psychrometric ratio on the Chilton-Colburn analogy, equations 5.2.4 and 5.2.5. This appeared reasonable, bearing in mind both the degree of uncertainty in the published data and that the equation was to be applied to a new geometry. Also approximate calculations indicated the Schmidt number for the vapour to be not very different from unity (2.0 approx).

Assuming the Chilton-Colburn analogy to be applicable

$$\frac{h}{k_\rho} = \rho C_p \, Le^{2/3} \qquad 5.2.8$$

where $Le = \frac{\alpha}{D} = \frac{Sc}{Pr}$ and $\alpha = \frac{k}{\rho C_p}$

In terms of the stagnant film hypothesis, it follows that

$$\frac{\delta_V}{\delta_M} = Sc^{1/3}$$

$$\frac{\delta_T}{\delta_M} = Le^{1/3}$$

For given values of concentration difference and Reynolds number, the proportionality between evaporative mass flux N_A and diffusion coefficient D is

$$N_A \propto \frac{D}{\delta_M} \propto \frac{D}{D^{1/3}} \propto D^{2/3}$$

It should be noted that a consequence of the Chilton-Colburn analogy is that the wet-bulb depression is independent of air velocity (Reynolds number).

5.3 Solvent Vapour Pressure

During constant rate drying, solvent evaporating from the free surface exerts the saturated vapour pressure corresponding to the liquid temperature. Solvent vapour pressures are relatively low, and consequently the saturated vapour concentration may be calculated from the ideal gas law

$$\rho_s = \frac{p_s M}{R T_s} \qquad 5.3.1$$

p_s = saturated vapour pressure, N/m^2

T_s = absolute temperature, K

ρ_s = mass concentration of saturated vapour kg/m^3

M = molecular weight of solvent

An equation relating p and T may be derived from thermodynamics as follows. In any phase change, involving a volume change ΔV and the corresponding entropy change ΔS, the Clapeyron equation must be satisfied

$$\frac{dp}{dT} = \frac{\Delta s}{\Delta V} \qquad 5.3.2$$

For the phase change from liquid to vapour (making the assumption that $\Delta V \approx v_g$) the Clausius-Clapeyron equation holds

$$\frac{dp}{dT} = \frac{h_{fg}}{T\, v_g} \qquad 5.3.3$$

where h_{fg} = enthalpy of evaporation, J/kg

v_g = specific volume saturated vapour, m^3/kg

Substituting equation 5.3.1 into equation 5.3.3 (also using $v = 1/\rho$ and $h_v = M\ h_{fg}$) gives

$$\frac{dp}{dT} = \frac{\Delta h_v\ p}{T^2\ R} \qquad 5.3.4$$

This equation may be integrated if it is assumed that Δh_v is a constant

$$\ell n\ p = -\frac{\Delta h_v}{RT} + c \qquad 5.3.5$$

which may be expressed in the form

$$\ell n\ p = A - \frac{B}{T} \qquad 5.3.6$$

where A and B are constants characteristic of a particular liquid. Note that

$$B = \frac{\Delta h_v}{R} \qquad 5.3.7$$

and $$\frac{dp}{dT} = \frac{Bp}{T^2} \qquad 5.3.8$$

Equation 5.3.6 is similar to the vapour pressure equation proposed by Antoine (1888)

$$\ell n\ p = A - \frac{B}{T + C} \qquad 5.3.9$$

where C is an additional constant.

Equations 5.3.6 and 5.3.9 are the desired equations relating vapour

pressure and temperature. Before equation 5.3.6 can be used in the theory which follows it must be linearised.

Linearisation of equation 5.3.6

Let T_o = datum temperature

p_o = datum pressure

from equation 5.3.6 $$p_o = e^{(A - B/T_o)} \qquad 5.3.10$$

Let $T = T_o + \theta$

$$p = e^{A - B/(T_o + \theta)}$$

$$= e^{A} \; e^{-\frac{B}{T_o}(1 + \theta/T_o)^{-1}}$$

using the binomial approximation $(1 + x)^{-1} \approx 1 - x$

$$p = p_o \, e^{B\theta/T_o^2} \qquad 5.3.11$$

using the binomial approximation $e^{x} \approx 1 + x$

$$p = p_o \, (1 + b\theta) \qquad 5.3.12$$

where $$b = \frac{B}{T_o^{\,2}}$$

The consistency of equation 5.3.12 can be checked if it is noted that linearity implies

$$b = \frac{1}{p_o} \left(\frac{dp}{dT}\right)_o \qquad 5.3.13$$

which is seen to be consistent with equation 5.3.8.

5.4 Relative Evaporation Rate, m_c

When comparing a variety of solvents it is useful to have some measure of their relative evaporation rates. For purposes of comparison it will be assumed that air, at atmospheric pressure, flows at a standard rate, and at a standard temperature T_o, over a surface of fixed geometry. The solvent will evaporate at a constant rate, and the mass flux m_c from the surface may be obtained from equation 5.2.1

$$m_c = k_\rho (\rho_s - \rho_o)$$

In the usual arrangement of wet-bulb thermometer, a large mass of air is directed normally across the thermometer bulbs. In this case, there is no recirculation of the drying air, and the humidity and temperature of the bulk air stream, remain constant and unaffected by the surface evaporation. This situation is consistent with the usual assumption in boundary layer theory, that for flow over an external surface, such as a flat plate, the free steam conditions remain constant. For such an external flow, it is the boundary layer which entrains ambient fluid, and the transferred quantity (heat, mass or momentum) is retained within the boundary layer. The stipulation that the free steam condition does not change in the stream wise direction is characteristic of external, developing boundary layer flows without recirculation. It follows that in this research, where evaporation occurs within a wall boundary layer, the vapour concentration in the free stream, ρ_o, may be taken as constant. In addition, because there was no arrangement to recirculate air and because the absolute quantity of solvent evaporated during a test was small, ρ_o was assumed to be zero. With this condition equation 5.2.1 becomes

$$m_c = k_\rho \rho_s \qquad 5.4.1$$

It is worth noting in passing, that the remarks of the previous paragraph, on the free-stream condition, do not apply to fully developed flows confined within a duct. Here, the heat or mass transferred from the duct wall produces an axial change of state of the bulk flow. The magnitude of this axial change may be determined by incorporating conservation equations into the theoretical model. Similar remarks apply when recirculation is employed.

The psychrometric ratio is obtained from equation 5.2.8

$$\frac{k_\rho}{h} = C_1 D^{2/3} \qquad 5.4.2$$

where $C_1 = (\rho C_p \alpha^{2/3})^{-1}$

At the low vapour concentrations which pertain, the fluid properties required to evaluate C_1 may be assumed to be those of pure air and treated as constants.

Let T_s = surface temperature

$\theta = T_o - T_s$ = wet bulb depression

$$T_s = T_o - \theta \qquad 5.4.3$$

In practice θ is usually small in comparison with the absolute temperature T_o. This fact allows the analysis to be simplified at two points:-

i) Because $\theta << T_o$

then $T_s \approx T_o$

Introducing this approximation into equation 5.3.1

$$\rho_s \approx C_2 \, p_s \, M \qquad 5.4.4$$

where $C_2 = (R \, T_o)^{-1}$

ii) The linearised form of the Antoine equation 5.3.12 can be used

$$p_s = p_o \, (1 - b\theta) \qquad 5.4.5$$

where p_o = saturated vapour concentration at standard temperature T_o

p_s = saturated vapour concentration at surface temperature T_s

Substituting equation 5.4.5 in equation 5.4.4

$$\rho_s = C_2 \, p_o \, (1 - b\theta) \, M \qquad 5.4.6$$

The wet bulb depression is obtained from equation 5.2.2 with $\rho_o = 0$

$$\theta = \frac{k_p}{h} \rho_s \, h_{f_g} \qquad 5.4.7$$

and substituting equation 5.4.2 and 5.4.6 in equation 5.4.7

$$\theta = C_1 \, D^{2/3} \, C_2 \, p_o \, (1 - b\theta) \, M \, h_{f_g}$$

Solving for θ

$$\theta = \frac{C \, r \, h_{f_g}}{1 + C \, b \, r \, h_{f_g}} \qquad 5.4.8$$

where $r = D^{2/3} \, p_o \, M$

$C = C_1 C_2$

This expression for θ can now be introduced into equation 5.4.6

$$\rho_s = C_2\, p_o\, M \left(1 - \frac{b\, C\, r\, h_{f_g}}{1 + C\, b\, r\, h_{f_g}}\right)$$

$$= \frac{C_2\, p_o\, M}{1 + Cbr\, h_{f_g}} \qquad 5.4.9$$

Finally the evaporation rate can be obtained by substituting equations 5.4.2 and 5.4.9 into 5.4.1

$$m_c = \frac{h\, C_1\, D^{2/3}\, C_2\, p_o\, M}{1 + Cbr\, h_{f_g}}$$

or putting $F = (1 + Cbr\, h_{f_g})^{-1}$

$$\underline{m_c = h\, C\, r\, F} \qquad 5.4.10$$

Since h and C are constant, then for comparative purposes the relative evaporation rate is proportional to the product of two factors

1) Primary evaporation index, $r = D^{2/3}\, p_o\, M$ 5.4.11

2) A correction factor, $F = \frac{1}{(1 + Cbr\, h_{f_g})}$ 5.4.12

which lies in the range, $0 \leqslant F \leqslant 1$

To test the above theory, predictions were made for a range of alcohols which included the research solvent, MIBC. The relevant properties of these solvents are listed in Table 5.1. The diffusion coefficient D, for solvent vapour through air, was calculated using the equation of Fuller et al equation 3.5.3. The constants in the Antoine equation were taken from Reid et al (40).

Relative evaporation rates, both the primary value r from equation 5.4.11 and the corrected value rF from equation 5.4.12, were calculated and are set out in Table 5.2. For comparison with these predictions of linear theory, two other sets of data are included. First an iterative method was used to solve Antoine's equation to give exact values of rF and θ. Second, published results from the Shell Liquid Film Evaporometer (29) have been listed. To facilitate the comparison each set of data has been normalised.

5.5 Comments on the Theory of the Relative Evaporation Rate

a) Table 5.2 shows that there is reasonable agreement between values of rF calculated by linear theory and by the Antoine equation. It is apparent that for volatile solvents evaporative cooling is significant and cannot be neglected. However, even at the volatile end of the range, the theory provides useful physical insight into those factors which influence the relative evaporation rate. The agreement between the present theory and results from the Shell Evaporometer is less good. One explanation of this discrepancy is that, because of heat leakages, the full wet bulb depression is not achieved in the evaporometer.

b) A limiting case is worthy of consideration. Table 5.1 shows that b is roughly constant, and therefore from equation 5.3.13

$$\left(\frac{dp}{dT}\right)_o \alpha\ p_o$$

For solvents of low volatility, p_o and h_{fg} are small, and the wet-bulb depression θ will approach zero. In the limit the correction factor F is unity, and for this case the equation for the relative

evaporation rate reduces to

$$m_c = hCr \qquad 5.5.1$$

c) Equation 5.4.10 shows m_c to be independent of h_{fg} and this will always be true when dp/dT is zero. The explanation is that the enthalpy of evaporation does not enter directly into equation 5.4.1 for the rate of evaporation, but enters via equation 5.4.7 for θ. The reduction in vapour pressure $(p_o - p_s)$ caused by evaporative cooling depends entirely upon the gradient of the vapour pressure curve dp/dT and when this is zero, p_s remains equal to p_o.

d) ~~For highly volatile solvent,~~ Where θ becomes relatively large and the ~~use of~~ equation 5.4.5 leads to significant errors. For such cases the actual non-linear equations must be solved, and a computer program was written to do this. This program will be described later.

e) Because of the non-linearity of the equations, the relative evaporation rates of solvents will change with temperature. This effect is probably significant and merits investigation in the future.

f) The error introduced into the analysis by making the approximation for the Antoine Equation (see equation 5.3.11) shown below:-

$$p = e^{\left(A - \frac{B}{T}\right)} \approx p_o \, e^{\frac{B\,\theta}{T_o^2}}$$

has the following explanation.

The exponent in Antoine's equation arises from the difference of two quantities, A and B/T, which are of approximately equal magnitude. Any small error made when approximating the term $\frac{B}{T}$ will lead to a significant error after exponentiation.

A diagramatic representation of wet-bulb theory

For a particular solvent, the dynamic balance between the energy flux q, to and from the evaporative surface, may be qualitatively illustrated on the type of diagram shown in Figures 5.1, a - c.

Let q_H = heat flux from bulk air

q_M = energy flux in evaporated solvent

At standard air flow conditions h and k_ρ are constants, and

$$q_H \alpha \theta$$

this proportionality is represented by the straight line on Figure 5.5.1. Assume that

$$q_M \alpha p_s$$

this relation is represented by the expontial curve on Figure 5.1. The point of intersection of these two curves

$$q_H = q_M$$

occurs when the surface takes on the wet-bulb temperature T_s.

The discrepancy due to linearisation of the Antoine equation is illustrated in Figure 5.1. It can be seen that both θ and q will be

underestimated by the linear theory, a trend which is confirmed by the data in Table 5.2.

This type of graph could prove useful in design to visualise the effects of changes in system variables. For example Figure 5.2 illustrates the effect on the wet-bulb depression of changing solvents. Figure 5.3 shows the effect of increasing the heat and mass transfer coefficients in the same proportion, say by an increase in Reynolds number. The designer might take advantage of the consequent increase in dryer performance either to evaporate more solvent with the same air temperature (q increased) or to evaporate the same quantity of solvent with a decreased air temperature (q constant).

Figure 5.4 is offered as a quantitive demonstration of this graphical technique. It shows the effect on q and θ of changing the air temperature while maintaining the air velocity constant. The data for this figure was obtained from Table 6.3

5.6 Theory of Constant-Rate Ink Drying

This section will be concerned with evaluating the effect of changes in air velocity and temperature on the rate of drying of a single solvent. The theory, which is based on the Chilton-Colburn analogy, is a development of that set out in Section 5.4.

Assuming fluid properties remain constant then the psychrometric ratio, equation 5.2.8 is itself a constant

$$\frac{k_\rho}{h} = \frac{1}{\rho C_p}\left(\frac{D}{\alpha}\right)^{2/3} = C_3 \qquad 5.6.1$$

The constant rate at which solvent evaporates from unit area of surface, m_c kg/m^{2}s, may be determined from

$$m_c = \frac{h\,\theta}{h_{fg}} \qquad 5.6.2$$

The effect of air velocity, V

It can be seen from the equation for the wet-bulb depression

$$\theta = \frac{k_\rho}{h}\ \rho_s\ h_{fg} \qquad 5.6.3$$

that when T_A is held constant, θ also remains constant. Thus the rate of evaporation is a function of the heat transfer coefficient h which can be obtained from a heat transfer correlation of the form

$$Nu = C_4\ Re^a\ Pr^{1/3}$$

or
$$h = C_4\ \frac{k}{L}\ Re^a\ Pr^{1/3} \qquad 5.6.4$$

where C_4 and a are constants, and L is a characteristic length scale.

The effect of air temperature, T_A

The effect of raising T_A is to raise T_s and p_s which will increase the evaporation rate. The change in T_s will be less than the change in T_A because θ must also increase to transfer the extra energy required for evaporation. This effect is qualitatively similar to that illustrated in Figure 5.4. The theory which follows derives the functional relation between θ and T_A.

Let T_s = surface temperature

p_s = saturated vapour pressure at T_s

Treating the vapour as a perfect gas

$$\rho_s = \frac{p_s M}{R T_s} = C_5 \frac{p_s}{T_s} \quad \text{where } C_5 = \frac{M}{R}$$

and making the approximation that $T_A \approx T_s$

$$\rho_s = C_5 \frac{p_s}{T_A} \qquad 5.6.5$$

using the linear relation between vapour pressure and temperature, equation 5.3.12

$$p_s = p_A (1 - b\theta) \qquad 5.6.6$$

where $p_A = e^{A - B/T_A}$

$$b = \frac{B}{T_A^2}$$

Let θ = wet bulb depression corresponding to T_A

$$\theta = \frac{k_\rho}{h} \rho_s h_{fg}$$

$$= C_3 \frac{C_5 p_A (1 - b\theta) h_{fg}}{T_A}$$

$$= \theta' (1 - b\theta) \qquad 5.6.7a$$

where $\theta' = C_3 C_5 p_A h_{fg}/T_A$

θ' is the hypothetical value of θ with $\rho_s = \frac{M P_A}{R T_A}$

$$\underline{\theta = F' \theta'} \qquad 5.6.7b$$

$$F' = \text{correction factor} = \frac{1}{1 + b\theta'} \qquad 5.6.8$$

F' lies in the range, $0 < F' < 1$

Constant rate drying time t_c

From equation 5.6.2

$$m_c = \frac{h\ \theta}{h_{fg}}$$

substituting equations 5.6.4 and 5.6.7

$$m_c = \frac{C_4\ k\ Re^a\ Pr^b\ F'\ \theta'}{L\ h_{fg}} \qquad 5.6.9$$

Let m_o = initial mass of solvent, kg/m^2

m_c = constant drying (evaporation) rate, $kg/m^2\ s$

The hypothetical constant rate drying time t_c (see section 4.4) is defined by the equation

$$t_c = \frac{m_o}{m_c} \qquad 5.6.10$$

substituting equation 5.6.9 in 5.6.10

$$t_c = \frac{m_o\ L\ h_{fg}}{C_4\ k\ Re^a\ Pr^b} \quad \frac{(1 + b\theta')}{\theta'} \qquad 5.6.11$$

where $\theta' = \dfrac{C_3\ C_5\ h_{fg}\ e^{A-B/T_A}}{T_A}$ 5.6.12

$$b = \frac{B}{T_A^{\,2}} \qquad 5.6.13$$

Although approximate in nature, equation 5.6.11, demonstrates the manner in which the physical variables affect the drying time t_c. It shows that the effect of air velocity V and air temperature T_A can be treated separately.

For constant T_A

$$t_c \propto \frac{1}{V^a}$$

For constant V

$$t_c \propto \frac{1}{\theta}$$

Equation 5.6.11 is also useful when a comparative estimate is required. Although apparently complex, when assessing changes for a single solvent, the constants C_3 and C_5 need be calculated only once. Then, for a particular value of T_A, the value of θ can be estimated on a pocket calculator without the need for iteration. To illustrate the method and to check its accuracy the calculation for the research solvent MIBC, is shown below.

$$p_A = e^{27.996 - 6544/T_A}$$

$$b = 6544/T_A^2$$

$$h_{fg} = 427{,}000$$

$$C_3 = \frac{1}{\rho C_p}\left(\frac{D}{\alpha}\right)^{2/3} = 4.006 \quad 10^{-4}$$

$$C_5 = \frac{M}{R} = 1.234 \quad 10^{-2}$$

$$C_3\, C_5\, h_{fg} = 2.113$$

TABLE 5.3

T_A (c)	20	40	60
p_A	287.6	1198	4206
b	0.0762	0.0668	0.059
θ'	2.074	8.09	26.69
F'	0.86	0.649	0.389
θ (equn 5.6.7)	1.76	5.25	10.36
θ (iterative caln)	1.8	5.8	13.4

From equations 5.3.4 and 5.3.7

$$\frac{dp}{dT} = \frac{Bp}{T^2} \qquad 5.6.14$$

Calculations show that because p rises exponentially with T, the magnitude of dp/dT increases with T. For reasons which have already been discussed in Section 5.5, the accuracy of predictions based on equation 5.6.7 will decrease as dp/dT increases. This trend is manifest in Table 5.3 above. Even so, an error of 30% in the largest value of θ, is probably acceptable in a first estimate.

In addition this linearised theory offers an approximate, but relatively quick method of modifying the relative evaporation rate for the effects of temperature changes.

5.7 Computer Program for Constant-Rate Drying

Based on the theory developed in this chapter a computer program was written to predict the hypothetical constant-rate drying time t_c for various combinations of air temperature and air velocity. In the program the approximations necessary for an analytic solution are avoided, the real non-linear equations being solved by iteration.

The first program will not be described at this point because its predictions, although qualitatively good, did not agree closely with experiment. It was apparent that the experimental technique was capable of further refinement, but more importantly, that the empirical data used as input to the program required detailed checking. An account of the work undertaken to reduce the discrepancy between theory and experiment, and a detailed description of the latest computer program is given in the next chapter.

5.8 Application of Constant-Rate Theory to Dryer Design

The theory developed in this chapter applies equally whether the inked web is moving or stationary. The primary objective of the designer is to calculate the length of the dryer. Drying time and distance moved by the web are related by the definition of webspeed, u

$$u = \frac{dx}{dt} \qquad 5.8.1$$

For a given web speed this equivalence can be used in two ways:

a) The total distance travelled by the web in its passage through the dryer can be divided into a large number of small discrete steps. The heat and mass transfer equations may be recast in

finite difference form (see Section 6.7). These equations can then be used to predict transient changes of ink temperature and solvent content as the web encounters a variable drying environment in its passage through the dryer. A computer program to carry out this type of calculation for a single nozzle is given in Section 7.5.

b) It is probably sufficiently accurate to assume that, for an array of nozzles, the space averaged value of the heat transfer coefficient, $\bar{h}$, can be used as a basis for dryer design. With this assumption the evaporation rate can be considered constant and the dryer length L evaluated from

$$L = u.\ t_c \qquad 5.8.2$$

Accordingly, as a separate part of this research effort, a computer program was written to evaluate $\bar{h}$ for slot nozzles. The input to the program is the space wise distribution of heat transfer coefficient under a nozzle as a function of air velocity and nozzle geometry. This program is used as a sub-routine to the main program. Specifying Reynolds number, Z/B, nozzle pitch etc. to the sub-routine will cause it to respond with $\bar{h}$, for use in the main program. The output from the main program is drying time, dryer length, number of nozzles, etc.

Such a program has been successfully developed. However, as the principal difference between this program and the program set out in Appendix 1, is the sub-routine for $\bar{h}$, it was decided to include here neither the program nor the results from it.

TABLE 5.1

Physical Property Data for a Range of Alcohols

Properties evaluated at a temperature of 20 C.

Diffusion coefficient calculated using equation of Fuller et al (16).

Vapour pressure data from Reid et al (33).

Alcohol	M	D $m^2/s.10^5$	M $D^{2/3}$ $m^2/s.10^{-2}$	p_o b at 20 C	h_{fg} $J/kg.10^{-6}$	Δh_v $J/kg\text{-}mol.10^{-6}$	b
methyl	32.03	1.638	2.067	0.1266	1.101	35.265	0.0494
ethyl	46.05	1.249	2.481	0.0586	0.854	39.326	0.0551
isopropyl	60.6	1.043	2.895	0.0440	0.665	40.299	0.05646
n propyl	60.6	1.043	2.895	0.0193	0.686	41.571	0.0582
sec butyl	74.08	0.909	3.229	0.0150	0.561	41.558	0.05822
iso butyl	74.08	0.909	3.229	0.0117	0.578	42.818	0.06
n butyl	74.08	0.909	3.229	0.0057	0.590	43.707	0.06123
MIBC $C_6 H_{13} OH$	102.11	0.72	3.810	0.00288	0.427	43.602	0.0611

TABLE 5.2

Alcohol	$r = M D^{2/3} p_o$		F	r F		Using Antoine equation r F			Shell Evaporometer	
	Actual	MIBC = 1		Actual	MIBC = 1	Actual	MIBC = 1	θ	n-butyl acetate = 1	MIBC = 1
methyl	261.7	23.9	0.1361	35.6	3.7	56.3	5.8	28.0	4.1	13.6
ethyl	145.4	13.3	0.2469	35.8	3.4				2.4	8.0
isopropyl	127.3	11.6	0.319	40.6	4.2	50.9	5.3	15.0	2.2	7.3
n propyl	55.8	5.1	0.501	30.0	3.1	29.3	3.0	9.0	1.2	4.0
sec butyl	48.4	4.4	0.586	28.4	2.9				1.1	3.7
isobutyl	37.8	3.4	0.633	23.9	2.5				0.85	2.8
n butyl	18.4	1.7	0.771	14.2	1.5				0.46	1.5
MIBC $C_{16} H_{13}OH$	11.0	1.0	0.886	9.7	1.0	9.7	1.0	2.0	0.30	1.0

$C = C_1 C_2 = 4.462.10^{-7}$

Relative Evaporation Rates for a Range of Alcohols

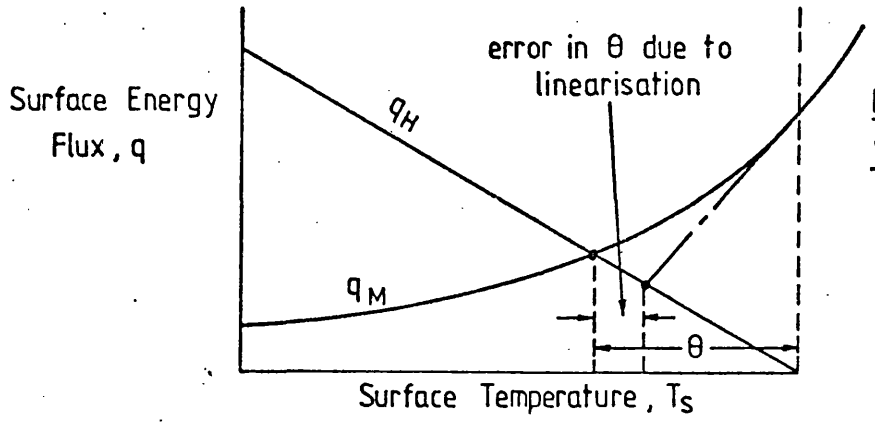

FIGURE 5.1.
WET-BULB DEPRESSION θ

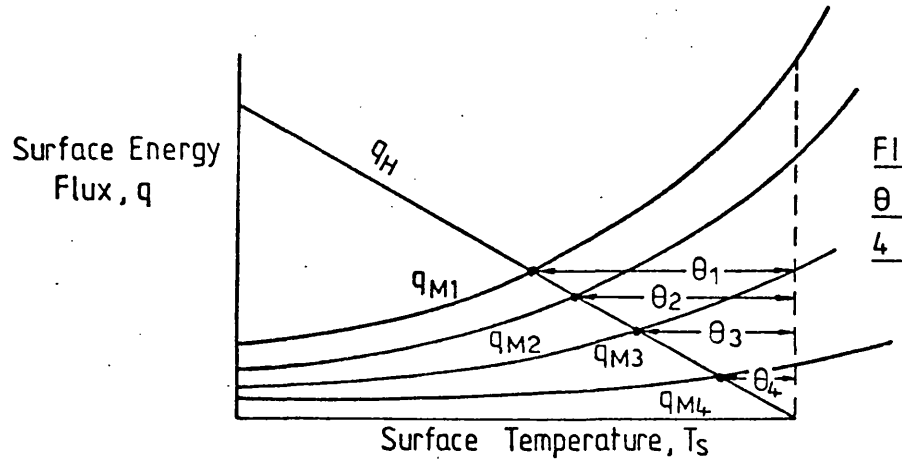

FIGURE 5.2.
θ FOR A RANGE OF
4 SOLVENTS

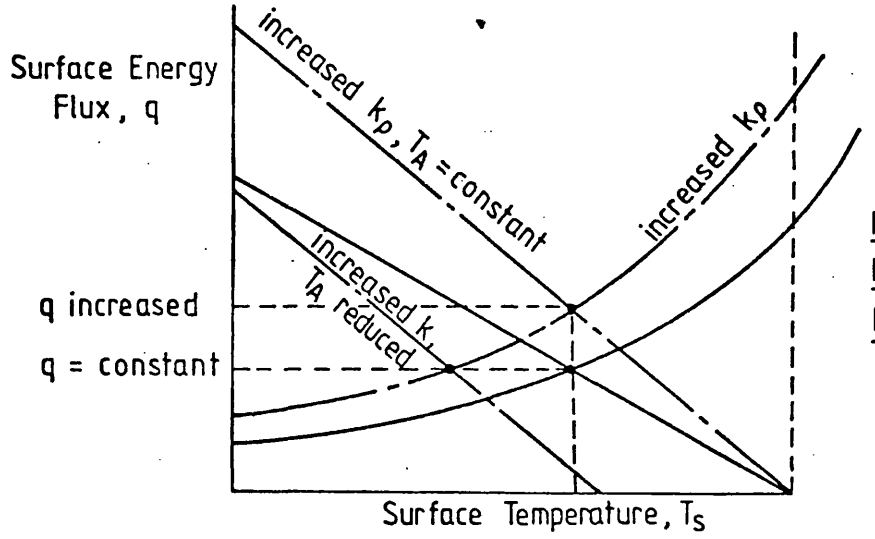

FIGURE 5.3.
EFFECT OF INCREASING
h AND k_ρ

q_H = heat flux from air to surface = $h(T_A - T_S)$

q_M = energy flux from surface = $k_\rho \rho_s h_{fg}$

FIGURE 5.4. THE EFFECT OF CHANGING AIR TEMPERATURE ON THE WET- BULB EQUILIBRIUM POINT.

Air velocity = 20 m/s (constant)

Data extracted from Table 6.3.

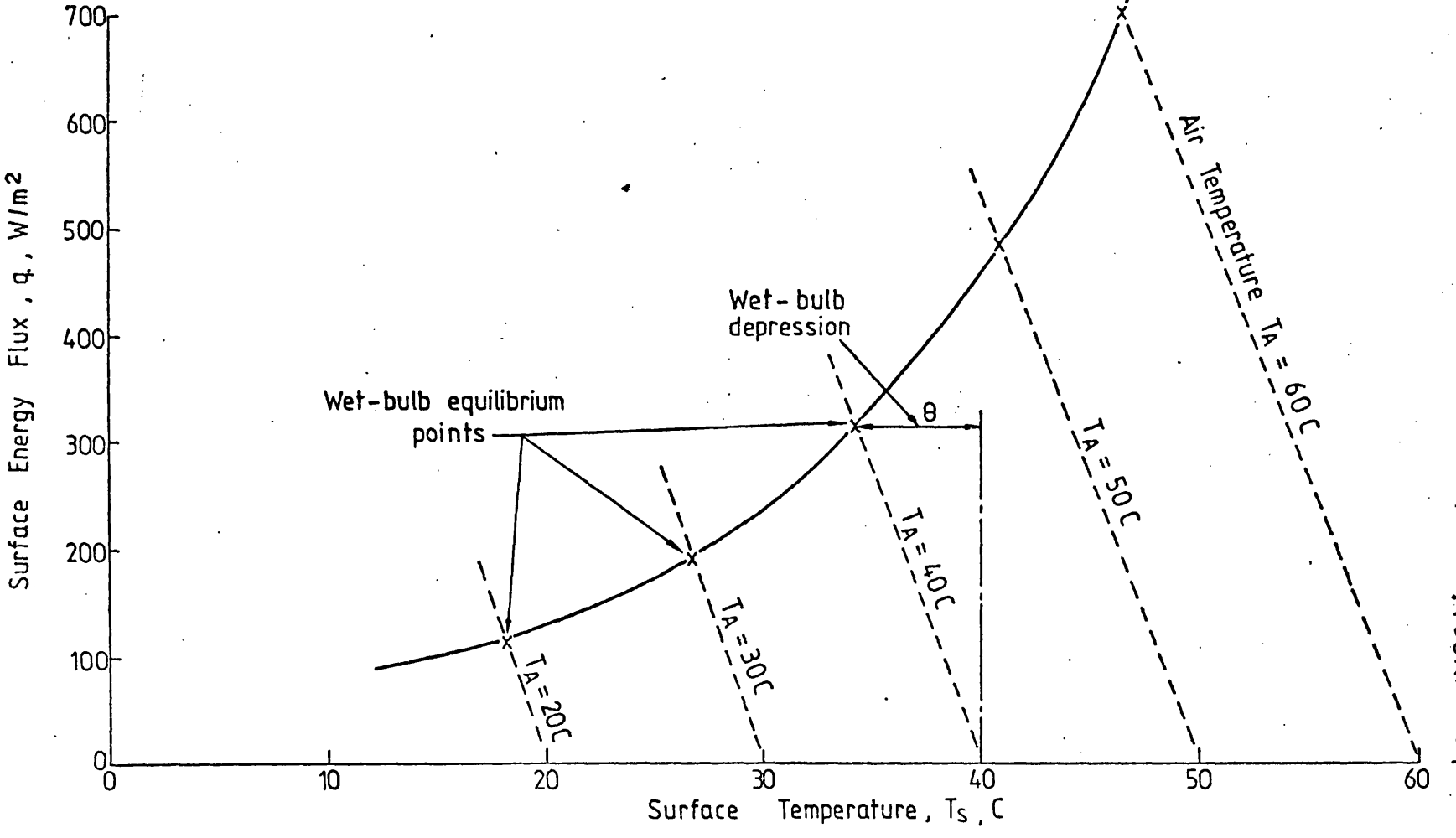

FIGURE 5.4

6. EXTERNALLY CONTROLLED DRYING I

EXPERIMENTAL REFINEMENTS LEADING TO COMPUTER PROGRAM

6.1 Introduction

The experimental technique and some early IR drying curves were described in Chapter 4 as background to the theory which followed. Numerical calculations showed that drying times predicted from theory appeared to be about 50% shorter than the experimental values. In an effort to locate, and if possible to eliminate this discrepancy, the theory, the experimental technique and the physical data were all subjected to critical appraisal.

These detailed checks showed that there was a calibration error in a commercial heat flux meter; also that refinements in the IR Technique were possible. This chapter begins with an account of this development work, which was spread over a period of approximately one year. Because different aspects of the work were being examined at the same time, the account is not in chronological order. By eliminating errors, the agreement between theory and experiment was significantly improved. The degree of agreement which was achieved is demonstrated later in this chapter. It is worth remarking, that although refinements to it were made, the experimental technique remained essentially unchanged from that described in Chapter 4.

Once the validity of the research technique had been established, further drying tests were carried out to extend the range of the constant-rate experiments described in Section 4.5. Experimental values of the constant rate drying time t_c were compared with those predicted by means of a computer program. These comparisons showed that the agreement between theory and experimental was reasonably good.

6.2 Vapour Pressure Data for MIBC (4 methyl pentan-2-ol)

In the early stages of this research little data could be found on the vapour pressure of 4 methyl pentan-2-ol. Initially, only two sources of data were located, Chatfield (41) and Durrans (42). These two sources agreed closely, only at one state point:-

i) Temperature, 20 C: Vapour pressure, 2.2 mm Hg (293.3 N/m^2).
However to evaluate the constants in equation 5.3.6

$$\ln p = A - B/T$$

the vapour pressure must be known at two temperatures. In the absence of further data, the chart method of Cox (43) was used to estimate the vapour pressure at a second point:-

ii) Temperature, 127 C: Vapour pressure, 32,410 N/m^2.
Sometime later, when checking the entire method for inconsistances, a further search in the sparse literature was made and two further references, Hovorka et al (44) and Monick (45) were found. Both of these sources gave higher values of vapour pressure than those assumed above. This was unexpected as the adoption of these higher vapour pressures would make worse the discrepancy between theory and experiment.

While the literature search to locate reliable vapour pressure data was proceeding, it was decided to try and determine this information by experiment. To do this a standard Ramsay-Young apparatus was used, which was available in the University Chemistry Laboratory. The basis of this method, is that the solvent boils at a sub-atmospheric pressure in an evacuated vessel. At the beginning of the experiment the

pressure is lowered to its minimum value and solvent temperature and corresponding vapour pressure are noted. Vapour pressure and temperature were recorded at five other points, as the pressure was allowed to rise from its lowest to its highest value.

At about the same time, the suppliers of the solvent, The Shell Company, were contacted. It was learned that Shell had in fact determined the properties of MIBC and that this information was contained in their Technical Data Sheet (46). Examination of this Data Sheet confirmed that the vapour pressure of 2.2 mm Hg at 20 C was correct, but indicated that the Cox chart method led to erroneous results. Shell's technical representative stated, that at such low vapour pressures, the presence of even small quantities of impurities, could lead to discrepancies between published data from different sources. Traces of impurity could arise when, what was nominally the same solvent, was supplied by different manufacturers.

The vapour pressure data from all of the above sources, including the Ramsay-Young apparatus, is plotted in Figure 6.1. It can be seen that the experimental results from the Ramsay-Young apparatus are in good agreement with the technical data supplied by the Shell Company. In addition both these sets of data, agree with the 20 C point previously quoted from references (41) and (42). In view of these agreements, it was decided that the Shell Company's data could be used to calculate the constants in the Antoine equation. The following two state points, one at either end of the test range, were selected for this purpose.

i) Temperature 20 C, Vapour pressure = 2.2 mm Hg (293.3 N/m^2)

ii) Temperature 91 C, Vapour pressure = 165.5 mm Hg (22,059 N/m^2)

From these two data points, the following vapour equation was derived

$$\ln p = 27.996 - \frac{6544}{T} \qquad 6.2.1$$

This equation is also shown in Figure 6.1 and it can be seen that it gives a good representation of the accepted data over the entire working range. Equation 6.2.1 was incorporated in the constant-rate computer program.

6.3 Experimental Heat Transfer Coefficients

A theoretical analysis of the impingement region was not attempted because, at the small nozzle/plate distances used in practice, theories of turbulence were not well developed. Instead heat transfer coefficients were measured experimentally using small flux meters of the type originally invented by Gardon (47); shown diagrammatically in Figure 6.2a. When positioned in a heated surface as shown in Figure 6.2b, the meter develops a small emf which is proportional to the heat flux from the cooled foil. For further details see Hardisty (5).

Considerable difficulties were experienced when attempts were made to manufacture Gardon meters in the University. Because of their small size and because the copper body acted as a heat sink it proved almost impossible to achieve a satisfactory weld between the constantan foil and the rim of the copper body. To circumvent this difficult problem a Gardon meter was purchased from a manufacturer (Medthern Corp.) in the USA, Figure 6.2c. Because this transducer was supplied with a calibration chart certified by the National Bureau of Standards this appeared to represent a considerable saving in effort. Later events were to show this optimism was misplaced.

In the early stages of the heat transfer work, the Gardon probes were positioned in a thick aluminium plate which was heated by an electric resistance heater placed behind it. With this arrangement, the following method was used to calibrate the flux meters. Under steady-conditions, the measured power supplied to the heater E, allows the average value of the heat transfer coefficient $\bar{h}$, to be calculated from

$$E = \bar{h} A (T_S - T_A) + Q_L \qquad 6.3.1$$

A = heated surface area, m^2

T_S = surface temperature, C

T_A = ambient air temperature, C

Q_L = heat loss, W

The plate and meter were then traversed under the jet while the flux meter output was recorded on an X-Y recorder. Figure 6.3 shows the record of three tests carried out at a constant jet Reynolds number, but at three different surface temperatures. The average value of probe output during the traverse $\bar{e}$ may be determined from the average height of the curves in Figure 6.3. The meter calibration factor K then follows from

$$K = \bar{q}/\bar{e} \quad W/m^2 \; V \qquad 6.3.2$$

where $\bar{q}$ = average heat flux (E/A)

From the calibration certificate supplied with the proprietry flux meter

$$1 \text{ mV} \equiv 6{,}320 \text{ w/m}^2 \qquad 6.3.3$$

or $K = 6.32.10^3 \text{ w/m}^2 \text{ mV}$

When this meter was calibrated at Bath, almost as a formality, a value of K almost double the above figure was determined. The following test data, illustrates this discrepancy.

TABLE 6.1

Re = 11,000 B = 3.4 mm (Z/B = 8)

	$\bar{h}$ from plate power			$\bar{h}'$ from flux meter			
Surface Temp T_s(C)	E (W)	Q_L (W)	$\bar{h}$ (W/m^2 K)	$\bar{e}$ (mV)	$\bar{q} = K\bar{e}$ (W/m^2)	$\bar{h}'$ (W/m^2 K)	$\bar{h}/\bar{h}'$
100	533.2	50.0	207	1.39	8823	117	1.77
60	307.2	16.8	266	.68	4341	124	2.15
50	169.2	20.0	192	.44	2793	112	1.71
					average ratio =		1.88

$A = 0.03108, \text{ m}^2$

$T_A = 25, \text{ C}$

$\bar{h} = (E - Q_L)/(T_s - T_A)A$

$K = 6.32.10^3 \text{ w/m}^2 \text{ mV}$

$\bar{h}' = \bar{q}/(T_s - T_A)$

Faced with such a wide discrepancy in the value of K, it was vital to carry out a more accurate calibration. The electrical method of heating the heat transfer is convenient, but significant temperature differences occur in the aluminium plate during a traverse. To avoid

this fault it was decided to build a new calibration apparatus in which the surface is heated by saturated steam. This apparatus and the method of calibration are described in Appendix 1. A number of careful calibration tests served to confirm the numerical value of 1.8 for the ratio $\bar{h}/h'$ of Table 6.1

Heat transfer data obtained at Bath for a single-slot-nozzle agree generally with the data of Gardon and Akfirat (48). This agreement is demonstrated in the comparative calculation carried out in Appendix 1. Gardon and Akfirat's data is represented by the correlation

$$Nu_o = 1.2\ Re_E^{0.58}\ (Z/B)^{-0.62} \qquad 6.3.4$$

where $Nu_o = h_o B/k$ and $Re_E = V_E B\rho/\mu$

h_o = stagnation point heat transfer coefficient, w/m^2 K

V_E = air velocity at nozzle outlet, m/s

B = width of slot nozzle, m

Z = height of slot above surface, m.

Because, at the time, these doubts about the calibration had not been resolved, computer predictions for Hardsity (7) were based upon equation 6.3.4.

It is gratifying to note that Medtherm eventually confirmed the accuracy of the Bath calibration. Their explanation of the error in their certificate of calibration was that, without declaring it, they had changed the type of transducer from a Gardon to a "Schmidt-Boelter", Figure 6.2d. Both transducers are externally identical. Factory calibration of the Schmidt-Boelter gauge had been carried out with the

sensor absorbing heat. However in the Bath research the sensor is losing heat and this difference in the direction of the heat flux was the source of the error. The Medtherm Company agreed that it was necessary to correct their original value of K, equation 6.3.3, by multiplying it by a factor of 1.8.

It is also worth noting that, after a period of development work, a method of manufacturing Gardon Type flux meters in the University was successfully evolved. In the process of this work the probe was completely re-designed and the problem of welding the constanton foil to the copper body was successfully overcome, Miller and Godoy (49).

Lateral variation of heat transfer coefficient

It will be recalled that the IR measuring point is a distance of 10 cm from the centre line of the nozzle, Figure 4.3. The heat transfer coefficient at this point, h_x, may be determined from a correlation such as equation 6.3.4 if the ratio h_x/h_o is known. At first, by extrapolating Gardon's data, this ratio was estimated to be 1/5. Later this ratio was measured experimentally and the results of a series of tests to do this are shown in Figure 6.4.

Two points are worth making about these experimental results. First, tests have shown that the heat transfer distribution under a slot jet depends upon the shape of the nozzle which produces the jet. The data in Figure 6.4 was obtained from the actual slot nozzle used in the drying tests. It can be seen from Figure 6.4 that the ratio V_x/V_o (identical with h_x/h_o) is in reasonable agreement with the estimated value of 1/5 and this later value was retained in the computer program. Secondly, the stagnation point heat transfer data of Figure 6.4 is in good agreement (±2%) with equation 6.3.4.

6.4 Secondary Effects on Heat and Mass Transfer

The effect of mass transfer on the heat transfer coefficient was analysed in Section 3.8. Equation 3.8.8 expressed this effect in terms of the parameter R

$$\gamma = \frac{\ln(1 + R)}{R} \qquad 6.4.1$$

where $R = \frac{(C_p\ \theta)}{h_{f_g}}$

$$\gamma = \frac{h}{h_o}$$

For the solvent vapour/air system

$$C_p = 1{,}005 \text{ J/kg K}$$

$$h_{f_g} = 427{,}000 \text{ J/kg K}$$

Research has shown that the wet-bulb depression, θ, lies in the range 2 - 13 C (see later computer results). Even with the extreme value of θ(13 C)

$$R = 3.06.10^{-2}$$

And since for small values of R

$$\ln(1 + R) \approx R$$

it is seen that γ will have a value close to unity (0.985).

It is concluded that, for 4 methyl 2 pentanol in this research, the

above effect on the heat transfer coefficient is within the margin of experimental error and can be neglected.

The following form of the mass transfer rate equation was used in the computer program (equation 3.6.4)

$$m = k_\rho(\rho_s - \rho_A) \qquad 6.4.2$$

m = mass transfer flux, kg/m^2 s

k_ρ = mass transfer coefficient, m/s

ρ = mass concentration (density) kg/m^3

To calculate the mass transfer coefficient from the empirically determined value of the heat transfer coefficient, the Chilton-Colburn analogy was used. This calculation will yield k_ρ^o, the mass transfer coefficient in the absence of bulk flow (equation 5.2.7b)

$$\frac{h}{k_\rho^o} = \rho\, C_p \left(\frac{Sc}{Pr}\right)^{2/3} \qquad 6.4.3$$

Because equation 6.4.2 is applied to mass transfer across a boundary layer then the effect of bulk flow (see Section 3.8) must be allowed for. Starting from equation 3.8.3.

$$k_c = k_c^o \quad \frac{C}{\bar{C}_B}$$

and noting that

$$k_c \equiv k_\rho \quad \text{(equation 3.6.5)}$$

$$c = \frac{P}{RT}$$

then $k_\rho = k_\rho^o \frac{p}{\bar{p}_B}$ 6.4.4

where p = atmos pressure

$\bar{p}_B$ = log mean pressure of air in boundary layer

By definition

$$\bar{p}_B = \frac{P_{B2} - P_{B1}}{\ln (P_{B2}/P_{B1})} \qquad 6.4.5$$

For this research the solvent concentration at the outer edge of the boundary layer is zero and $p_{B2} = p$. Thus

$$\bar{p}_B = \frac{P_{A1}}{\ln \left(\frac{P}{P - P_{A1}}\right)} \qquad 6.4.6$$

p_{A1} = saturated vapour pressure at surface.

Finally substituting equation 6.4.4 into equation 6.4.3

$$k_\rho = h \frac{p}{\bar{p}_B} \frac{Le^{-2/3}}{\rho C_p} \qquad 6.4.7$$

In the program equation 6.4.7 was used to calculate both k_ρ and the psychrometric ratio h/k_ρ.

6.5 Refinements in Experimental Technique

Infragauge response time

The early portion of the IR drying curve is unreal because the Infragauge cannot respond quickly enough to a step change in solvent, Figure 4.4. Because this is perhaps the least satisfactory aspect of the experimental technique an attempt was made to eradicate it. Tests to measure the time constant of the system soon showed that the delay was in the electronic integrating circuits within the Infragauge control unit. Discussions with the manufacturer confirmed that this was an inherent characteristic of these circuits and could not be eliminated. Minor electronic adjustments were made, before finally setting the overall time constant of the instrument to 1.1 second. This was the lowest value which would permit stable operation.

The initial steeply rising part of the IR curve can be eliminated if the experimental technique is modified in the following ways. Before starting the time base on the X-Y recorder, printed web is fed continuously through the IR beam for a sufficient time for the Infragauge output to rise to its maximum value. When this has been attained the web is brought to rest and simultaneously the time base of the recorder is started. Drying curves obtained by this modified technique are shown in Figure 6.5.

The results for band 1 (the thinnest ink film) show that the initial transient has been entirely eliminated and that the early portion of the drying curve is virtually a straight line. This is a valuable experimental demonstration of constant-rate drying. In spite of this success in band 1 this modified technique was not persevered with for the following reasons:-

a) The web could not be stopped suddenly without the risk of jerking it.

b) Continuous running wastes materials.

c) It is only worthwhile on band 1. On the thicker bands of ink, the true maximum voltage is never registered because the sensitivity of the Infragauge is saturated (see Section 4.2). Tests were normally run on band 3 because this produced measurable drying times at practical values of air velocity and temperature.

During constant-rate drying the graph of ink solvent content against time may be represented as a descending ramp function.

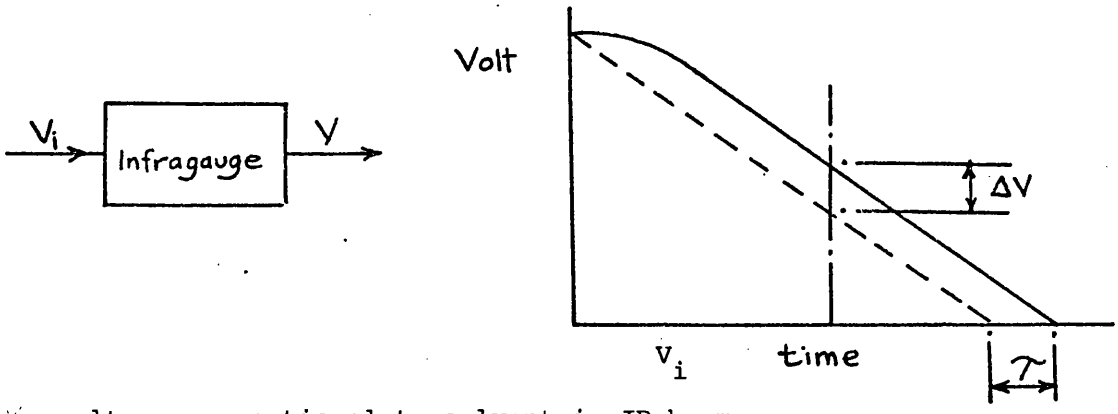

v_1 = voltage proportional to solvent in IR beam

V = Infragauge output voltage

Because the origin of the time delay resides in resistance and capacity of the electrical circuit, the response of the system is first order, and may be represented by the following differential equation

$$V + \tau \frac{dV}{dt} = V_i$$

τ = time constant

When V_i is a ramp function

$$v_i = V_o - Kt$$

and after the initial transient

$$V = V_i + \Delta V \quad \text{and} \quad \frac{dV}{dt} = -K.$$

Substitution into the original differential equation gives

$$\Delta V = \tau K$$

The Infragauge voltage will lag behind the "true" voltage V_i by one time constant. Accordingly, values of ${}_1t_c$ estimated by extrapolating the IR curves, were reduced by one time constant (1.1 second) before comparing them with theoretical predictions.

Web Support

Originally, the plastic web rested on a thick aluminium plate which both provided support for the web and scattered radiation back to the IR detector. This arrangement can be criticised on the grounds that conduction of heat from plastic to aluminium is possible. To counter this criticism, the web was supported on a smooth wooden track. At the IR scanning point a shallow recess was cut across the track parallel to the slot nozzle and a reflector plate fitted flat to the bottom of it, Figure 4.3. With the web clear of the aluminium conduction from the under side of the web is largely eliminated.

At this time, a closely fitting cover was fitted over the web to prevent solvent evaporation from the web on its transit from the printing press to the IR measuring point.

Adjustments of Infragauge

To eliminate direct reflection from ink to IR detector the Infragauge head is tilted at an angle of 20 degrees from the vertical, Figure 4.3. It is difficult to maintain this angle exactly when, for instance, the head is moved to scan another ink band. Small changes in head angle in turn cause changes in instrumental gain. In spite of exercising care in lining up the head, it was not possible entirely to eliminate this source of discrepancy. In addition it proved difficult to detect changes in instrumental gain which occurred fortuitously over a period of time.

6.6 The Effect of Dissolved Resin on Drying Rate

The effect of a dissolved solute is to modify the vapour pressure, and hence the evaporation rate, of the solvent. In an ideal solution, which obeys Raoult's Law, the solvent vapour pressure is reduced in direct proportion to the mole fraction of the solute. Solvent evaporation from an ideal solution would be accompanied by a progressive lowering of solvent vapour pressure; the evaporation rate, although externally controlled, is then no longer constant, but diminishes with time. The drying curve is modified from the straight line characteristic of evaporation from a porous solid to that of a decaying exponential.

Inspection of the experimental drying curves (see band 1, Figure 6.5) showed that the behaviour characteristic of an ideal solution did not

occur and that the early portions of these curves were almost straight. In fact when the solute is a high polymer, the above simple ideal behaviour should not be expected. In addition to non-ideal effects, there are two further points which may influence the behaviour of the real solution:-

i) The resin may not be completely dissolved, but may be present as a swollen gel

ii) Because the molecular weight of the solvent is extremely large, the mol fraction of the solvent will remain approximately constant even though quite large changes of mass fraction take place.

In spite of discussions with the ink-maker, the supplier of the resin and academic colleagues, no definite explanation of the behaviour of the real ink system has been arrived at. This point is discussed in greater detail in Appendix 2. An associated point, also commented upon in Appendix 2, is the modification of the evaporation rate, caused by blending the solvent with other solvents.

Because of the complexity of its molecules, it is not possible to make theoretical predictions of the effect of the resin on the evaporation rate of the pure solvent. However the difference in drying rate between ink and pure solvent can be determined empirically as follows. A series of drying curves were first determined for pure solvent, Figure 6.6. When the "printing" of the pure solvent was first contemplated, it was though that the difficulty of wetting the plastic would prevent the application of a coating. However, these apprehensions proved to be ill-founded, when practical trials showed

that pure solvent could be successfully printed. Figure 6.6 shows drying curves for pure solvent, and it is clear that the early stage of drying does indeed take place at constant-rate.

Immediately following the runs on pure solvent, and for identical test conditions, drying curves were recorded for the research ink, Figure 6.7. The constant-rate slopes from Figures 6.6 and 6.7 are compared in Table 6.2 below.

TABLE 6.2

Air Velocity m/s	Constant-rate Slope		Ratio of Slopes
	Pure Solvent	Ink	
20	0.82	.68	1.2
30	1.17	.96	1.2
40	1.45	1.2	1.21
50	1.66	1.39	1.19

The data in Table 6.2 shows that pure solvent dries more quickly than ink by a factor of 1.2. Other similar comparisons have shown this factor to lie in the range 1.2 to 1.4 and an average value of it was taken as 1.3. Accordingly, in the computer program which is described in the next section, theoretical constant-rate drying times for pure solvent were divided by 1.3 to predict to ink drying times.

6.7 Computer Program to Predict Time of Externally Controlled Drying

When freshly printed ink at ambient temperature is suddenly brought to rest in the drying environment of a wall jet, initially the temperature rises. The Biot number (Bi) may be calculated for the plastic substrate from the following data

$h = 100\ w/m^2\ C$

$L\ (thickness) = 25.10^{-6}\ m$

$k = 0.2\ w/m^2\ C$

$$Bi = \frac{hL}{k} = \frac{100.25}{0.2.10^6} = 0.0125$$

It can be seen that with such thin films, the Biot number is low and consequently a lumped parameter analysis is permissable. A separate experimental investigation, Wheeler and Mulervy (50), has confirmed the validity of this reasoning. Thus a single temperature T_s is used to designate the ink/substrate system.

During a short time interval Δt, an energy balance may be written for unit surface area as follows

$$h(T_A - T_s) = k_\rho\ (\rho_s - \rho_A)\ hf_g + \frac{(\Delta T_s \Sigma\ m\ C_p)}{\Delta t} \qquad 6.7.1$$

where, $\Sigma\ m\ C_p$ = heat capacity of plastic, ink and solvent, J/K

subscript A refers to drying air

This equation is identical with equation 5.2.1 except for the introduction of the last term to represent the initial transient. Equation 6.7.1 may be reformulated as a finite difference equation for ΔT_s.

With the boundary condition, $\rho_A = 0$

Let $\Delta m = k_\rho \rho_s \Delta t$ 6.7.2

$$Q_H = h(T_A - T_s) \Delta t \quad 6.7.3$$

$$Q_D = \Delta m \, h_{fg} \quad 6.7.4$$

$$\Delta T_s = \frac{Q_H - Q_D}{\Sigma \, m \, C_p} \quad 6.7.5$$

Using the theory and data presented in the earlier section of this Chapter, and based upon equations 6.7.1 - 5 above, a computer program was written to predict drying time. The flow chart for this program is shown in Figure 6.7 and the program itself is set out in Appendix 3.

For purposes of calculation the total drying time was split into two periods.

i) The initial adjustment period, t_1

During this period the system temperature T_s changes from the ambient temperature T_A, to the wet-bulb temperature T_{WB}. The time t_1 taken up by this transient is the sum of a number of discrete time steps each one based on the finite difference equations 6.7.2 - 5

$$t_1 = \Sigma \Delta t \quad 6.7.6$$

The period ends when the change in system temperature ΔT_s is less than a prescribed value (0.1 C).

ii) The constant-rate period, t_c

In this program, it is assumed that there is no falling-rate period. It is further assumed that the second period of drying continues at a constant rate until all of the solvent is evaporated. It should be noted that in practice the second period of drying would end at the critical point. Because it is a theoretical concept t_c is called the hypothetical constant-rate drying time.

A finite difference solution is not required in the second period as the system temperature remains constant at the wet-bulb value.

Let $\Sigma \Delta m$ = solvent evaporated in first period

m_o = initial solvent deposit

m_2 = solvent evaporated in second period

$$m_2 = m_o - \Sigma \Delta m \qquad 6.7.6$$

$$Q_2 = m_2 h_{fg} \qquad 6.7.7$$

$$q_2 = h \theta \qquad 6.7.8$$

θ is the wet-bulb depression which may be calculated from the known value of the psychrometric ratio

$$t_c = \frac{Q_2}{q_2} \qquad 6.7.9$$

The total drying time t is given by

$$_1t_c = t_1 + t_c \qquad 6.7.10$$

The hypothetical time, $_1t_c$, is a measure of the drying period which is controlled by the condition of the external air. $_1t_c$ may be estimated graphically from the experimental drying curves (see section 4.5) and compared with predictions from the computer program.

A typical matrix of outputs from the program is shown in Table 6.3. To illustrate the effects of air velocity and temperature, values of $_1t_c$ from Table 6.3 are shown graphically in Figure 6.9.

6.8 IR Drying Curves - Comparison of Theory and Experiment

To provide a background for the description of the experimental method, an early series of drying curves was presented in Section 4.5. Drying curves from a later test series, to extend and complement the earlier research, are now presented. As far as possible, consistency of test method has been maintained between both series of tests.

Figure 6.10, shows the effect of changing the jet velocity V_E, the jet temperature being maintained constant throughout. To complement the curves already presented in Figure 4.8, the air temperature at the IR measuring point T_A was raised to the maximum value consistent with safe operation of the inlet ducting and nozzle box.

Figure 6.11, shows the effect of changing the air temperature T_A, while maintaining the air velocity V_E constant. The air velocity of 60 m/s in this test was the maximum value attainable from the fan. These curves complement the curves already presented in Figure 4.9.

Experimental drying time, $_1t_c$, taken from the drying curves are compared with values predicted by the computer program, in Table 6.4 below.

TABLE 6.4

T_A = 25 C (constant) from Figure 4.8

Air Velocity, m/s		20	30	40	50	60	70
l^{t}_{c}	Experiment	31.0	22.7	17.3	15.1	13.2	12.5
	Theory	23.1	18.3	15.5	14.2	12.4	
Ratio Expt/Theory		1.34	1.24	1.12	1.06	1.06	

T_A = 60 C (constant) from Figure 6.10

Air Velocity, m/s		20	30	40	50
l^{t}_{c}	Experiment	7.5	4.8	3.5	2.9
	Theory	5.6	4.5	3.8	3.3
Ratio Expt/Theory		1.34	1.07	0.92	0.88

V_E = 30 m/s (constant) from Figure 4.9

Air Temperature, C		25	30	35	40	45	50	55	60
l^{t}_{c}	Experiment	15.8	14.5	10.8	8.1	6.3	5.3	4.3	3.6
	Theory	18.3	14.4		8.9		6.0		4.5
Ratio Expt/Theory		.86	1.01		.91		.88		0.8

V_E = 60 m/s (constant) from Figure 6.11

Air Temperature, C		30	40	50	60
l^{t}_{c}	Experiment	10.2	6.6	4.9	3.4
	Theory	9.8	6.0	4.1	3.0
Ratio Expt/Theory		1.04	1.1	1.2	1.13

The data in Table 6.4 shows that the agreement between theory and experiment is quite reasonable. The average of the ratios in the table is 1.05. When considering this agreement the following points should be borne in mind:-

a) It is difficult, over a long period of time, to operate the gravure press so that it always deposits exactly the same quantity of ink on the web. Note for example the discrepancy between a value of $_1t_c$ of 4.8 s obtained in one test for 60 C/30 m/s and a value of 3.6 s obtained in another test for 30 m/s/60 C.

b) The theoretical model used as a basis for calculation, represents a considerable simplication of the chemical and physical processes which actually take place.

c) Drying times of the order of 2 - 3 s probably represent the limit of accuracy of the experimental technique.

After making allowances for these points, the disagreement between theory and experiment, shown up in Table 6.4, appears to lie within the expected range of theoretical and experimental error. Hence, although the data appears to indicate that experimental drying times are longer than those predicted by theory, further tests are required to confirm the magnitude of this inconsistency.

1 constant rate drying thk=11.3

0 air vel	air temp	surf temp	hx	qdot	hdx	mdotd	mdoth	d	t1	t2	total
10.0	20.0	18.3	34.8	78.7	0.01395	0.00014	0.00014	0.00000713	4.0	45.7	49.7
20.0	20.0	18.2	52.1	111.0	0.02085	0.00021	0.00021	0.00000713	3.1	29.9	33.0
30.0	20.0	18.2	65.9	138.2	0.02638	0.00027	0.00027	0.00000713	2.5	23.5	26.0
40.0	20.0	18.2	77.8	168.3	0.03117	0.00032	0.00032	0.00000713	2.0	20.1	22.1
50.0	20.0	18.2	88.6	198.6	0.03547	0.00036	0.00036	0.00000713	1.6	17.9	19.5
60.0	20.0	18.3	98.5	239.4	0.03942	0.00040	0.00040	0.00000713	1.2	16.6	17.8
0 air vel	air temp	surf temp	hx	qdot	hdx	mdotd	mdoth	d	t1	t2	total
10.0	30.0	26.7	34.6	132.3	0.01430	0.00027	0.00027	0.00000753	6.0	21.4	27.4
20.0	30.0	26.7	51.8	190.0	0.02137	0.00040	0.00040	0.00000753	4.4	13.8	18.2
30.0	30.0	26.7	65.5	243.3	0.02704	0.00051	0.00051	0.00000753	3.4	11.0	14.4
40.0	30.0	26.7	77.4	287.4	0.03195	0.00060	0.00060	0.00000753	2.9	9.3	12.2
50.0	30.0	26.7	88.1	334.0	0.03636	0.00068	0.00068	0.00000753	2.4	8.4	10.8
60.0	30.0	26.7	97.9	395.4	0.04040	0.00074	0.00074	0.00000752	1.9	7.9	9.8
0 air vel	air temp	surf temp	hx	qdot	hdx	mdotd	mdoth	d	t1	t2	total
10.0	40.0	34.3	34.4	213.3	0.01463	0.00046	0.00046	0.00000792	6.4	10.5	16.9
20.0	40.0	34.3	51.4	315.0	0.02188	0.00069	0.00069	0.00000792	4.4	6.8	11.2
30.0	40.0	34.2	65.1	394.8	0.02768	0.00088	0.00088	0.00000792	3.6	5.2	8.9
40.0	40.0	34.2	76.9	467.2	0.03270	0.00104	0.00104	0.00000792	3.1	4.4	7.5
50.0	40.0	34.3	87.5	540.0	0.03722	0.00117	0.00117	0.00000792	2.6	4.1	6.6
60.0	40.0	34.4	97.3	619.7	0.04136	0.00128	0.00128	0.00000791	2.1	3.9	6.0
0 air vel	air temp	surf temp	hx	qdot	hdx	mdotd	mdoth	d	t1	t2	total
10.0	50.0	40.9	34.2	324.3	0.01495	0.00073	0.00073	0.00000829	6.4	5.1	11.5
20.0	50.0	40.9	51.1	481.2	0.02236	0.00109	0.00109	0.00000830	4.4	3.2	7.6
30.0	50.0	40.9	64.7	611.6	0.02828	0.00137	0.00137	0.00000830	3.4	2.7	6.0
40.0	50.0	40.9	76.4	722.9	0.03342	0.00162	0.00162	0.00000830	2.9	2.3	5.1
50.0	50.0	41.0	87.0	831.1	0.03803	0.00184	0.00184	0.00000829	2.4	2.1	4.5
60.0	50.0	41.0	96.7	932.7	0.04227	0.00203	0.00203	0.00000829	2.1	2.0	4.1
0 air vel	air temp	surf temp	hx	qdot	hdx	mdotd	mdoth	d	t1	t2	total
10.0	60.0	46.6	34.0	466.2	0.01526	0.00106	0.00106	0.00000866	6.0	2.5	8.5
20.0	60.0	46.6	50.8	694.3	0.02282	0.00159	0.00159	0.00000866	4.1	1.6	5.6
30.0	60.0	46.6	64.2	881.6	0.02886	0.00200	0.00200	0.00000866	3.1	1.4	4.5
40.0	60.0	46.6	75.9	1041.3	0.03410	0.00237	0.00237	0.00000866	2.6	1.1	3.8
50.0	60.0	46.6	86.4	1183.6	0.03882	0.00270	0.00270	0.00000866	2.4	0.9	3.3
60.0	60.0	46.8	96.0	1331.0	0.04314	0.00297	0.00297	0.00000865	2.0	1.0	3.0

TABLE 6.3

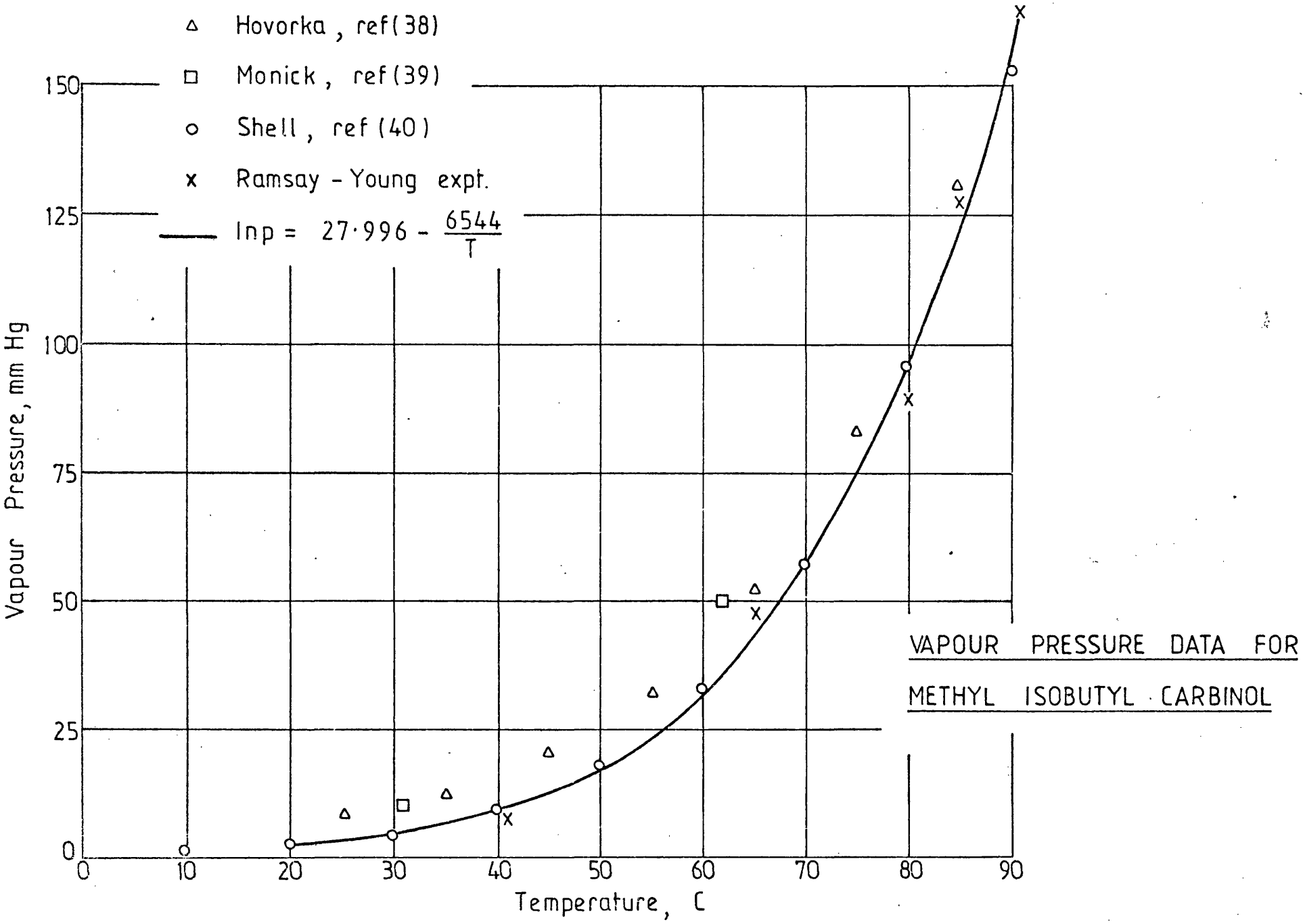

VAPOUR PRESSURE DATA FOR METHYL ISOBUTYL CARBINOL

FIGURE 6.1

FIGURE 6.2

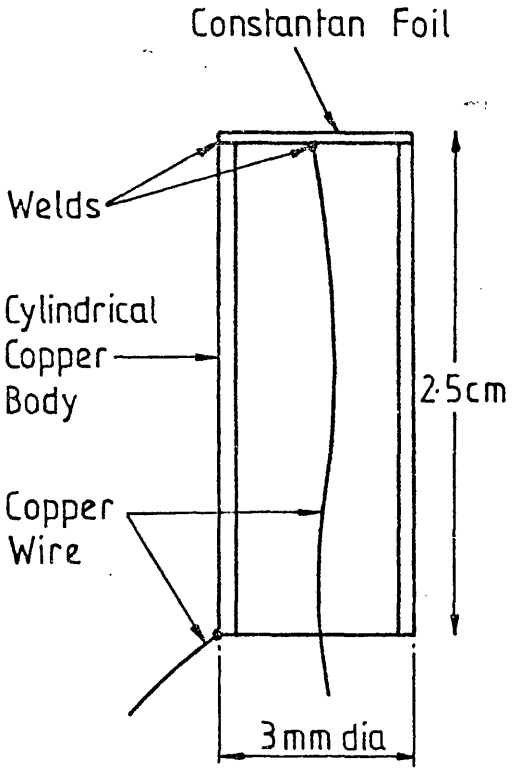

(a) Principle of "Gardon" meter

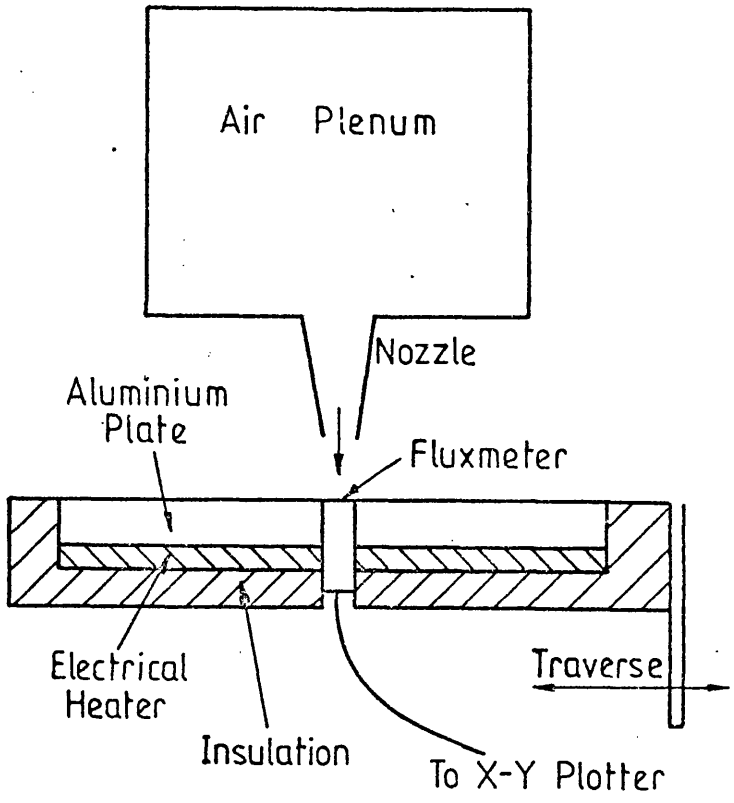

(b) Heat transfer rig

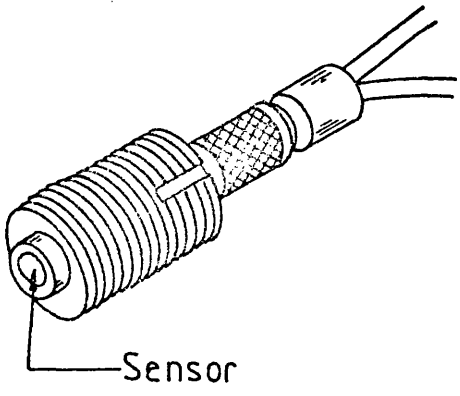

(c) "Medtherm" Fluxmeter

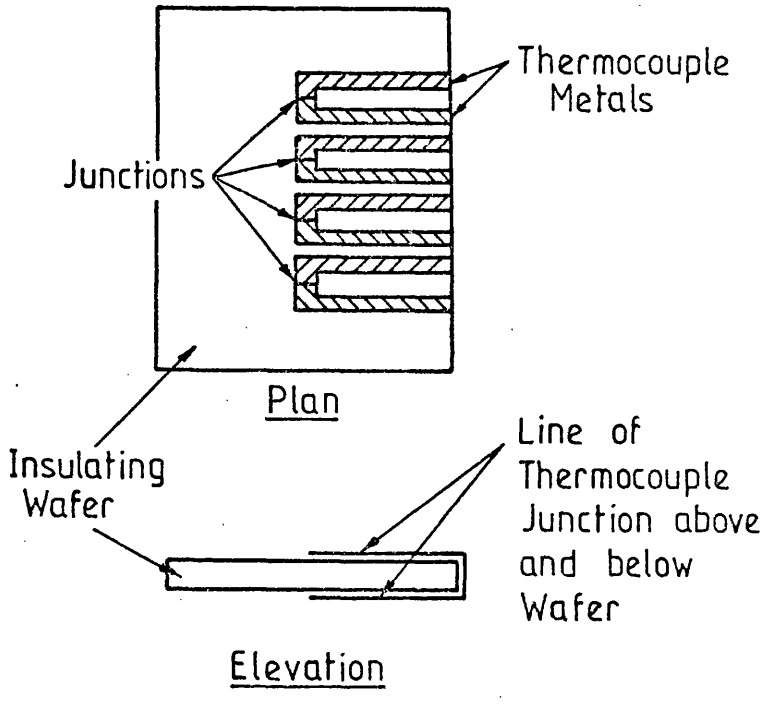

(d) Principle of "Schmidt-Boelter" meter

FIGURE 6.2. HEAT TRANSFER INSTRUMENTATION

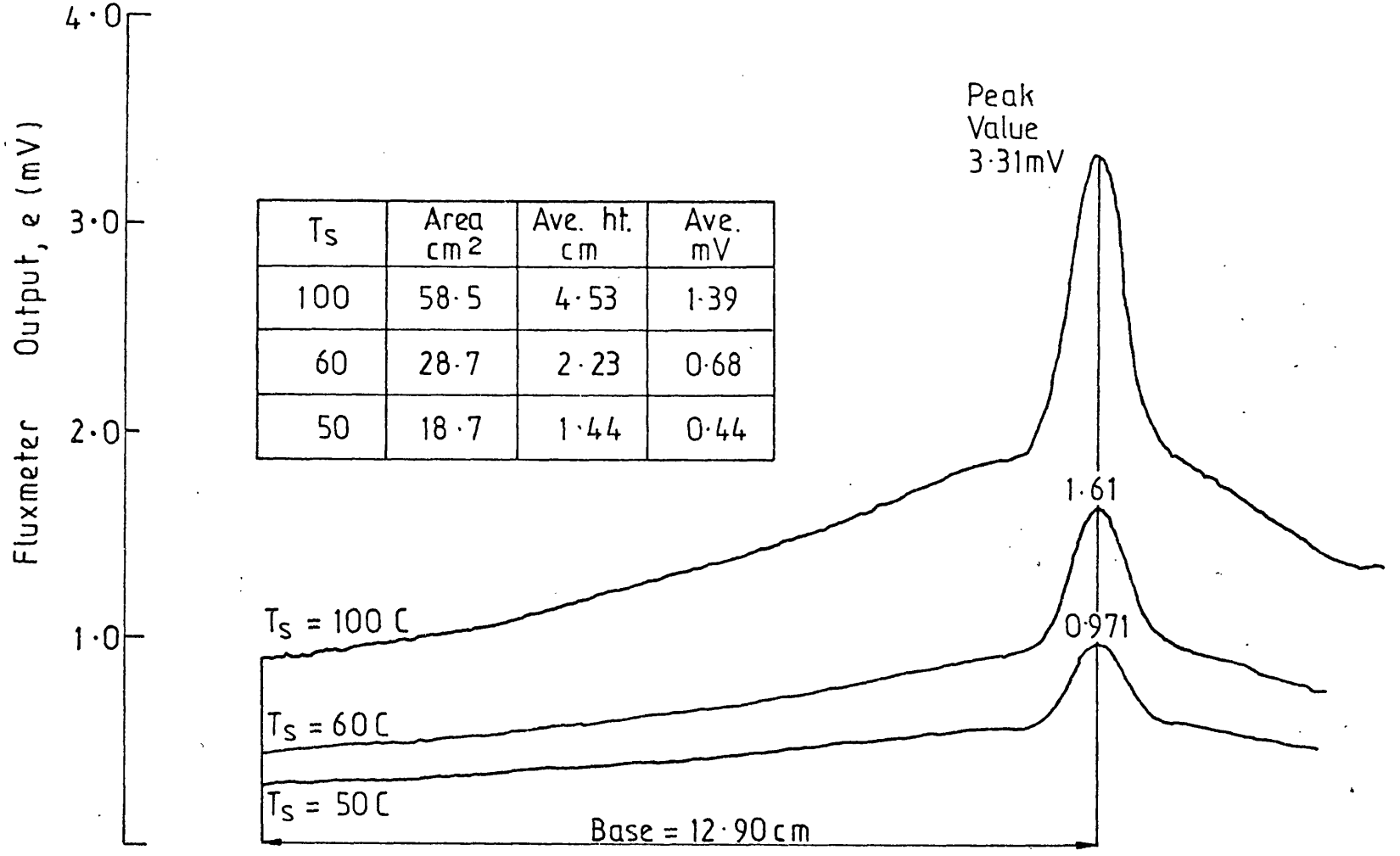

T_S	Area cm^2	Ave. ht. cm	Ave. mV
100	58·5	4·53	1·39
60	28·7	2·23	0·68
50	18·7	1·44	0·44

FIGURE 6.3. CALIBRATION OF FLUXMETER IN ELECTRICALLY HEATED PLATE

FIGURE 6.3

LATERAL VARIATION OF HEAT TRANSFER COEFFICIENT UNDER A ONE-DIMENSIONAL SLOT NOZZLE

B = 3·18 mm

Z/B = 8

Air Temperature = 25·5C

Test	$Re_E = \frac{V_E B \rho}{\mu}$	V_o	V_x	$\frac{V_x}{V_o} \left(\equiv \frac{h_x}{h_o}\right)$
1	12,170	5·15	1·0	0·1945
2	10,140	4·6	0·9	0·195
3	8,110	4·1	0·75	0·183
4	6,080	3·55	0·58	0·1635
5	4,060	2·63	0·45	0·172

V_o = maximum voltage

V_x = voltage 10cm from nozzle

1 volt ≡ 116 W/m^2K

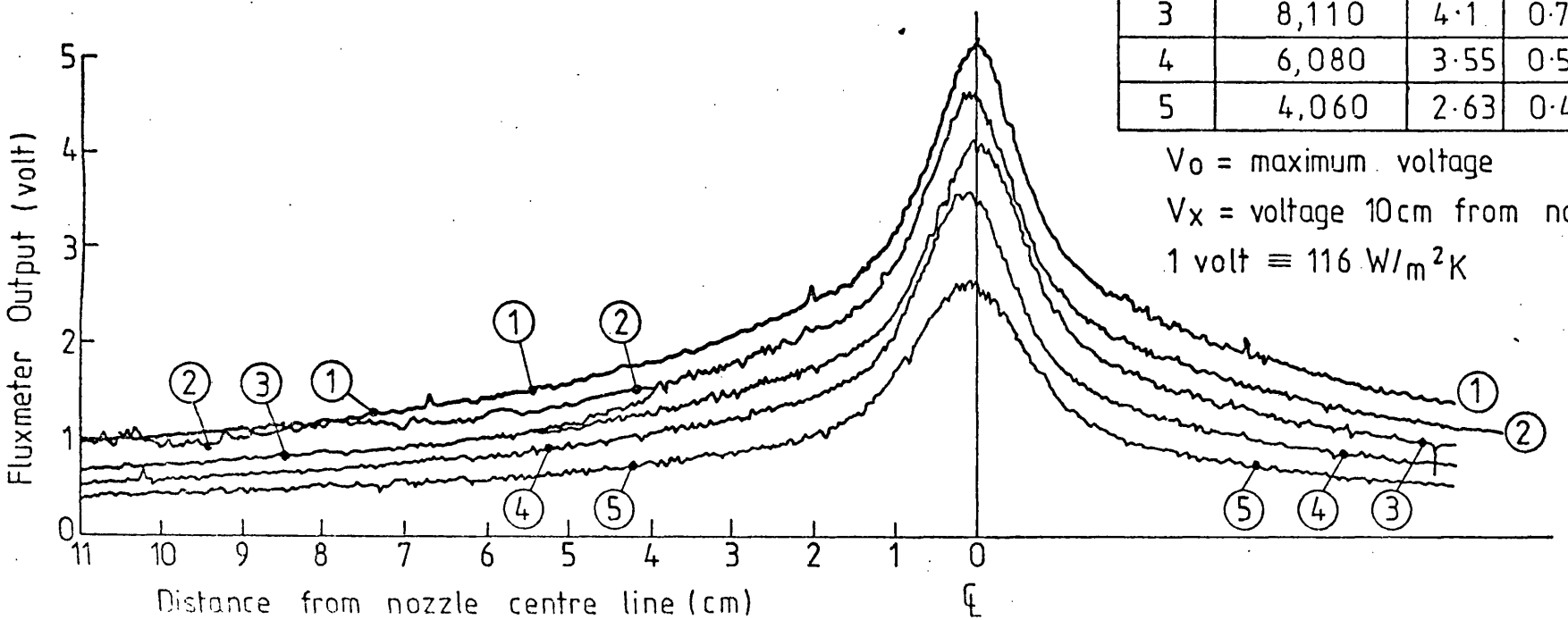

FIGURE 6.4

FIGURE 6.5. EXTENDED WEB TRAVEL TO ERADICATE INITIAL TRANSIENT

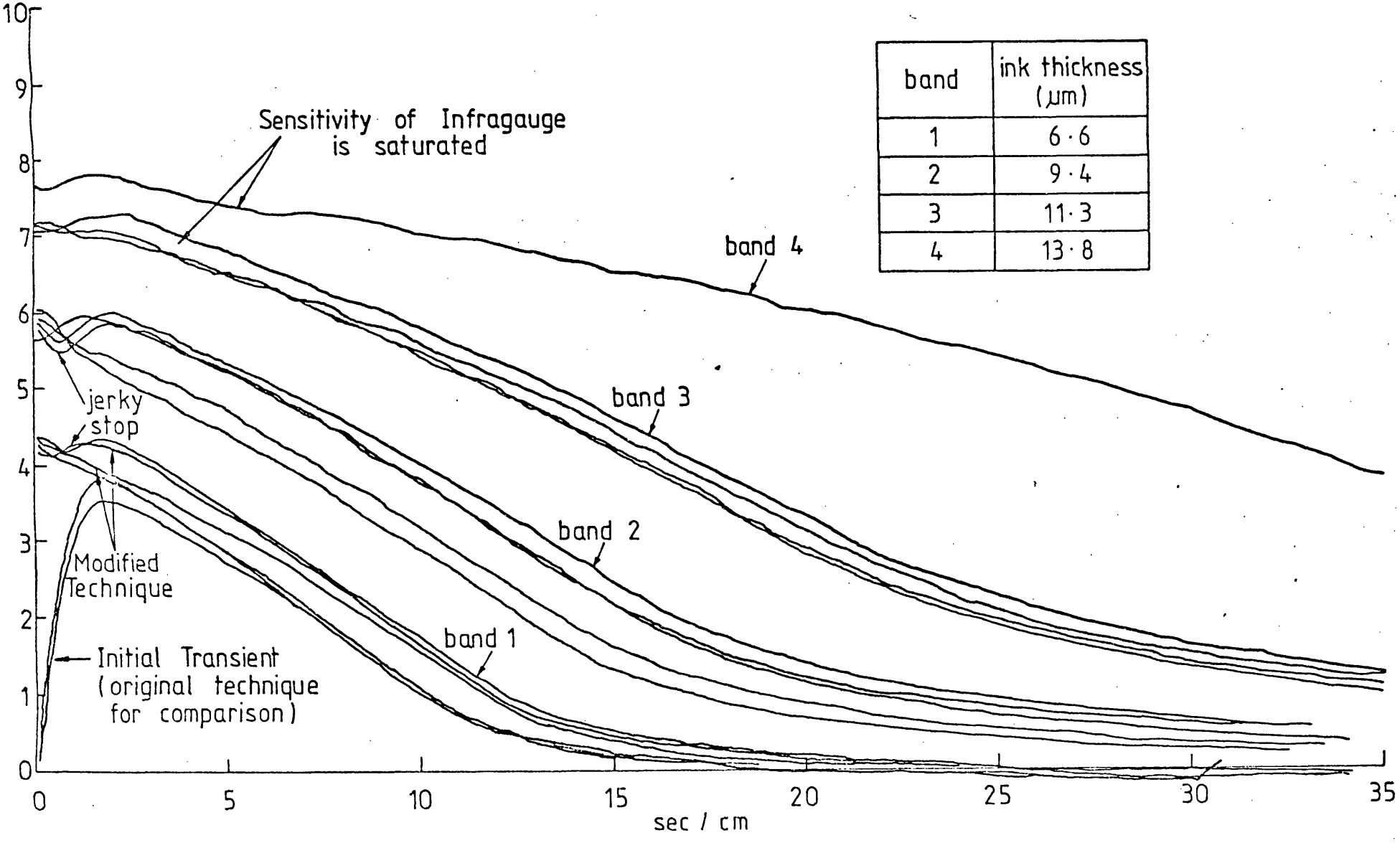

band	ink thickness (μm)
1	6·6
2	9·4
3	11·3
4	13·8

FIGURE 6.5

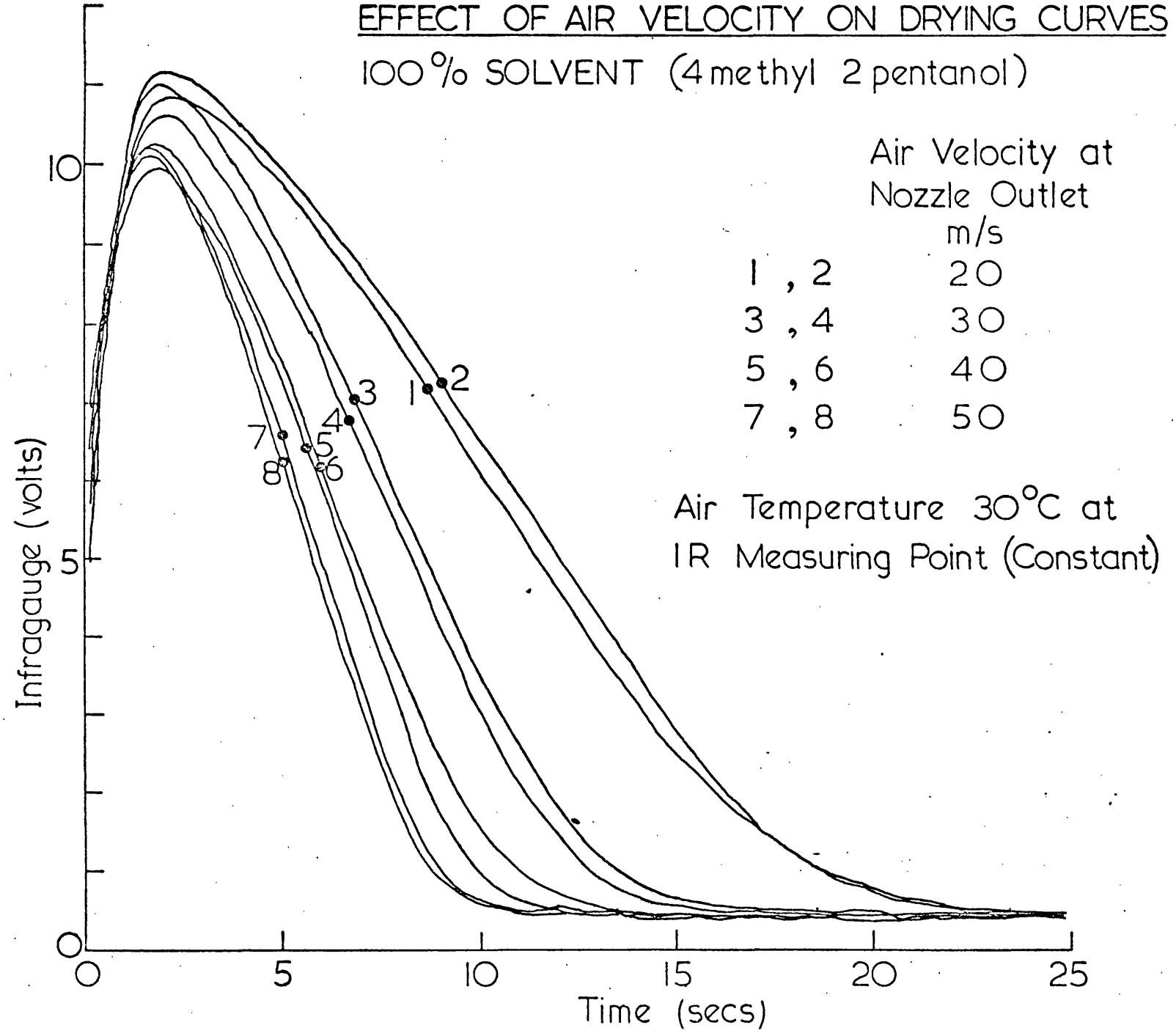
EFFECT OF AIR VELOCITY ON DRYING CURVES
100% SOLVENT (4 methyl 2 pentanol)
Air Velocity at Nozzle Outlet m/s
1 , 2 20
3 , 4 30
5 , 6 40
7 , 8 50
Air Temperature 30°C at IR Measuring Point (Constant)
Infragauge (volts)
Time (secs)
0
5
10
15
20
25
1
2
3
4
5
6
7
8

FIGURE 6.6

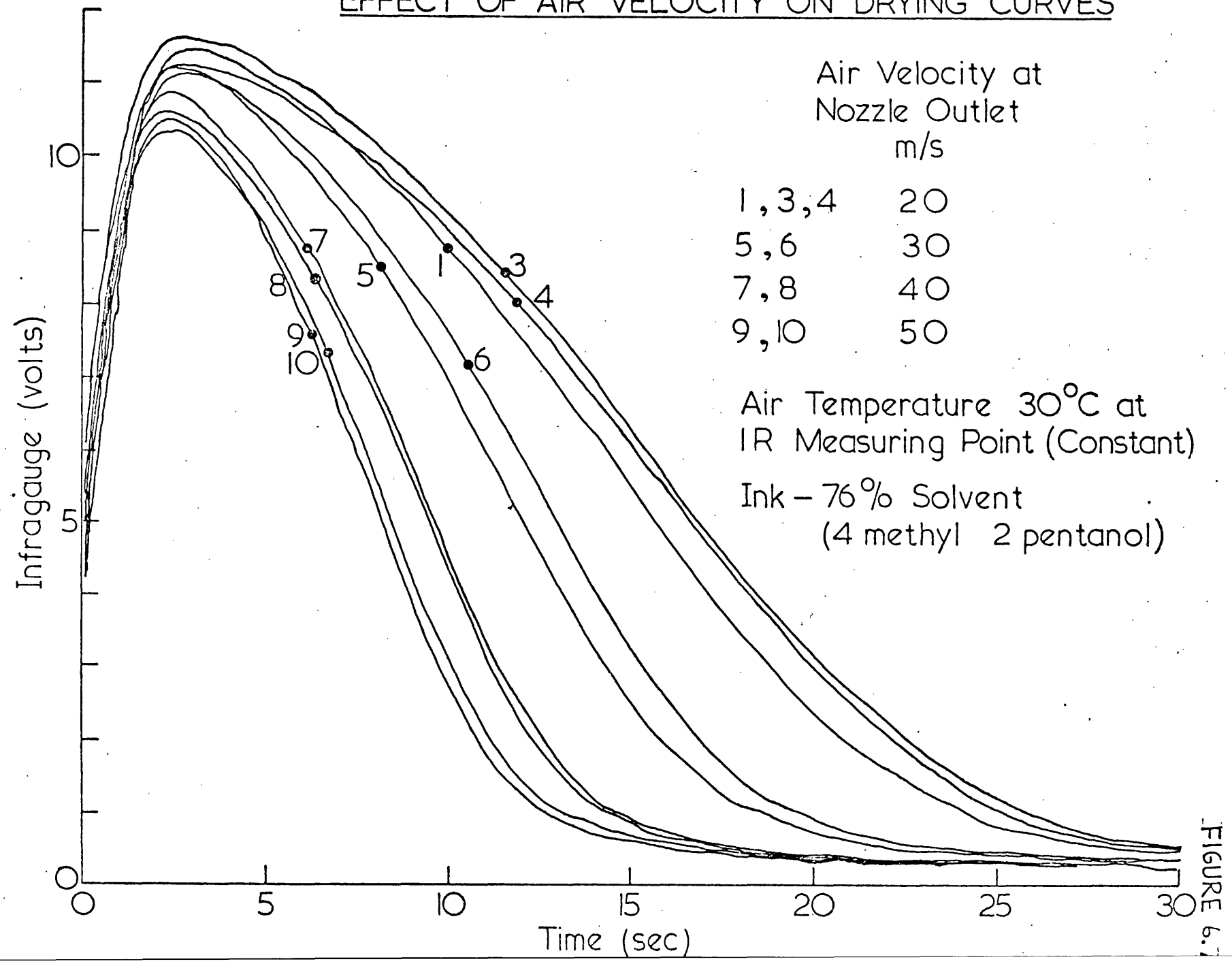
EFFECT OF AIR VELOCITY ON DRYING CURVES
Air Velocity at Nozzle Outlet m/s
1, 3, 4 20
5, 6 30
7, 8 40
9, 10 50
Air Temperature 30°C at IR Measuring Point (Constant)
Ink – 76% Solvent (4 methyl 2 pentanol)
Infragauge (volts)
Time (sec)
0
5
10
15
20
25
30
1
3
4
5
6
7
8
9
10

FIGURE 6.7

FIGURE 6.8

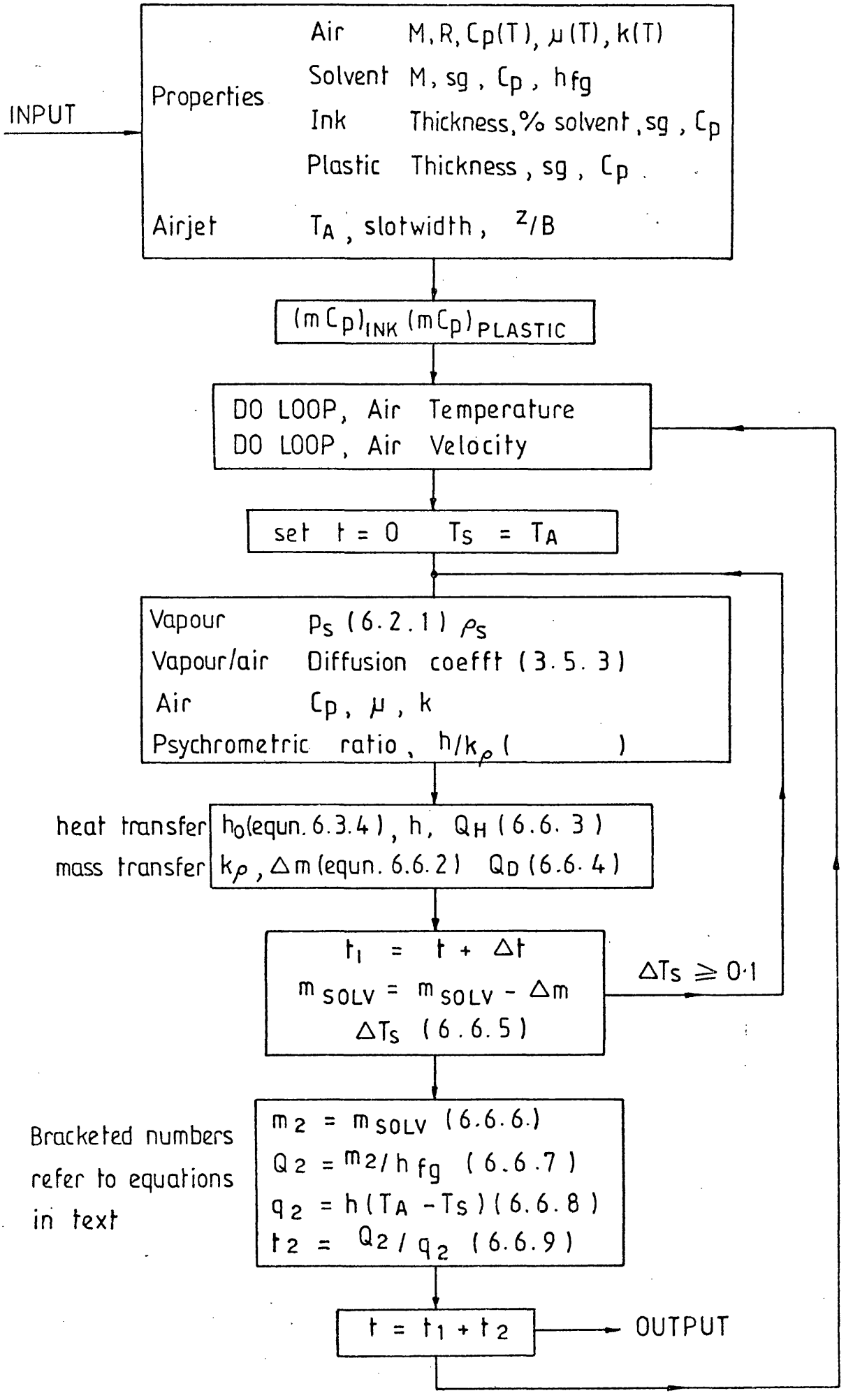

FIGURE 6.7. FLOW CHART FOR CONSTANT-RATE PROGRAM

FIGURE 6.9. CHARACTERISTICS OF EXTERNALLY CONTROLLED DRYING

Solvent : 4 methyl 2 pentanol
Ink deposit : Thickness 11·3 μm , 76 % solvent

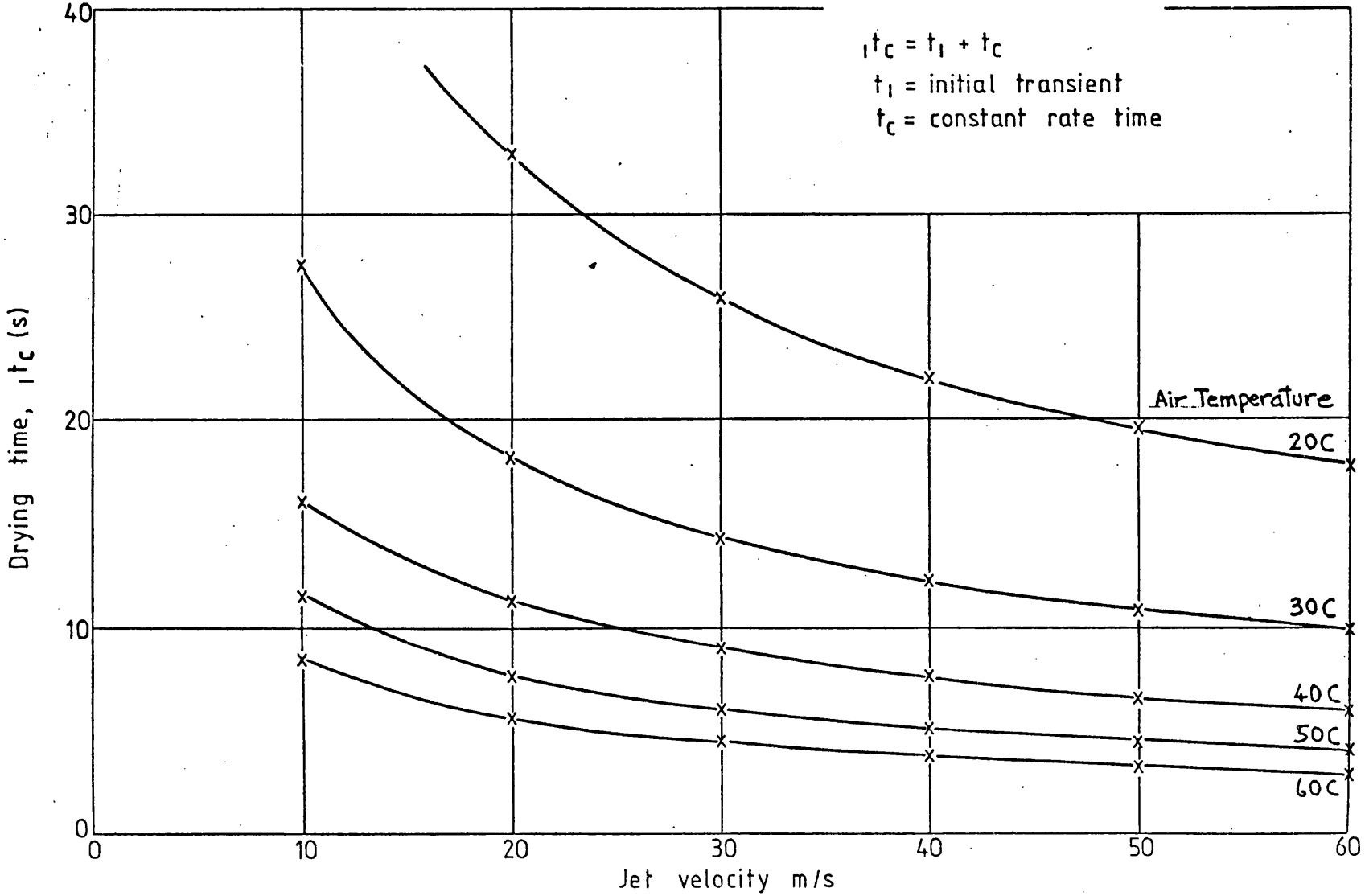

FIGURE 6.9

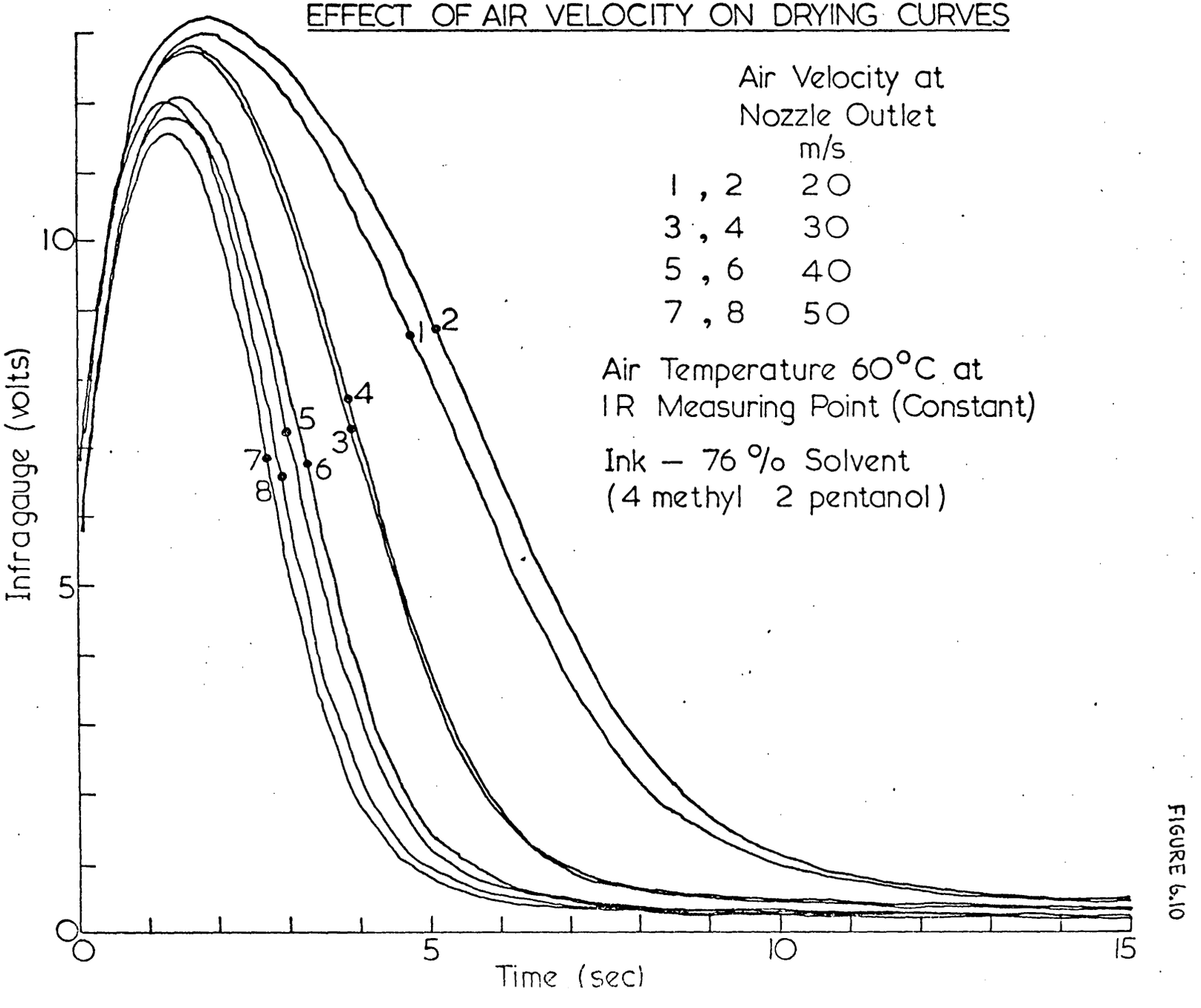
EFFECT OF AIR VELOCITY ON DRYING CURVES
Air Velocity at Nozzle Outlet m/s
1 , 2 20
3 , 4 30
5 , 6 40
7 , 8 50
Air Temperature 60°C at IR Measuring Point (Constant)
Ink – 76 % Solvent (4 methyl 2 pentanol)
Infragauge (volts)
Time (sec)
0
5
10
15
1
2
3
4
5
6
7
8

FIGURE 6.10

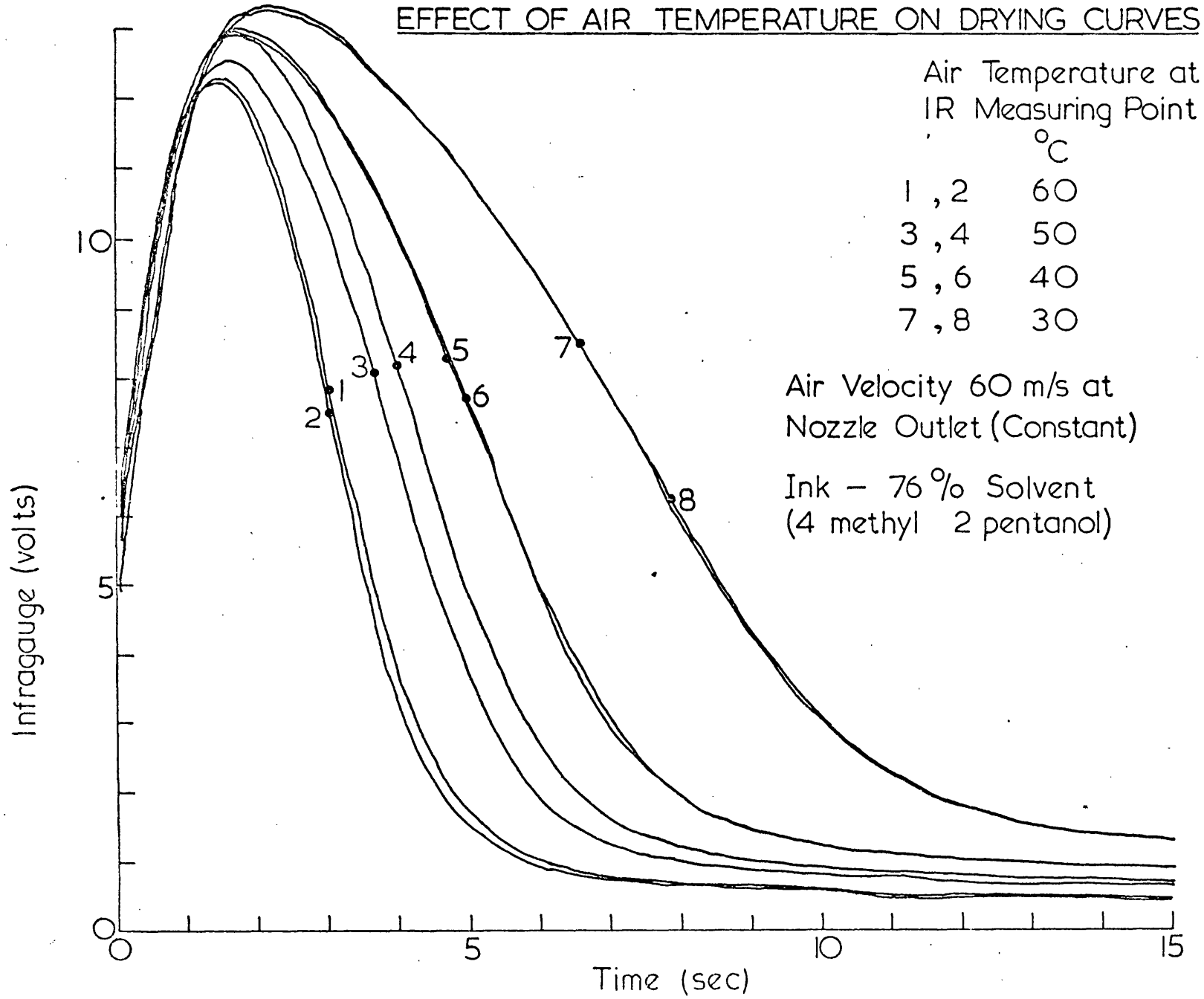
EFFECT OF AIR TEMPERATURE ON DRYING CURVES
Air Temperature at IR Measuring Point °C
1 , 2 60
3 , 4 50
5 , 6 40
7 , 8 30
Air Velocity 60 m/s at Nozzle Outlet (Constant)
Ink – 76 % Solvent (4 methyl 2 pentanol)
Infragauge (volts)
Time (sec)
0
5
10
15
1
2
3
4
5
6
7
8

FIGURE 6.11

7. EXTERNALLY CONTROLLED DRYING II - FURTHER DEVELOPMENTS

7.1 Introduction

The IR drying curves presented in Chapters 4 and 6 represent, within the limitations of the research rig, a relatively complete investigation of the effect of changing air conditions on the drying characteristics of the single solvent research ink. In addition to this test series, other associated tests were carried out; for clarity these further results are reported separately in this chapter.

Accurate measurements of ink surface temperature provide a valuable check on theory, but such measurements are difficult to obtain. The background to these difficulties and the results of an attempt to measure plastic temperature by means of an IR thermometer are given in section 7.2

To relate the basic research of the earlier chapters more closely to industrial practice the IR method was extended in two aspects. First, tests were carried out on a faster, more volatile solvent, n-propanol. Second, measurements were made of the total quantity of solvent evaporated during the passage of the ink under the air jet.

7.2 Ink Temperature Measurement

The physical properties of the ink/plastic system, and the rates of the physical and chemical processes within the system, all depend upon the temperature attained during drying. Hence a knowledge of this temperature would be extremely useful to both press designer and operator. Unfortunately, it is extremely difficult to measure the temperature of a thin, moving transparent film. In the packaging industry, attempts to measure web temperature have not met with success.

Industrial tests have been reported to the writer, in which small proprietry temperature indicators have been attached to the web. In principle these indicators respond to high temperature by changing colour. In fact, tests carried out during the course of this research, have shown that, because of their relatively large thermal inertia and slow reaction rate, such indicators are unsuitable for this task.

An entirely different method of web temperature measurement was therefore tested by the writer. In this method an extremely thin strip of gold was deposited on the surface of the plastic (by vacuum evaporation) to act as a resistance thermometer. For research purposes, a section of plastic complete with gold strip was mounted on a small trolley. Web movement was simulated by moving the trolley along rails and under a heated air jet. Experimental results were excellent, see Wheeler and Mullervy,(50) but the method suffers from a practical defect. The gold strips are fragile and must be connected by wires to a measuring system. Thus, the technique cannot, at present, be used on a practical printing press.

Next, the temperature of the web was measured by means of a radiation thermometer. Initially this method appeared attractive because it avoided those difficulties, outlined above, associated with contacting the web. To this end a number of commercial radiation thermometers were assessed and some proving trials were carried out. These investigations brought out the following points:-

i) Because of the extreme thinness and variability of the ink layer it is necessary to measure the temperature of the plastic substrate. Both ink and plastic are assumed to be at the same temperature (section 6.7).

ii) In this application, temperatures in the range 0 - 60 C must be measured. At this relatively low temperature the intensity of IR radiation is low and a specialised instrument is required.

iii) For valid temperature measurement the radiation from the plastic film must be emitted wholly by the film itself.

iv) The plastic used in this research, polypropylene, is a selective emitter. Because of this and because of its thinness, the plastic can transmit radiation from hot bodies behind it or reflect radiation from hot bodies in front of it. This extraneous radiation can be picked up by the IR detector and so falsify the indicated temperature.

v) The difficulties of iv) can be avoided by using a thermometer which operates on a narrow spectral band. In this band the plastic should have an absorptivity of unity and consequently act as a black-body.

Following the above deliberations, trials were conducted on a commercial IR thermometer. This instrument was of the narrow band type centered on a wavelength of 3.43 μm; at this wavelength the absorptivity of the polypropylene substrate is unity. Even with such a specialised instrument success could not be guaranteed, as its range of operation started at a temperature of 30 C.

The experimental method used to record the temperature of the printed web was almost the same as the method already used to record IR drying curves and described in section 4.1. The principal difference was that the measuring head the Infragauge was removed and replaced by the measuring head of the IR thermometer. By connecting the electrical

output of the IR thermometer to the X-Y plotter a temperature record was obtained from a stationary inked specimen during drying.

Figure 7.1 shows the results of five tests to assess the effect of different air temperatures on the temperature of the web during drying. To confirm repeatability two curves were recorded at each test condition. The curves all appear to exhibit a characteristic "arrest" at a low temperature, before rising up to the air temperature towards the end of the test. It is considered that this arrest corresponds to constant-rate drying. Although the records of transient temperature shown in Figure 7.1 lack precision, when allowances are made for the experimental difficulties, the tests may be considered successful. The transient curves have been used to estimate experimental values of the wet-bulb depression. For comparison with these experimental values, theoretical. predictions of the wet-bulb temperature have also been included in Figure 7.1. It can be seen that there is good agreement between experiment and theory. In view of the difficult nature of these temperature measurements, this degree of confirmation of the constant-rate theory of ink drying is probably as much as can be achieved by this approach.

Although the above tests were successful, they demonstrated that the temperature of a thin transparent film could only be successfully measured with very specialised and expensive equipment. Consequently this line of investigation was not pursued further at that time.

7.3 Tests on a More Volatile Solvent - n-Propanol

The original research ink, 4 methyl pentan-2-ol, had been selected because its relatively low volatility allowed sufficient time for its

drying characteristics to be studied. Having gained experience with this slowly evaporating ink it was decided to apply the same experimental technique to n propanol a faster commercial solvent.

As before the ink supplier formulated a single solvent ink. A sample of this ink, as supplied, was weighed in a chemical balance, evaporated to dryness and then weighed again. By this means it was established that the ink contained 66% solvent by mass. To calculate the mass of ink deposited on the plastic by number 3 band of the gravure cylinder, 3 strips of dry printed plastic were cut from appropriate portions of the web. Each strip was weighed on a chemical balance, n-proponal was used to remove the ink, and the strips were weighed once again. The ink deposit on the three strips, estimated by difference, was as follows:-

i) 4.1 gm/m^2

ii) 3.9 gm/m^2

iii) 3.8 gm/m^2 Average dry ink deposit = 3.93 gm/m^2

Non-volatiles in ink = 100-66 = 34%

Average ink deposit from gravure roller = 3.93/0.34 = 11.57 gm/m^2

Results of further drying tests on the n-propanol based ink are shown in Figures 7.2 and 7.3. Figure 7.2 shows the effect on the IR drying curves of changing the air velocity and Figure 7.3 shows the effect of changing air temperature. Because the ink now dryed at a faster rate, a slight modification was made to the experimental technique, to ameliorate the effect of the slow response time of the Infragauge. The printing press and the time base on the X-Y plotter were started

simultaneously, and the press was kept running for about 10 seconds. This was sufficient time for the Infragauge signal from the wet, moving web to become roughly constant. After 10 seconds the press was stopped and a drying curve was then recorded from the stationary web. The effect of this modification in technique, was to remove the initial rising transient from the drying curve. The drying curve proper, was now preceded by a roughly horizontal trace.

From Figures 7.2 and 7.3, it can be seen that the IR curves for the n-proponal based ink exhibit two characteristic differences from the previous curves for 4 methyl 2 pentanol:-

i) Although the initial ink deposit (gm/m^2) is somewhat greater than previously, the voltage which the n-propanol based ink produces from the Infragauge, is smaller. Previously, with 4 methyl 2 pentanol, the virtual voltage at zero time V_o was of the order of 20 volts; with n-propanol V_o is reduced to roughly 13 volts. Changing the solvent has altered the calibration of the IR instrument.

ii) The fraction of the initial solvent deposit still remaining at the critical point has increased. Consequently, the IR drying curves show only the last portion of the constant-rate period. Thus estimation of the gradient of the curves in the constant rate region, and the extrapolation of this slope to obtain t_c, has now become more difficult. In spite of this, it is considered that the estimates of t_c made from these curves are of an acceptable accuracy.

The computer program described in section 6.7 may be used to predict theoretical drying times for any solvent provided that appropriate

physical property data is inserted. For n-propanol (C_3H_8O) the following data was obtained from Reid et al (40)

Molecular weight = 60.09

Specific gravity (liquid) = 0.805

Specific heat (liquid) = 2,453 J/kg C

Enthalpy of evaporation = 686,635 J/kg

Relation between saturated vapour pressure p and absolute temperature T:-

$$p = \exp\left(22.43 - \frac{3166.0}{(T - 80.15)}\right)$$

There was insufficient time to carry out the necessary tests to determine, for n-propanol, the ratio of the drying rates of ink and pure solvent. In the absence of empirical data on this ratio, the value of 1.3 determined in the previous test series (section 6.6) was retained.

Using the above physical information, the input data to the computer program of Appendix 3 was suitably amended for n-propanol. Table 7.1 shows, for gravure band No. 3, predicted drying times for various combinations of air velocity and temperature. These theoretical predictions are compared with the experimental drying times of Figures 7.2 and 7.3 in Table 7.2 below:-

TABLE 7.2

Air Velocity, m/s		20	30	40	50	60
$1^{t}c$	Experiment	8.9	6.3	5.4	4.5	4.0
	Theory	8.4	6.6	5.6	4.9	4.5
Ratio Expt/Theory		1.06	0.95	0.96	0.92	0.89

T_A = 28 C (constant)

V_E = 30 m/s (constant)

Air Temperature, C		30	40	50	60
l^t_c	Experiment	6.4	4.4	3.9	3.2
	Theory	6.2	4.6	3.6	3.0
Ratio Expt/Theory		1.03	0.96	1.08	1.07

The comparison shows that the agreement between theory and experiment is reasonably good.

It is also possible to compare, for the same air conditions, the experimental drying times of n-propanol and 4 methyl pentan-2-ol:-

TABLE 7.3

Air Velocity 30 m/s (constant)

Air Temperature, C		30	60
l^t_c	4 methyl pentan-2-ol	14.5	4.8
	n propanol	6.3	3.0
Ratio of drying times		2.3	1.6

The ratio shown in Table 7.3 are less than the value of 4.0 predicted by the Shell Evaporometer and shown in Table 5.2. The ratios are even less than the value of 3.0 predicted by evaporation rate theory in Table 5.2. This difference arises because the results in Table 5.2 apply to an air temperature of 20 C.

The Critical Point

Estimates of the position of the critical point on the drying curve, are more difficult to make for n-propanol than previously for 4 methyl 2 pentanol. This is because, for n propanol, the IR curves exhibit less of the constant-rate period. Nevertheless, it can be seen from Figures 7.2 and 7.3 that the behaviour of the critical point is similar to that previously described in Section 4.6. Changing the rate of drying in the constant-rate region, by a factor of the order of 2, appears not to have a corresponding effect on the position of the critical point. The following approximate estimates were made from Figures 7.2 and 7.3

V_o = 13 volt

V_c = 6.5 volt

$$\frac{V_c}{V_o} = 0.5$$

V_o = virtual voltage at zero time

V_c = voltage at critical point.

The magnitude of (V_c/V_o) determined above, is larger, by a factor of approximately two, than previous values of this parameter for the ink based on 4 methyl 2 pentanol. This trend is, at least, in line with the suggestion made in section 4.6, that the value of V_c/V_o is dependent upon the percentage of non-volatiles in the ink. However, since the non-volatiles have increased by only 50%, this explanation is a partial one. To test the theory further, a detailed analysis of the non-volatiles in the n-propanol based ink is required, and this is not available.

7.4 Cumulative Drying Effect of a Single Nozzle - Experiments

When this research was originally planned, it was intended that drying effectiveness should be assessed by measuring the rate at which solvent is removed by the dryer during continuous, steady-state operation of the press. To achieve this objective the research rig was fitted with two IR measuring heads one placed before the dryer (air nozzle) and one after it. The intention was to calculate the rate at which solvent was evaporated by the dryer from the difference in the two IR signals. In fact, this intention was never persevered with. The preferred technique was to use a single IR head to record drying curves from a stationary specimen as described in Chapter 4. However, tests were carried out to extend the experimental method and to fulfil the original research objective.

Modified experimental technique

The IR measuring head was moved from its position before the nozzle and placed in a similar position after the nozzle, Figure 7.4. Thus the inked specimen now passed under the air jet before reaching the IR measuring station 10 cm beyond the nozzle centreline.

To obtain the results shown in Figures 7.5 to 7.7, the following change was made to the experimental technique. The time base on the X-Y plotter and the printing press were started simultaneously at a time of minus 10 s. Printing was continued for 10 s, sufficient time for the IR reading from the moving web to attain a quasi steady-state condition. After 10 s (time zero) the press was stopped, which led to the subsequent recording of a drying curve from a stationary specimen.

Experimental results

Figure 7.5 shows the effect of increasing the air velocity at constant temperature. It can be seen that the increased heat transfer coefficient causes a progressive lowering of the solvent content at the IR measuring point, the wavy horizontal trace in the -7 s to 0 s region. It should be pointed out, that to ensure that the Infragauge operated within its linear range (see section 4.1) it was necessary to carry out these tests on gravure band No. 1 (the thinnest band). Thus the vertical distance of the horizontal wavy trace below the "air-off" trace is proportional to the total quantity of solvent evaporated by the nozzle. Figure 7.3 also shows drying curves from stationary specimens recorded after stopping the web. Except for a systematic lowering of their point of origin these curves are similar to those analysed in section 6.8.

Figure 7.6 shows the results of a similar series of tests to assess the effect of increasing the air temperature. Figure 7.8 shows the effect of increasing both air velocity and air temperature to their maximum values attainable on this rig. Because of the increased drying effect achieved, it was possible to carry out these tests on gravure band No. 3.

7.5 Cumulative Drying Effect of a Single Nozzle - Computer Program

To calculate the amount of solvent evaporated as an element of ink passes under the air jet at a speed of 0.3 m/s it was necessary to modify the program described previously in section 6.7 and set out in Appendix 3. The inked element travels a total distance of 20 cm, from a point 10 cm on one side of the nozzle centreline to a point 10 cm on the other side. For purposes of computation, this transit was

modelled as a series of small discrete steps. At each step the energy balance equation, 6.7.5 was solved and the differential change of temperature was computed from equation 6.7.5.

The modified program is given in Appendix 4. In essence the modification consists of adjusting the value of the heat and mass transfer coefficients (h_x and k_x) and the air temperature T_{Ax} to simulate the changing position of the web. The following ratios were obtained from experiment, at 10 cm from the nozzle centreline

$$\frac{h_x}{h_o} = \frac{1}{5}$$

$$\frac{T_{Ax}}{T_{Ao}} = \frac{2}{3}$$

h_o = heat transfer coefficient at nozzle centreline

T_{Ao} = air temperature at nozzle centreline

Simple symmetrical, linear distributions of h_x and T_A were assumed, typically as shown in Figure 7.8. The actual equations of these distributions, are to be found on page 3 of the program in the section entitled "hxovho, ta change with x".

Figure 7.9 shows the transient variation of ink temperature first as the web passes under the nozzle and finally as the stationary web settles down to the equilibrium wet-bulb temperature. The data in Figure 7.9 is taken from a detailed computer print-out of the transient calculation. One section of this print-out for an air velocity of 10 m/s is shown in Table 7.4. The manner in which h_x and T_A change with distance can also be seen from Table 7.4.

For computational purposes the drying time is split into three sub-periods:-

t1 = time to pass under air-jet (20 cm, 0.67 s)

t2a = time subsequent to t1 for the ink temperature to adjust to the wet-bulb temperature

t2 = time subsequent to t2a for the solvent content to fall to zero at constant drying rate

The computer output shown in Table 7.5 shows drying data for gravure band No. 1. It shows the effect on the above drying times of systematically varying both air velocity and air temperature. In the print-out

total = t2a + t2

In addition the fraction of the initial solvent deposit evaporated during the time period t1 was calculated and designated "frac 1". Table 7.6 shows similar data calculated for gravure band No. 3.

In Table 7.7 below, values of frac 1 extracted from Tables 7.5 and 7.6 are compared with values estimated from experiment.

TABLE 7.7

Gravure Band No 1

T_A = 30 C (constant) from Figure 7.5

Air Velocity, m/s		20	30	40	50	60
frac 1	Experiment	0.12	0.15	0.22	0.26	0.36
	Theory	0.138	0.197	0.252	0.306	0.356
Ratio Expt/Theory		0.78	0.76	0.87	0.85	1.01

V_E = 20 m/s (constant) from Figure 7.6

Air Temperature, C		30	40	50	60	70
frac 1	Experiment	0.13	0.23	0.39	0.55	0.87
	Theory	0.138	0.212	0.32	0.47	0.67
Ratio Expt/Theory		0.94	1.08	1.22	1.17	1.3

Gravure Band No 3

From Figure 7.7 (estimated value of V_o = 11.0 volt)

Air Velocity, m/s		20	30	40	50	60	60	60	60
Air Temperature, C		25	25	25	25	25	30	40	60
frac 1	Experiment	0.05	0.13	0.16	0.25	0.32	0.43	0.58	0.86
	Theory	0.06	0.09	0.11	0.13	0.15	0.19	.525	0.78
Ratio Expt/Theory		0.84	1.0	1.45	1.9	2.1	2.3	1.1	1.1

In assessing the data in Table 7.7 two points should be borne in mind. First, the temperature distribution used in the program is a crude appoximation and could be refined. Second, it is difficult to estimate V_o, the IR voltage for no air flow, because at that point the Infragauge may be outside the linear operating range. Bearing these two points in mind the agreement between experiment and computer prediction is encouraging. It is believed that the large discrepancies of the Band 3 data arise from errors in estimating voltages at zero time.

A further comparison of experiment with theory is possible. In Figures 7.5 - 7.7, the portions of the drying curves which lie beyond zero time may be extrapolated forward to yield the hypothetical drying time $_1t_c$. It can be seen that values of $_1t_c$ obtained in this matter agree reasonable well with values of the "total" time in Tables 7.5 and 7.6.

CONSTANT RATE DRYING TIMES n-propanol TABLE 7.1

Band 3 Initial ink deposit 11.57 gm/m²

air vel	air temp	surf temp	hx	qdot	hdx	mdotd	mdoth	d	t1	t2	total
10.0	28.0	15.9	34.5	432.7	0.01759	0.00061	0.000610	.00001012	1.6	11.0	12.6
20.0	28.0	15.8	51.6	642.9	0.02630	0.00092	0.000920	.00001012	1.4	7.0	8.4
30.0	28.0	15.8	65.3	812.6	0.03327	0.00116	0.001160	.00001012	1.1	5.5	6.6
40.0	28.0	15.8	77.2	961.9	0.03931	0.00137	0.001370	.00001012	0.9	4.7	5.6
50.0	28.0	15.9	87.9	1100.0	0.04474	0.00155	0.001550	.00001012	0.6	4.3	4.9
60.0	28.0	16.1	97.7	1242.9	0.04972	0.00170	0.001700	.00001011	0.3	4.2	4.5
air vel	air temp	surf temp	hx	qdot	hdx	mdotd	mdoth	d	t1	t2	total
10.0	30.0	16.9	34.5	466.3	0.01767	0.00066	0.000660	.00001021	2.4	9.3	11.7
20.0	30.0	16.9	51.6	695.1	0.02641	0.00098	0.000980	.00001021	1.7	6.1	7.8
30.0	30.0	16.9	65.2	877.9	0.03341	0.00125	0.001250	.00001021	1.4	4.8	6.2
40.0	30.0	16.9	77.1	1040.7	0.03948	0.00147	0.001470	.00001021	1.1	4.1	5.2
50.0	30.0	16.9	87.7	1185.1	0.04493	0.00167	0.001670	.00001021	1.0	3.7	4.6
60.0	30.0	17.1	97.5	1330.1	0.04993	0.00184	0.001840	.00001020	0.7	3.5	4.2
air vel	air temp	surf temp	hx	qdot	hdx	mdotd	mdoth	d	t1	t2	total
10.0	40.0	21.7	34.3	646.6	0.01803	0.00091	0.000910	.00001065	3.2	5.5	8.7
20.0	40.0	21.5	51.2	960.8	0.02696	0.00138	0.001380	.00001066	2.4	3.4	5.8
30.0	40.0	21.5	64.8	1213.6	0.03411	0.00175	0.001750	.00001066	2.0	2.6	4.6
40.0	40.0	21.6	76.6	1438.3	0.04030	0.00206	0.002060	.00001066	1.5	2.3	3.9
50.0	40.0	21.6	87.1	1642.8	0.04586	0.00233	0.002330	.00001065	1.3	2.1	3.4
60.0	40.0	21.7	96.9	1833.1	0.05097	0.00258	0.002580	.00001065	1.1	2.0	3.1
air vel	air temp	surf temp	hx	qdot	hdx	mdotd	mdoth	d	t1	t2	total
10.0	50.0	25.5	34.0	843.3	0.01839	0.00121	0.001210	.00001109	3.6	3.2	6.8
20.0	50.0	25.5	50.8	1259.5	0.02749	0.00182	0.001820	.00001109	2.4	2.2	4.6
30.0	50.0	25.4	64.3	1591.6	0.03478	0.00230	0.002300	.00001109	2.0	1.6	3.6
40.0	50.0	25.5	76.0	1884.8	0.04109	0.00271	0.002710	.00001109	1.5	1.5	3.1
50.0	50.0	25.6	86.5	2152.0	0.04676	0.00307	0.003070	.00001109	1.3	1.4	2.7
60.0	50.0	25.8	96.2	2401.2	0.05197	0.00339	0.003390	.00001108	1.1	1.3	2.4
air vel	air temp	surf temp	hx	qdot	hdx	mdotd	mdoth	d	t1	t2	total
10.0	60.0	29.0	33.8	1061.0	0.01873	0.00152	0.001520	.00001151	3.2	2.4	5.6
20.0	60.0	29.0	50.5	1585.9	0.02799	0.00228	0.002280	.00001151	2.0	1.7	3.8
30.0	60.0	28.9	63.9	2003.5	0.03542	0.00289	0.002890	.00001151	1.7	1.3	3.0
40.0	60.0	28.8	75.5	2364.7	0.04185	0.00342	0.003420	.00001151	1.5	1.0	2.5
50.0	60.0	29.0	85.9	2697.0	0.04763	0.00388	0.003880	.00001151	1.3	0.9	2.2
60.0	60.0	29.2	95.5	3006.9	0.05293	0.00429	0.004290	.00001151	1.1	0.9	2.0

Passage under air-jet

web stationary

Transient

x	time	T_A	T_S	h_x/h_o	h_x	q_h	q_d	dT	m_{sol}
m	sec	C	C		w/m²K	J	J	C	Kg
0.00000	0.00000	20.00	15.00	0.20	36.23	12.08	3.25	0.126	0.00411
0.02000	0.06667	22.00	15.13	0.30	53.82	24.66	4.88	0.283	0.00410
0.04000	0.13333	24.00	15.41	0.39	71.36	40.87	6.64	0.491	0.00409
0.06000	0.20000	26.00	15.90	0.49	88.87	59.83	8.61	0.735	0.00407
0.08000	0.26667	28.00	16.63	0.59	106.33	80.57	10.94	0.999	0.00405
0.10000	0.33333	30.00	17.63	1.00	180.48	148.79	20.10	1.849	0.00403
0.12000	0.40000	28.00	19.48	0.59	106.05	60.22	13.62	0.671	0.00398
0.14000	0.46667	26.00	20.15	0.49	88.51	34.50	11.91	0.325	0.00395
0.16000	0.53333	24.00	20.48	0.39	70.97	16.66	9.75	0.100	0.00392
0.18000	0.60000	22.00	20.58	0.30	53.41	5.06	7.37	-0.033	0.00390
0.20000	0.66667	20.00	20.55	0.20	35.84	-1.30	4.92	-0.090	0.00388
0.22000	0.73333	20.00	20.46	0.20	35.86	-6.54	29.23	-0.517	0.00387
0.34000	1.13333	20.00	19.94	0.20	35.87	0.88	28.13	-0.395	0.00380
0.46000	1.53333	20.00	19.54	0.20	35.87	6.55	27.32	-0.302	0.00373
0.58000	1.93333	20.00	19.24	0.20	35.88	10.88	26.71	-0.231	0.00367
0.70000	2.33333	20.00	19.01	0.20	35.88	14.19	26.25	-0.176	0.00361
0.82000	2.73333	20.00	18.84	0.20	35.89	16.72	25.91	-0.135	0.00355
0.94000	3.13333	20.00	18.70	0.20	35.89	18.65	25.65	-0.103	0.00349
1.06000	3.53333	20.00	18.60	0.20	35.89	20.13	25.45	-0.078	0.00343
1.18000	3.93333	20.00	18.52	0.20	35.89	21.25	25.30	-0.060	0.00337
1.30000	4.33333	20.00	18.46	0.20	35.89	22.11	25.19	-0.046	0.00331
1.42000	4.73333	20.00	18.41	0.20	35.89	22.77	25.11	-0.035	0.00325
1.54000	5.13333	20.00	18.38	0.20	35.89	23.26	25.04	-0.026	0.00319
1.66000	5.53333	20.00	18.35	0.20	35.89	23.64	24.99	-0.020	0.00313
1.78000	5.93333	20.00	18.33	0.20	35.89	23.93	24.95	-0.015	0.00307
1.90000	6.33333	20.00	18.32	0.20	35.89	24.15	24.92	-0.012	0.00301
2.02000	6.73333	20.00	18.31	0.20	35.89	24.32	24.90	-0.009	0.00296

Computer Prediction of Transient Drying

TABLE 7.4

Final Summary

cumulative drying effect thk=6.6

air vel	air temp	surf temp	hx	qdot	hdx	mdotd	fract	t1	t2a	t2	total
10.0	20.0	18.3	35.9	60.8	0.01368	0.00015	0.055	0.67	6.47	19.92	26.39

gravure band no 1

4 methyl 2 pentanol

intdry

1 cumulative drying effect thk=6.6

0 air vel	air temp	surf temp	hx	qdot	hdx	mdotd	frac1	t1	t2a	t2	total
10.0	20.0	18.2	35.9	50.3	0.01368	0.00015	0.055	0.67	3.27	22.64	25.91
20.0	20.0	18.2	53.7	78.5	0.02045	0.00022	0.090	0.67	2.79	13.86	16.65
30.0	20.0	18.2	67.9	99.4	0.02587	0.00028	0.120	0.67	2.31	10.37	12.67
40.0	20.0	18.2	80.2	119.1	0.03057	0.00033	0.147	0.67	2.05	8.33	10.38
50.0	20.0	18.2	91.3	128.1	0.03480	0.00038	0.173	0.67	1.67	7.13	8.79
60.0	20.0	18.2	101.5	122.2	0.03869	0.00043	0.197	0.67	1.27	6.32	7.58
0 air vel	air temp	surf temp	hx	qdot	hdx	mdotd	frac1	t1	t2a	t2	total
10.0	30.0	26.6	35.6	103.4	0.01403	0.00028	0.076	0.67	1.67	11.86	13.53
20.0	30.0	26.7	53.3	163.5	0.02096	0.00041	0.138	0.67	2.79	5.53	8.32
30.0	30.0	26.7	67.4	205.9	0.02652	0.00052	0.197	0.67	2.31	3.72	6.03
40.0	30.0	26.7	79.6	244.7	0.03134	0.00062	0.252	0.67	2.05	2.66	4.71
50.0	30.0	26.7	90.6	271.2	0.03567	0.00071	0.306	0.67	1.67	2.14	3.80
60.0	30.0	26.6	100.7	280.7	0.03966	0.00080	0.356	0.67	1.27	1.86	3.13
0 air vel	air temp	surf temp	hx	qdot	hdx	mdotd	frac1	t1	t2a	t2	total
10.0	40.0	34.3	35.4	192.9	0.01436	0.00047	0.106	0.67	0.47	7.28	7.75
20.0	40.0	34.3	52.9	287.6	0.02146	0.00071	0.212	0.67	2.45	1.88	4.33
30.0	40.0	34.3	66.9	363.4	0.02715	0.00090	0.318	0.67	2.03	0.82	2.85
40.0	40.0	34.3	79.1	432.8	0.03208	0.00106	0.421	0.67	1.83	0.16	1.99
50.0	40.0	34.3	90.0	487.4	0.03652	0.00121	0.520	0.67	1.51	-0.10	1.41
60.0	40.0	34.7	100.0	525.3	0.04060	0.00136	0.614	0.67	1.07	0.00	1.07
0 air vel	air temp	surf temp	hx	qdot	hdx	mdotd	frac1	t1	t2a	t2	total
10.0	50.0	41.0	35.1	311.4	0.01467	0.00074	0.148	0.67	0.47	4.26	4.73
20.0	50.0	41.0	52.5	464.6	0.02193	0.00111	0.320	0.67	2.45	-0.17	2.27
30.0	50.0	41.2	66.4	582.6	0.02775	0.00141	0.497	0.67	1.47	0.00	1.47
40.0	50.0	41.9	78.4	633.6	0.03282	0.00174	0.669	0.67	0.73	0.00	0.73
50.0	50.0	43.1	89.2	617.2	0.03742	0.00213	0.831	0.67	0.39	0.00	0.39
60.0	50.0	46.3	98.8	363.8	0.04180	0.00291	0.983	0.67	0.07	0.00	0.07
0 air vel	air temp	surf temp	hx	qdot	hdx	mdotd	frac1	t1	t2a	t2	total
10.0	60.0	46.7	34.8	453.2	0.01498	0.00109	0.204	0.67	1.27	1.73	3.00
20.0	60.0	47.0	52.1	675.8	0.02239	0.00163	0.469	0.67	1.43	0.00	1.43
30.0	60.0	47.8	65.8	806.3	0.02836	0.00215	0.742	0.67	0.63	0.00	0.63
40.0	60.0	52.3	77.4	595.2	0.03375	0.00336	0.999	0.67	0.07	0.00	0.07
50.0	66.0	54.7	130.6	1480.2	0.05831	0.00667	1.127	0.60	0.00	0.00	0.00
60.0	72.0	56.1	192.3	3054.2	0.08697	0.01081	1.161	0.53	0.00	0.00	0.00
0 air vel	air temp	surf temp	hx	qdot	hdx	mdotd	frac1	t1	t2a	t2	total
10.0	70.0	51.5	34.6	623.8	0.01527	0.00149	0.278	0.67	1.67	0.28	1.94
20.0	70.0	52.4	51.6	908.6	0.02284	0.00229	0.665	0.67	0.75	0.00	0.75
30.0	70.0	58.3	64.7	759.0	0.02942	0.00413	1.050	0.67	0.00	0.00	0.00
40.0	84.0	61.0	150.2	3450.0	0.07035	0.01155	1.087	0.53	0.00	0.00	0.00
50.0	91.0	62.6	212.4	6039.3	0.10096	0.01804	1.075	0.47	0.00	0.00	0.00
60.0	91.0	61.9	236.4	6884.6	0.11208	0.01928	1.313	0.47	0.00	0.00	0.00

CUMULATIVE DRYING EFFECT

Gravure band no 1

TABLE 7.5

intdry
1 cumulative drying effect thk= 11.3
0

air vel	air temp	surf temp	hx	qdot	hdx	mdotd	frac1	t1	t2a	t2	total
10.0	25.0	22.5	35.8	70.8	0.01386	0.00021	0.036	0.67	1.27	31.39	32.65
20.0	25.0	22.5	53.5	112.7	0.02071	0.00031	0.062	0.67	2.79	18.49	21.28
30.0	25.0	22.5	67.6	145.5	0.02620	0.00039	0.085	0.67	2.59	13.77	16.36
40.0	25.0	22.5	79.9	163.5	0.03096	0.00046	0.107	0.67	2.05	11.33	13.38
50.0	25.0	22.5	91.0	185.0	0.03524	0.00053	0.127	0.67	1.83	9.62	11.45
60.0	25.0	22.5	101.1	179.5	0.03919	0.00060	0.147	0.67	1.37	8.53	9.89
10.0	20.0	18.2	35.9	46.5	0.01368	0.00015	0.031	0.67	2.87	42.45	45.32
20.0	20.0	18.2	53.6	73.6	0.02045	0.00022	0.051	0.67	2.79	26.96	29.74
30.0	20.0	18.2	67.9	98.5	0.02587	0.00028	0.068	0.67	2.59	20.57	23.16
40.0	20.0	18.2	80.2	108.8	0.03057	0.00033	0.083	0.67	2.05	17.07	19.12
50.0	20.0	18.2	91.3	123.2	0.03480	0.00038	0.097	0.67	1.83	14.69	16.51
60.0	20.0	18.2	101.4	112.8	0.03869	0.00043	0.111	0.67	1.37	13.02	14.39
air vel	air temp	surf temp	hx	qdot	hdx	mdotd	frac1	t1	t2a	t2	total
10.0	30.0	26.8	35.6	123.4	0.01402	0.00027	0.042	0.67	0.47	24.59	25.06
20.0	30.0	26.7	53.3	161.0	0.02097	0.00041	0.075	0.67	2.79	12.72	15.50
30.0	30.0	26.7	67.4	198.7	0.02653	0.00053	0.106	0.67	2.31	9.37	11.68
40.0	30.0	26.7	79.6	234.5	0.03134	0.00062	0.137	0.67	2.05	7.44	9.49
50.0	30.0	26.6	90.6	265.7	0.03568	0.00071	0.166	0.67	1.83	6.19	8.01
60.0	30.0	26.6	100.7	279.4	0.03966	0.00080	0.194	0.67	1.47	5.42	6.89
air vel	air temp	surf temp	hx	qdot	hdx	mdotd	frac1	t1	t2a	t2	total
10.0	40.0	34.5	35.4	212.4	0.01435	0.00046	0.056	0.67	2.47	12.14	14.61
20.0	40.0	34.2	52.9	285.4	0.02146	0.00071	0.111	0.67	2.45	6.18	8.63
30.0	40.0	34.3	66.9	363.1	0.02715	0.00090	0.167	0.67	2.31	3.97	6.27
40.0	40.0	34.3	79.1	429.7	0.03208	0.00106	0.222	0.67	2.05	2.84	4.89
50.0	40.0	34.2	90.0	480.9	0.03652	0.00121	0.277	0.67	1.67	2.28	3.95
60.0	40.0	34.2	100.0	522.5	0.04060	0.00136	0.329	0.67	1.37	1.90	3.26
air vel	air temp	surf temp	hx	qdot	hdx	mdotd	frac1	t1	t2a	t2	total
10.0	50.0	41.2	35.1	324.3	0.01466	0.00072	0.076	0.67	2.87	6.24	9.10
20.0	50.0	40.9	52.5	461.5	0.02194	0.00111	0.163	0.67	2.45	2.67	5.12
30.0	50.0	40.9	66.4	581.7	0.02775	0.00141	0.255	0.67	2.03	1.44	3.47
40.0	50.0	40.9	78.5	690.5	0.03279	0.00166	0.348	0.67	1.83	0.68	2.51
50.0	50.0	40.9	89.3	781.1	0.03732	0.00190	0.438	0.67	1.51	0.36	1.87
60.0	50.0	40.8	99.3	852.9	0.04150	0.00213	0.525	0.67	1.17	0.23	1.40
air vel	air temp	surf temp	hx	qdot	hdx	mdotd	frac1	t1	t2a	t2	total
10.0	60.0	47.0	34.9	468.8	0.01497	0.00106	0.102	0.67	2.47	3.61	6.07
20.0	60.0	46.7	52.1	677.8	0.02239	0.00162	0.234	0.67	2.11	1.03	3.13
30.0	60.0	46.7	65.9	858.2	0.02833	0.00205	0.378	0.67	1.75	0.16	1.91
40.0	60.0	46.9	77.9	1010.8	0.03347	0.00243	0.520	0.67	1.39	0.00	1.39
50.0	60.0	47.2	88.6	1110.2	0.03812	0.00285	0.655	0.67	0.87	0.00	0.87
60.0	60.0	48.1	98.3	1121.0	0.04245	0.00339	0.782	0.67	0.47	0.00	0.47

TABLE 7.6

CUMULATIVE DRYING EFFECT

Gravure band no 3

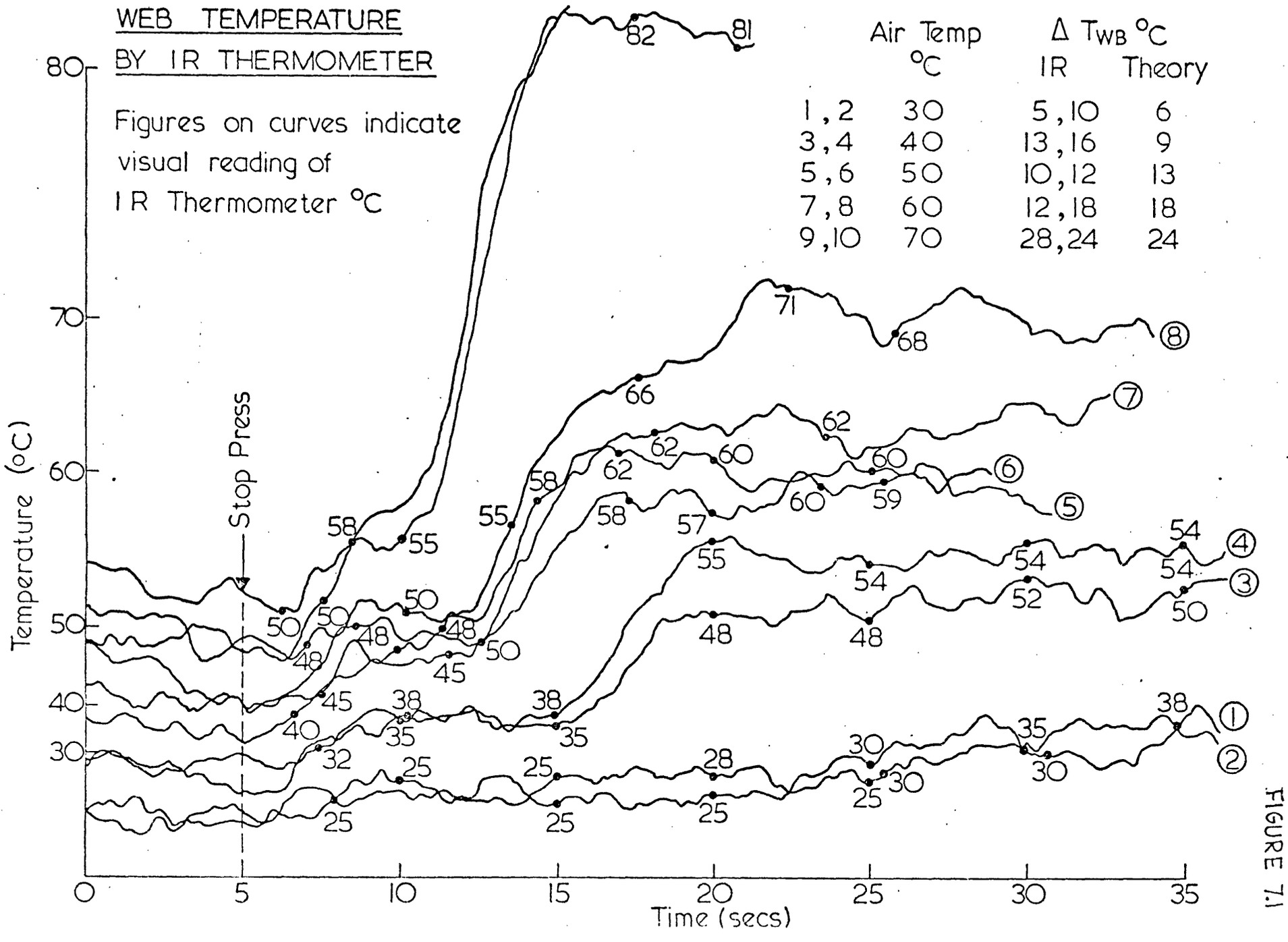
WEB TEMPERATURE
BY IR THERMOMETER
Figures on curves indicate visual reading of IR Thermometer °C
Air Temp °C
Δ TWB °C
IR
Theory
1,2 30 5,10 6
3,4 40 13,16 9
5,6 50 10,12 13
7,8 60 12,18 18
9,10 70 28,24 24
Stop Press
Temperature (°C)
Time (secs)
80
70
60
50
40
30
0
5
10
15
20
25
30
35
①
②
③
④
⑤
⑥
⑦
⑧

FIGURE 7.1

THE EFFECT OF AIR VELOCITY ON DRYING

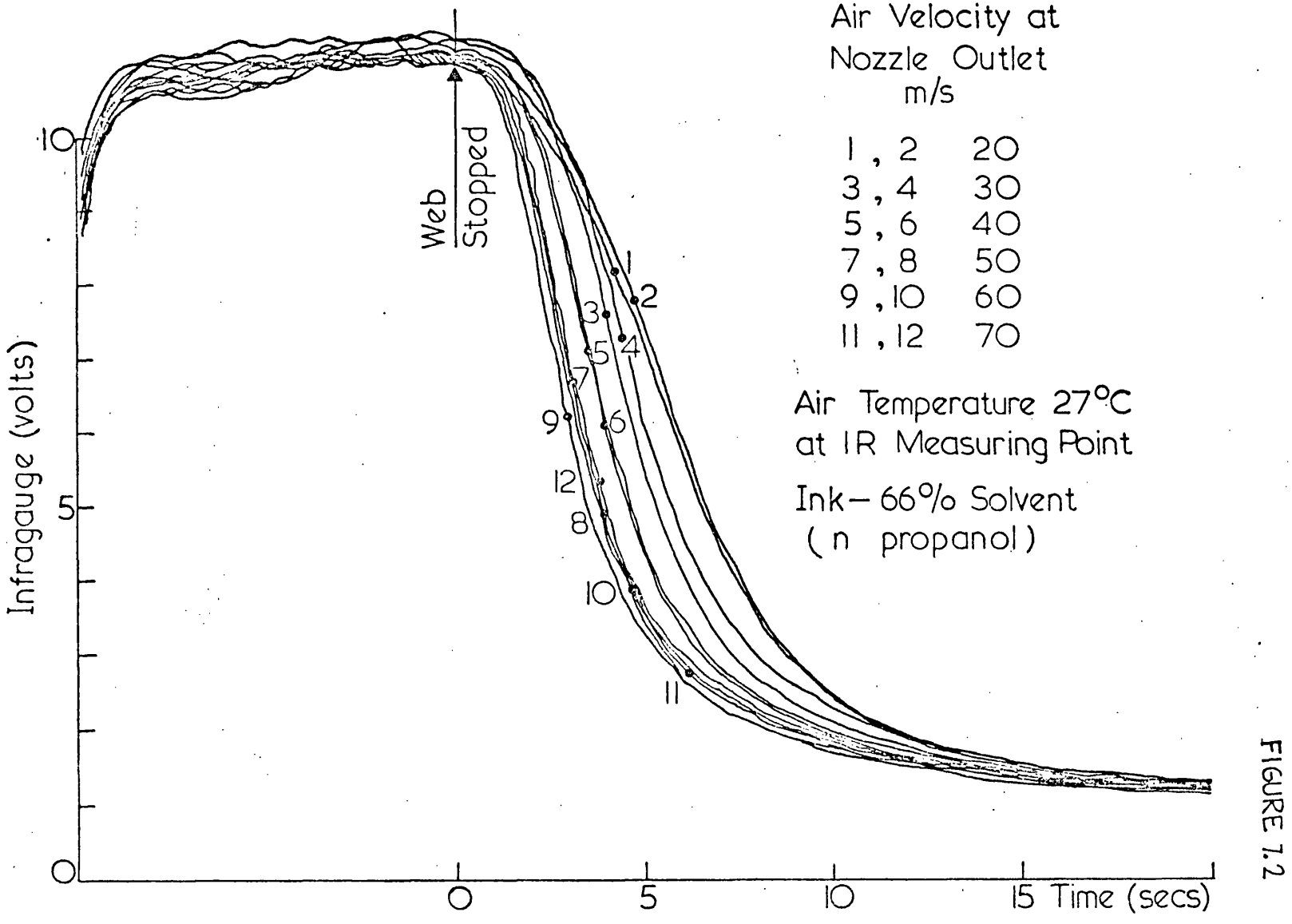

FIGURE 7.2

THE EFFECT OF AIR TEMPERATURE ON DRYING

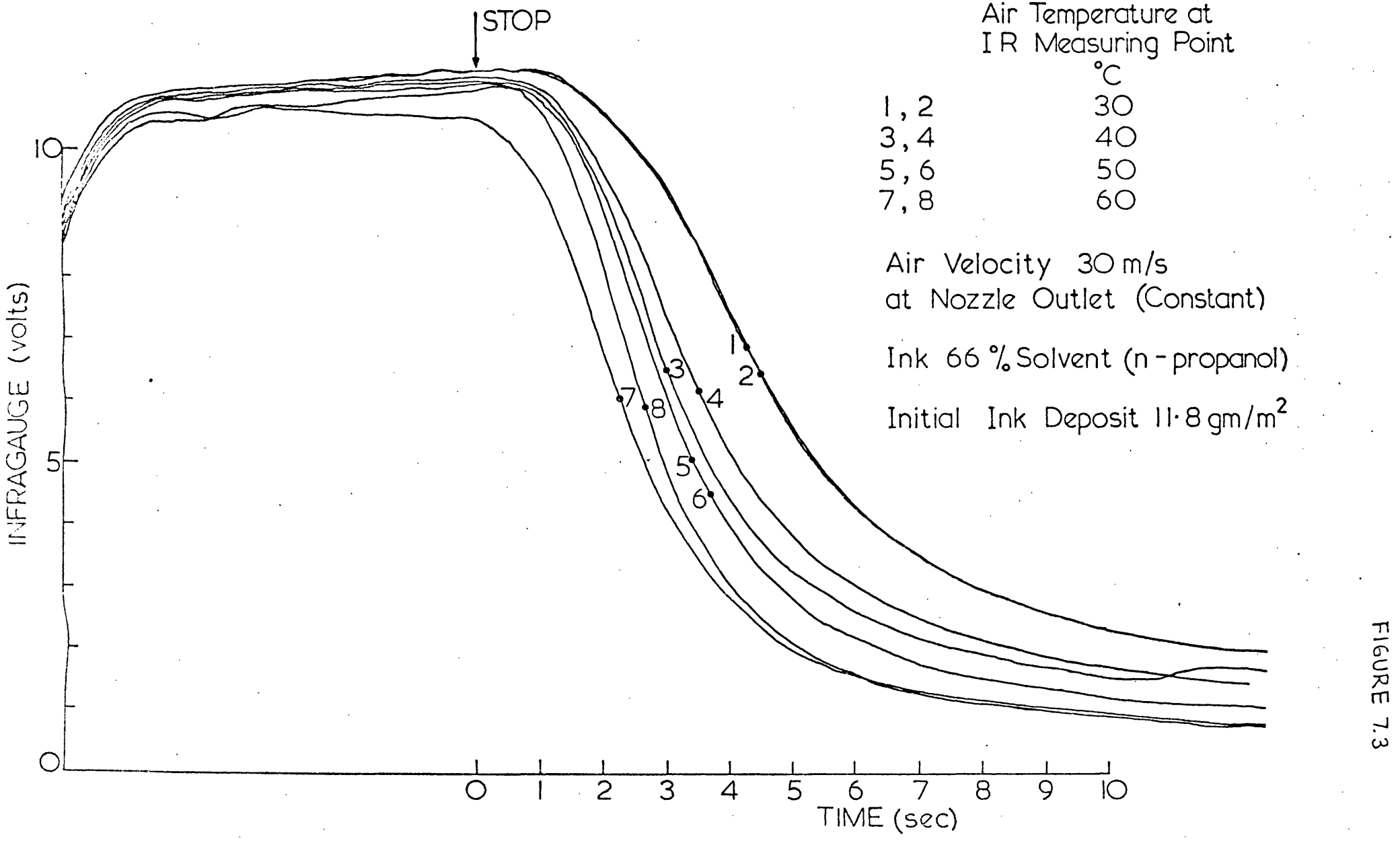

FIGURE 7.3

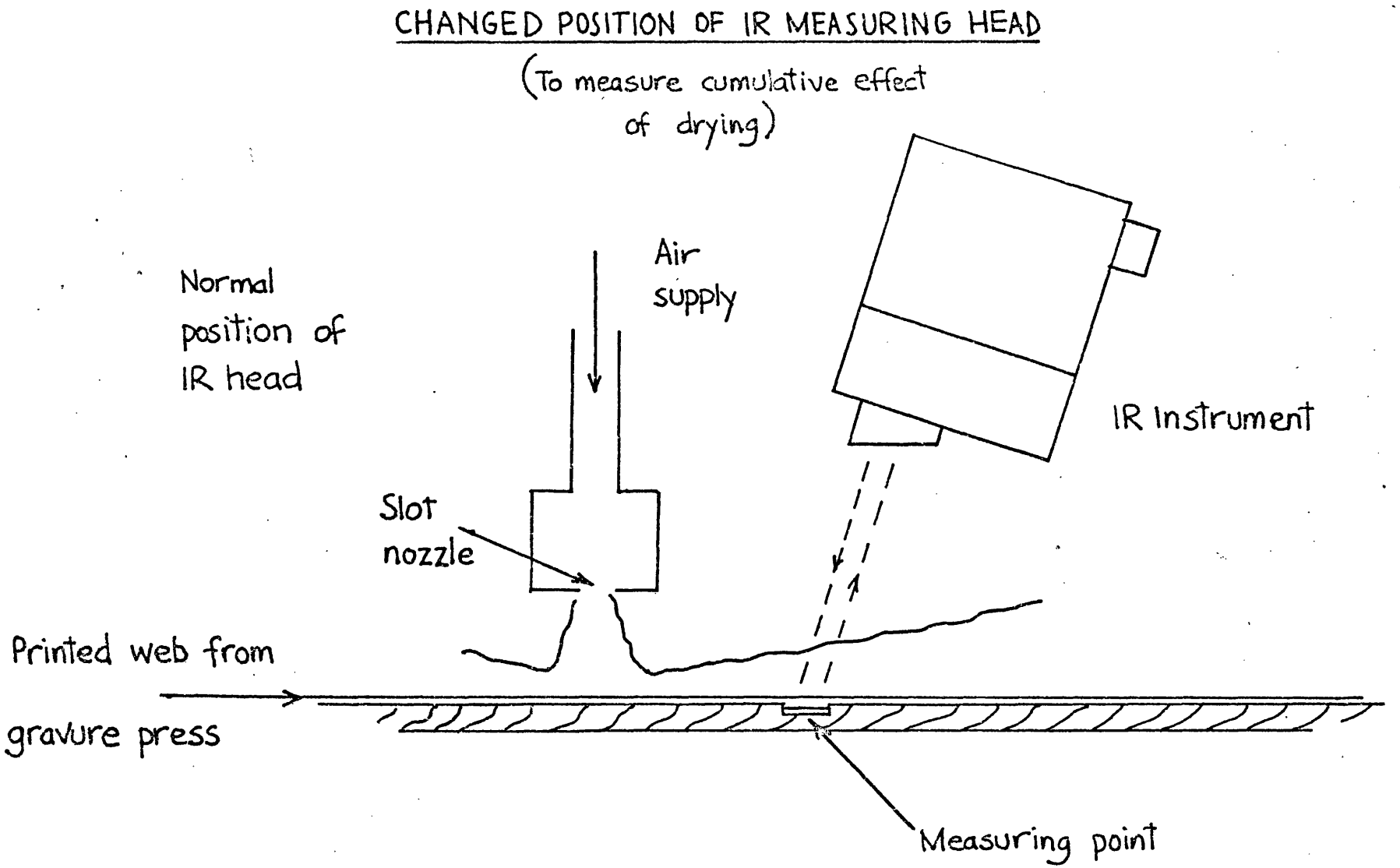
CHANGED POSITION OF IR MEASURING HEAD
(To measure cumulative effect of drying)
Normal position of IR head
Air supply
IR Instrument
Slot nozzle
Printed web from gravure press
Measuring point

FIGURE 7.4

CUMULATIVE DRYING EFFECT OF A SINGLE NOZZLE

THE EFFECT OF AIR VELOCITY

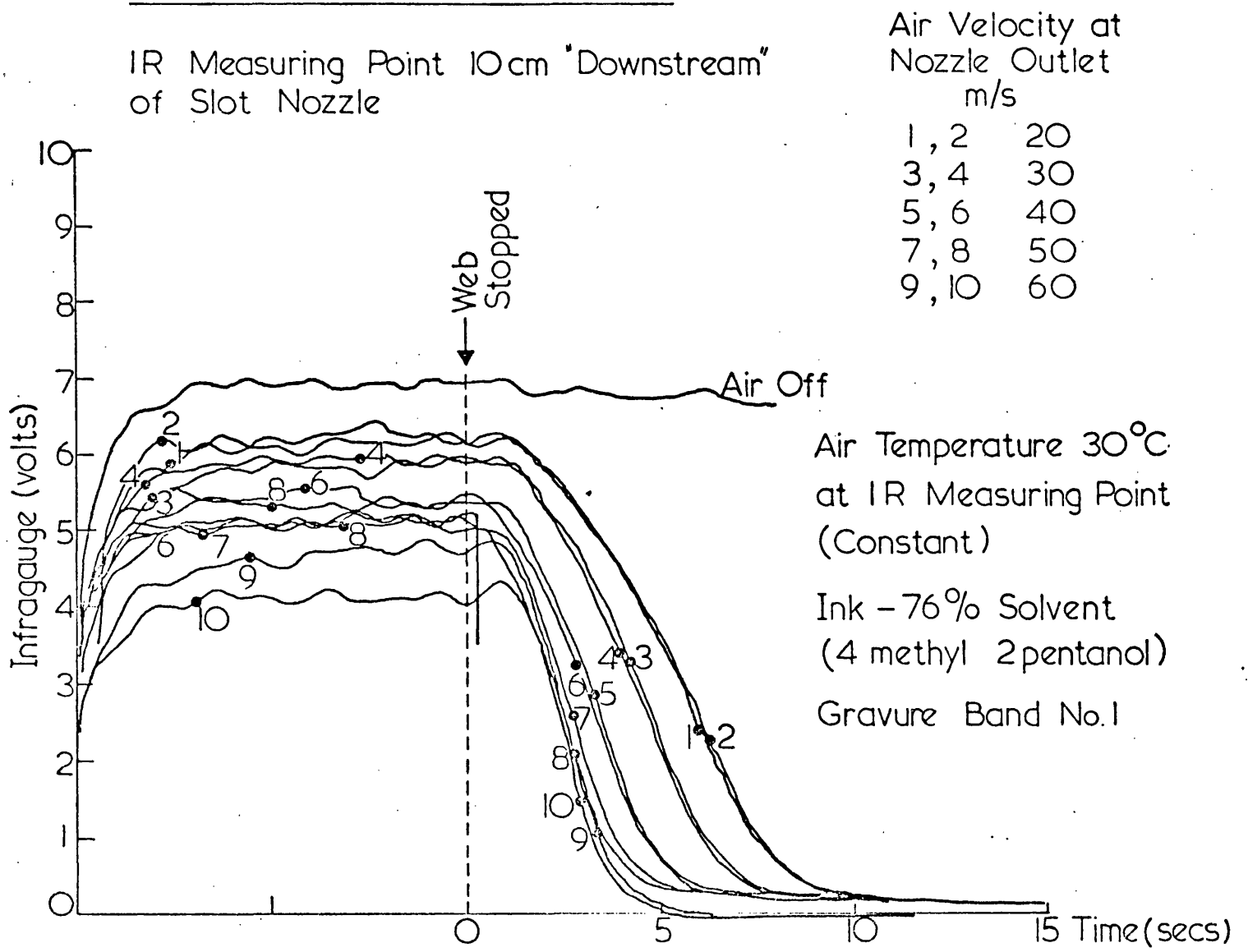

FIGURE 7.5

CUMULATIVE DRYING EFFECT OF A SINGLE NOZZLE

THE EFFECT OF TEMPERATURE

IR Measuring Point 10 cm "Downstream" of Slot Nozzle

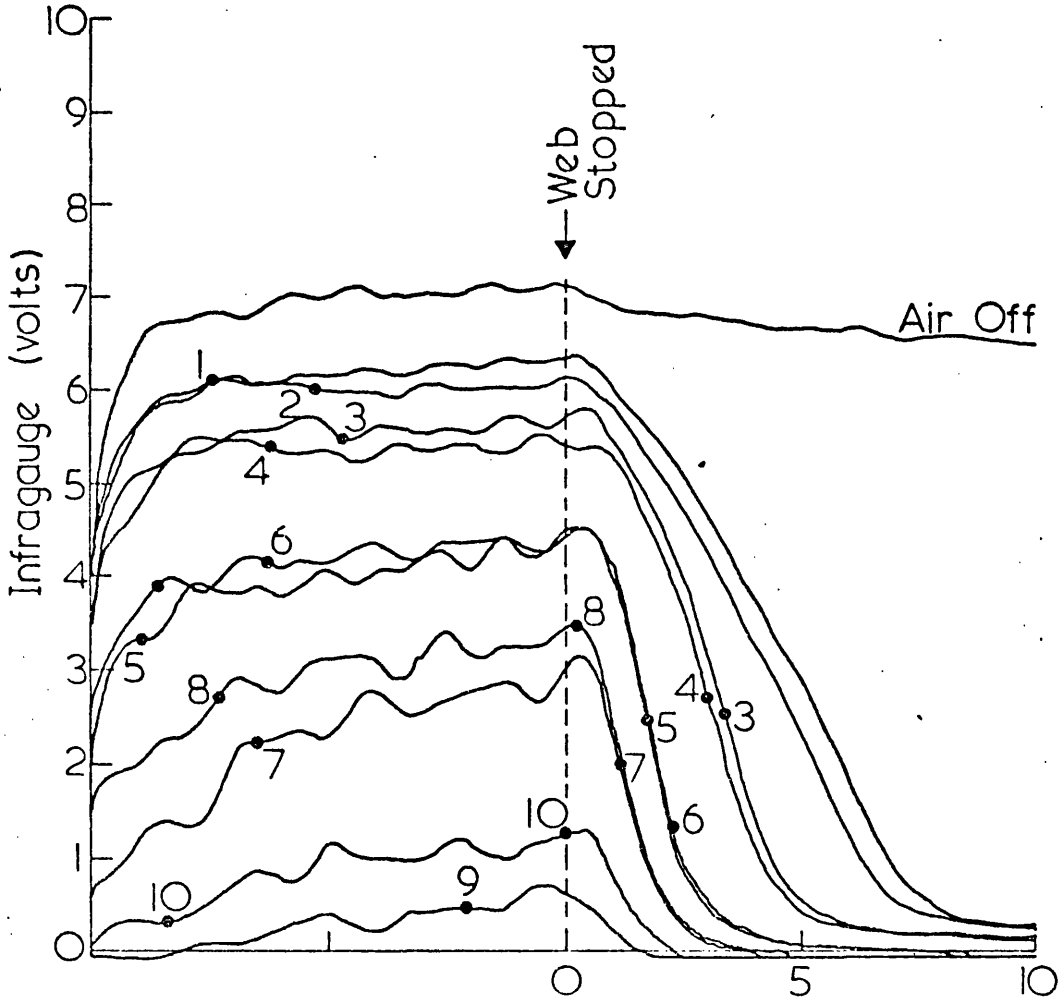

Air Temperature at IR Measuring Point	°C
1 , 2	30
3 , 4	40
5 , 6	50
7 , 8	60
9 , 10	70

Air Velocity 20 m/s at Nozzle Outlet (Constant)

Ink – 76 % Solvent (4 methyl 2 pentanol)

Gravure Band No. 1

FIGURE 7.6

CUMULATIVE DRYING EFFECT OF A SINGLE NOZZLE

IR Measuring Point 10 cm "Downstream" of Slot Nozzle

	Air Velocity m/s	Air Temp C
1 and 2	20	25
3 , 4	30	25
5 and 6	40	25
7 , 8	50	25
9 , 10	60	25
11 , 12	60	28
13 , 14	60	40
15	60	60

Ink 76% Solvent (4 methyl 2 pentanol)

Gravure Band No. 3

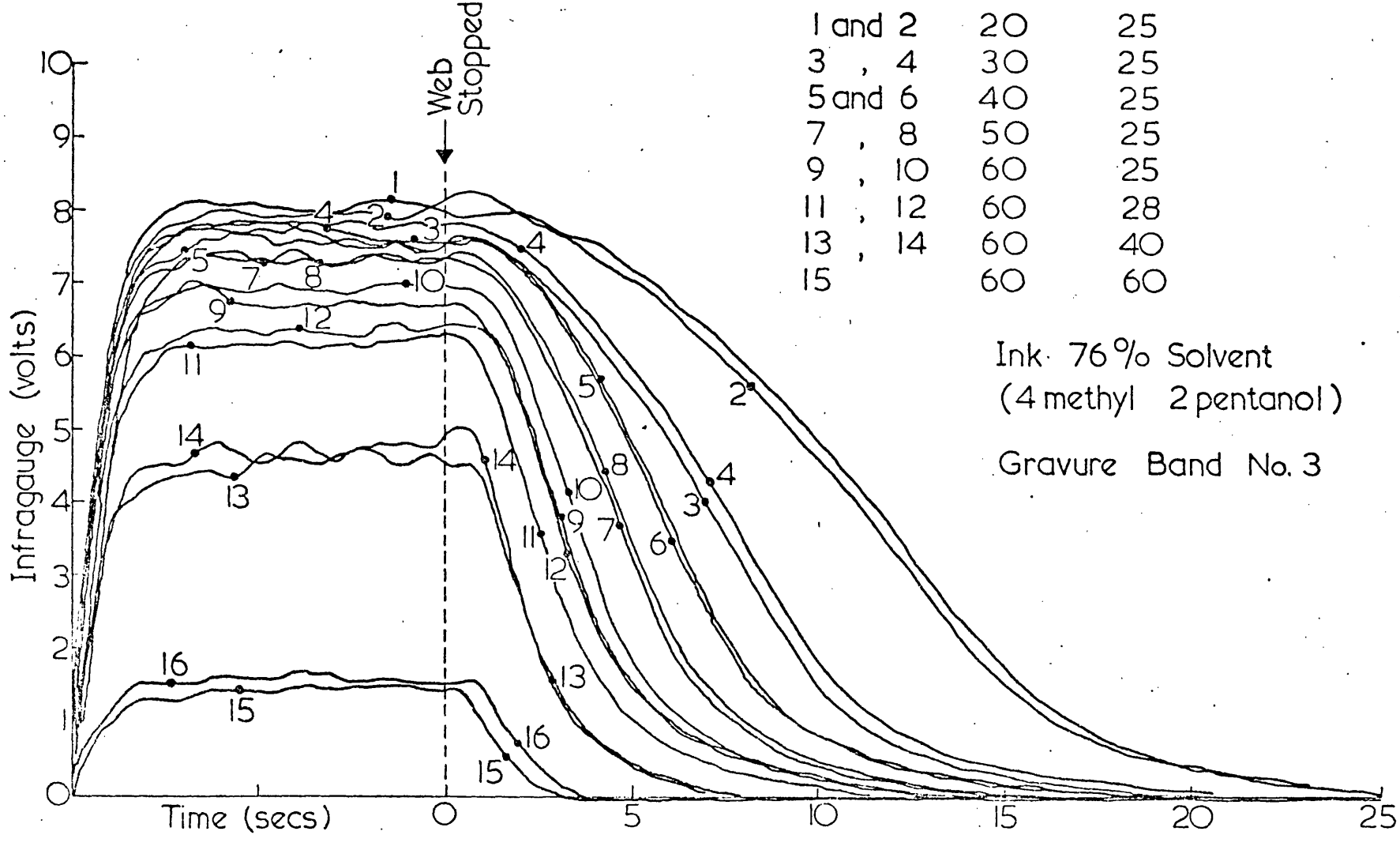

FIGURE 7.7

FIGURE. 7.8 DISTRIBUTION OF h_x AND T_A FOR COMPUTER PROGRAM OF APPENDIX 2

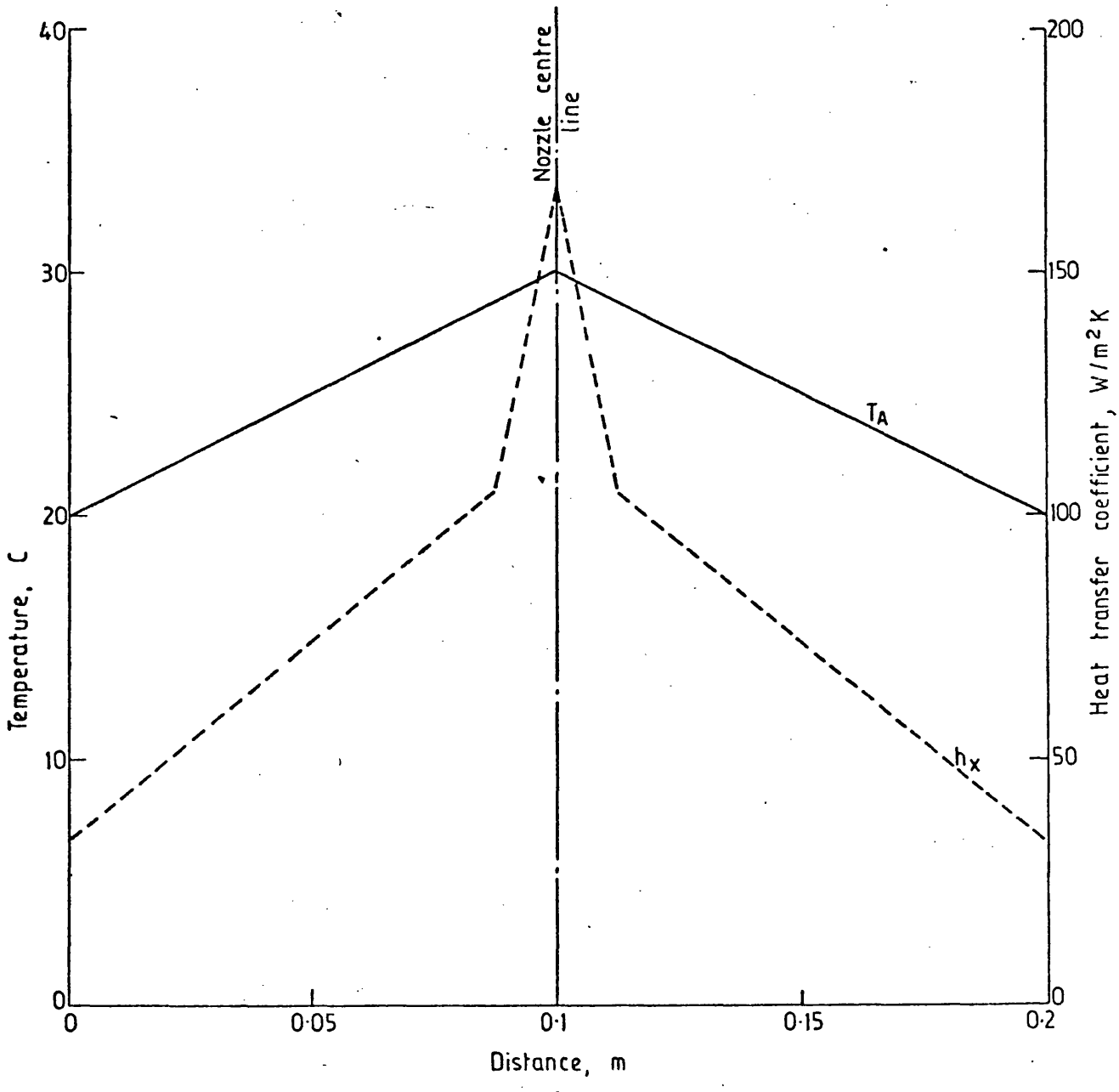

FIGURE 7.9 TRANSIENT TEMPERATURE DURING DRYING

Gravure band no. 1

4 methyl 2 pentanol

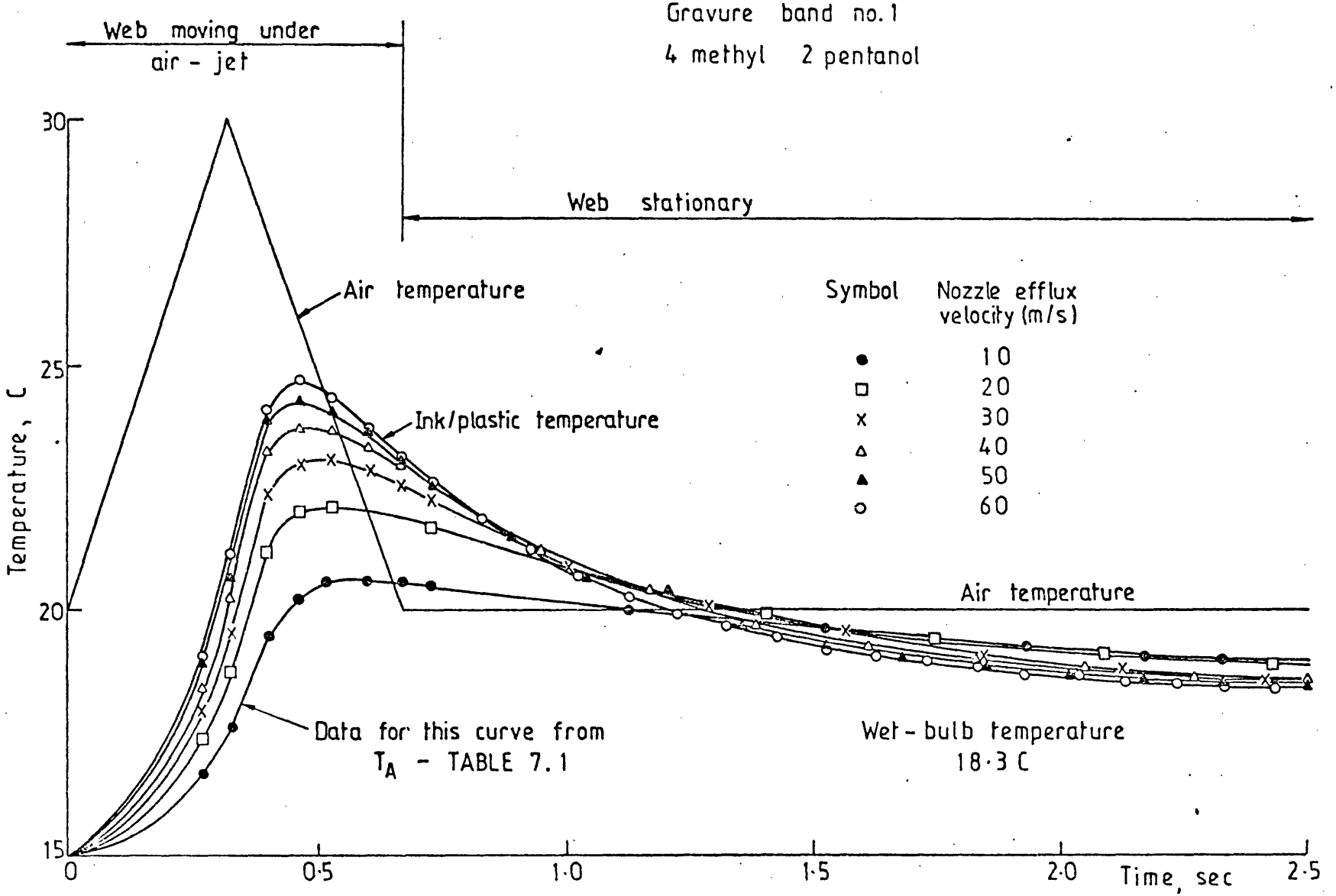

FIGURE 7.9

8. FALLING-RATE INK DRYING - DIFFUSION IN POLYMERS

8.1 Introduction

The experiments described in previous chapters have confirmed that when the drying is externally controlled, the rate of ink-drying is largely unaffected by the nature of the non-volatile constituents of the ink. This is no longer the case in the falling-rate period of drying. In this period, the solvent molecules must pass through the solidifying layer of non-volatiles and it is the resistance to this movement which controls the drying rate. Results from the present research are consistent with the premise that solvent is transferred through the residual ink film, by diffusion.

The writer has made some effort to relate this ink-drying research to generally accepted drying theory, eg. Keey (51), but this objective has proved difficult to attain. The reason for this is that drying theory is largely concerned with the transfer of water by capillary action through relatively large porous bodies. The fundamental difference in the transfer process upon which normal drying theory is based has prevented its detailed use in this research. However the theory has provided both a conceptual framework and some useful concepts.

To provide insight into the solvent-in-polymer diffusion process, attention was turned to research being actively pursued in the field of plastics technology. This research is authoratatively reviewed in the monograph edited by Crank and Park (52). Surprisingly perhaps, relevant research in the field of paint technology appeared to be less useful, in that it was more empirical in nature. This may have been because the more basic research was not readily accessible to an engineer.

In a review article, Park (53) has stressed the fundamental role of molecular transport for plastics technology,

> "Transport of low molecular weight materials through polymer layers is important in every stage of surface coating. Thus the rate of drying of a paint film is controlled almost entirely by the rate of migration of solvent to the surface, while the protective action of the coating results mainly from its action as a barrier to the transport of water, oxygen and other agressive materials"

The various theories of molecular migration through polymers described in Crank and Park (52), Park (53), Rogers (54) etc., are all based on diffusion as the transport mechanism.

To gain insight into the solvent diffusion process it is necessary to study the physics and chemistry of the ink at the molecular level. Liquids and materials such as plastics and rubbers have similar physical structures, in that they consist of random arrangements of closely packed molecules. According to Rogers (54), "Solubility and transport in amorphous elastomers appear to be quite similar to the corresponding processes in low molecular weight liquids". For this reason, and because initially the ink is in the liquid state, the review of relevant diffusion theory set out in this chapter, begins by briefly describing diffusion in liquids.

The diffusion of solvents through polymers is first described qualitatively. The research referred to above has shown that diffusion through plastics can be explained in terms of the "Free-volume Theory". Ths theory is used here to obtain relations which

express the manner in which the diffusion coefficient changes with solvent concentration and temperature. These expressions are then available for incorporation into a theoretical solution of the diffusion equation which is developed later in Chapters 9 and 10. Later still these theoretical predictions are compared with experimental data in Chapter 11.

A word of caution must be inserted at this point. Diffusion of an organic solvent through a high polymer is an extremely complicated physico/chemical process. Because of this, it is not possible in practice, to deduce equations to predict numerical values of the diffusion coefficient for a particular solvent/polymer system. Nor, in general, are these values available from empirical measurements.

The more general aspects of drying theory are taken up again in Chapter 11, where they are used in an attempt to correlate experimental drying curves in the falling rate region.

8.2 General Description of Diffusion Within the Ink Layer

Within homogeneous mixture such as solutions and gels, matter transfer takes place by diffusion. In this research, the ink consisted of a finely ground pigment uniformly distributed through a solution of a resin in a solvent. Thus the capillary porous model upon which a great deal of drying theory is based, was inappropriate. Instead the following simple homogeneous model of the ink layer is proposed. The pigment particles are inert and impervious to solvent; therefore they are considered as a separate phase and excluded from consideration. Similarly, measurements have shown the polypropylene substrate to be impervious to solvent penetration, and this may be excluded from the

model. The resin is a high molecular weight polymer, through which the solvent, of relatively low molecular weight, is transferred by diffusion. In the falling-rate region, the rate of drying is limited by the rate at which solvent can diffuse through the polymer to the free surface.

In practice, during the initial period of drying the mixture consists largely of solvent. The above model is assumed to apply to this period, with the diffusion coefficient having a suitably large value. As the limiting case of pure solvent is approached, the value of the diffusion coefficient should approach that of the self-diffusion coefficient of pure solvent. It should be borne in mind, however, that this early period has already been treated under constant-rate drying.

8.3 Review of Research into "Retained Solvents" in Paint Films

It is characteristic of diffusion controlled drying processes that the drying rate diminishes exponentially with time. In ink drying this undesirable characteristic is exercerbated, because, research has shown, that solvent-in-polymer diffusion coefficients are markedly concentration dependent. In such conditions, the last vestiges of solvent are usually extremely difficult to remove from the so-called "dry" ink layer.

Solvent retained by coatings can cause a variety of practical problems, Nunn and Newman (55). Solvent release is a major factor in determining the maximum film thickness that can be laid down in a single application. A slow rate of solvent release may require an excessively long time before the applied coat achieves the desired degree

of hardness and water resistance. In the food-packaging industry, to avoid problems of odour or taint, it is common practice to specify that only quite minute quantities of solvent remain in the ink after drying. It is worth noting that the usual method of increasing the drying rate by increasing the air jet velocity will have no effect in this situation. It can be seen that the problem of retained solvents is an important industrial problem.

The problem of retained solvent has received the attention of a number of workers in the paint industry, but until comparatively recently the controlling factors remained unresolved. For example it was thought that a "strong" solvent for a polymer would be preferentially retained by that polymer. The volatility of the solvent and hydrogen bonding are two other factors which were thought to influence solvent retention.

In a systematic series of experiments Hansen (56) measured drying rates and solvent retention, and estimated diffusion coefficients for selected solvents and polymers. The only consistent conclusion from the data was that solvent retention was caused by a low solvent diffusion coefficient. Hansen also demonstrated that solvent diffusion coefficients were primarily dependent on molecular geometry. None of the factors suggested in the previous paragraph appeared to affect the value of the diffusion coefficient. In reporting his theoretical investigations, Hansen (57) stated that solvent loss during the falling-rate period of lacquer drying is controlled by solvent-in-polymer diffusion coefficients. In these investigations he used a diffusion coefficient which was exponentially dependent upon solvent concentration (see equation 8.4.9). Nunn and Newman (58) report, that

the results of their retention experiments can be explained on the basis that, in the falling-rate period the rate of solvent release is diffusion controlled.

8.4 Diffusion in Liquids

General

Because of the dense packing of liquid molecules and the force fields which exists between them, diffusion coefficients of liquids are numerically smaller than for low pressure gases. Also in contrast to gases, diffusion coefficients in liquids often show a marked variation with concentration. The theory of the liquid state has not yet been developed to a level where fundamental molecular data can be used with confidence to predict values of the transport properties.

To establish some fundamental definitions and relationships, this review of diffusion begins with a physical treatment of particle transport.

Movement of a particle in a field of force

Consider the movement of charged particles (ions) in a fluid, under the action of an electrical field of strength E. Each particle experiences a force F' given by

$$F' = Z\ e\ E \qquad 8.4.1$$

Z = number of electrical charges on ion

e = charge on an electron

The particles are accelerated to a steady drift velocity ν, at which point the applied force F' is equal and opposite to the drag force. The mobility of an ion, m, is defined as its drift speed in a field of unit strength

$$m = \frac{\nu}{E} \qquad 8.4.2.$$

using equation 8.4.1 $\qquad \nu = \frac{mF'}{Ze} \qquad 8.4.3$

Assuming that the particle is sufficiently large for the surrounding medium to be treated as a continuum then Stokes's Law applies

$$F' = 6\pi r \mu \nu \qquad 8.4.4$$

r = radius of particle

μ = viscosity of fluid

Stoke's Law then yields an equation for the mobility

$$m = \frac{Ze}{6\pi r \mu} \qquad 8.4.5$$

Thermodynamic basis of diffusion

Diffusion is a spontaneous movement of particles to reduce the concentration gradient and to produce equilibrium. Thermodynamics teaches, Atkins (59), that a system may undergo a spontaneous change of state only if the net result of this change is to bring about a reduction in the chemical potential of the system. The amount of work required to move 1 mole of material against a gradient of chemical potential is

$$dW = \frac{d\mu}{dy}\ dy \qquad 8.4.6$$

μ = chemical potential, J/mol

W = work, J/mol.

From mechanics the analgous equation for work done is

$$dW = -F\ dy \qquad 8.4.7$$

F = force, N/mol

Comparison of equations 8.2.6 and 8.2.7 shows that the gradient of the potential plays the role of a force

$$F = -\frac{d\mu}{dy} \qquad 8.4.8$$

The thermodynamics of diffusion is set out rigorously by Tyrell (60).

The chemical potential μ of the solute in an ideal solution is defined by

$$\mu = \mu^{o} + RT \ln x \qquad 8.4.9$$

μ^{o} = chemical potential in the standard state, J/mol

x = mol fraction of solute

Equation 8.4.9, when substituted into equation 8.4.8, gives the force on a molecule

$$F' = \frac{RT}{Lc}\frac{dc}{dy} = -\frac{kT}{c}\frac{dc}{dy} \qquad 8.4.10$$

c = concentration of solute, mol/m^3

k = Boltzmann's constant = R/L = $1.38.10^{-23}$ J molecule/K

L = Avogadro's number, molecules/mol

The drift velocity ν may be interpreted as a flux of molecules

$$J' = \nu\, c\, L \qquad 8.4.11$$

J' = molecular flux, $molecules/m^2$ s

Fick's Law may also be written to express the flux of molecules

$$J' = -D\, L \frac{dc}{dy} \qquad 8.4.12$$

Equating equations 8.4.11 and 8.4.12 and also using equation 8.2.10

$$\nu = -\frac{D}{c}\frac{dc}{dy} = D\frac{F'}{kT} \qquad 8.4.13$$

The friction coefficients f' and f

Some of the previous equations may be written in terms of a molecular friction coefficient f', which is defined as the force required to maintain a particle at unity velocity

$$f' = \frac{F'}{\nu} \qquad 8.4.14$$

From equations 8.3 and 8.13

$$f' = \frac{Ze}{m} = \frac{kT}{D} = \frac{RT}{LD} \qquad 8.4.15$$

The molar friction factor f is defined by the equation

$$f = Lf' \qquad 8.4.16$$

The intrinsic mobility m_I is the reciprocal of f

$$m_I = \frac{1}{f} = \frac{m}{ZEL} = \frac{D}{RT} \qquad 8.4.17$$

Hydrodynamic equations for the diffusion coefficient

Equations 8.4.3 and 8.4.13 are both expressions for the drift velocity and may therefore be equated to yield the Einstein relation

$$D = \frac{mkT}{Ze} = \frac{kT}{f'} = m_I RT \qquad 8.4.18$$

Substituting for the mobility obtained from Stoke's Law, equation 8.4.4, yields the Stokes/Einstein equation

$$D = \frac{kT}{6\pi r\eta} \qquad 8.4.19$$

Both these expressions are hydrodynamic in character, in that they are based on the assumption of a large particle moving through a continuum. Thus they are suitable for large isolated particles diffusing in a dilute solution.

If the Stokes/Einstein relation remains valid for molecules of equal size, then it may be used to predict the self-diffusion coefficient of a pure liquid, D_{AA}. For molecules arranged in a close packed cubic lattice, then from Treybal (61)

$$D_{AA} = \frac{kT}{2\pi\mu}(cL)^{\frac{1}{2}} \qquad 8.4.20$$

Non-ideal solutions

The activity satisfies the following definition

$$a = \gamma x$$

a = activity

γ = activity coefficient (unity for ideal solutions)

For non-ideal solutions the chemical potential may be written in terms of the activity

$$\mu = \mu^{o} + RT \ln a \qquad 8.4.21$$

Using the drift velocity ν to express a molar flux J

$$J = \nu c$$

Obtaining ν from equation 8.4.13 and using equation 8.4.8

$$\nu = \frac{DF}{RT} = - D \frac{d}{dy} (\ln a)$$

substitution gives

$$J = - D \frac{d(\ln a)}{d(\ln c)} \frac{dc}{dy} \qquad 8.4.22$$

In the real solution the diffusion coefficient is defined by Fick's Law

$$J = - D_{AB} \frac{dc}{dy} \qquad 8.4.23$$

comparing equations 8.4.22 and 8.4.23

$$D_T = D_{AB} \frac{d(\ln c)}{d(\ln a)} \qquad 8.4.24$$

The diffusivity D_T is sometimes called either the activity corrected diffusion coefficient or the thermodynamic diffusion coefficient. It is often less sensitive to changes in composition than D_{AB}.

8.5 Diffusion in Polymer Membranes - Physical Description

General

Transport of low molecular weight substances through polymer (plastic or rubber) membranes has been extensively studied because of the industrial importance of polymers as barriers. This research has shown that the degree of interaction between penetrant and polymer varies markedly and that this interaction affects the diffusion coefficient. It is helpful to classify low molecular weight penetrants into three groups:-

a) Permanent gases

Because of their low solubility, permanent gases interact little with the polymer and hence their diffusion coefficients are not markedly dependent upon concentration.

b) Liquids and vapours

Compared with simple gases, liquids and vapours have both higher molecular weights and higher solubility. Consequently their diffusion coefficients are both lower than those of simple gases and concentration dependent.

c) Water

It appears that water constitutes a unique solvent because of the molecular interactions which arise from hydrogen bonding.

Further discussion will be limited to the subject of diffusion of solvents in polymers.

Solubility and Permeability

Experimental research on diffusion in polymers is frequently concerned with the problem of steady (or unsteady) absorption (or desorption) of a solvent by a membrane. According to Kishimoto (62), when a pressure difference causes permeation through a polymer film, the condensed penetrant dissolves at one surface of the film, diffuses through the barrier, and evaporates from the other surface at the low pressure side.

Consider unit area of polymer film of thickness, H. The equilibrium concentrations of penetrant in the surface layers C_1 and C_2 are related to the partial vapour pressures p_1 and p_2 by the solubility relation

$$C = S\ p \qquad 8.5.1$$

s = solubility coefficient

When Henry's Law is obeyed s is a constant

The flux of pentrant J through the film may be written

$$J = \frac{-P\ (p_2 - p_1)}{H} \qquad 8.5.2$$

P = permeability constant

H = film thickness

Before equation 8.5.2 can be used to determine the diffusion coefficient D solubility data must be known. For the case when Henry's is obeyed and D is constant, then

$$P = D\,S \qquad 8.5.3$$

Molecular description of diffusion

The microscopic movements of the polymer molecules constituting the membrane, profoundly influence the rate of diffusion. Macromolecules are built up from monomer units, or segments, into a chain-like structure. In amorphous polymers, the type used in this research, the polymer chains are intermingled in a tangled, disorderly manner. Intuitively it can be seen that the ease with which a pentrant molecule can migrate through such a structure will depend upon the amount of free space available within the tangled chains. Also, the ability of the chain to flex in response to random thermal fluctuations and so redistribute the free volume, will influence the ease of migration. A tightly packed, highly ordered and inflexible molecular structure is associated with low penetrant diffusivity.

In a random arrangement of molecules, migration of an individual molecule is prevented by the cage of molecules which surround it. Random thermal motions rearrange the positions of molecules and "holes" in the cage are continuously being created and destroyed. Provided the hole is of sufficient size and the molecule has sufficient energy to occupy it, diffusive transport will take place. The amount of energy required to form a hole will be proportional to the size of the hole. Thus, consequent upon Boltzmann's Law, the number of holes should decrease exponentially with their size. This migratory movement of particles is regarded by some investigators as

a sequence of jumps; during each jump the particle passes over a potential barrier separating one position from the next, Rogers (54).

The relation of free volume to the glass transition temperature

The physical properties of amorphous polymers change significantly over a small range of temperature termed the glass transition temperature T_g. Below T_g, the polymer is a hard, brittle and glassy substance, while above T_g it is a soft, pliable and rubbery material. In particular it is found that the rate of increase of specific volume with temperature is much greater above T_g than below it. This phenomenon has the following explanation. Below T_g polymer chain molecules are immobilised and thermal movements are restricted to vibrations about an equilibrium position. Above T_g the expansion of the polymer chain is sufficient to permit motions of chain segments.

At a particular temperature, the free volume within a polymer v_f may, in principle, be defined as follows:-

$$v_f = v - v_o \qquad 8.5.3$$

v = specific volume of system

v_o = volume occupied by molecules

The fractional free volume f is defined as

$$f = \frac{v_r}{v_o} = \frac{(v - v_o)}{o} \qquad 8.5.4$$

A rigorous operational definition of free volume presents difficulties, but conceptually it is related to the hole concept in the theory of

liquids. The total free volume is the sum of two sub-volumes:-

i) The interstitial volume within the chains themselves. Segmental motion causes a redistribution of this volume. A relatively greater proportion of free volume is associated with chain ends.

ii) The holes and vacancies between chains.

It has been suggested by Kummins and Kwei (63) that, at temperatures above T_g, the diffusion rate of organic vapour in a polymer is primarily controlled by the mobility of the polymer segmental units. In turn, this segmental mobility is a function of the free volume of the system.

8.6 Free Volume Theory of Diffusion of Organic Pentrants in Polymers

Introduction

Experimental researches show that when a penetrant is a good solvent for the polymer, the diffusion coefficient of the system is usually markedly dependent upon concentration level. Various explanations of this dependency have been advanced. For example equation 8.4.24 shows the thermodynamic diffusion coefficient D_T to be a product of D_{AB} and a term d(ln c)/d(ln a) which describes the non-ideality of the solution. It appears that this correction for non-ideality is seldom of sufficient magnitude to account for the observed concentration dependency of the diffusion coefficient, Fujita (64).

According to Rogers (54) good solvents swell and plasticize the polymer structure leading to increased mobility of both polymer segments and penetrant molecules. Solvents or plasticizers (a low molecular weight substance added to a polymer to soften it) separate

the polymer chains and so decrease the cohesive interactions between them.

Although there is agreement that hole formation is required before a diffusion jump can occur, there are two principal theories of hole formation. In the first, the formation of an hole requires an activation energy; only those processes which possess the activation energy are permitted. In the second, the free volume theory, the total free volume within the polymer structure may be redistributed according to probability theory. Because it is successful and increasingly used, and because it offers an elegantly simple physical model of transport processes, a brief account of free volume theory will be given.

Unfortunately, despite a detailed literature search, telephone discussions with the manufacturer of the resin and a visit to a leading researcher in this field, it proved to be not possible to use free volume theory to deduce quantitative equations for the diffusion coefficient. However the theory does form a basis for the semi-empirical equations for the concentration dependency of the diffusion coefficient.

Free Volume Theory

Doolittle (65) appears to have been the first to propose that the free volume concept could be used, on an empirical basis, to correlate viscosity data of oil. Various theoretical treatments have stemmed from this proposal. The free volume theory of Fujita (64) is widely used, and it is this version which is briefly outlined here. The starting point is the demonstration by Cohen and Turnbull (66) that, for a liquid composed of identical molecules, the probability P of

finding a free volume exceeding a given value v^* is

$$P = \exp\left(-\frac{b\,v^*}{\bar{v}}\right) \qquad 8.6.1$$

$\bar{v}$ = average free volume of one molecule

b = numerical factor of order unity

Fujita assumes that equation 8.6.1 may be applied to polymer/diluent mixtures and that the product $b\,v^*$ may be written B and interpreted as a measure of hole size.

$$P = \exp\left(-\frac{B}{f}\right) \qquad 8.6.2$$

f = average fractional free volume of system (equation 8.5.4)

The mobility of a diluent (solvent) molecule should be proportional to the probability that this molecule finds in its vicinity a hole large enough to permit a diffusion jump. Let B correspond to the minimum value of B which will permit this jump

$$m_I = A \exp(-B/f) \qquad 8.6.3$$

m_I = intrinsic mobility

A = proportionality factor (largely dependent upon size and shape of penetrant molecule)

Using the relation between D and m_I, equation 8.4.17, yields

$$D = RTA \exp(-B/f) \qquad 8.6.4$$

D is the diffusion coefficient relative to a fixed polymer network. From equation 8.6.4. it is immediately apparent that D will decrease with increasing size of diffusant. Equation 8.6.4 will be used to deduce the effect on D of changes both in diluent concentration and in temperature.

Concentration dependence of D

Experiments show that the addition of a low molecular weight solvent increases polymer segmental mobility. This is manifest as an increased mobility of solvent molecules. This can be explained in the basis that, because of their small size, the addition of solvent molecules to a polymer increases the average free volume of the system.

Assume that the fractional free volume in the system increases linearly with solvent volume fraction V_s

$$f = (1 - V_s)\, f_o + V_s\, f_s = f_o + \beta V_s \qquad 8.6.5$$

f_o = average fractional free volume of pure polymer at T_o

f_s = average fractional free volume of pure solvent at T_o

$\beta = f_s - f_o$

The introduction of equations 8.6.5 into equation 8.6.4 gives

$$D = RTA \exp\left(-\frac{B}{f_o + \beta V_s}\right) \qquad 8.6.6$$

which, after some manipulation, yields

$$\ln (D/D_o) = \frac{B\, \beta\, V_s}{f_o^{\,2} + f_o \beta\, V_s} \qquad 8.6.7$$

D_o is the value of D extrapolated to zero penetrant concentration.

At low concentrations equation 8.6.6 reduces to

$$\ln (D/D_o) = \frac{B \beta V_s}{f_o^2} \qquad 8.6.8$$

In many cases these equations represent the experimental data quite well; indeed at low concentrations the data is usally correlated by exponential formulae of the form

$$D = D_o \exp (C V_s) \qquad 8.6.9$$

where C is a constant.

It is perhaps worth noting that equation 8.6.8 is similar in form to the equation proposed by Doolittle (65) to correlate viscosity data of oil. Indeed the whole point of dissolving the polymer in a solvent is to lower the viscosity so that the mixture can be printed.

Glass transition temperature

The glass-transition temperature T_g marks the onset of segmental mobility for a polymer. In a mixture of two substances of different T_g, each should contribute to the free volume of the system in proportion to the amount of each substance present. Thus T_g for a mixture of solvent and polymer should be the weighted average of the T_g of the components, Rodriguez (67). The addition of a solvent to a polymer lowers the glass transition temperature because the smaller solvent molecules have proportionately more free volume associated with their free ends. Machin and Rogers (59) discuss various theoretical attempts to quantify this effect.

Temperature dependence of D

Because of thermal expansion, the fractional free volume f is expected to increase with temperature in the following manner

$$f - f_g = \Delta\alpha(T - T_g) \qquad 8.6.10$$

f = fractional free volume of pure polymer at T

f_g = fractional free volume of pure polymer at T_g

$\Delta\alpha$ = the difference in thermal expansion coefficient of pure polymer above and below T_g

Introducing equation 8.6.10 into equation 8.6.4 gives

$$D = RTA \exp\left(- \frac{B}{(f_g + \Delta\alpha(T - T_g))}\right) \qquad 8.6.11$$

which, after some manipulation, yields

$$\ln (D/D_g) = \frac{B\ \alpha\Delta(T - T_g)}{f_g^{\,2} + \Delta\alpha(T - T_g)}$$

where D_g is the value of D at T_g

It has been found that, over a restricted range, experimental data can frequently be correlated by plotting ln D against 1/T. This has lead to the view that diffusion may be regarded as a thermally activated process with the relation between D and T expressed by an equation of the Arrhenius type

$$D = D_o \exp\ (-\ E/RT)$$

where D_o and E are constants for a particular polymer. E may be

regarded as an activation energy for hole formation. The theory of Fujita can be used to deduce equations for the activation energy, Machin and Rogers (68).

Restriction on free-volume theory

The free volume theory of Fujita strictly applies at temperatures above the glass transition temperature, and there are two main reasons for this. First, it can be agreed that the free volume is zero at T_g. Second, below T_g, lattice relaxation times may be longer than molecular migration times and consequently free volume cannot be re-distributed. However later developments, such as Machin and Rogers (68), extend Fujita's basic approach by applying it above and below T_g.

9. FALLING RATE DRYING - THE DIFFUSION EQUATION

9.1 Introduction

The evidence presented in the previous chapter indicated that in the later stages, the rate at which an ink film dries is governed by the rate of diffusion of solvent to the surface. This evidence also showed that, in practical situations, the diffusion coefficient is concentration dependent. Incorporation of a concentration dependent diffusion coefficient into the diffusion equation renders this equation non-linear and consequently increases the difficulty of solution.

In this chapter analytic solutions of the diffusion equation with a constant diffusion coefficient are presented to clarify dimensionless variables and boundary conditions. It is demonstrated that the exponential form of the concentration dependency of the diffusion coefficient allows a transformation of the equations which simplifies subsequent numerical analysis. Finally the transfored equations are converted into finite-difference form preparatory to their incorporation in a computer program in Chapter 10.

9.2 The Diffusion Equation

The general differential equation of mass transfer expresses conservation of substance for a control volume of differential extent. Using a cartesian co-ordinate system, the diffusive transfer of component A in the x-direction is shown below

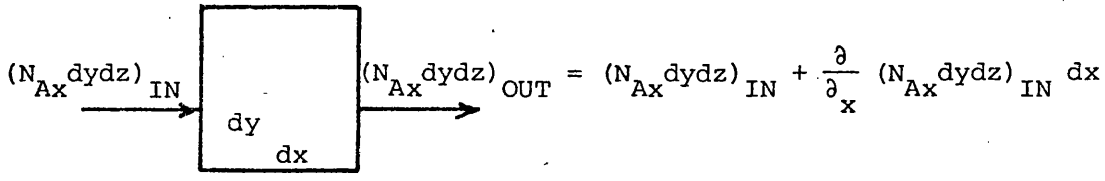

For the x-direction, the net rate of transfer of component A into the control volume is

$$-\frac{\partial}{\partial x}(N_{Ax}dydz)$$

and similar expressions may be written for the y and z directions. In the absence of chemical reactions, the rate of accumulation of A within the control volume is

$$dxdydz\ \frac{\partial c_A}{\partial t}$$

Hence, conservation of mass gives immediately

$$\frac{\partial N_{Ax}}{\partial x} + \frac{\partial N_{AY}}{\partial y} + \frac{\partial N_{AZ}}{\partial z} + \frac{\partial c_A}{\partial t} = 0 \qquad 9.2.1$$

N_{Ax}, N_{AY} and N_{AZ} are the rectangular components of the mass flux vector N_A. Expressing N_A by means of equation 3.3.2 and for conciseness adopting vector notation

$$\nabla \cdot x_A N - \nabla \cdot c D_{AB} \nabla x_A + \frac{\partial c_A}{\partial t} = 0 \qquad 9.2.2$$

Equation 9.2.2 is the general form of the binary diffusion equation.

Particular forms of the general diffusion equation are valid for important special cases. For example for stationary systems where the overall concentration may be considered constant, then

$$\nabla \cdot D_{AB} \nabla c_A = \frac{\partial c_A}{\partial t} \qquad 9.2.3$$

and for one-dimensional diffusion in cartesian co-ordinates.

$$\frac{\partial}{\partial x}\left(D_{AB}\frac{\partial c_A}{\partial x}\right) = \frac{\partial c_A}{\partial t} \qquad 9.2.4$$

If the diffusion coefficient is constant

$$D_{AB}\frac{\partial^2 c_A}{\partial x^2} = \frac{\partial c_A}{\partial t} \qquad 9.2.5$$

Equation 9.2.5 is sometimes referred to as Fick's Second Law or simply as the diffusion equation. In the above equations the concentration c has been expressed in molar units, but it is apparent that equations 9.2.4 and 9.2.5 remain valid irrespective of the units of c. Later, when these equations are converted into dimensionless form, the symbol C will be used to express the dimensionless concentration.

Equation 9.2.4 is the starting point of the computer program.

9.3 Classical Solutions when the Diffusion Coefficient is Constant

The authoratative monograph by Crank (69) constitutes an invaluable compendium of solutions of the diffusion equation, from which the classical equations of this section have been drawn. It is easy to see by differentiation that

$$c = \frac{A}{t^{\frac{1}{2}}}\exp\left(-x^2/Dt\right) \qquad 9.3.1$$

where A is an arbitrary constant, is a solution of the diffusion equation (equation 9.2.5). The constant A may be evaluated for the case of a mass m deposited at time t = 0 in the plane x = 0, to give

$$c = \frac{m}{2(\pi Dt)^{\frac{1}{2}}}\exp\left(-x^2/4Dt\right) \qquad 9.3.2$$

The principle of superpostion, can then be used to build up solutions for more complex situations by infinite sums of the elemental solution, equation 9.3.2. These integrals are conveniently expressed in terms of the error function (a standard mathematical function written erf Z) and the dimensionless variable $x/\sqrt{Dt}$. This type of solution is most suitable for evaluation at small times. In a finite medium, this is equivalent to limiting its use to the early stages of diffusion when penetration is localised and the body can, for practical purposes, be treated either as an infinite or semi-infinite medium.

Alternatively the diffusion equation can be solved by the method of separation of the variables to yield solutions in the form of trigonometrical series. Of interest for drying is the case of diffusion from a plane slab of thickness 2L in which the diffusing substance is initially at a uniform concentration c_o and at zero time the surface concentrations are reduced to a constant value of c_1. For this case the solution is

$$\frac{c - c_1}{c_o - c_1} = \frac{4}{\pi} \sum_{n=o}^{\infty} \frac{(-1)^n}{2n + 1} \exp \left[- D(2n + 1)^2 \pi^2 t/4L^2 \right] \cos \frac{(2n + 1)\pi x}{2L} \qquad 9.3.3$$

n takes on the values 1, 2, 3 .....

If m denotes the total amount of diffusing substance remaining in the sheet at time t and m_o the amount initially present, then

$$\frac{m}{m_o} = \frac{4}{\pi} \sum_{n=o}^{\infty} \frac{8}{(2n + 1)^2 \pi^2} \exp \left[- D(2n + 1)^2 \pi^2 t/4L^2 \right] \qquad 9.3.4$$

The above trigonometrical series converges satisfactorily for moderate and large times. The dimensionless concentration profile is conveniently

expressed in terms of

x/L, a dimensionless length scale

Dt/L^2, a dimensionless time scale

The analogy between the diffusion equation and the heat conduction equation should be pointed out. It follows therefore that a solution of one is, after making the appropriate change of notation, a solution of the other.

An equation equivalent to equation 9.3.3 was used by Sherwood (3) in his pioneering researches into drying. Sherwood assumed that the constant-rate period ended when the surface concentration fell either to zero or an equilibrium value, and that equation 9.3.3 then applied to the subsequent falling-rate period. This surface boundary condition is equivalent to the assumption that the surface mass transfer coefficient is infinite; an assumption that was criticised by Newman (65).

Surface boundary condition

When evaporation takes place from the surface, it is often assumed, Crank (69, p. 36), that the following boundary condition holds

$$D\left(\frac{\partial c}{\partial x}\right)_s = \alpha\ (c_s - c_l) \qquad 9.3.5.$$

α = constant of proprtionality

c_s = concentration in the surface

c_l = concentration in equilibrium with the vapour pressure in the drying air remote from the surface.

Equation 9.3.5 is analagous to Newton's Law of Cooling in convective heat transfer, but it should be noted that 9.3.5 is not compatible with a constant drying rate.

In an endeavour to make his solution of the diffusion equation relevant to the conditions of falling rate drying, Newman (70) incorporated the boundary condition of equation 9.3.5. Newman integrated his solution to evaluate the free liquid concentration $\bar{c}$ at any time and presented his results as tables of the dependent variable E, defined as

$$E = \frac{\bar{c} - c_1}{c_o - c_1} \qquad 9.3.6$$

The constant-rate period

At zero time, it may be assumed that the concentration has the uniform value c_o throughout the slab. When constant-rate drying has been established, the concentration profiles within the solid must take on an equilibrium shape. The effect of a constant-rate of surface evaporation will be to lower the concentration profile but not to change its shape. Under such conditions $\frac{\partial c}{\partial t}$ will be a constant. Hence the diffusion equation reduces to

$$\frac{d^2c}{dx^2} = \text{constant} \qquad 9.3.7$$

Thus the concentration profile is a parabola which satisfies the equation

$$\frac{c_m - c}{c_m - c_s} = \frac{(x - L)^2}{L^2} \qquad 9.3.8$$

where

c_m = maximum concentration at centre of slab

c = concentration at distance x from one surface

L = half thickness of slab

The surface gradients at z = 0 and x = 2L are

$$\left(\frac{dc}{dx}\right)_s = \pm \frac{2(c_m - c_s)}{L} \qquad 9.3.9$$

The critical point

The critical point marks the end of constant-rate drying. It occurs when liquid can no longer reach the free surface at a sufficient rate to maintain the surface vapour pressure at its equilibrium, saturated value. Keey (51) gives an empirical definition, which locates the critical point at the discontinuity on the drying rate curve, see Figure 11.1. The average moisture content of the solid at this point is then defined as the critical moisture content.

Gilliland and Sherwood (71) proposed that the critical point occurred when the surface moisture concentration reached either zero or the equilibrium value. This explanation has been widely accepted in the theory of hygroscopic drying (51). This criterion, together with the parabolic concentration profile of equation 9.3.8, entails that the critical moisture content will be dependent upon the drying rate. This may be demonstrated as follows. Starting with equation 9.3.9

$$c_m - c_s = \frac{L}{2}\left(\frac{dc}{dx}\right)_s = \frac{L}{2D}\left(\frac{dm}{dt}\right) \qquad 9.3.10$$

dm/dt is the constant drying rate.

The average moisture concentration at the critical point, $\bar{c}_c$, may be obtained by integration. Using equation 9.3.8 and putting $c_s = 0$

$$\bar{c}_c = \frac{1}{L}\int_0^L c\, dx = \frac{2\, C_m}{3} = \frac{1}{3}\frac{L}{D}\frac{dm}{dt} \qquad 9.4.10$$

It would appear from the above that the critical moisture content is directly proportional to the drying rate during the constant-rate period of drying.

In opposition to the above theory, Broughton (72) presented experimental evidence to show that in some cases the surface concentration at the critical point $(c_s)_c$ was greater than zero. It has already been pointed out in section 4.6 that evidence from IR drying curves is not consistent with equation 9.4.10. This point is discussed further in Chapter 11.

The falling-rate period

Sherwood (3) has suggested that there are two periods of falling-rate drying. In the first, dry patches appear on the surface, but constant-rate drying continues unabated from the remaining wetted area. The total surface area covered by dry patches increases linearly with time; consequently the drying rate diminishes linearly with time. The second period of falling-rate drying begins when the surface is entirely dry.

9.4 Diffusion in Ink Drying - The Exponentially Varying Diffusion Coefficient

The solutions of the diffusion equation based on a constant diffusion coefficient provide valuable insight into the nature of the problem and indicate the appropriate dimensionless variables. However, it

was argued in Chapter 8 that to be relevant to ink drying the solution should incorporate a diffusion coefficient which is exponentially dependent on concentration (equation 8.6.9). Of course incorporation of a concentration dependent diffusion coefficient renders the diffusion equation non-linear and makes it difficult to solve by analytical methods.

The monograph by Crank (69) contains a number of purely analytical solutions of the diffusion equation. However the adaption of such solutions to practical problems may present difficulties for the following reasons:-

a) For the most part the solutions are restricted to a constant diffusion coefficient.

b) The solutions are restricted to a particular geometry and to a particular boundary condition.

c) The effort involved in the numerical evaluation of an analytic solution is usually by no means trivial.

Because the details of the ink-drying process were unknown at the outset of this research, it was essential to keep the theoretical solution as flexible as possible. For this reason, and because of the difficulties mentioned above, a numerical solution of the diffusion equation was preferred over an analytic solution for this research.

Because of mathematical difficulties, the early drying researchers used simple models of the drying process. Recently and in particular for the permeation of water through a porous medium, quite complex computer models have been proposed. In particular, for high intensity

drying of porous slabs, it is no longer necessary to assume that the plane of evaporation remains on the surface. When the rate of evaporation becomes sufficiently intense the plane of evaporation will recede into the material and may sweep through it, Keey (51). The movement of the evaporative surface, and the incorporation of internal vapour diffusion to the free surface, adds further complexity to the model and to its solution.

Taking into account, the extreme thinness of the ink film during the falling-rate period (band 3, thickness $\approx 2 - 4\ \mu m$), it appeared doubtful if it could sustain the internal gradients required by the receding plane, (see (51) p. 170). Other considerations reinforced this view. In his early research, Sherwood (3) suggested that receding plane evaporation probably occurred only in porous solids and not in colloid like materials. In addition in the present research, the rate of evaporation did not appear to be intense; for example the maximum air temperature was 70 C. Finally, although it was aimed to make the computer program reasonably general, the complexity of incorporating in it a receding plane of evaporation did not appear to be justified.

To summarise, the numerical model proposed for computer solution incorporated an exponentially dependent diffusion coefficient with evaporation taking place at the free surface.

9.5 Transformation Of The Equations By Means Of The S-Variable Dimensionless Form

When the diffusion coefficient depends upon concentration, the relevant form of the diffusion equation is 9.2.4. Rewriting and for convenience omitting subscripts

$$\frac{\partial}{\partial x}\left(D\frac{\partial c}{\partial x}\right) = \frac{\partial c}{\partial t} \qquad 9.5.1$$

For a general solution, it is usual to express this equation in non-dimensional form. The classical solutions of the previous section suggest the following dimensionless variables

$$C = \frac{c}{c_o}, \quad X = \frac{x}{L}, \quad T = \frac{D_o t}{L^2}, \quad D^* = \frac{D}{D_o}$$

the introduction of these into equation 9.5.1 yields

$$\frac{\partial}{\partial x}\left(D^*\frac{\partial C}{\partial x}\right) = \frac{\partial C}{\partial T} \qquad 9.5.2$$

An Alternative Variable S

Hansen (56) has drawn attention to the proposal by Crank (69, p. 207) to transform equation 9.5.2 into a form which facilitates numerical solution. Crank points out that although both D^* and $\partial C/\partial x$ vary separately, the variation of their product $D^* \partial C/\partial x$ may be smaller in magnitude. Based on this, he has suggested that the convergence of a numerical iterative method may be improved by the introduction of a new variable S, defined by

$$S = \frac{\int_o^C D^* \, dC}{\int_o^1 D^* \, dC} \qquad 9.5.3$$

Equation 8.6.9 may be expressed non-dimensionally

$$D^* = \exp(KC) \qquad 9.5.4$$

where K is a constant.

Let D_1^* = maximum value of D*, occurs when C = 1.

$$K = \ln D_1^* \qquad 9.5.5$$

Inserting equation 9.5.4 into the definition of S

$$S = \frac{\int_o^C e^{KC}\, dC}{\int_o^1 e^{KC}\, dC}$$

giving

$$S = \frac{e^{KC} - 1}{e^K - 1} \qquad 9.5.6$$

or alternatively

$$C = \frac{1}{K} \ln\left[S\,(e^K - 1) + 1\right] \qquad 9.5.7$$

It can be seen that when equation 9.5.4 holds, S is a pure function of C. Also that

$$0 \leqslant C \leqslant 1 \qquad 0 \leqslant S \leqslant 1$$

and that when D^1 is constant, S = C.

For convenience let

$$Z = \int_0^1 D^* \, dC = \frac{1}{K} (e^K - 1) = \text{constant} \qquad 9.5.8$$

It is easy to show that

$$\frac{\partial S}{\partial C} = \frac{D^*}{Z} \qquad 9.5.9$$

Transformation of the diffusion equation to S-form

Rewriting equation 9.5.2

$$\frac{\partial}{\partial x}\left(D^* \frac{\partial C}{\partial x}\right) = \frac{\partial C}{\partial T}$$

l.h.s $$\frac{\partial}{\partial x}\left(D^* \frac{\partial C}{\partial x}\right) = \frac{\partial}{\partial x}\left(Z \frac{\partial S}{\partial x}\right) = Z \frac{\partial^2 S}{\partial x 2}$$

r.h.s $$\frac{\partial C}{\partial T} = \frac{Z}{D^*} \frac{\partial S}{\partial T}$$

giving finally

$$D^* \frac{\partial^2 S}{\partial x^2} = \frac{\partial S}{\partial T} \qquad 9.5.10$$

The Boundary Condition at the Surface

It will be assumed for the present that the surface boundary condition can be represented by an equation similar to 9.3.5

$$D\left(\frac{\partial C}{\partial x}\right)_s = k \, (c_s - c_1) \qquad 9.5.11$$

k = mass transfer coefficient

C_S = solvent concentration in the surface

C_1 = solvent concentration in drying air remote from surface

Making the further assumption that C_1 is zero, equation 9.5.11 may be transformed to non-dimensional form

$$D^* \left(\frac{\partial C}{\partial X}\right)_s = \frac{kL}{D_o} C_s \qquad 9.5.12$$

The dimensionless group (kL/D_o) is a program parameter which has a form similar to that of the Biot number (Bi = hL/k) which arises in problems of convective heating or cooling. It will be denoted by the symbol Bi_2. For any single program run Bi_2 is assigned a constant value. The value of the parameter Bi_2, and the boundary condition above, have considerable physical significance for matching theoretical to experimental drying processes. This point is discussed in detail in the next chapter.

The boundary condition must now be transformed into S-form. Using the subscript zero to denote the surface where X = 1

from equation 9.5.9 $\quad D^* \left(\frac{\partial C}{\partial X}\right)_1 = Z\left(\frac{\partial S}{\partial X}\right)_1$

from equation 9.5.7 $\quad C_1 = \frac{1}{K} \ln \left[S_1 (e^K - 1) + 1 \right]$

Introducing these transformations into equation 9.5.12, gives

$$\left(\frac{\partial S}{\partial X}\right)_1 = \frac{Bi_2}{(e^K - 1)} \ln \left[S_1 (e^K - 1) + 1 \right] \qquad 9.5.13$$

which is the transformed boundary condition at the surface. It is non-linear.

The Boundary Condition at the Substrate

Tests have indicated that the plastic substrate, to which the ink is applied, is essentially impervious to solvent penetration. Thus the following boundary condition must be satisfied

$$D\left(\frac{\partial C}{\partial X}\right)_s = 0 \qquad 9.5.14$$

Using the S-variable, and using the subscript L to denote the substrate boundary where X = L, the transformed boundary condition is

$$\left(\frac{\partial S}{\partial X}\right)_L = 0 \qquad 9.5.15$$

Modified Variation of D* with C

The above mathematical development was used as the basis of the numerical analysis. It has been presented because it allows a straightforward demonstration of the transformation of the diffusion equation and boundary conditions to S-form. However a later, more detailed, analysis of both theoretical and experimental results suggested a possible improvement. Results appeared to show, that during the early period of drying the value of the diffusion coefficient would be fairly high and could be considered to be approximately constant. A reasonable hypothesis is that D* starts to fall, only when the concentration falls below some characteristic value C_E. The actual value of C_E is to be selected to achieve agreement with experimental data. For example it may be appropriate to identify C_E with the critical point. This type of relationship is illustrated in the diagram below

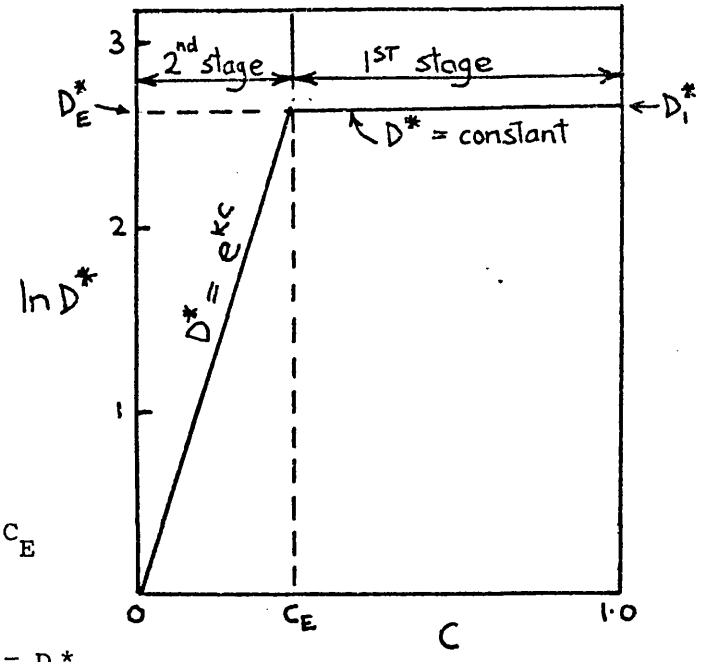

D_E^* = value of D* when $C = C_E$

From the diagram, $D_E^* = D_1^*$

for this case $$K = \frac{\ln D_1^*}{C_E} \qquad 9.5.16$$

With this modified variation of D*, the integrals in equation 9.5.3 which defines the transformation variable S, must now be carried out in two steps, as shown below.

The S-Transformation for the Modified Variation of D* with C

First-Stage $C_E \leqslant C \leqslant 1.0$

$$D^* = D_2^* = D_1^* = \text{constant}$$

$$S = \frac{\int_0^C D^* \, dC}{\int_0^1 D^* \, dC} = \frac{\int_0^{C_E} D^* \, dC + D_1^* \int_{C_E}^C dC}{\int_0^{C_2} D^* \, dC + D_1^* \int_{C_E}^1 dC}$$

$$S = \frac{K D_1^* C + A_1}{A_2} \qquad 9.5.17$$

$$C = \frac{SA_2 - A_1}{K D_1^*} \qquad 9.5.18$$

where

$$A_1 = D_1^* - 1 - K D_1^* C_2 = \text{constant}$$

$$A_2 = \left[D_1^* - 1 + K D_1^* (1 - C_2)\right] = \text{constant}$$

convective boundary condition, equation 9.5.12

$$D^* \left(\frac{\partial C}{\partial X}\right)_s = Bi_2 \, C_s$$

which may be transformed to

$$\left(\frac{\partial S}{\partial X}\right)_s = \frac{Bi_2}{D_1^*} \left(S_s - \frac{A_1}{A_2}\right) \qquad 9.5.19$$

Second-Stage $0 \leqslant C \leqslant C_E$

$$D^* = e^{KC}$$

$$S = \frac{\int_0^C D^* \, dC}{\int_0^1 D^* \, dC} = \frac{\int_0^C e^{KC} \, dC}{\int_0^{C_E} D^* \, dC + D_1^* \int_{C_E}^1 dC}$$

$$S = \frac{D^* - 1}{A_2} \qquad 9.5.20$$

$$C = \frac{1}{K} \ln (SA_2 + 1) \qquad 9.5.21$$

A_2 is a constant defined above.

onvective boundary condition, equation 9.5.12

$$D^* \left(\frac{\partial C}{\partial X}\right)_s = Bi_2 \, C_s$$

which may be transformed to

$$\left(\frac{\partial S}{\partial X}\right)_s = \frac{Bi_2}{A_2} \, (S_s A_2 + 1) \qquad 9.5.22$$

It is straightforward to show that both equation 9.5.17 and 9.5.20 can be differented to yield a relation of the form

$$\frac{\partial S}{\partial C} = \frac{D^*}{\text{constant}}$$

This relation is identical in form to the previous equation 9.5.9. Thus the transformation of the diffusion equation to S-form is unaffected by the modified variation of D* with C, and equation 9.5.10 remains valid.

9.6 The Finite-Difference Equations

An implicit finite-difference method (of the type originally proposed by Crank and Nicolson) was adopted. An implicit method was chosen to avoid the stability problems inherent in explicit methods when the time-step criterion is exceeded. Crank (69, p. 210) proposed the finite-difference form of equation 9.5.10 as

$$\frac{S_{i,j+1} - S_{i,j}}{\delta T} = \frac{D^*_{i,j+1} + D^*_{i,j}}{4 \, \delta x^2} \left(S_{i+1,j+1} - 2S_{i,j+1} + S_{i-1,j+1} + S_{i+1,j} - 2S_{i,j} + S_{i-1,j}\right) \qquad 9.6.1$$

The subscript notation is used to refer to a general value, $S_{i,j,}$ on a grid within the X-T region. Details of this grid are shown in Figure 9.1; the subscripts of S-values at grid points adjacent to $S_{i,j,}$ and used in equation 9.6.1, are also shown.

The diffusion equation is a partial differential equation of the type classified as "parabolic", and as such, its solution has a characteristic form. Prior to calculation, the initial values of S(at T = 0) must be specified together with the boundary values of S for all T. The finite-difference solution then evolves in a manner which is sometimes characterised as "marching forward in time". For example, using the known values of S at time T = 0(j = 0) a set of equations 9.6.1 can be written which implicitly contains the unknown S-values at the time δT.(j = 1) known values of S along the j^{th} row are referred to as "present" values while values of S along the $(j + 1)^{th}$ row are called "future" values. The set of implicit equations is next solved for the future values of S (when D* is constant the set of linear equations can be solved by standard methods of elimination). A time-step is complete when the set of equations has been solved.

At the beginning of the next time-step, future S-values from the previous step become present S-values. The above procedure is repeated, the solution marches forward in time, filling in one row of the open-ended X-T space at each step.

The surface boundary condition

To obtain greater accuracy it is usual to represent the boundary point by a central difference formula, Smith (73). To do this, it is necessary to introduce the fictitious S-value at the external mesh point j = 0 (see Figure 9.1). Starting from equation 9.5.13, with the

subscript 1 denoting the free surface

$$\left(\frac{\partial S}{\partial X}\right)_1 = \frac{Bi_2}{(e^K - 1)} \ln\left[S_1 (e^K - 1) + 1\right] \qquad 9.6.2$$

then representing the derivative in finite-difference form

$$\frac{S_{2,j} - S_{o,j}}{2\delta X} = \frac{Bi_2}{(e^K - 1)} \ln\left[S_{1,j} (e^K - 1) + 1\right]$$

which given an equation for the fictitious point

$$S_{o,j} = S_{2,j} - \frac{B_{i2}\ 2\,\delta X}{(e^K - 1)} \ln\left[S_{1,j} (e^K - 1) + 1\right] \qquad 9.6.3$$

Equation 9.6.3 may then be substituted into the general finite difference equation 9.6.1, to obtain an implicit equation for the future surface point $S_{1,j+1}$

$$\frac{S_{1,j+1} - S_{1,j}}{\delta T} = \frac{(D^*_{1,j+1} + D^*_{1,j})}{4\,\delta x^2} \left\{ S_{2,j+1} - 2S_{1,j+1} + S_{2,j+1} \right.$$

$$- \frac{Bi_2\ 2\delta X}{(e^K - 1)} \ln\left[S_{1,j+1} (e^K - 1) + 1\right] + S_{2,j} - 2S_{1,j} + S_{2,j}$$

$$\left. - \frac{B_{i2}\ 2\ \delta X}{(e^K - 1)} \ln\left[S_{1,j} (e^K - 1) + 1\right] \right\} \qquad 9.6.4$$

The substrate boundary condition

Let the value of i at the substrate boundary be L.

To satisfy the condition that the substrate is impervious to solvent, equation 9.5.15, it is necessary to introduce an S-value at the external point (L + 1, j). In finite-difference form, the boundary condition becomes

$$S_{L+1,j} = S_{L-1,j} \qquad 9.6.4$$

and inserting this into the general equation 9.6.1, yields

$$\frac{S_{L,j+1} - S_{L,j}}{\delta T} = \frac{(D^*_{L,j+1} + D^*_{L,j})}{2\delta X^2}\left(S_{L-1,j+1} - S_{L,j+1} + S_{L-1,j} - S_{L,j}\right) \qquad 9.6.5$$

Initial conditions

Any set of S-values may be specified at time zero. However the most usual would be

$$t = 0, \quad c = c_o \quad 0 \leqslant x \leqslant L \qquad 9.6.6$$

which transform to

$$T = 0, \quad C = 1.0, \quad S = 1.0 \quad 0 \leqslant X \leqslant 1.0 \qquad 9.6.7$$

Final conditions

It will be assumed that the equilibrium content of the ink-film is

zero, giving

$$t = \infty, \quad c = 0, \quad 0 \leqslant x \leqslant L \qquad 9.6.8$$

which transforms to

$$T = \infty, \quad C = 0, \quad S = 0, \quad 0 \leqslant X \leqslant 1.0 \qquad 9.6.9$$

FIGURE 9.1.

FINITE - DIFFERENCE GRID

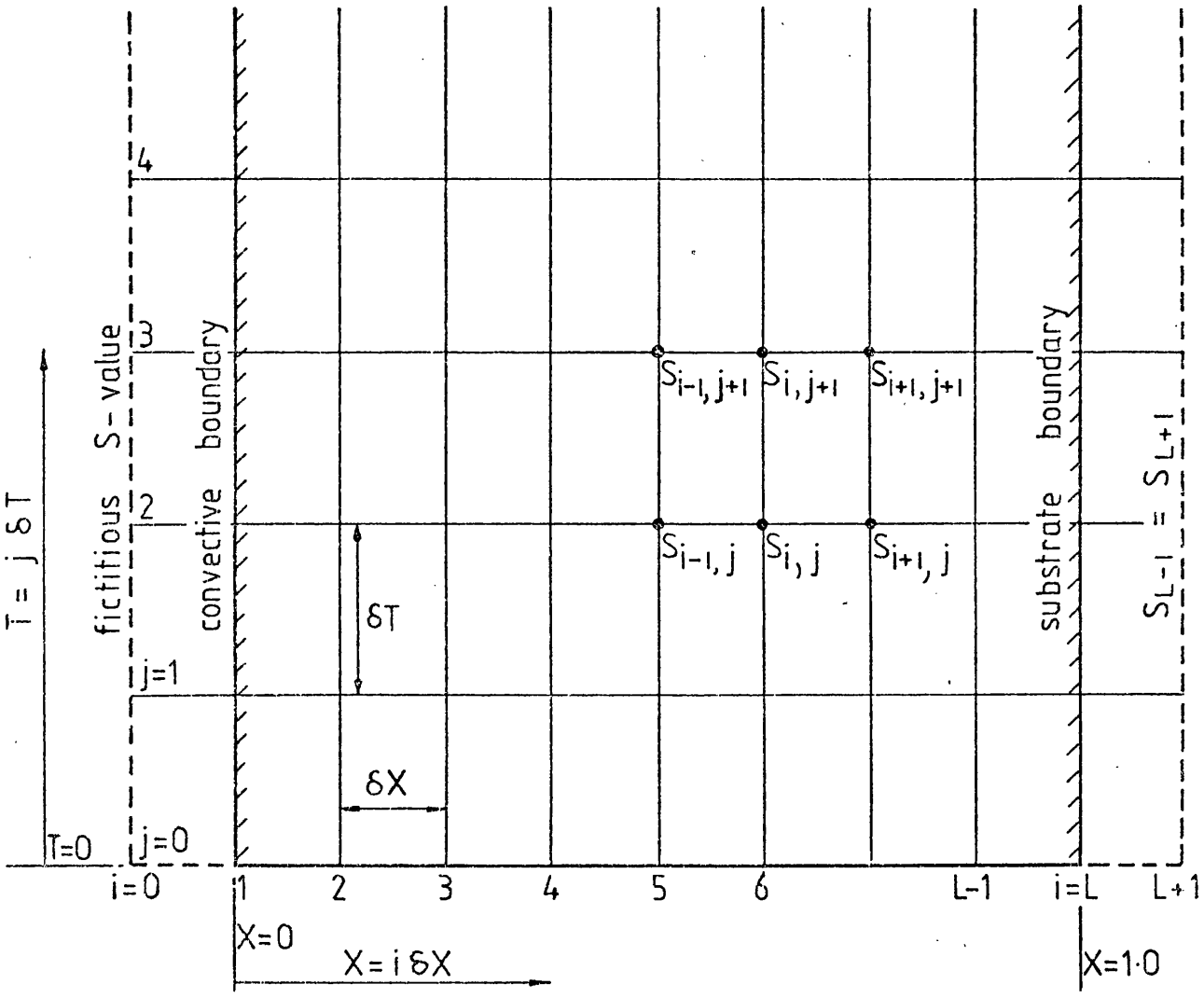

i and j take on integer values

In the program the thickness of the ink is sub-divided into 8 intervals, i.e. $\delta X = 1/8$

At the substrate boundary, $i = L$

10. A COMPUTER PROGRAM TO SOLVE THE DIFFUSION EQUATION WITH A CONCENTRATION DEPENDENT DIFFUSION COEFFICIENT

10.1 Introduction

In this chapter the finite-difference equations, derived in the previous chapter, are developed into a computer program. The non-linear equations are solved by an iterative method. Initially, because the details of the problem, and the nature of the solution, were largely unknown, the program was kept general. By this it is meant, that computation began at the beginning of the constant-rate period, "marched" through the critical point, and ended at a suitable point in the falling-rate region. To accomplish this task, the computational technique, had to be stable over a large range of the parameters D_1^*, Bi_2 and Fo. It was hoped that such a program would allow the implications of various boundary conditions to be investigated.

Early trial runs were largely unsuccessful. The source of the difficulty was traced to the divergence of the iterative technique used to solve the non-linear equations. It became necessary to analyse those factors which influenced the convergence of the iterative technique. This analysis showed that, for particular values of the parameters, this convergence depended upon the manner in which the finite-difference equations were formulated prior to iteration. Although these difficulties were overcome, and eventually satisfactory program operation was achieved, program development was rather protracted. Only the salient features of this development work are described in this chapter.

Successful computer runs showed up the fundamental role played by the dimensionless parameters, D_1^* and Bi_2. A graphical facility, available as standard computer software, was used to obtain internal concentration profiles during drying.

Later, attention was concentrated on the falling-rate region alone. The objective of this work, was to match the behaviour of the computer model to data drom the IR curves, obtained during parallel experimental investigations in the falling-rate region. The manner in which the computer model must be modified to achieve this matching is described.

10.2 Parameters in Numerical Analysis of Transient Mass Transfer

Dimensionless groups in transient heat transfer

It has been previously remarked upon that the two processes of heat and mass transfer are analogous. Thus it should be expected, that dimensionless groups used to express transient heat transfer data, can be transformed to express similar results in mass transfer. In convection the following two gropus are employed:-

Fourier Number, $Fo = \alpha t/L^2$

The Fourier number is usually regarded as a dimensionless time scale.

Biot Number, $Bi = hL/k$

The Biot number is the ratio of the internal thermal resistance of the body (L/k) to the external thermal resistance of the boundary layer (1/h). When the Biot number is small (say < 0.1) internal temperature differences within the body are negligible in comparison with the temperature difference between the body and its surroundings. In such a case, when the temperature of the body may be assigned a single value the body may be treated as a lumped parameter system.

It is easy to demonstrate, for a body cooling by convection, when the thermodynamic properties are constant, that

$$\frac{\theta}{\theta_o} = e^{-Bi\ Fo} \qquad 10.2.1$$

θ = Temperature difference between body and its surroundings.

Analagous groups in mass transfer

If the situation is changed from heat transfer to mass transfer the analagous groups follow immediately.

$$\text{Fourier number, } Fo = \frac{Dt}{L^2}$$

Again, Fo is a dimensionless time scale

$$\text{Biot number, } Bi = \frac{k_\rho L}{D}$$

The mass transfer Biot number may also be regarded as a measure of the rate of surface evaporation. For each program run, the mass transfer coefficient, k_ρ, was regarded as constant. At high values of the evaporation rate (large Bi and k_ρ) concentration differences develop within the body. At extremely high values of Bi, the surface concentration falls to zero.

Newtonian Drying

When transient heat transfer can be expressed in the form

$$\frac{\theta}{\theta_o} = e^{-t/\beta} \qquad 10.2.1$$

where β is the time constant.

The characteristic exponential decay of temperature with time may be termed Newtonian cooling. By analogy,"Newtonian Drying" satisfies the following equation

$$\frac{m}{m_o} = e^{-t/\beta'} \qquad 10.2.2$$

m = average moisture content of body

β' = time constant for mass transfer

Since evaporation from the surface takes place according to

$$\frac{dm}{dt} = k_\rho A(\rho_s - \rho_\infty) \qquad 10.2.3$$

where ρ_s = vapour concentration at the surface

then mass transfer will take place according to equation 10.2.2 in the following three characteristic situations:-

a) $Bi \leqslant 0.1$

The internal liquid concentrations c are equal, and ρ_s falls in step with c_s

b) $Bi > 1.0$

After an initial adjustment period, when the liquid diffusion coefficient is constant, the internal concentration profiles take on an equilibrium shape

c) $Bi >> 1.0$

The surface concentration is virtually zero. In this case the

rate of evaporation is limited entirely by the internal resistance to diffusion. The evaporation rate is independent of Bi

$$\frac{m}{m_o} = e^{-Fo} \qquad 10.2.4$$

Finite-difference parameters in the computer program

In the computer program, the dimensionless form of the diffusion equation, (9.5.2) is solved. The computer solution is in terms of the Fourier and Biot numbers, absolute values of the transport coefficients are not used.

Definition of Biot number

When the diffusion coefficient is concentration dependent the precise definition of the Biot number requires care. Although the mass transfer coefficient k_ρ can be maintained constant during drying, the diffusion coefficient D will change. In this situation it is necessary to distinguish between the two following, slightly different, definitions of the Biot number

$$Bi_1 = \frac{k_\rho L}{D} \qquad \text{and} \qquad Bi_2 = \frac{k_\rho L}{D_o} \qquad 10.2.5$$

D_o = smallest value of D (at C_o)

Recalling that

$$D^* = \frac{D}{D_o} = \exp\,(KC)$$

then

$$Bi_1 = \frac{k_\rho L}{D} \cdot \frac{D}{D_o} \cdot \frac{D_o}{D} = \frac{Bi_2}{D^*} \qquad 10.2.6$$

Bi_1 is the normal mass transfer Biot number described above. Bi_1 will change continuously during drying, having its smallest value at the beginning of drying and its largest value at the end. Although it is incorporated implicitly in the analysis, it does not appear explicitly in the finite difference-equations.

Bi_2 is a program parameter, the constant value of which must be specified as input for each computer run. The value of Bi_2 represents the value of the extremum, which Bi_1 increases to at the end of drying.

An estimate the the value of Bi_2 was necessary for insertion in the program. The following value was considered appropriate for preliminary test. At the beginning of constant-rate drying

$$Bi_1 \approx 10^{-1}$$

Say diffusion coefficient varies by a factor of 1000

$$D_1^* = 1{,}000$$

$$Bi_2 = Bi_1 . D_1^* = 10^{-1}.10^3 = 10^2$$

Definition of Fourier number

Inspection of equations 9.6.1 and 9.6.4 will show that the following dimensionless group arises naturally

$$\frac{(D^*_{i,j+1} + D^*_{i,j}) \ \delta T}{2 \ \delta X^2} \qquad 10.2.7$$

Making a slight modification, the group may be regarded as a Fourier

number which is a dimensionless criterion of step-length

$$Fo = \frac{D^*_{i,j}\ \delta T}{\delta X^2} \qquad 10.2.8$$

When the finite-difference method is an explicit one, the length of the time step must not exceed a definite value or the solution will be unstable. Each finite-difference equation in the set must be examined for stability and usually the severest restriction on step-length arises from the stability criterion at a convective boundary. It was to avoid the restriction on step length associated with explicit methods than an implicit method was chosen.

Unfortunately, it has been found that the necessity of ensuring convergence of the iterative method of solution, itself introduces constraints. More will be said of these difficulties later, but normally the step-length was determined by setting the Fourier number in the program equal to 1/2

$$Fo = \frac{D^*\ \delta T}{\delta X^2} = \frac{1}{2} \qquad 10.2.9$$

Note that with this restriction increasing D^* serves to reduce δT

Having set the value of Fo, the time-step δT may be calculated for equation 10.2.9. The dimensionless total time T, required to carry out n time steps, follows from

$$T = \sum_{1}^{n} \delta T \qquad 10.2.10$$

10.3 The Computer Program

Solving the finite-difference equations by iteration

Because the diffusion coefficient is concentration dependent its "future" magnitude, at the time (j+1), is unknown. Thus the implicit equations cannot be solved by the standard elimination methods normally used to solve sets of linear equations. The solution of non-linear partial differential equations is difficult and it is usually necessary to consider each problem individually, as general methods are not available.

Examination of the finite-difference equation 9.6.1, shows that it can be made the basis of an iterative method if it is re-formulated as follows:-

$$S_{i,j+1} = S_{i,j} + \frac{\delta T}{4\delta X^2}(D^*_{i,j+1} + D^*_{i,j})(S_{i+1,j+1} - 2S_{i,j+1} + S_{i-1,j+1}$$

$$+ S_{i+1,j} - 2_{i,j} + S_{i-1,j}) \qquad 10.3.1$$

In this implicit form, the principal unknown $S_{i,j+1}$ appears on both sides of the equation, and this may be expressed

$$S_{i,j+1} = g(S_{i,j+1}) \qquad 10.3.2$$

Provided that an estimate of $S_{i,j+1}$ (called SG_i) can be made then this can be substituted into $g(S_{i,j+1})$ and equation 10.3.2 used to generate what it is hoped will be an improved estimate. Equation 10.3.2 can then be used recursively.

To obtain an initial approximation to the value of $S_{i,j+1}$, put

$$S_{i,j+1} = SG_i = S_{i,j} \qquad 10.3.2$$

This approximation is then used to evaluate the improved estimate of $S_{i,j+1}$ on the l.h.s. of equation 10.3.1 (SP_i in the program). Of course in practice equation 10.3.2 is used to obtain the initial approximation to all S-values on the future (j+1) line.

Provided that the iterative procedure is convergent, then it can be used in a program loop to generate a sequence of improved approximations to $S_{i,j+1}$. Iteration continues until the difference between SG_i and SP_i is less than some pre-set tolerance, signifying an approach to a stationary state.

In a similar manner the finite-difference equation for the boundary point, equation 9.6.4 can be reformulated for iteration

$$S_{1,j+1} = S_{1,j} + (D_{1,j+1} + D_{1,j}) \frac{\delta T}{4\delta X^2} \left\{ S_{2,j+1} - 2S_{1,j+1} + S_{2,j+1} \right.$$

$$- \frac{Bi_2\, 2\delta X}{(e^k - 1)} \ln\left[S_{1,j+1} (e^k - 1) + 1 \right]$$

$$\left. + S_{2,j} - 2S_{1,j} + S_{2,j} - \frac{Bi_2\, 2\delta X}{(e^k - 1)} \ln\left[S_{1,j} (e^k - 1) \right] \right\} \qquad 10.3.3$$

The Program

The original version of the program to solve the diffusion equation with exponentially varying diffusion coefficient and convective boundary condition is set out in Appendix 5. Figure 10.1 shows the flow chart for the program. In essence the program consists of iterative loops to solve equations 10.3.1 and 10.3.3 at each time step. The solution marches forward in steps of length δT, as described in section 9.6

To specify the finite-difference grid in the X direction, 8 intervals were used, i.e. at the substrate boundary i = 9. At time zero the concentration C was put equal to unity: At the beginning of program development, the simplest dependency of D* on C was chosen, namely equation 9.5.4 and 9.5.5

$$D^* = \exp(KC)$$

$$K = \ln D_1^*$$

Values of D_1^* (the value of D* when C = 1) were selected in the range 1.05 - 10^6, this was in line with the findings of Hansen (56). Various values of the Fourier and Biot numbers were tried in the ranges

$$10 < Bi_2 < 10^4$$

$$0.5 < Fo < 10$$

The iterative sequence continues until the difference between consecutive values of S is less than a pre-set value of tolerance. Although the program equations are written in terms of the variables D* and S, at the end of each time step the concentrations C_i are also evaluated and profiles of all three variables are printed out. In addition the average concentration $\bar{C}$ is calculated, as shown below, and printed out.

$$\bar{C} = \frac{1}{L} \sum_{1}^{i=L} C_i \qquad 10.3.4$$

Initial development

After normal debugging of the program had been completed, checking showed that numerical values from the program agreed with hand calculations. Even so program performance was far from satisfactory. In the early runs quite large values of Bi and D_1^* had been used, 10^4 and 10^6 respectively. Since, from equation 10.2.4

$$\delta T = \frac{Fo\ \delta X^2}{D^*}$$

it appeared reasonable to accompany the large value of D* with a relatively large value of Fo, in the range 10 - 100. A number of test runs were carried out, with various values of the program parameters, but either computing time was impractically long or the program failed. The failure always occurred during the iterative solution of the finite-difference equation at the boundary, equation 9.6.4. Eventually the iterative method computed a value of $S_{o,j+1}$ which was negative; the consequent attempt to evaluate the logarithm of a negative argument, caused program failure.

Later, to overcome these difficulties, the program parameters were modified to the following values

$$Fo = \tfrac{1}{2},\ Bi_2 = 100,\ D_1^* = 10$$

With the incorporation of these changes, successful runs became possible. Even so program operation was still unsatisfactory. Results showed that long runs were required to bring about significant changes in concentration. Detailed print-outs of the iterative sequence showed that at times, the rate at which it converged onto the "true" value was, impractically slow. The guessed values of S

oscillated above and below the true value; the difference between any two values in the sequence being alternatively positive and negative. The usual method of overcoming stability problems is to reduce the magnitude of the time-step (Fo). However when this was tried, extremely long computer runs were required to reduce the average concentration.

Because of these difficulties, it was decided to modify the program and to solve the non-linear S-equation by Newton's method. It will be recalled that Newtons method is based on the recursion formula

$$x_{n+1} = x_n - f(x_n)/f'(x_n)$$

Further trials on the modified program soon demonstrated that no improvement had been achieved. Newton's method was abandoned and the program reverted to its original form.

At this point it became essential to determine the factors controlling the rate of convergence, or divergence, of iteration. This investigation is described in the next section.

NOTE

The program development work described above took place over a period of weeks. Considerable time and effort were invested in it, but it was essentially unproductive. After consideration, it was decided not to include detailed results from these development runs in this thesis.

10.4 The Convergence of Fixed Point Iteration

Theory

To illustrate the convergence of a non-linear algebraic equation, consider the problem of finding a root of the equation

$$f(x) = 0 \qquad 10.4.1$$

First express this equation in the form

$$x = g(x) \qquad 10.4.2$$

In general, the function g(x) can have many forms depending upon how f(x) is rearranged to produce equation 10.4.2. For example if f(x) is a polynomial in x, then any x may be manipulated to the l.h.s. of equation 10.4.2. Not all of these arrangements are equally satisfactory for iterative purposes.

Let $x = x_o$ be an initial approximation to the desired root x = Z. Equation 10.4.2 may be written as a recursion formula to generate successive approximations to the root

$$x_{n+1} = g(x_n) \quad n = 0, 1, 2 \ldots\ldots \qquad 10.4.3$$

It can be shown, Conte and de Boor (74) that the conditions to ensure convergence of the recursion formula are contained in the following theorem.

Convergence Theorem

Let I be an interval containing the point x = z. Let g(x) and g'(x)

be continuous in I. Then if $|g'(x)| < 1$ for all points in I, and if the initial approximation x_o is chosen in I, the iteration (equation 10.4.3) converges to the root Z.

By interpreting the theorem geometrically, its application can be illustrated. A root of equation 10.4.3 occurs at the point where the line y = x intersects the curve y = g(x). Two consequences follow from the theorem

i) The smaller the value of g'(z) the faster will iteration converge

ii) If the modulus of the slope g'(z) is greater than unity, then the iteration will diverge.

The manner in which convergence and divergence is influenced by the value of $|g'(x)|$ is shown diagrammatically in Figure 10.2.

One additional point is illustrated on Figure 10.2.c. In the program, convergence is tested by computing for the n^{th} iteration the error between the estimate of $S(SG_i)$ and the improved estimate of $S(SP_i)$

$$(ERROR)_n = (SG_i - SP_i)_n \qquad 10.4.4$$

If the error is greater than the allowable tolerance then for the $(n + 1)^{th}$ iteration

$$(SG_i)_{n+1} = (SP_i)_n = (SG_i - ERROR)_n \qquad 10.4.5$$

Equation 10.4.5 can be re-written in a somewhat more useful form

$$(SG_i)_{n+1} = (SP_i)_n + PARAM1.ERROR_n \qquad 10.4.6$$

where 0 < PARAM1 < 1 is an adjustable coefficient.

When PARAM1 has the value of zero the original recursion formula holds. Figure 10.2.c shows that putting PARAM1 equal to 0.5, convergence can be achieved even for $|g'(x)| > 1$.

Rearrangement of finite-difference equation to improve convergence

From the above theory it appeared probable that the program failures at the surface boundary, described in the previous section, were caused by divergence of the iterative sequence. A possible reason for this was that equation 10.3.2. had been poorly formulated for iteration and did not satisfy the convergence theorem. It was decided to test this hypothesis by formulating an alternative recursion formula for the boundary point. Equation 9.6.4 was rearranged to bring the value of $S_{i,j+1}$ under the log sign, to the l.h.s. of the equation.

$$S_{1,j+1} = \frac{e^c - 1}{e^k - 1} \qquad 10.4.7$$

where

$$C = -\frac{(e^k - 1)}{2RBi_2\ \delta X}\left\{\frac{(S_{1,j+1} - S_{1,j})\ 4\delta X^2}{(D^*_{1,j+1} + D^*_{1,j})\ \delta T} - S_{2,j} + 2S_{1,j} - S_{o,j} - 2S_{2,j+1} + 2S_{1,j+1}\right]$$

$$S_{o,j} = S_{2,j} - \frac{2\ Bi_2\ \delta X}{(e^k - 1)}\ \ln\left[S_{i,j}\ (e^k - 1) + 1\right]$$

The development runs carried out with the modified recursion formula, indicated that for high values of Bi_2 and D_1^* a significant improvement had been achieved. Encouraged by this success, a subroutine was added to the program to give the following graphical output:-

a) A graph of average concentration ($\bar{C}$) against time (TD^*/L^2) - A drying curve.

b) Graphs of C against X - Concentration profiles.

In spite of a significant amount of time spent in trying to build on the improvements made, the program was still liable to fail. For example, for a large number of runs D* was held constant by setting D_1^* equal to unity. In practice, the avoid program failures D_1^* was set close to 1.0 , a value of 1.05 being used. A constant value of D* was used to facilitate numerical checks both on the program itself and on the iterative sequence. With values of D_1^* and Bi_2 set at 1.05 and 100 respectively, and using equation 10.4.4, two characteristic modes of failure became apparent

a) Fo = ½

A stable solution was obtained, but after a 2 or 3 time steps the surface concentration C_1, became negative

b) Fo = 0.005

To avoid C_1 becoming negative it appeared reasonable to limit reductions in C_1 to 5%. A hand calculation showed that to achieve this objective, a Fourier number of 0.005 was required. However when this value of Fourier number was used in the program, it resulted in divergence of the iterative sequence.

Because of these failures further analysis of the iterative method was necessary.

Further analysis of convergence of the iterative method at the surface boundary

Both forms of the recursion formula at the surface boundary, equations 10.3.1 and 10.4.7, were checked for convergence. Previous failures indicated that these checks should be carried out at two characteristic values of Fourier number, 0.5 and 0.005. D_1^* was held constant at 1.05, initially Bi_2 was set at 100, but later other values of this parameter were tried.

Equations 10.3.3 and 10.4.4 may both be written in the form

$$SP_1 = g(SG_1) \qquad 10.4.5$$

SG_1 = first estimate of $S_{i,j+1}$

$g(SG_1)$ = r.h.s. either of equation 10.3.1 or of equation 10.4.7

SP_1 = improved estimate of $S_{i,j+1}$

To gain insight into the convergence problem the type of graphical analysis illustrated in Figure 10.2 was carried through by means of a hand calculation. For the first time-step, the function $g(SG_1)$ was evaluated for a series of avlues of SG_1. Checking the convergence of two equations at two values of Fourier number gives four graphs, and these can be seen in Figure 10.3.

When it is recalled that iteration will diverge when $| g'(SG_1) | > 1$, then the reasons for the previous characteristic program failures are immediately apparent from the graphs of Figure 10.3. For $Bi_2 = 100$, then

Equation 10.3.3

Converges for Fo = 0.005; Diverges for Fo = 0.5

Equation 10.4.7

Diverges for Fo = 0.005; Converges for Fo = 0.5

It can be seen by comparison that the graphs are consistent, i.e. for the same values of Fo and Bi_2, the intersection point of the curves of SG_1 and $g(SG_1)$ yields the same root regardless of whether equation 10.3.3 or equation 10.4.7 is used. However, when the gradient of $g(SG_1)$ is steep, the iterative sequence will spiral away from the intersection point no matter how close the initial estimate was to it.

Because of the insight it gave into convergence a second graphical analysis was carried through for the second time-step (j = 3). The results of this are shown in Figure 10.4. Again the graphs are consistent one with another and for Bi_2 = 100 they confirm what was stated above, namely that equation 10.3.3 will converge only for small values of Fo and that equation 10.4.7 will only converge for large values of Fo.

These characteristics lead to the following difficulty. A Fourier number of 0.005 is so small, that little change occurs and computer runs are long and inefficient. Because of the large time-step associated with a Fo number of 0.5, the boundary value of C is negative. However, it should be noted that further investigations showed that convergence was improved by increasing the value of D_1*.

It should be pointed out that the recursion formula for the general internal point, equation 10.3.1, may also be re-formulated in an alternative form. Further calculation showed that the two versions had convergence characteristics generally similar to those of the surface boundary point, i.e. one formulation converged for high values of Fourier number and the other converged for low values.

Although the analysis of the convergence of the iterative method had not overcome the difficulties, it had indicated that solutions were possible. For example, both forms of the recursion formula were included in the program as separate modules. The module actually used in a computer run was selected to suit the particular value chosen for the Fourier number.

10.5 Further Consideration of the Constant-Rate Surface Boundary Condition

If the vapour concentration the drying air is assumed to be zero, then the following boundary condition must be satisfied at the free surface

$$D\left(\frac{\partial c}{\partial x}\right)_s = k_\rho \rho_s \qquad 10.5.1$$

c_s = liquid concentration at the surface

ρ_s = vapour concentration at the surface

k_ρ = mass transfer coefficient

It is generally assumed that during the constant-rate period thermodynamic equilibrium is established at the free surface. Thus, during this period, even though c_s falls continuously, sufficient liquid is present to maintain the vapour pressure at the free surface at the saturated value, and consequently ρ_s remains constant.

The physical significance of the Biot number was pointed out in section 10.2

$$Bi_l = \frac{k_\rho L}{D} = \frac{\text{internal resistance to mass transfer}}{\text{external resistance to mass transfer}}$$

During the constant-rate period, experiment shows that the mass transfer rate depends entirely on the resistance of the external boundary layer, and consequently Bi_l must be small. As drying proceeds D will decrease, however, until the critical point is reached, the internal resistance must remain a small fraction of the total resistance.

In the absence of additional hypotheses, it is implicit in equation 10.5.1 that constant-rate drying will continue until the liquid concentration at the surface (c_s) falls to zero. This can lead to difficulties when matching the behaviour of the present simple mathematical model to that of the real system. For example, Newman (69) has pointed out that c_s cannot in fact fall to zero, since this would cause mass transfer from the surface to cease entirely. This is a somewhat pedantic point, since the small mass transfer rates of the falling-rate period could be maintained with an almost negligible surface vapour pressure.

However, for this research, there is a more serious difficulty that has already been touched upon in section 9.4. Because of the low internal resistance to mass transfer during the constant-rate period, internal concentration gradients will be small. This, when coupled with a surface concentration of zero, entails that at the critical point the average concentration within the solid, $\bar{c}$, must be almost zero. This inference clearly contradicts experimental evidence from the drying curves which show that approximately 20% of the solvent still remains unevaporated

at the end of the constant-rate period. An explanation of this experimental behaviour was proposed in section 4.6.

To match the behaviour of the computer model to the experimental drying curves, it was assumed that the end of the constant-rate period occurred when the surface concentration reached a critical value C_{sc}. A numerical value of the parameter C_{sc}, suitably chosen to ensure good agreement with experiment, was assigned as input data to the program. It is an advantage of a numerical, over an anylitical, solution, that such matching becomes possible and allows the physical implications of departures from standard conditions to be investigated.

It was assumed that at the end of the constant-rate period, the equilibrium relation between saturated vapour pressure and liquid concentration could be expressed as

$$\rho_s = R\, C_{sc} \qquad 10.5.2$$

where R and C_{sc} are constants.

That the evaporation rate remains unchanged until the surface concentration falls to the value C_{sc}, and decreases thereafter, is contained in the following conditions

$$C_{sc} \leqslant C_s \leqslant 1.0 \qquad \rho_s = R\, C_{sc} \qquad 10.5.3.a$$

$$0 \leqslant C_s \leqslant C_{sc} \qquad \rho_s = R\, C_s \qquad 10.5.3.b$$

Using equations 10.5.1 and 10.5.3a, the constant-rate boundary condition can now be written

$$D\left(\frac{\partial c}{\partial x}\right)_s = k_\rho R C_{sc} \qquad 10.5.4$$

or, in non-dimensional terms

$$D^*\left(\frac{\partial C}{\partial X}\right)_s = \frac{k_\rho L}{D_o} R C_{sc} \qquad 10.5.5$$

and then in terms of the S-variable

$$\left(\frac{\partial S}{\partial X}\right)_s = \frac{R Bi_2}{(e^k - 1)} \ln\left[S_{sc} (e^k - 1) + 1\right] \qquad 10.5.6a$$

where

S_{sc} is the value of S corresponding to C_{sc}

During the falling rate period, the surface vapour pressure falls and equation 10.5.3b is applicable. The boundary equation is identical to equation 10.5.6a except thatnow the constant S_{sc} is replaced by the variable S_c

$$\left(\frac{\partial S}{\partial X}\right)_s = \frac{R Bi_2}{(e^k - 1)} \ln\left[S_s (e^k - 1) + 1\right] \qquad 10.5.6b$$

The finite-difference equation for the surface boundary is obtained by substituting equation 10.5.6 into the general finite-difference equation 9.6.1

$$\frac{S_{1,j+1} - S_{1,j}}{\delta T} = \frac{(D^*_{1,j+1} + D^*_{1,j})}{4\ \delta x^2}\left[S_{2,j+1} - 2S_{1,j+1} + S_{2,j+1} + S_{2,j} - 2S_{1,j} + S_{2,j} - 2A\right] \quad 10.5.7$$

where $A = \frac{2\ \delta X\ R\ Bi}{(e^k - 1)} \ln\left[S_s\ (e^k - 1) + 1\right]$

rearranging as a recursion formula

$$S_{1,j+1} = S_{2,j+1} + S_{2,j} - S_{1,j} - A - \frac{2\ \delta X^2}{\delta T}\ \frac{(S_{1,j+1} - S_{1,j})}{(D^*_{1,j+1} + D^*_{1,j})} \quad 10.5.8$$

Equation 10.5.8 was incorporated into the contant-rate section of the program.

Figure 10.5 shows extracts from the computer output for the following conditions

$$Fo = 0.5,\quad Bi_2 = 100,\quad D_1^* = 10,\quad DENRAT = 0.1$$

It can be seen that after 10 time-steps both the gradient of S at the surface, $(\partial S/\partial X)_s$, and the drying rate, $\partial \bar{c}/\partial t$, had settled to constant values.

10.6 Constant-Rate Period - Some Computational Difficulties

$D_1^* = 1.05$ and $Bi_2 = 0.1$

A constant value of diffusion coefficient (in practive $D_1^* = 1.05$) was selected both because it represented an important special case and because it facilitated program checks. The discussion of the previous

section has shown that during the constant-rate period the Biot number (for constant D*, $Bi_1 = Bi_2$) should be less than unity.

Each test case consisted of running the program for 21 time-steps; no convergence problems were encountered. The difficulty was that, because of the small Biot number, at the end of a trial the reduction in the average concentration $\bar{c}$ was quite small. At first it was thought that larger reductions in $\bar{c}$ could be produced simply by increasing the length of the time step (Fo). Preparatory to doing this, the recursion formula, equation 10.5.8, was tested for convergence. The graphical analysis of Figure 10.6a shows that the iterative sequence will become increasingly stable as the Fourier number is increased.

Next, the program was tested with three values of Fo (5,50 and 500) and extracts from the computer outputs are set out in Figure 10.7. These results were unexpected, they show that increasing the Fourier number from 5 to 500 lowers the concentration profile only slightly. Values of $\bar{c}$ at the end of each of the three runs are given in Table 10.1 below.

TABLE 10.1

	Fo		
	5	50	500
Average concentration after 20 time-steps, $\bar{c}$	0.988	0.964	0.956

It is clear from the data in the above table that as Fo is increased $\bar{c}$ approaches a limiting value. The existence of such a limit may be demonstrated by evaluating equation 10.5.8 for the first time-step.

(J = 2)

Input data:- $D_1^* = 1.05$, $Bi_2 = 0.1$, $C_{sc} = 0.1$, $R = 1.0$

By calculation $A = 0.00244$

$$\frac{2\ \delta X^2}{\delta T(D^*_{1,j+1} + D^*_{1,j})} \approx Fo$$

For $j = 1$ $\quad S_{2,j} - 2S_{1,j} + S_{2,j} - A = 0 \quad (S_o = S_1 = S_2 = 1;\ A = 0)$

For $j = 2$ $\quad$ Assume $S_{2,j+1} = 1.0$, then using equation 10.5.8

$$S_{1,j+1} = 1.0 - .00122 - \frac{1}{Fo}(S_{1,j+1} - 1)$$

or $$S_{1,j+1} = \frac{0.99878 + 1/Fo}{1 + 1/Fo}$$

As Fo increases to infinity, $S_{1,j+1}$ approaches the limiting value of 0.99878, which agrees closely with the value of 0.99876 taken from program output for a Fourier number of 500. Such a limiting value cannot be realistic, since $\bar{c}$ should be inversely proportional to Fo. It was concluded that the computer results for Fo > ½ were spurious.

To gain insight into this difficulty, the explicit form of the finite difference equation, with the constant-flux boundary condition, was solved on a hand calculator. Based on these calculations the following explanation is proposed for the behaviour described above. The effect of the flux at the boundary on the finite-difference mesh is simulated by progressively reducing the surface concentration while maintaining the concentration gradient constant. When the Biot number is small, the reduction in concentration and the associated gradient, are both small.

This surface effect is then transmitted from point to point across the mesh. If a large time-step is used (large Fo) then this would be expected to produce a commensurately large reduction in the surface concentration. But such a reduction, because it produces a large surface gradient, invalidates the original boundary condition for small Biot number. It follows therefore, that when the Biot number is small, a large number of small time-steps (Fo < 0.5) are required for a real solution. This difficulty was discussed with a numerical analyst who agreed that solutions of the finite-difference equation at large values of Fourier number, could not be regarded as true solutions of the original differential equation. Following this difficulty, for subsequent computer runs, the greatest value of Fourier number was limited to 0.5.

Figure 10.6a shows that, the iterative sequence based on equation 10.5.8 will not converge at low values of Fourier number. To meet the requirement for convergence when using Fourier numbers less than 0.5, the following alternative recursion formula was obtained from equation 10.5.7

$$S_{1,j+1} = S_{1,j} + (D^*_{1,j+1} + D^*_{1,j}) \frac{\delta T}{4\delta X^2} \left[S_{2,j+1} - 2S_{1,j+1} + S_{2,j+1} + S_{2,j} - 2S_{1,j} + S_{2,j} - 2A\right] \qquad 10.5.9$$

A graphical analysis of convergence carried out on equation 10.5.9 is illustrated in Figure 10.6b. This analysis confirms that an iterative sequence based on equation 10.5.9 will converge increasingly rapidly as Fo is decreased.

Both recursion formulas, equations 10.5.8 and 10.5.9 were retained in the program.

The final form of the program

At this point, the computer program had been developed into virtually its final form. The difficulties of iterative convergence had been largely overcome by including in the program two separate formulations of all finite-difference equations, one suitable for high Fourier number and one suitable for low Fourier number. Either formulation could be called upon, as the conditions demanded. When started at time zero, and with all concentrations equal to unity, the program first calculated a constant-rate period, $C_s \geqslant C_{sc}$. Subsequently, for $C_s < C_{sc}$ a falling-rate period was computed. This final version of the program to solve the non-linear form of the diffusion equation is shown in Appendix 6.

Successful computer runs

Figures 10.8a and 10.8b show graphical output from the computer, concentration profiles and drying curve, corresponding to the following conditions

$$D_1^* = 1.05, \quad Bi_2 = 1.0, \quad Fo = 0.5, \quad C_{sc} = 0.2$$

The value of 0.5 was used for the Fourier number because of the difficulties experienced with higher values described earlier in this section. To avoid excessively long computer runs, it was decided to increase Bi_2 to 1.0 and to accept the consequent small internal concentration gradients. This latter point was turned to advantage since it allowed the following check to be made on program consistency. It was

demonstrated in section 9.3, that when the diffusion coefficient is constant the concentration profiles are parabolic. The following concentration data has been extracted from Figure 10.8a for J = 400

	X=0	X=0.25	X=0.5	X=0.75	X=1.0
C_{max}	0.4322	0.4322	0.4322	0.4322	0.4322
C	0.3341	0.3771	0.4077	0.4261	0.4322
$C_{max} - C$	0.0981	0.0551	0.0245	0.0061	0.0000

To be parabolic, $(C_{max} - C)$ should be proportional to the square of the distance from C_{max} to C, i.e. to

1.0	0.5625	0.25	0.0625	0.0

multiplying 0.0981 by these factors gives

0.0981	0.05518	0.0245	0.0061	0.000

By comparison it can be seen that the values of $(C_{max} - C)$ taken from Figure 10.8a, lie on a parabola.

It can also be seen by inspection of Figure 10.8a that the concentration gradients at the free surface (X = 0.0) are constant as they should be in constant-rate drying. Finally, equation 10.5.5 may be evaluated to check the value of the gradient at the surface

$$D^* \left(\frac{\partial C}{\partial X}\right)_s = Bi_2 \, R \, C_{sc}$$

For J = 400 from Figure 10.8a

$$D^* \left(\frac{\partial C}{\partial X}\right)_s = D^* \frac{(C_2 - C_1)}{\delta X} = \frac{1.017 \cdot 0.02299}{0.125} = 0.187$$

and

$$Bi_2 \; R \; C_{sc} = 1.0 \cdot 1.0 \cdot 0.2 = 0.2$$

It can be seen that these values of concentration satisfy the boundary condition at the surface.

Thus the spot checks have demonstrated the consistency and validity of the numerical results.

Difficulties with high values of D*

Based on the theory of diffusion in polymers described in Chapters 8 and 9, the diffusion coefficient is expected to vary significantly with concentration. This exponential variation, expressed mathematically by equations 9.5.4 and 9.5.5, is illustrated graphically in Figure 10.9, for various values of the parameter D_1^*. Figure 10.10a shows concentration profiles from a computer run in which D_1^* was set equal to 10 i.e. D* changes by a factor of 10 when C varies from 0 to 1. For consistency with experimental drying curves, assume that at the critical point

$$C_s = C_{sc} = 0.2 \qquad 10.6.1$$

$$Bi_1 = 1.0 \qquad 10.6.2$$

Note: This choice of Bi_1 is discussed in more detail below.

The value of D_{sc}^* corresponding to C_{sc} may be obtained from Figure 10.9.

With both D^*_{sc} and Bi_1 known at the critical point, equation 10.2.2 can be used to deduce Bi_2.

$$Bi_2 = Bi_1 \cdot D^*_{sc} \qquad 10.6.3$$

and for $Bi_1 = 1$

$$Bi_2 = D^*_{sc} \qquad 10.6.4$$

Values of Bi_s corresponding to various values of D^*_1 and each consistent with Bi_1 equal to unity at the critical point, are set out in Table 10.2 below

TABLE 10.2

D^*_1	D^*_{sc}	Bi_2
1	1.0	1.0
10	1.58	1.58
100	2.5	2.5
1000	3.98	3.98

Experimental drying curves indicate that during the constant-rate period Bi_1 is quite small. For good agreement between theory and experiment, the preferred value for Bi_1 at the critical point would have been 0.1, rather than the value of 1.0 actually used in equation 10.6.2. However it can be seen from Table 10.2 that, because of the high value of D* at time zero, Bi_1 will be much less than unity throughout the constant-rate period. Bearing this in mind, and remembering that a decrease in Bi_1 causes an increase in computing time, the numerical value of equation 10.6.2 appears reasonable.

Figure 10.10b shows concentration profiles for $D_1^* = 100$ and $Bi_2 = 2.5$, these values being selected from Table 10.2. Examination of Figures 10.10a and 10.10b indicates that, during the constant-rate period, the concentration profiles are quite flat, and that these profiles become flatter as D_1^* is increased in magnitude. Thus, in spite of the large variation in D* between the beginning and end of the run, at any instant of time, D* is virtually constant across the solid layer. (It is worth noting that under these conditions a lumped parameter analysis would be satisfactory).

A computer run was carried out with $D_1^* = 1000$ and $Bi_2 = 3.98$, but the results have not been presented because the reduction in concentration achieved, even after 1000 time-steps, was negligible ($\bar{c} = 0.99329$). This run highlights the computational difficulty of operating with high values of D_1^* and low values of Bi_2. The manner in which the difficulty arises can be seen from equation 10.2.5 with Fo = 0.5

$$\delta T = \frac{\delta X^2}{2D^*}$$

At the start of the run, D* has its maximum value (1000 in this case) and the time-step is correspondingly small.

An attempt was made to overcome this problem of long inefficient computer runs by means of an approximate method based on an extrapolation technique. In the time available this method could not be made to operate successfully, but the basis of it is described in Appendix 7.

10.7 Computer Results - Further Variations of D_1^* and Bi_2

The associated values of D_1^* and Bi_2 listed in Table 10.2 were calculated to produce a suitably low value of Biot number throughout the constant-rate period, to give good agreement with drying experiments. This constraint, although it represented an interesting numerical problem, entailed that the concentration profiles of Figures 10.8 and 10.10a and b, exhibited only a small variation across the ink-layer. To exploit the capability of the program, it was considered worthwhile to run tests on combinations of D_1^* and Bi_2 outside those given in Table 10.2.

Figure 10.11 shows concentration profiles for two computer runs at the following conditions:-

Figure 10.11a : $D_1^* = 1.05$, $Bi_2 = 100$

Figure 10.11b : $D_1^* = 100$, $Bi_2 = 100$

A comparison of the concentration profiles in these two figures indicates that, in spite of Bi_2 having the same value in both, the shape of the concentration profiles is different. This follows because the shape of the profile depends not upon Bi_2, but upon Bi_1, which from equation 10.2.2

$$Bi_1 = \frac{Bi_2}{D^*}$$

will change as D* changes. With reference to Figure 10.11b, Bi_1 is small at the beginning of constant-rate drying (flat profiles) and large at the end (curved profiles).

The drying curves corresponding to Figure 10.10 and 10.11 appear in Figure 10.12. The rate of drying is proportional to the Biot number.

10.8 Program Modifications to Restrict Operation to Falling-Rate Period Only

Preliminaries

As a necessary preliminary to concentrating attention entirely on the falling-rate period, the form of functional relation between diffusion coefficient and concentration was re-examined. Two formulations of the exponential dependency were considered.

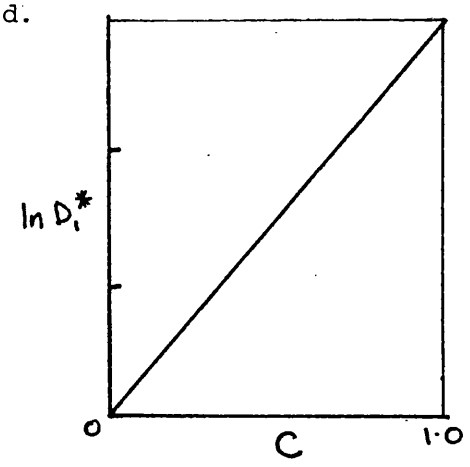

Case 1. $D^* = \exp(DC)$, for all C

This is the programmed relationship

$$K = \ln D_1^*$$

Normal program operation, with values of D_1^* and Bi_2 selected from Table 10.2, leads to following difficulty in the falling-rate region. An examination of Figure 10.9 will show that, for even quite high values of D_1^*, most of the variation in D* occurs at concentrations greater than 0.2. Enormous values of D_1^* must be used to produce quite modest variations of D* in the region C < 0.2.

Case 2. $D^* = \exp(KC)$, for $0 \quad C \quad C_c$

The theoretical treatment of this case has already been set out in section 9.5

$$D_c^* = D_1^*$$

D_c^* = value of D* at critical point

$$K = \frac{\ln D_1^*}{C_c}$$

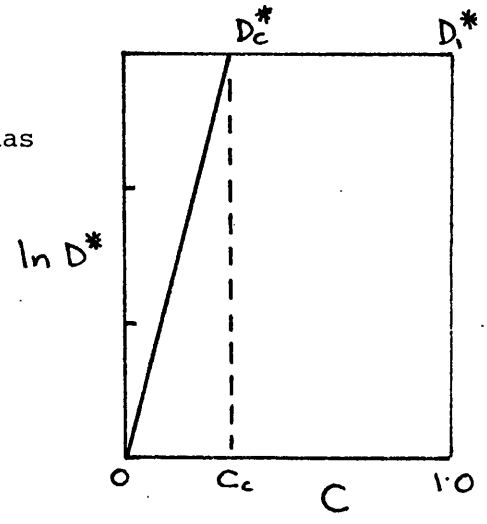

It should be noted that in this proposed form of case 2 behaviour, the discontinuity in the graph of D* and the change in the surface boundary condition, both occur at the critical point. This form of the relationship between the diffusion coefficient and concentration can be justified if the critical point marks the outset of hindered drying. Alternatively, this relationship may be regarded as a practical form of case 1, suitable for large values of D_1^*; enormous values of D* are of no practical interest since they represent negligible resistance to diffusion through the solid.

It follows that for this case 2 proposal:-

For, $C_c < C < 1.0$, D* = constant and therefore Bi_1 = constant

Assume, as before, $(Bi_1)_c = \frac{k_\rho \delta X}{D_c} = 1.0$

$$Bi_2 = \frac{k_\rho \delta X}{D_o} = \frac{k_\rho \delta X}{D_o} \cdot \frac{D_o}{D_c} \cdot \frac{D_1}{D_o} = \frac{k_\rho \delta X}{D_c} \cdot D_1^* = (Bi_1)_c \, D_1^*$$

$$Bi_2 = D_1^* \qquad 10.8.1$$

To run this case exactly as described, some program modifications would have been required. These arise because the integrals which define the S-variable (equation 9.5.3)

$$S = \frac{\int_o^1 DdC}{\int_o^1 DdC}$$

must be amended to take account of the modified form of the functional relationship between D and C. The new integrals, and the new equations for S and C were determined. These have already appeared as equations 9.5.17 - 21.

Program modifications

Case 2 behaviour can be implemented and the program modifications described above can be avoided if the computer runs are restricted entirely to the falling-rate region.

Experimental ink drying curves show, and theoretical analysis confirms, that at the critical point

$$C = C_{sc} = \text{constant}; \qquad Bi_1 = 1.0$$

The existing program may be used if the initial conditions are slightly changed, as follows

at t = 0 $\quad 0 \leqslant X \leqslant L \qquad C = 1.0$ 10.8.2a

$$Bi_1 = 1.0 \qquad 10.8.2b$$

$$C_{sc} = 1.0 \qquad 10.8.2c$$

With these initial conditions, then for a given value of D_1^*

$$K = \ln D_1^* \qquad 10.8.3$$

and from equation 10.8.1 above

$$Bi_2 = D_1^* \qquad 10.8.4$$

These changes are equivalent to a normalisation of the drying process based on conditions at the critical point. In the program, the constant-rate boundary condition is omitted by setting

$$\text{icrit} = 2 \qquad 10.8.4$$

The program was modified in accordance with equations 10.8.2 to 10.8.4. Subsequent results, described in the next section, are relevant entirely to the falling-rate period.

10.9 Computer Results - Falling-Rate Period

Initially with Diffusion Coefficient Constant

To allow a check on the program in the falling-rate region, initial tests were carried out using a constant diffusion coefficient ($D_1^* = D^* = 1.0$). For this case, standard transient heat and mass transfer data are available in the literature for comparison. The analogous dimensionless groups are

	Mass Transfer	Heat Transfer
Time Scale	$\frac{T\ D^*}{\delta x^2}$	$\frac{T\alpha}{L^2}$
Biot Number	$\frac{k_\rho\ \delta X}{D^*}$	$\frac{hL}{k}$

T = time

α = thermal diffusivity ($k/\rho\ C_p$)

Figure 10.13 illustrates concentration profiles for the case $Bi_2 = 1.0$. It can be seen that the concentration gradients at the surface are proportional to the surface concentration itself. This is consistent with the falling-rate boundary condition, equation 9.3.5. Data from this test has been replotted in Figure 10.14. The manner in which the surface concentrations change with time is shown in Figure 10.14a. A comparison with the heat transfer data of Schneider (75), shows excellent agreement. The manner in which the average concentration changes with time, for the case $Bi_2 = 1.0$, is shown in Figure 10.14b.

Data from two further computer runs at Bi_2 = 10 and Bi_2 = 100 are also included in Figure 10.14. It can be seen that the comparison with standard heat transfer, once more shows excellent agreement.

Newtonian Drying (Section 10.2)

The graphs of Figure 10.14 show that when the diffusion coefficient is constant, after an initial transient, non-dimensional drying curves are straight-lines when plotted on log/linear co-ordinates. This behaviour follows from the boundary condition equation 9.5.18

$$D^*\left(\frac{\partial C}{\partial X}\right)_s = Bi_2\, C_s$$

equating the surface evaporation rate to the drying rate

$$\frac{d\bar{C}}{dT} = -\, Bi_2\, C_s \qquad 10.9.1$$

For equation 10.9.1 to be analoagous to Newton's Law of Cooling, the mean concentration $\bar{C}$ must bear a fixed relation to the surface concentration C_s. This will occur after the initial transient, when the concentration profiles have achieved an equilibrium parabolic shape, so that

$$C_s = A\bar{C} \qquad 10.9.2$$

where A is a constant

Introducing equation 10.9.2 into equation 10.9.1, and remembering that initially $\bar{C}$ is equal to unity gives

$$\ln \bar{C} = -\, A\, Bi_2\, T \qquad 10.9.3$$

Thus, in Figure 10.14, the slopes of the curves are proportional to the Biot number.

One further comparison can be made with standard date for the important special case of zero surface resistance or infinite Biot number. For practical purposes, this case was approximated by setting Bi_2 in the program to a value of 1000. Concentration profiles from this test are shown in Figure 10.15. A comparison between the data contained in this Figure and data for this case in Crank (64) shows good agreement. To demonstrate this agreement, one profile from Crank has been included in Figure 10.15.

Computer runs with variable D_1^*

Three computer runs were carried out in which the range of exponential variation of the diffusion coefficient was systematically increased. Figure 10.16, a, b and c, shows concentration profiles from these runs, in which the value of D_1^* was 10, 100 and 1000, respectively. Additional data from these runs is set out in Table 10.3. To maintain the Biot number (Bi_1) equal to unity at the critical point for all tests, equation 10.8.4 was used

$$Bi_2 = D_1^*$$

Examination of the drying times recorded in Table 10.3 shows that, as anticipated, high values of Bi_2 and D_1^* produce a rapid decrease in solvent content during the early part of falling-rate drying. Towards the end of this period, the difference in drying times between the three cases becomes marked. This behaviour can be explained from Figure 10.9; at low concentrations numerical values of the diffusion

coefficient approach each other for all values of D_1^*.

Drying curves corresponding to the three cases of Figure 10.16 are illustrated in Figure 10.17.

TABLE 10.3

Rate of Drying Data - Figure 10.17

For all computer runs,

At T = 0; Concentration C = 1.0 = constant, $Bi_1 = 1$ (ie $Bi_2 = D_1^*$)

$D_1^* = 1$			
T	$\bar{C}$	$d\bar{C}/dT$	f
0.0	1.0	1.0	1.0
0.070	.93	.768	.768
0.147	.88	.656	.656
0.304	.782	.574	.574
0.461	.696	.508	.508
0.617	.619	.455	.455
0.773	.552	.406	.406
0.93	.491	.363	.363
1.085	.438	.325	.325
1.24	.390	.29	.29
1.4	.347	.259	.259
1.55	.310	.23	.23

$D_1^* = 10$			
T	$\bar{C}$	$d\bar{C}/dT$	f
0.0	1.0	10.0	1.0
.019	.855	5.86	.586
.043	.74	4.19	.419
.072	.63	3.26	.326
.110	.527	2.28	.228
.159	.432	1.71	.171
.22	.346	1.16	.116
.297	.271	.85	.085
.39	.207	.566	.057
.50	.154	.405	.041
.627	.112	.266	.027

$D_1^* = 100$			
T	$\bar{C}$	$d\bar{C}/dT$	f
0.0	1.00	100.0	1.0
.00198	.856	48.7	.487
.00458	.761	28.3	.283
.00828	.679	18.1	.181
.0136	.601	11.9	.119
.0213	.526	7.93	.079
.0324	.456	5.28	.053
.0483	.388	3.52	.035
.0710	.323	2.34	.023
.103	.263	1.55	.016
.147	.208	1.02	.010

$D_1^* = 1000$			
T	$\bar{C}$	$d\bar{C}/dT$	f
0.0	1.0	1000.0	1.0
.000356	.815	232.7	.233
.00098	.722	105.5	.11
.0021	.637	54.0	.054
.00428	.554	28.3	.028
.00826	.474	14.9	.015
.0156	.395	7.87	.0079
.0292	.319	4.14	.0041
.0537	.247	2.15	.0022
.0971	.18	1.11	.0011
.170	.122	.56	.0006

10.10 Rate of Drying - The Characteristic Drying Curve

The manner in which the rate of drying changes is also of interest. Dimensionless drying rates ($d\bar{C}/dT$) were computed for all three cases of Figure 10.17 and these appear in Table 10.3 overleaf. Drying rates may be normalised, by dividing them by the drying rate at the critical point

$$f = \frac{(d\bar{C}/dT)}{(d\bar{C}/dT)_c} \qquad 10.10.1$$

Since the program now starts from the critical point, ($d\bar{C}/dT$) must be evaluated at zero time. The general surface boundary condition is given by equation 9.5.12.

$$D^* \left(\frac{\partial c}{\partial x}\right)_s = Bi_2 \, C_s$$

And the surface evaporation rate may be equated to the drying rate

$$\frac{d\bar{c}}{dt} = Bi_2 \, C_s \qquad 10.10.2$$

But, at zero time,

$$C_s = \bar{c} = 1.0 \qquad 10.10.3$$

Hence

$$\left(\frac{d\bar{C}}{dT}\right)_{T=0} = \left(\frac{d\bar{C}}{dT}\right)_c = Bi_2 \qquad 10.10.4$$

Limiting values of the drying rate at zero time, are extremely difficult to estimate from the computed data. Instead, the limiting values of $(d\bar{C}/dT)$ given in Table 10.3 were calculated from equation 10.10.4.

A graph of the function f against $\bar{c}$, for falling-rate drying, is termed a "Characteristic Drying Curve". The four characteristic curves shown in Figure 10.18 correspond to earlier computer runs as indicated in the list below:-

	D_1^*	Bi_2	Corresponding Figure
1	1	1	10.14
2	10	10	10.16a
3	100	100	10.16b
4	1000	1000	10.16c

In recent drying research, the concept of the characteristic drying curve has attained some prominence. It was used (section 11.4) to normalise the IR drying curves in the falling-rate region.

For completeness the characteristic drying curve for Newtonian drying with a constant diffusion coefficient ($D_1^* = 1$) has been included on Figure 10.18. After an initial transient (which takes up a proportionately greater fraction of the total drying time at larger Biot numbers) this graph becomes a straight line. Thus, for drying with a constant diffusion coefficient, the characteristic drying curve is a straight line.

When the diffusion coefficient changes during drying ($D_1^* > 1$) the concentration profiles can never attain an equilibrium shape and

consequently the characteristic drying curve can never become a straight-line.

The characteristic drying curve - 2-stage model for diffusion coefficient

Replotting data from the IR curves (described in section 11.6) showed that the experimental characteristic drying curve could be divided into two regions, as shown diagrammatically below.

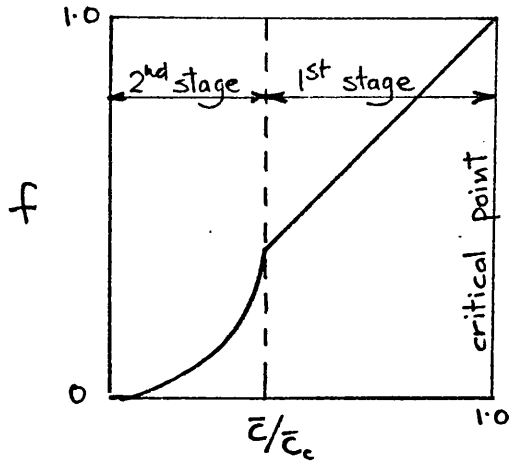

f = relative drying rate

$$= \frac{(d\bar{C}/dT)}{(d\bar{C}/dT)_c}$$

In the first stage of falling rate drying, the relative drying rate (f) decreases approximately linearly with solvent content. In the second stage, the gradient of the f curve diminishes as zero solvent content is approached.

Consideration showed that it should be possible to model the above experimental behaviour by making one further adjustment to the model of the diffusion coefficient. In section 10.8, a 2 stage model of the diffusion coefficient was adopted, but to avoid complexity, it was postulated that the discontinuity in the graph of D*, occurred at the critical point. To match the experimentally determined characteristic drying curve, shown diagrammatically above, it is now proposed that the discontinuity in the graph of D* should occur at the end of the first stage of falling-rate drying. This proposal is illustrated in the diagram overleaf.

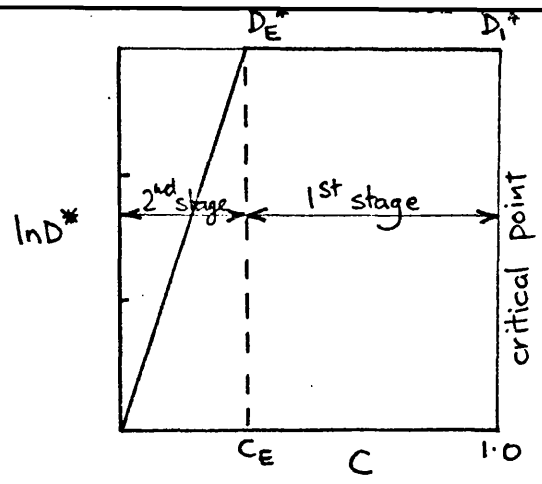

C_E = Concentration at end of 1st stage drying

The theoretical treatment of this model of the diffusion coefficient has already been presented in section 9.5, under the title "Case 2 behaviour". It can be seen that the algebraic transformations, from the C to the S variable, are more complex than for the simple case 1 model. Thus, to adopt this model some modifications to the program were required; these are summarised in Appendix 6.

It should be noted that the first stage behaviour of the experimental drying curve could have been modelled in a somewhat different manner. Sherwood (3) has suggested that this behaviour is caused by the appearance of dry patches on the surface, evaporation continuing at the constant-rate from the remainder. The present proposal was adopted because of its convenience, however the type of behaviour suggested by Sherwood could be programmed if desired.

Results of tests with the 2 stage diffusion coefficient are shown in Figure 10.19. To give agreement with experimental drying curves, it was assumed that the parameter C_E (see diagram above) had a value of 0.5. This remodelling of the diffusion coefficient was quite successful, in that the shape of the curves shown in Figure 10.19, resembles the shape of similar curves derived from experiment. However, there is one discrepancy. The first stage of the curves in Figure 10.19 is not linear. The cause of this non-linearity resides in the fact that, to economise in computing time, the value of the Biot number (Bi_2) was set at 1.0.

For the final series of computer runs, it was considered worthwhile to attempt to linearise the first stage of the characteristic drying curve. To do this it was necessary to reduce the value of the Biot number at the beginning of falling-rate drying, $(Bi_1)_c$, from unity to a value of 0.1. To determine the value of the program parameter Bi_2, recall from equation 10.2.6 that

$$Bi_1 = \frac{Bi_2}{D^*}$$

also that, when $Bi_1 = (Bi_1)_c$ $\qquad D^* = D_1^*$

For $(Bi_1)_c$ to have the desired value of 0.1, then

$$\underline{Bi_2 = 0.1 \cdot D_1^*} \qquad 10.10.5$$

The results of 4 computer runs, at various values of D_1^*, are shown in Figure 10.20. For each run the value of Bi_2 was determined from equation 10.10.5. As for the previous test, the first stage of falling-rate drying ended when the concentration C_E fell to 0.5. It can be seen that the desired linearisation of the first stage of drying has been achieved. Also that the characteristic drying curves from the computer now closely resemble those derived from experimental data.

Two observations will be made on the curves in Figure 11.20:-

a) By comparing the curves in Figure 11.20 with the curves in Figure 11.19, it can be seen that, in the second stage of drying, the shape of the curves appears to be dependent upon the value of the product

$D_l^* \ (Bi_l)_c$

The lower the value of the Biot number at the beginning of the falling-rate period, the larger must be the variation in D* to produce a given shape of curve in the second stage of drying.

b) Having established the theoretical basis of the model for the first falling-rate period of ink drying, an economy of computing time may be achieved by concentrating attention on the second period. If this was down, the characteristic drying curves for this second period alone would be similar to those appearing in Figure 10.18.

Addendum - Limitations of the Theoretical Model

It should be noted that as presently formulated the general theoretical model described in Chapter 10 is strictly applicable only to isothermal systems of fixed dimensions. These implicit assumptions were made to avoid complexity. In the falling-rate region, when comparing theoretical results from the model with experimental ink-drying data, the following remarks should be borne in mind:-

a) Isothermal System

During the falling-rate period the temperature of the system rises from the wet-bulb to the dry-bulb temperature. This temperature rise will cause the diffusion coefficient to increase, see page 135. For relatively non-volatile solvents, where the wet-bulb depression is small, it should be possible to neglect this effect. When the change in system temperature becomes significant, a more complex theoretical model, which incorporates the dependency of the diffusion coefficient on the absolute temperature is required.

b) System of Fixed Dimensions

It has been assumed that the free volume of the resin/solvent system decreases with solvent concentration. For this assumption to remain valid for a system of fixed dimension, the model is strictly applicable only to those situations where the volume vacated by the departing solvent does not serve to increase the free volume of the resin/solvent system. This dimensional effect will approach zero as the solvent content diminishes to zero. For systems where the effect of a dimensional change during drying is significant, then a modification to the model, to incorporate such a change of length scale, should be made.

FIGURE 10.1

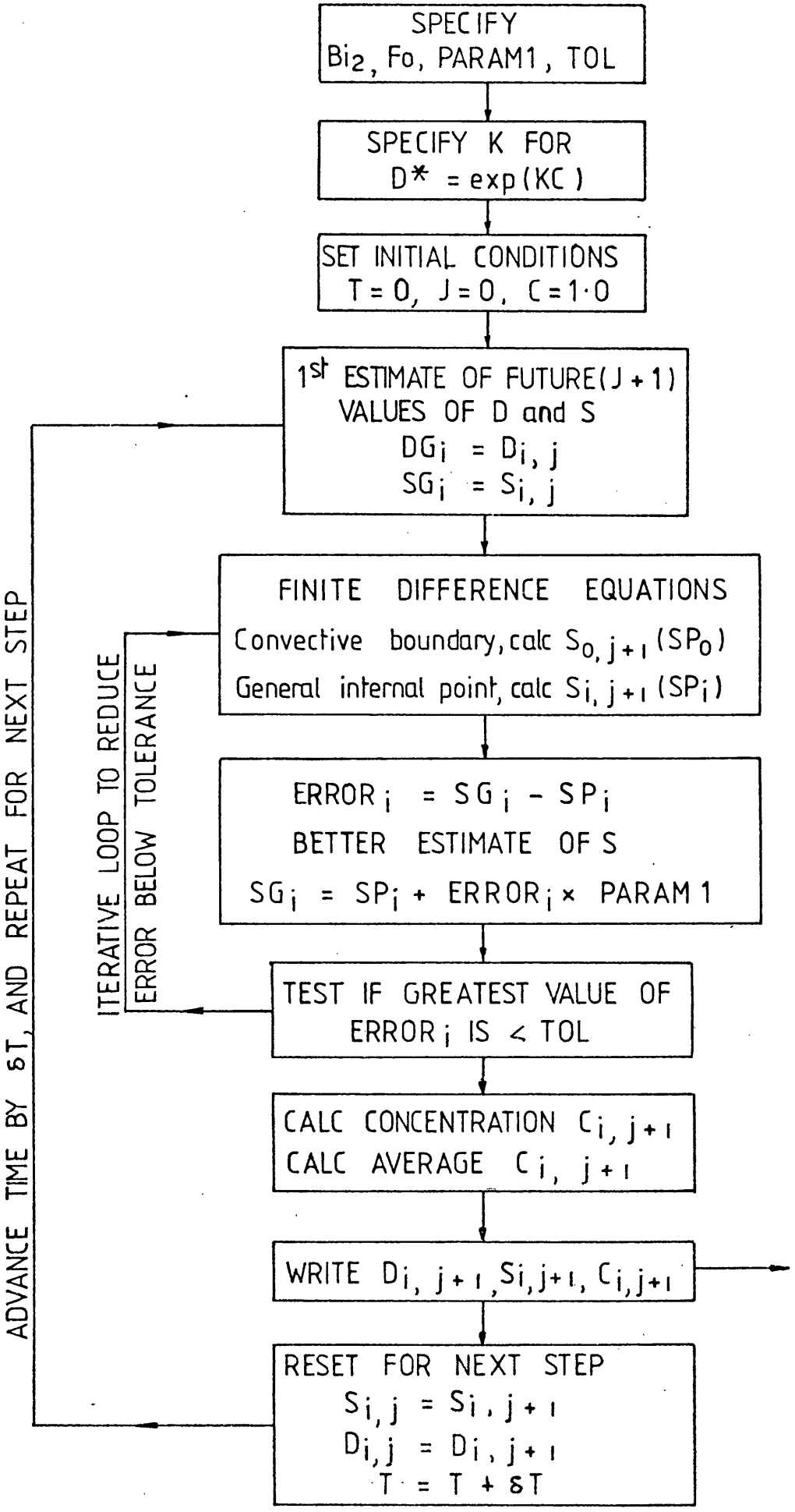
SPECIFY
Bi2, Fo, PARAM1, TOL
SPECIFY K FOR
D* = exp(KC)
SET INITIAL CONDITIONS
T = 0, J = 0, C = 1·0
1st ESTIMATE OF FUTURE(J + 1)
VALUES OF D and S
DGi = Di, j
SGi = Si, j
FINITE DIFFERENCE EQUATIONS
Convective boundary, calc S0, j+1 (SP0)
General internal point, calc Si, j+1 (SPi)
ERRORi = SGi − SPi
BETTER ESTIMATE OF S
SGi = SPi + ERRORi × PARAM 1
TEST IF GREATEST VALUE OF
ERRORi IS < TOL
CALC CONCENTRATION Ci, j+1
CALC AVERAGE Ci, j+1
WRITE Di, j+1, Si, j+1, Ci, j+1
RESET FOR NEXT STEP
Si, j = Si, j+1
Di, j = Di, j+1
T = T + δT
ITERATIVE LOOP TO REDUCE
ERROR BELOW TOLERANCE
ADVANCE TIME BY δT, AND REPEAT FOR NEXT STEP

FIGURE 10. 2.

THE CHARACTERISTICS OF ITERATION

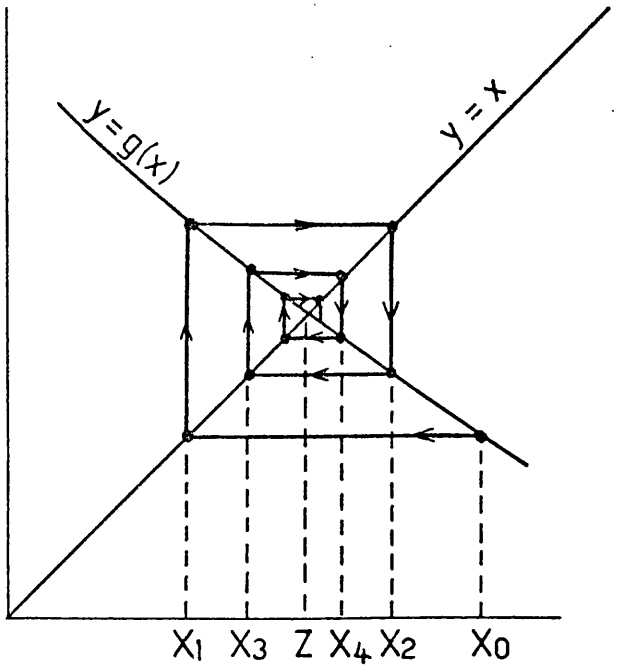

(a) Convergence , $|g'(x)| < 1$

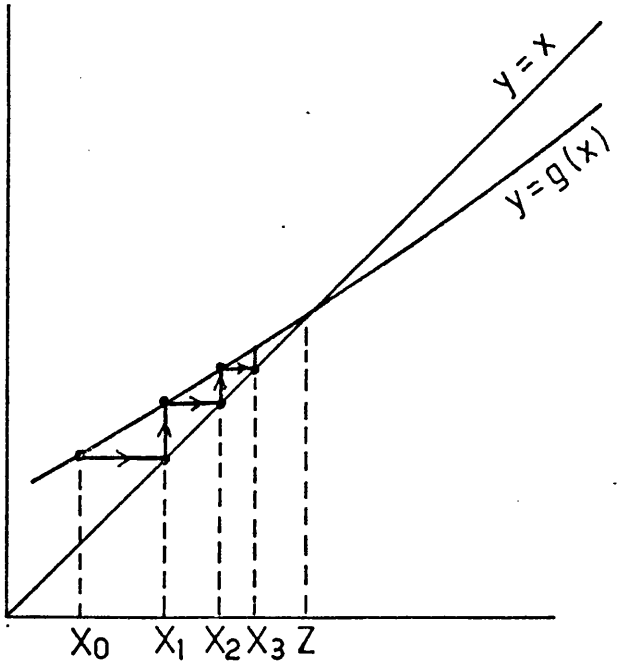

(b) Convergence , $g'x < 1$

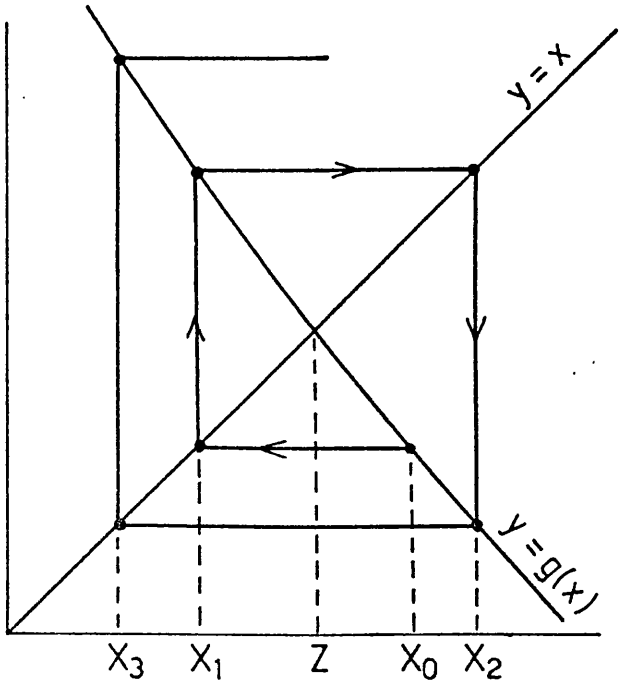

(c) Divergence , $|g'(x)| > 1$

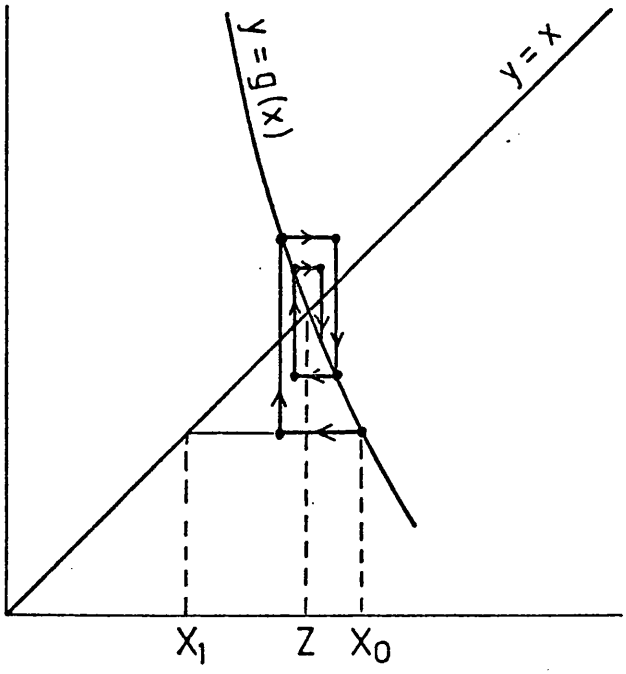

(d) Modified iteration technique

$$x_{n+1} = \frac{g(x_n) + x_n}{2}$$

Produces convergence even when $|g'(x)| > 1$

FIGURE 10.3.

CONVERGENCE CHARACTERISTICS OF FINITE-DIFFERENCE EQUATIONS

Equation 10.3.3. (1^{st} time step, j = 2)

$F_o = 0 \cdot 005$

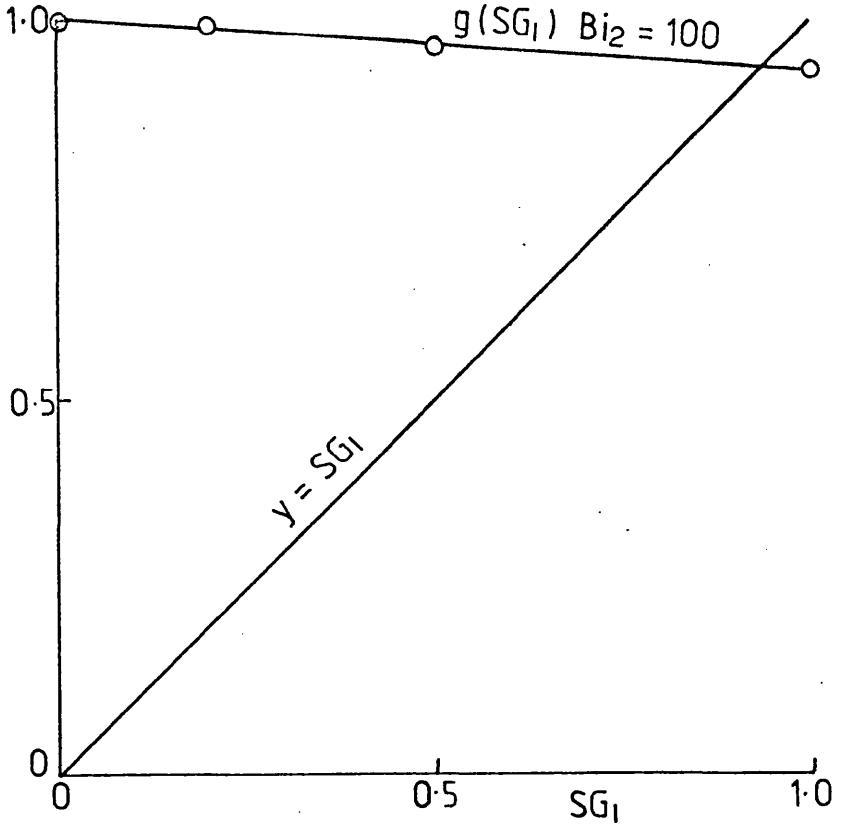

$F_o = 0 \cdot 5$

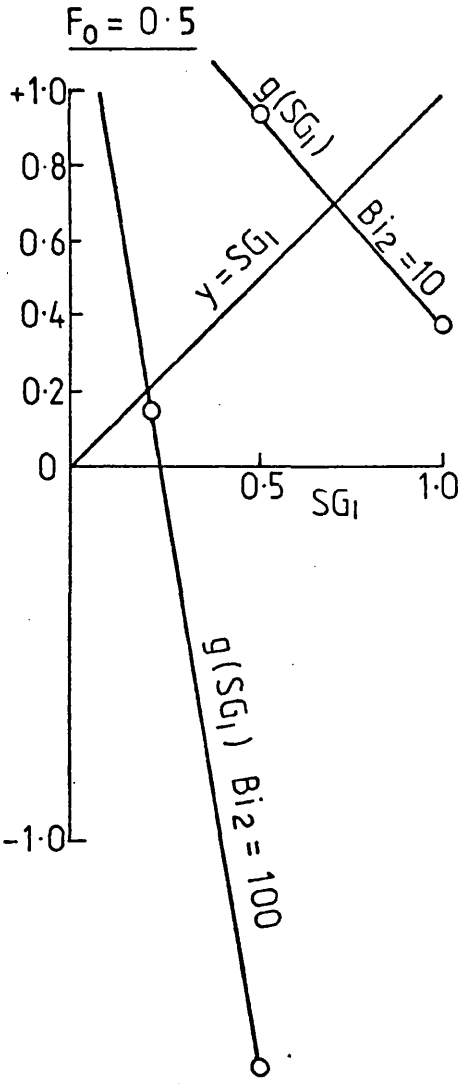

Equation 10.4.4.

$F_o = 0 \cdot 005$

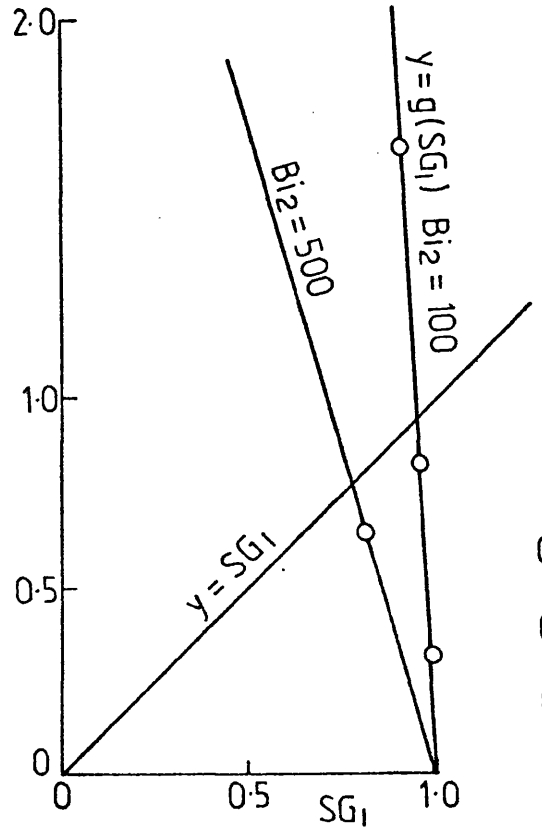

$F_o = 0 \cdot 5$

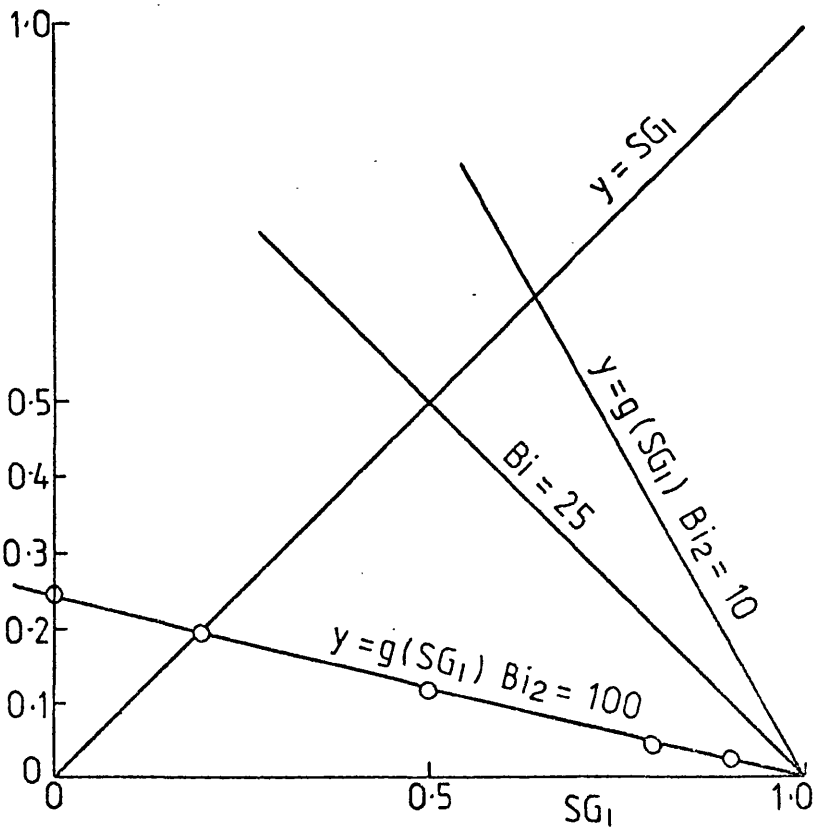

FIGURE 10.4.

CONVERGENCE CHARACTERISTICS OF FINITE-DIFFERENCE EQUATIONS

(2^{nd} time step, j = 3)

Equation 10.3.3

Changing F_o ($Bi_2 = 100$)

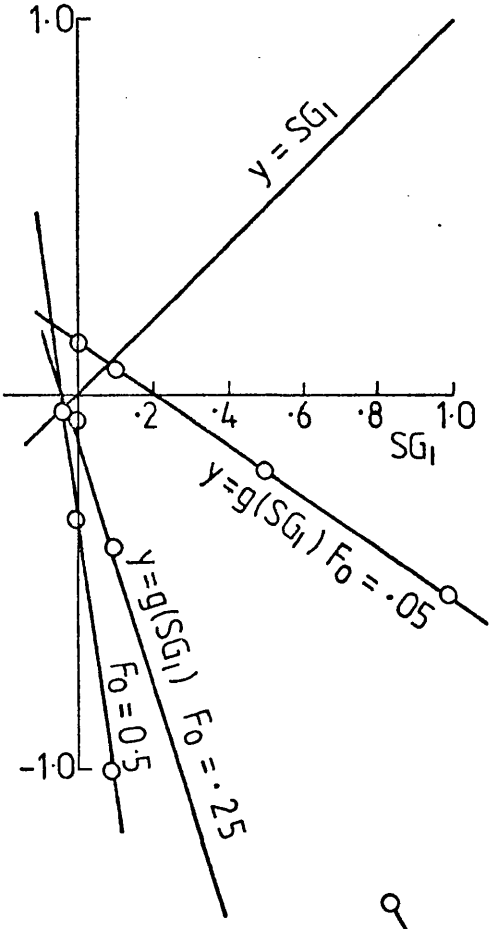

Equation 10.3.3

Changing Bi_2 ($F_o = 1/2$)

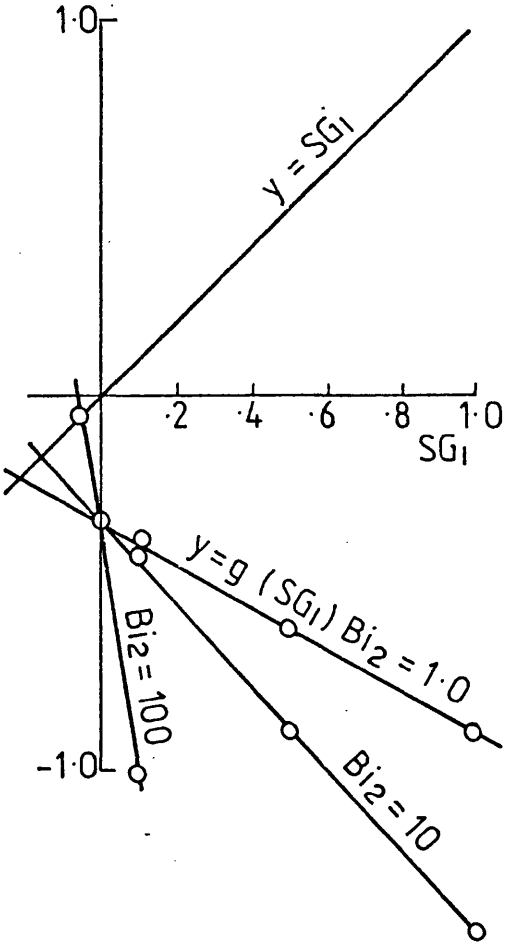

Equation 10.4.4

Changing F_o ($Bi_2 = 100$)

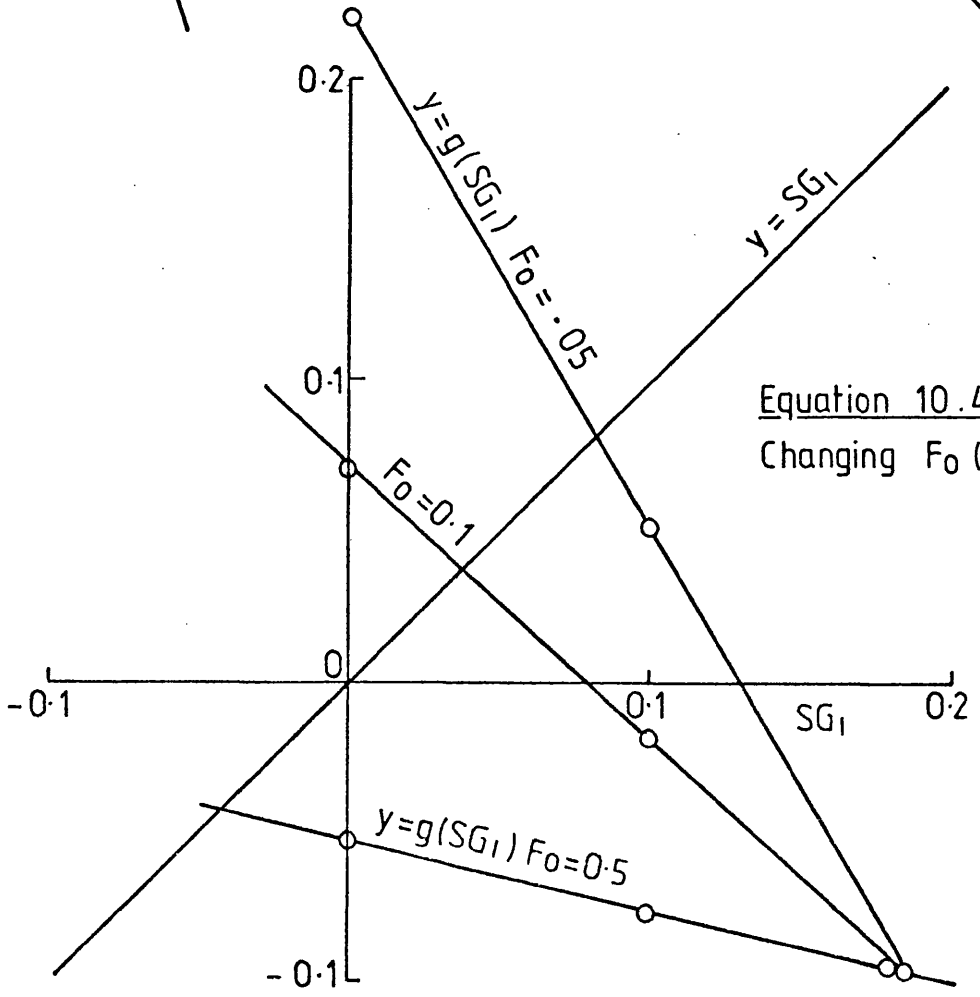

CONSTANT-RATE DRYING

J= 1 T= 0.00000000 BI= 100.0

	X=0	X=0.125	X=0.25	X=0.375	X=0.5	X=0.625	X=0.75	X=0.865	X=1.0
D*	0.100000E 02	0.100000E 02	0.100000E 02	0.100000E 02	0.100000E 02	0.100000E 02	0.100000E 02	0.100000E 02	0.100000E 02
S	0.000000E 00	0.000000E 00	0.000000E 00	0.000000E 00	0.000000E 00	0.000000E 00	0.000000E 00	0.000000E 00	0.000000E 00
C	1.00000	1.00000	1.00000	1.00000	1.00000	1.00000	1.00000	1.00000	1.00000

CBAR = 1.00000

J= 10 T= 0.00703372 BI= 100.0

	X=0	X=0.125	X=0.25	X=0.375	X=0.5	X=0.625	X=0.75	X=0.865	X=1.0
D*	0.442073E 01	0.666061E 01	0.809716E 01	0.897992E 01	0.948936E 01	0.976210E 01	0.989596E 01	0.995383E 01	0.996962E 01
S	0.628956	0.328056E 00	0.738573E 00	0.836658E 00	0.943262E 00	0.973567E 00	0.988440E 00	0.994371E 00	0.996625E 00
C = ΔS1/2	0.245875	0.64540	0.82351	0.90833	0.95327	0.97724	0.98954	0.99546	0.99799	0.99863

CBAR = 0.92106

J = 20 T = 0.00149894 2 BI = 100

	X=0	X=0.125	X=0.25	X=0.375	X=0.5	X=0.625	X=0.75	X=0.865	X=1.0
D*	0.237663E 01	0.464876E 01	0.628541E 01	0.747225E 01	0.831751E 01	0.889815E 01	0.927165E 01	0.947999E 01	0.954544E 01
S	0.405417	0.405417E 00	0.597268E 00	0.719139E 00	0.813057E 00	0.877573E 00	0.919072E 00	0.942121E 00	0.949403E 00
C = ΔS1/2	0.252458	0.37596	0.66734	0.79833	0.87345	0.91999	0.94930	0.96716	0.97677	0.97980

CBAR = 0.83423

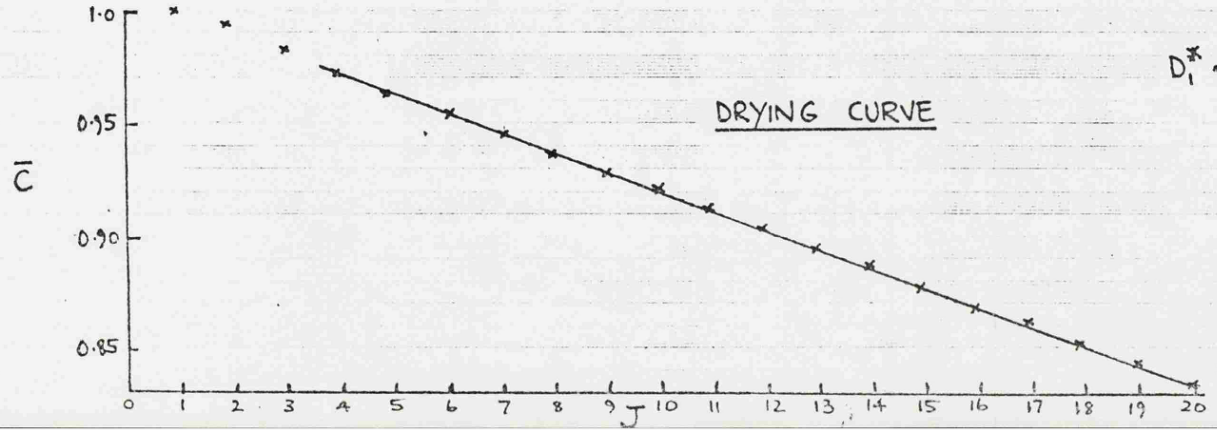

$D_1^* = 10{\cdot}0$, $F_0 = 0{\cdot}5$, DENRAT 0·01

$\bar{C}$ = AVERAGE CONCENTRATION

J = NUMBER OF TIME STEPS

FIGURE 10.5

FIGURE 10.6.

CONVERGENCE OF CONSTANT - RATE BOUNDARY CONDITION

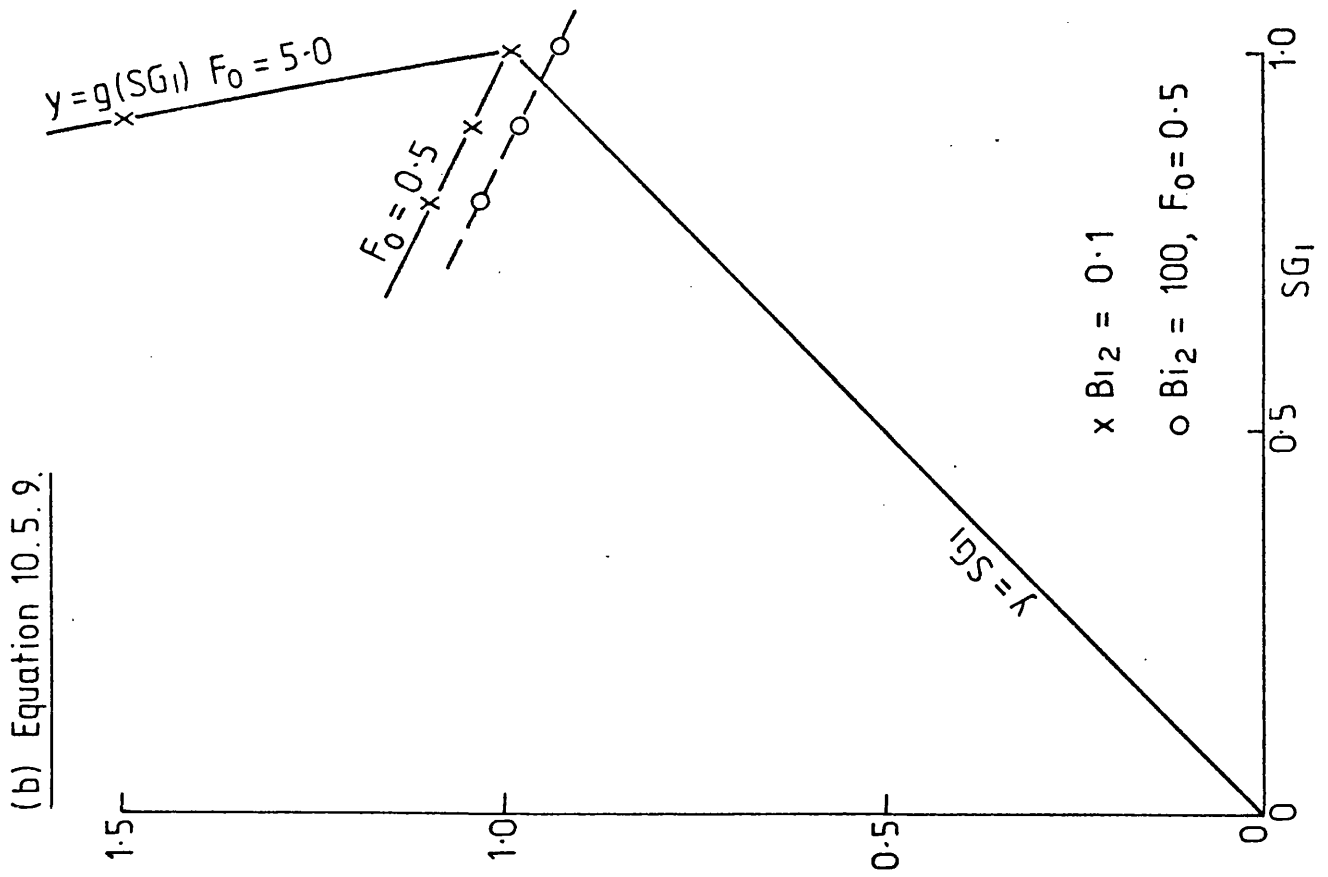

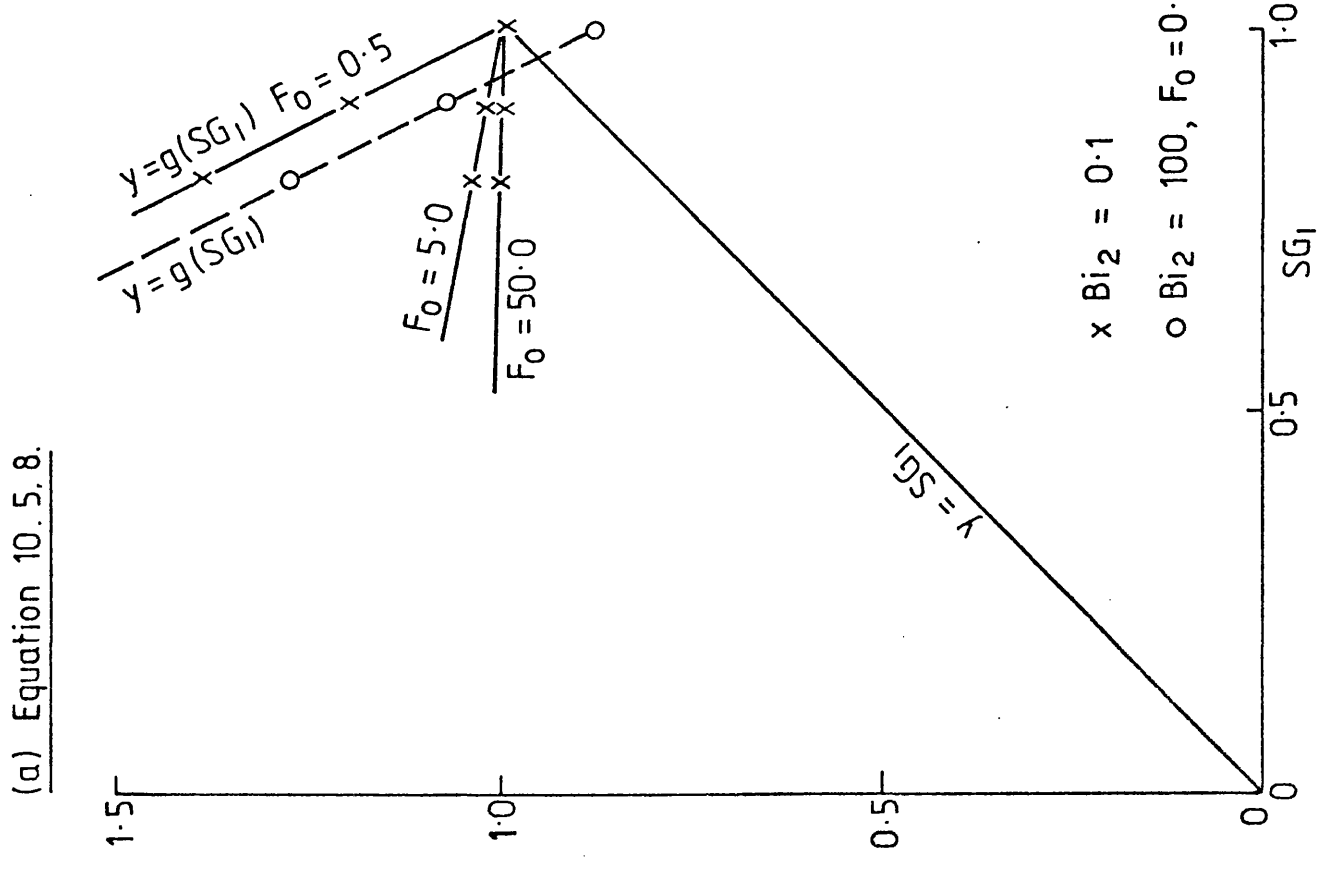

CONSTANT RATE DRYING

J = 21 T = 1·4883660 BI = 0·1 Fo = 5·0

	X=0	X=0.125	X=0.25	X=0.375	X=0.5	X=0.625	X=0.75	X=0.865	X=1.0
D*	0.104058E 01	0.104012E 01	0.104008E 01	0.104070E 01	0.104038E 01	0.104012E 01	0.104069E 01	0.104057E 01	0.104014E 01
S	0.991660E 00	0.982471E 00	0.981512E 00	0.993918E 00	0.987527E 00	0.982409E 00	0.993716E 00	0.991426E 00	0.982721E 00
C	0.99179	0.98287	0.98193	0.99406	0.98782	0.98281	0.99386	0.99162	0.98313

CBAR = 0.98776

J=21 T = 14·887988 BI = 0·1 Fo = 50·0

	X=0	X=0.125	X=0.25	X=0.375	X=0.5	X=0.625	X=0.75	X=0.865	X=1.0
D*	0.104329E 01	0.104736E 01	0.104778E 01	0.104879E 01	0.104769E 01	0.104804E 01	0.104847E 01	0.104813E 01	0.104808E 01
S	0.979335E 00	0.947207E 00	0.955671E 00	0.975368E 00	0.953759E 00	0.960796E 00	0.969406E 00	0.962525E 00	0.961629E 00
C	0.98020	0.94841	0.95667	0.97642	0.95481	0.96169	0.97010	0.96339	0.96251

CBAR = 0.96331

J=21 T = 148·892 BI = 0·1 Fo = 500

	X=0	X=0.125	X=0.25	X=0.375	X=0.5	X=0.625	X=0.75	X=0.865	X=1.0
D*	0.104376E 01	0.104781E 01	0.104738E 01	0.104844E 01	0.104722E 01	0.104764E 01	0.104808E 01	0.104771E 01	0.104767E 01
S	0.975124E 00	0.943273E 00	0.947604E 00	0.968305E 00	0.944314E 00	0.952841E 00	0.961524E 00	0.954163E 00	0.953468E 00
C	0.97569	0.94380	0.94837	0.96952	0.94557	0.95391	0.96240	0.95520	0.95453

CBAR = 0.95503

$D_1^* = 1.05$ DENRAT = 0·1

FIGURE 10.7

(a) CONTRATION PROFILES

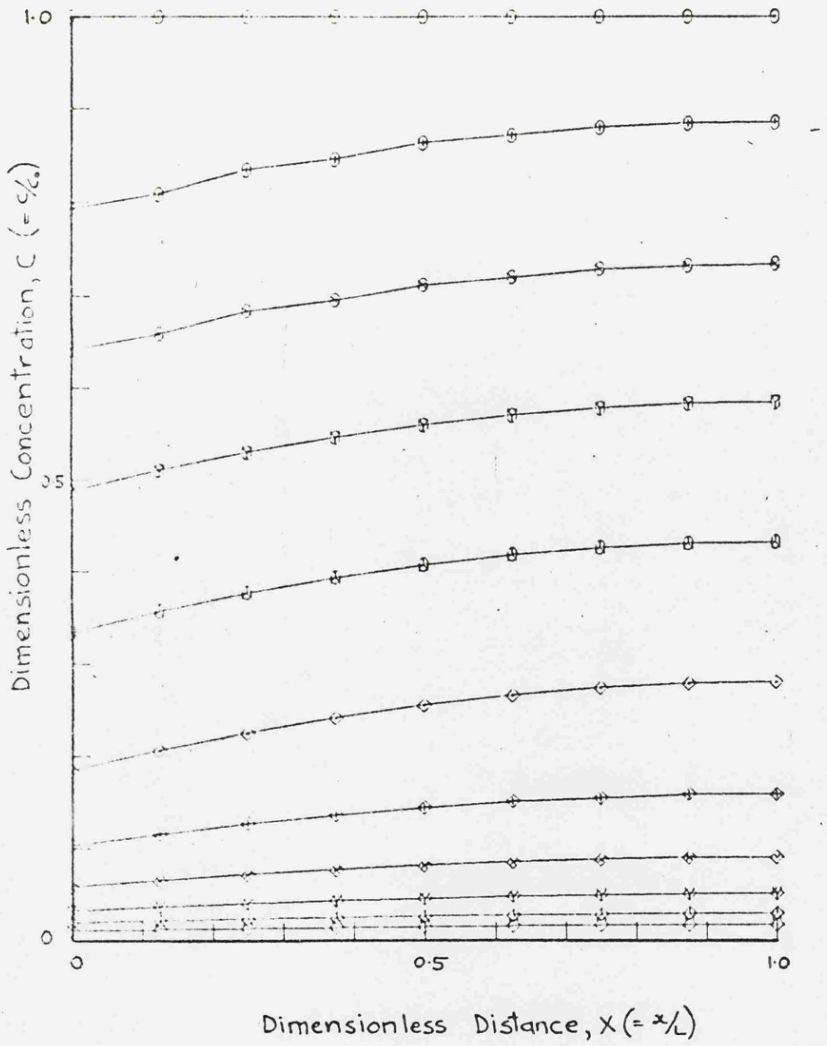

COMPUTER GRAPHICAL OUTPUT

$D_1^* = 1.05$, $Fo = 0.5$, $Bi_2 = 1.0$, $C_{sc} = 0.2$

(b) DRYING CURVE

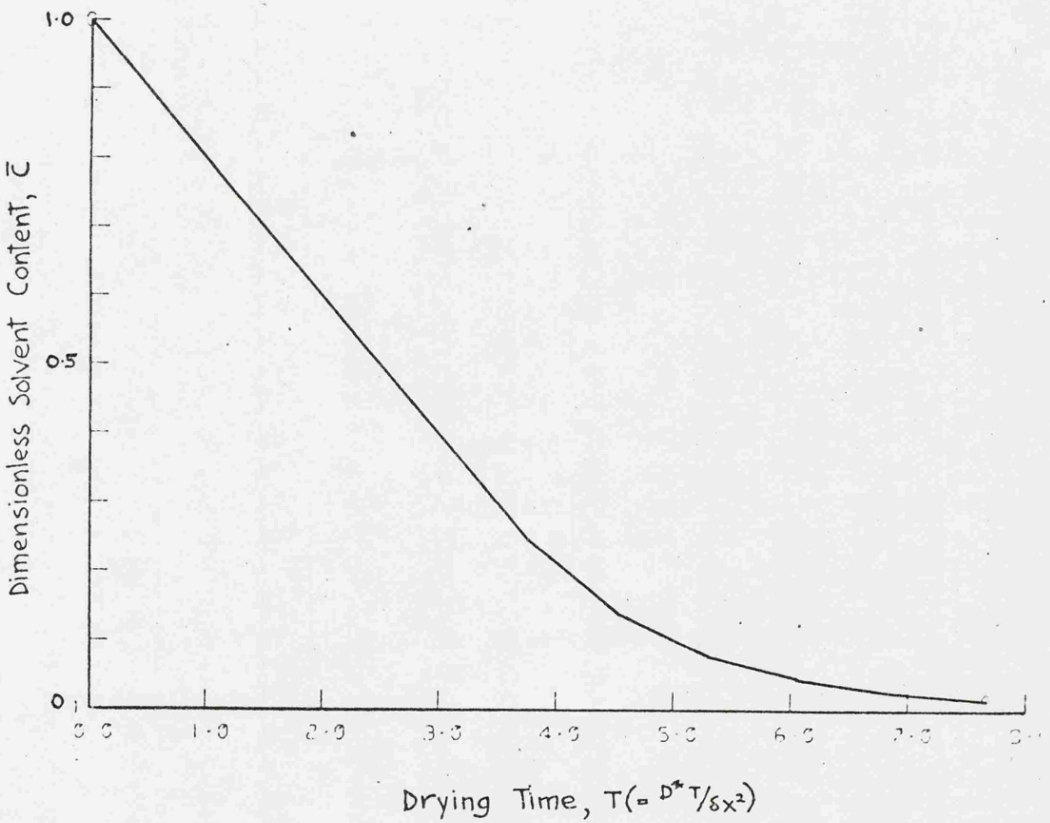

FIGURE 10.8

GRAPHS OF THE RELATION $D^* = e^{KC}$

$K = \ln(D_1^*)$

D_1^*	K
1	0
10	2·3026
100	4·605
1000	6·9077

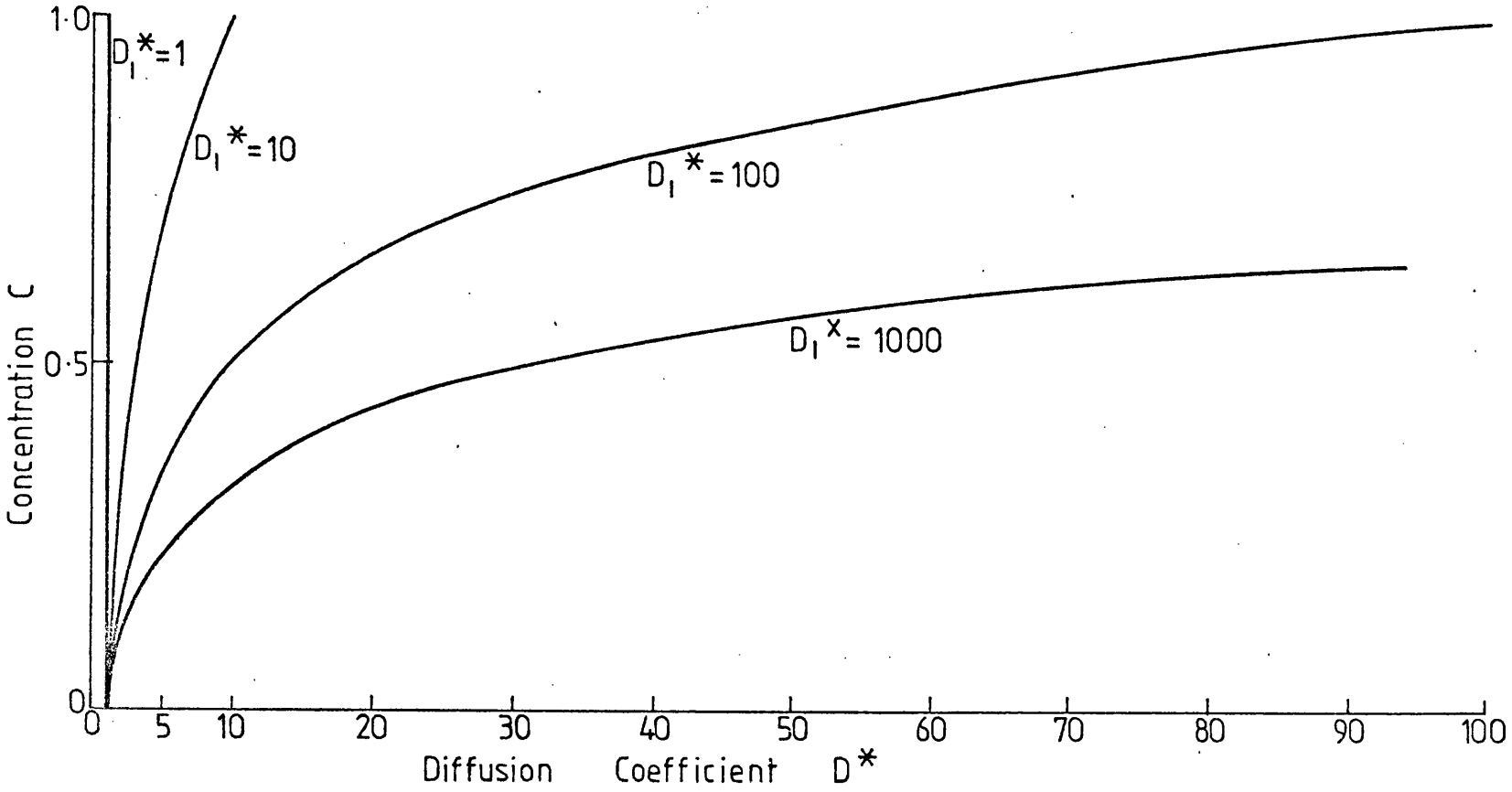

FIGURE 10.9.

FIGURE 10.10a

CONCENTRATION PROFILES

$D_1^* = 10$, $Bi_2 = 1{\cdot}58$, $C_{sc} = 0{\cdot}2$

Profiles at intervals of 200 time steps

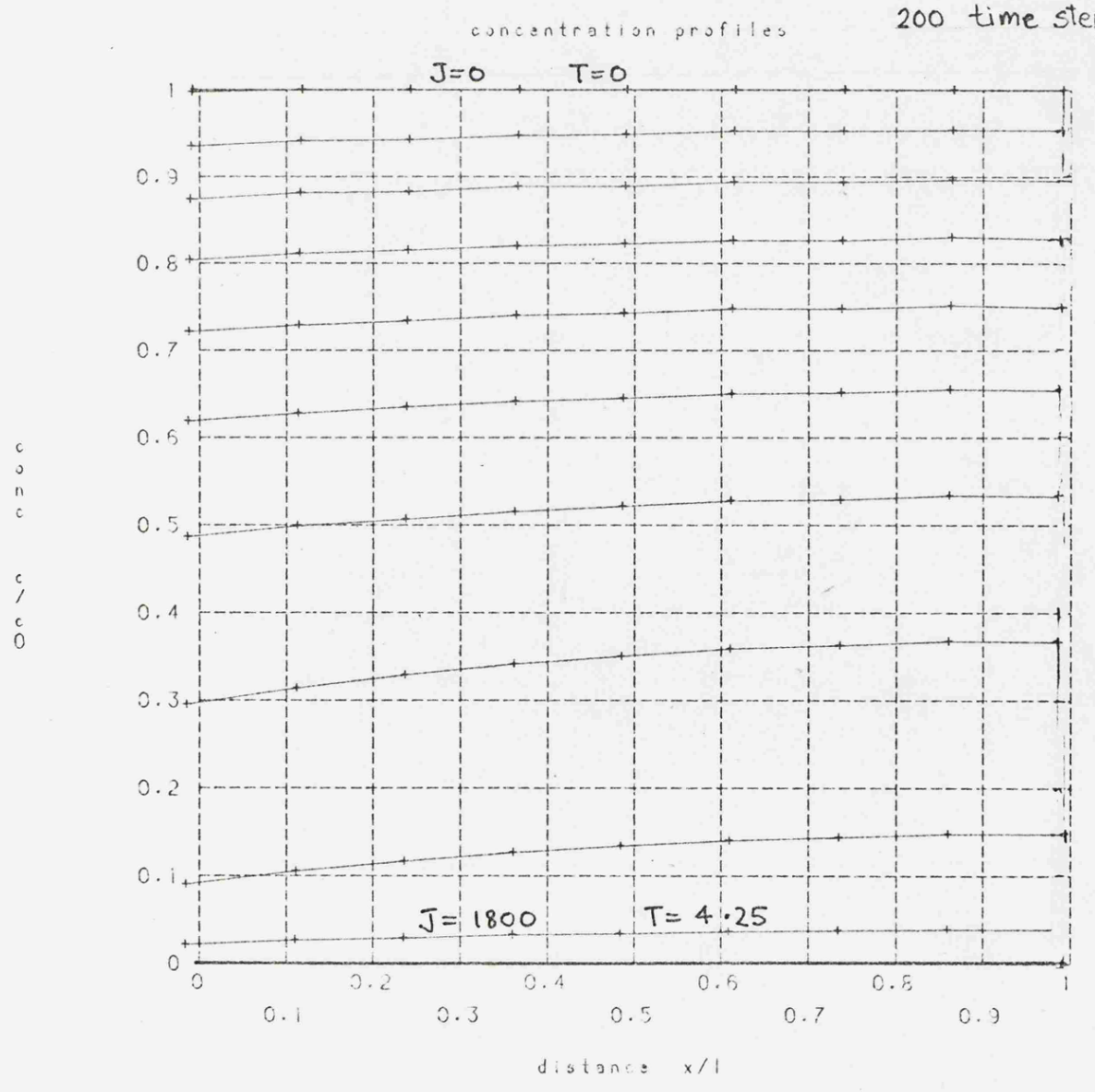

29/4/80

FIGURE 10.10b

CONCENTRATION PROFILES

$D_1^* = 100$, $Bi_2 = 2{\cdot}5$, $C_{sc} = 0{\cdot}2$

Profiles at intervals of 500 time-steps

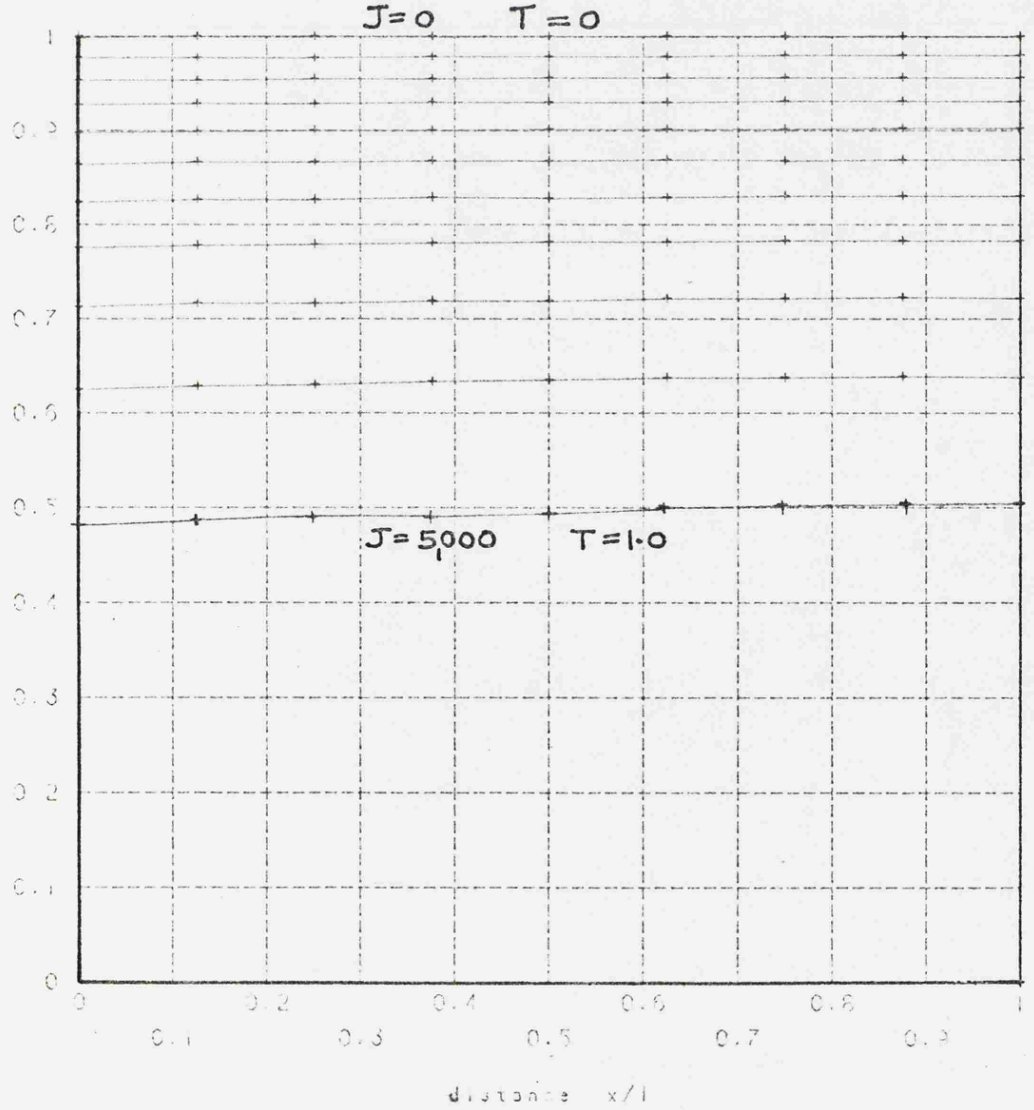

CONCENTRATION PROFILES

($C_{sc} = 0.2$)

a) $D_1^* = 1$, $Bi_2 = 100$, $Fo = 0.1$

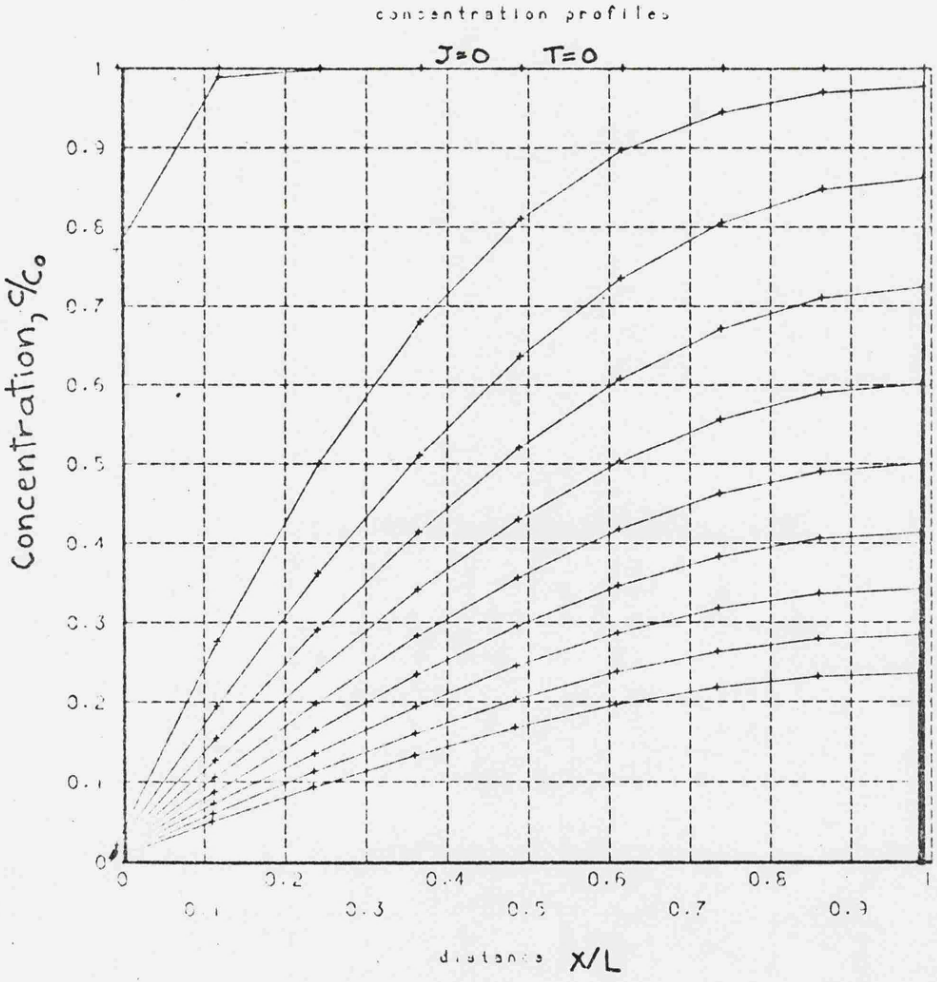

b) $D_1^* = 100$, $Bi_2 = 100$, $Fo = 0.1$

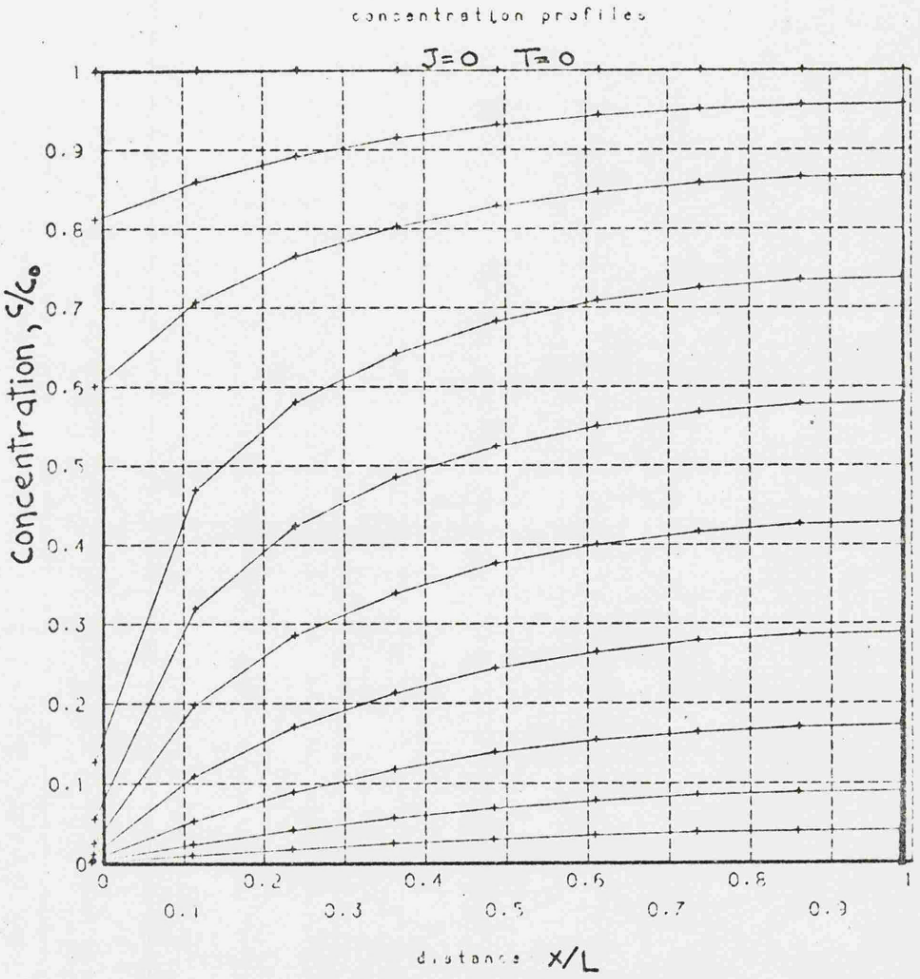

FIGURE 10.11

FIGURE 10.12

DRYING CURVES – COMPUTER PREDICTIONS

□ $D_1^* = 10$, $Bi_2 = 1.58$ Corresponds to Figure 10.10a
△ $D_1^* = 100$, $Bi_2 = 2.5$ Corresponds to Figure 10.10b
\+ $D_1^* = 1.0$, $Bi_2 = 100$ Corresponds to Figure 10.11a
× $D_1^* = 100$, $Bi_2 = 100$ Corresponds to Figure 10.11b

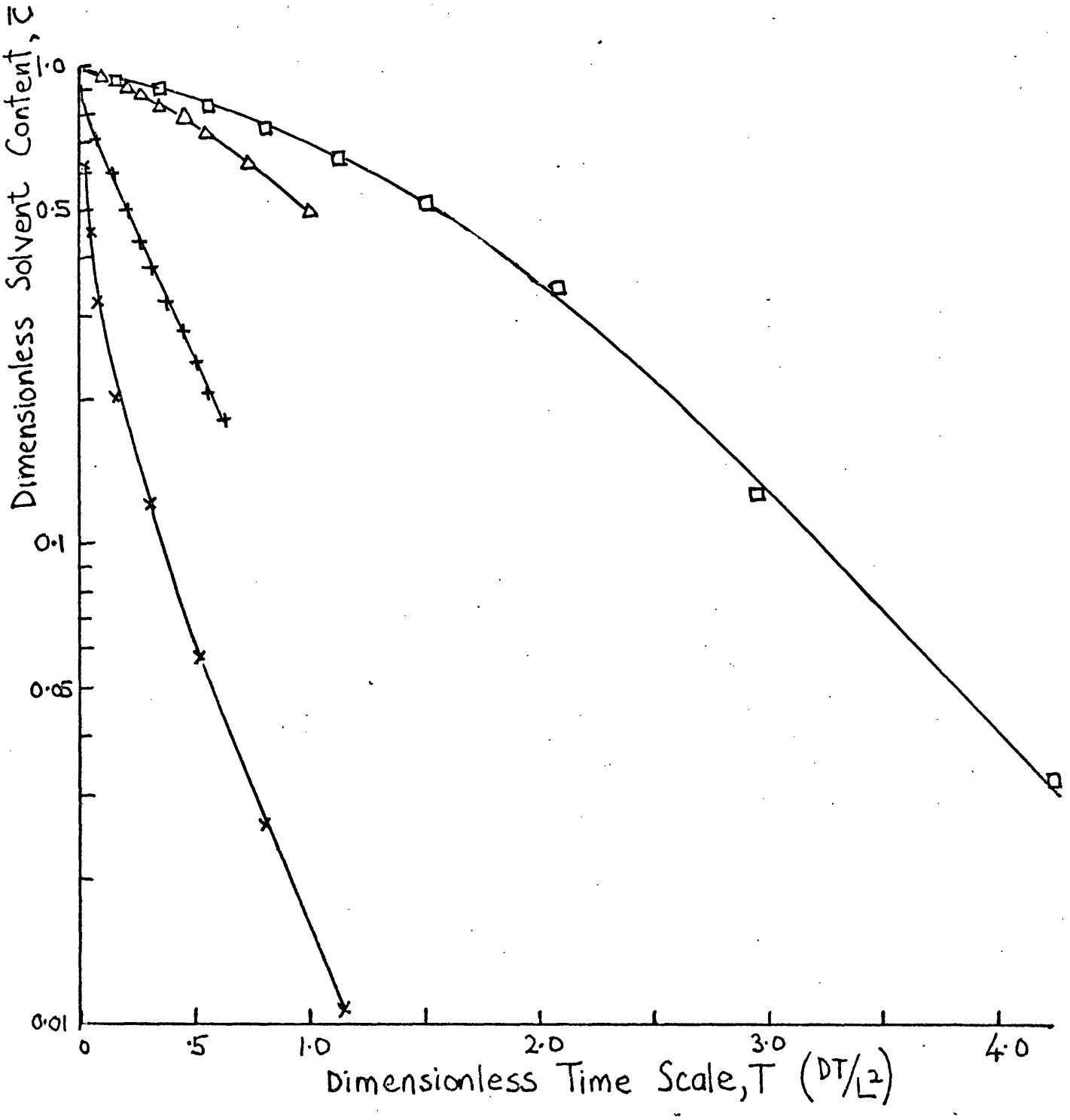

FIGURE 10.13

FALLING RATE PROFILES

$D_1^* = 1.00$, $Bi_2 = 1.0$

Profiles at intervals of 40 time steps

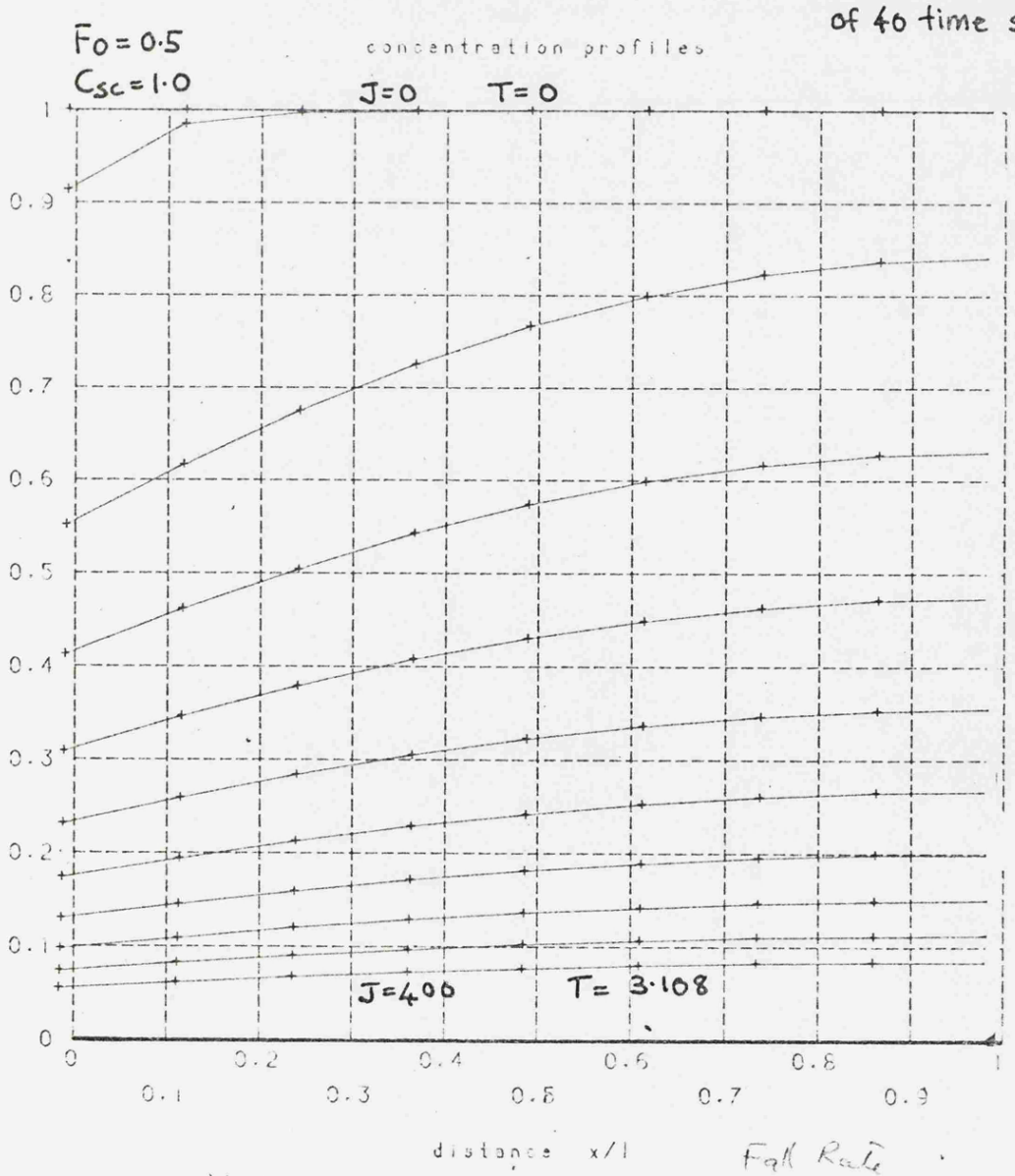

Fall Rate

$D_1^* = 1.0$ $Bi_2 = 1.0$

FIGURE 10.14

FALLING - RATE PERIOD, D^* = CONSTANT

COMPARISON OF COMPUTER PREDICTION WITH STANDARD DATA.

(a) CHANGE OF CONCENTRATION WITH TIME

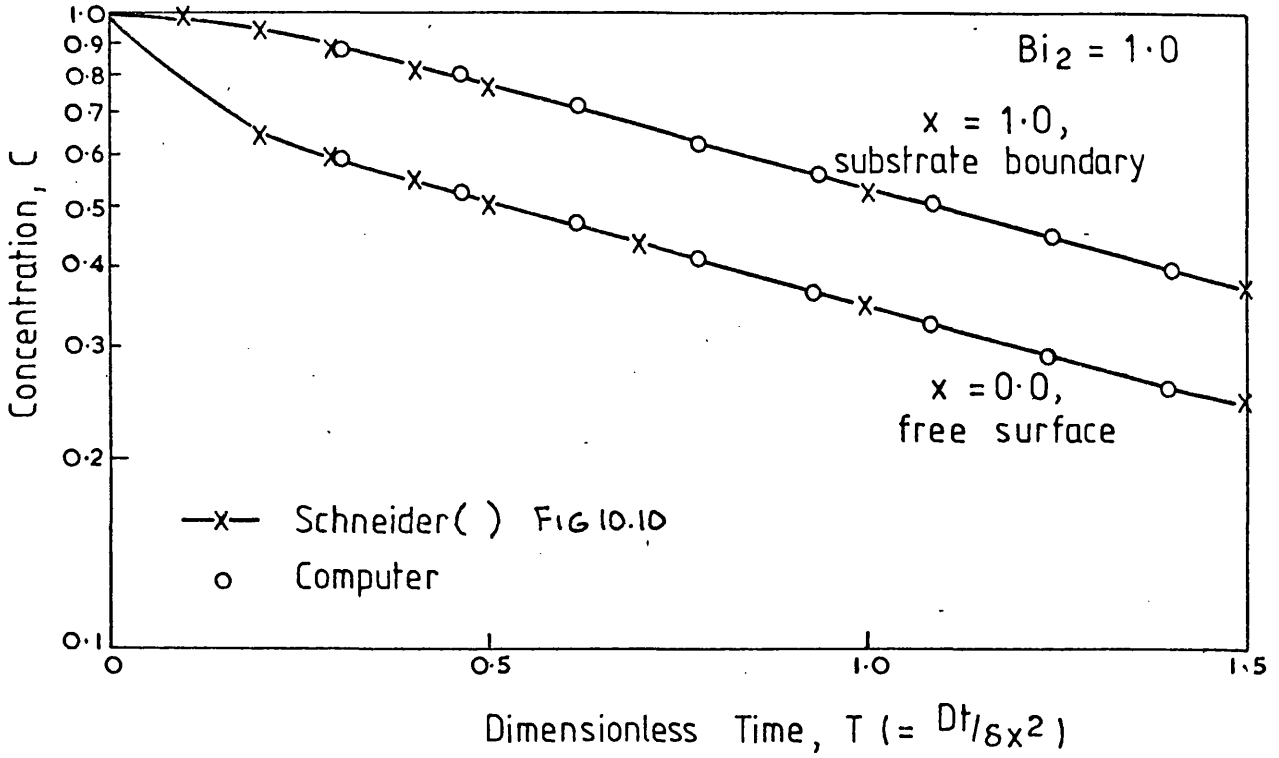

(b) DIMENSIONLESS DRYING CURVES

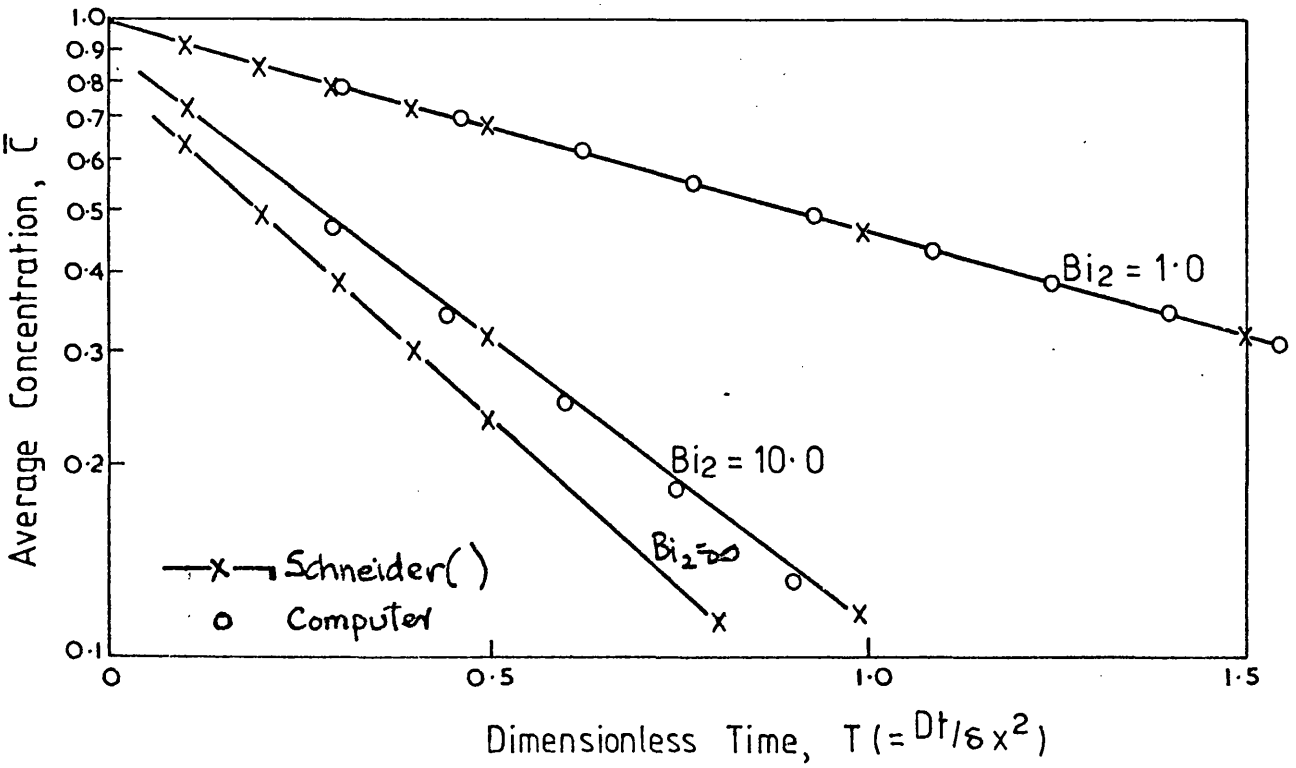

FIGURE 10.15

FALLING RATE PROFILES

$D_1^* = 1.00 \quad Bi_2 = 1000$

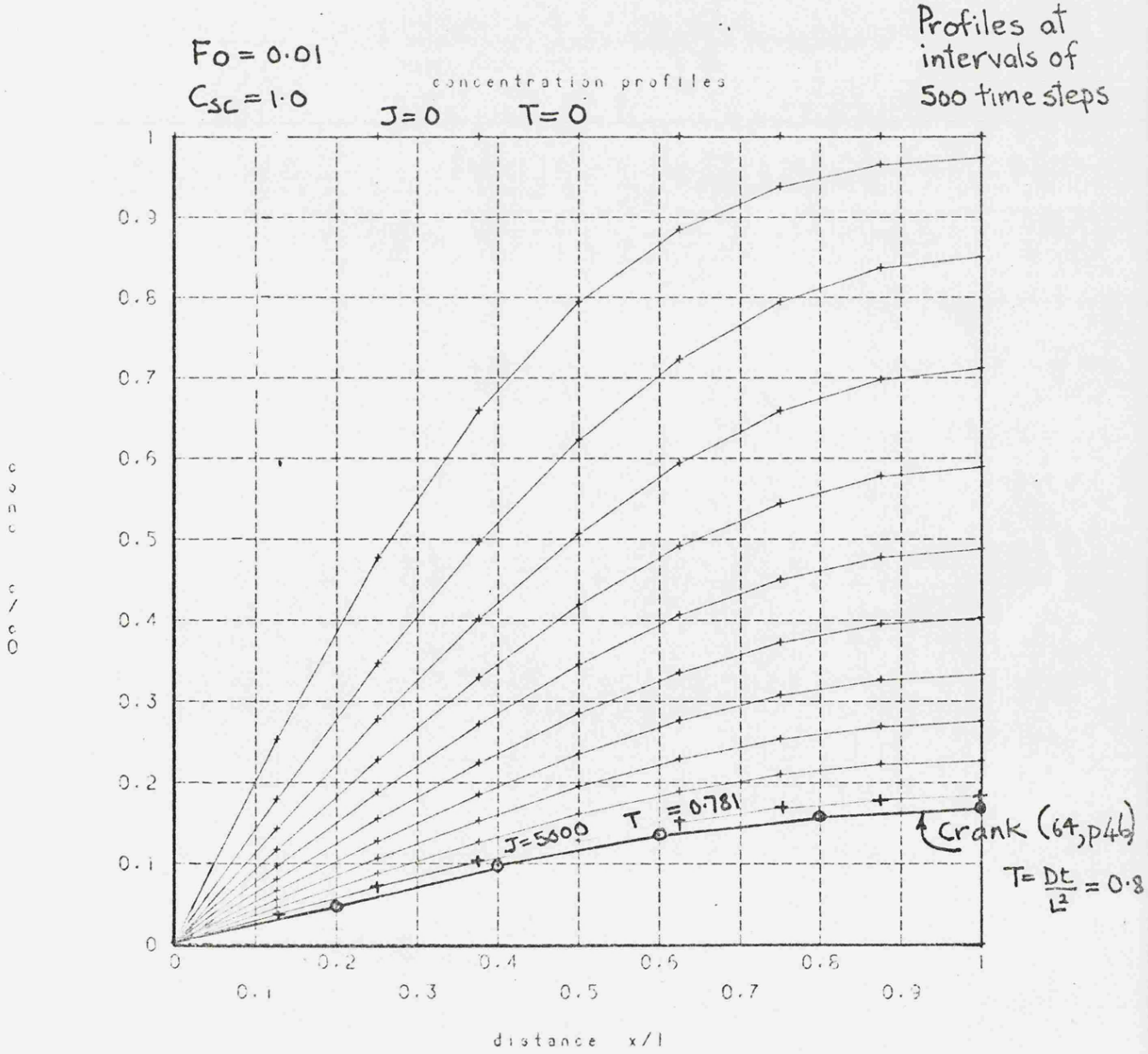

FIGURE 10.16 a

FALLING RATE PROFILES

$D_1^* = 10, \quad Bi_2 = 10$

$Fo = 0.5$

$C_{sc} = 1.0$

Profiles at intervals of 40 time steps

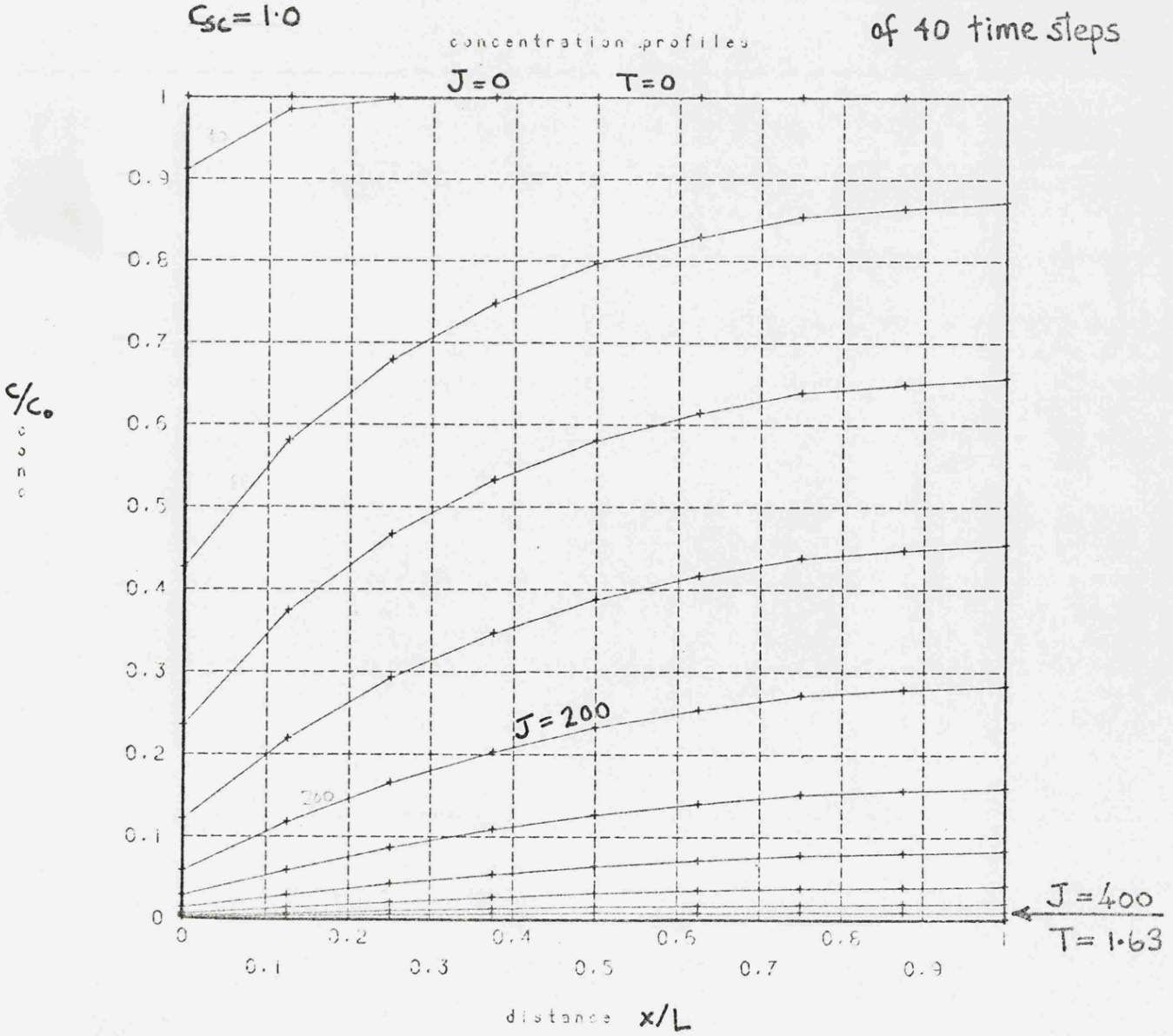

FALLING RATE CONCENTRATION PROFILES

b) $D_1^* = 100$, $Bi_2 = 100$

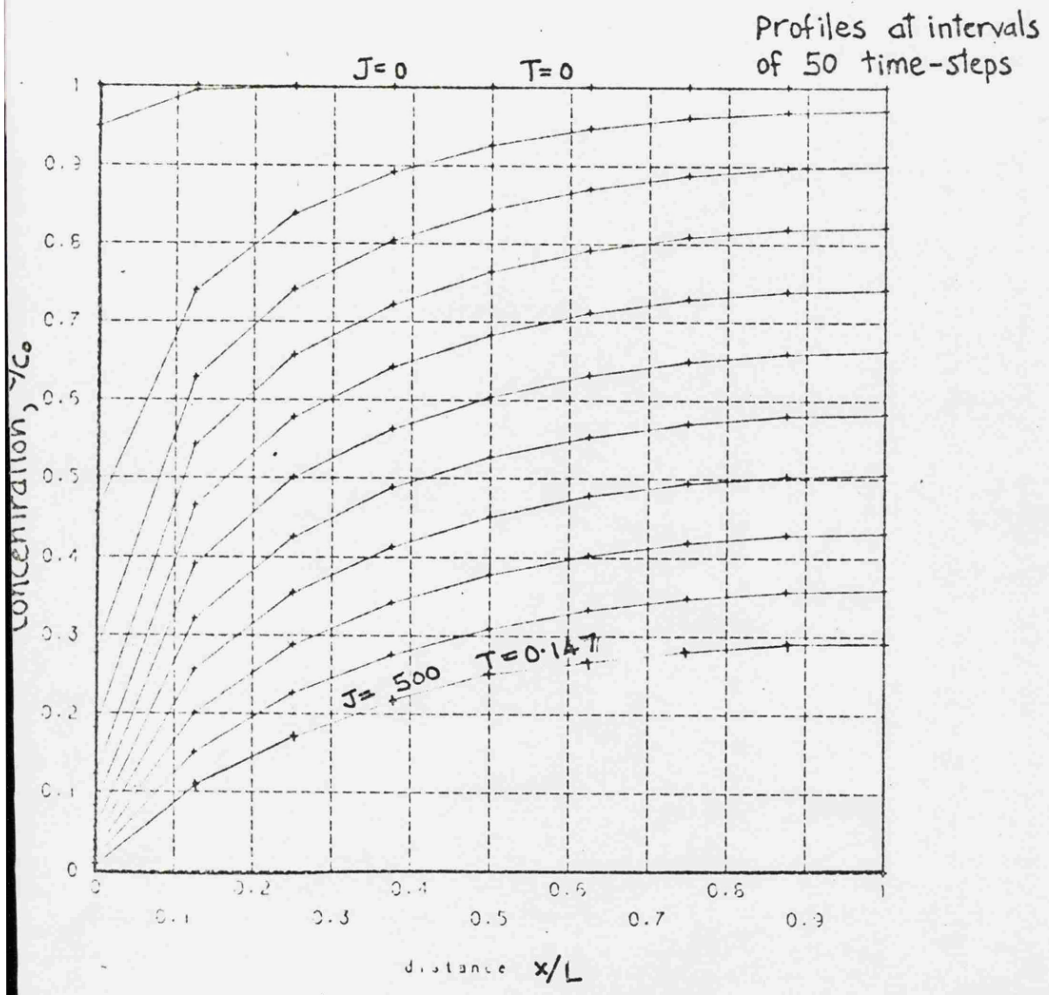

c) $D_1^* = 1{,}000$, $Bi_2 = 1{,}000$

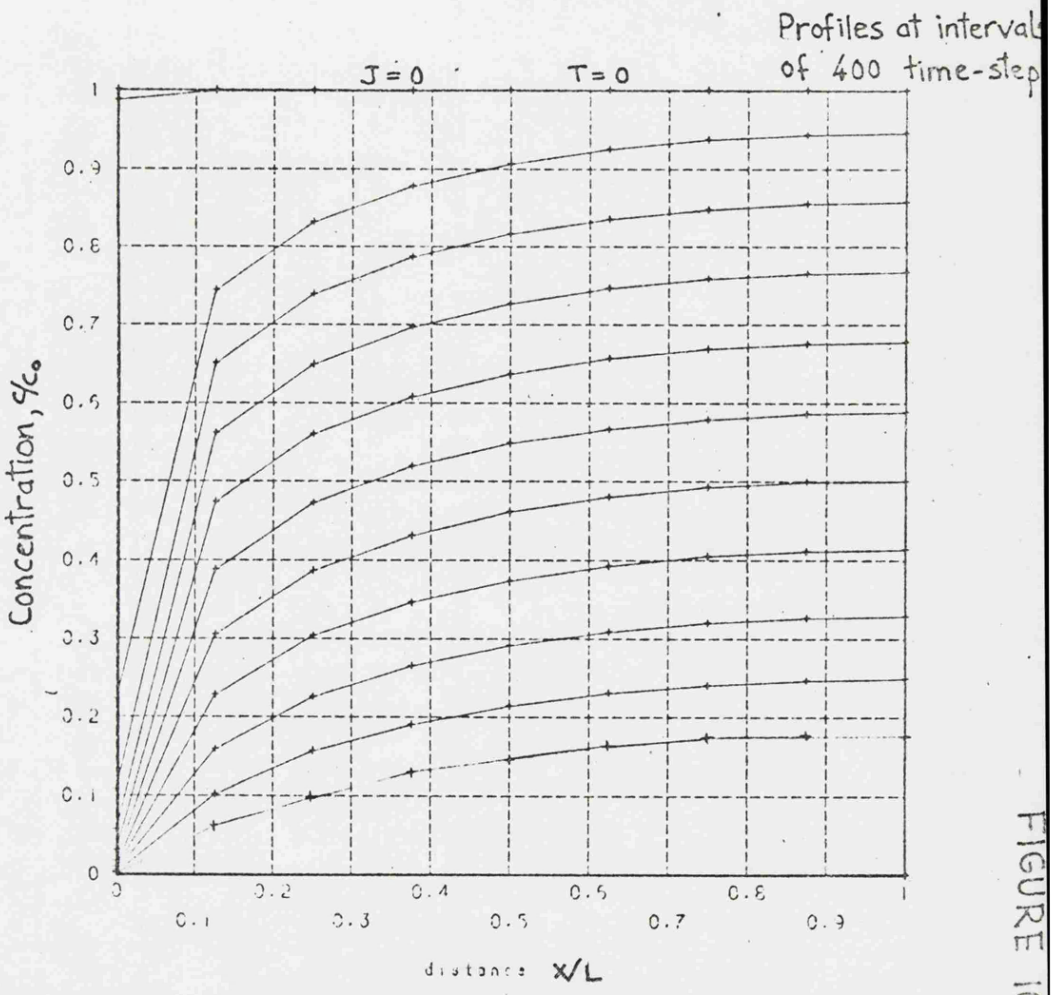

FIGURE 10.16B

FIGURE 10.17

FALLING RATE DRYING CURVES

Corresponding to Figure 10.16

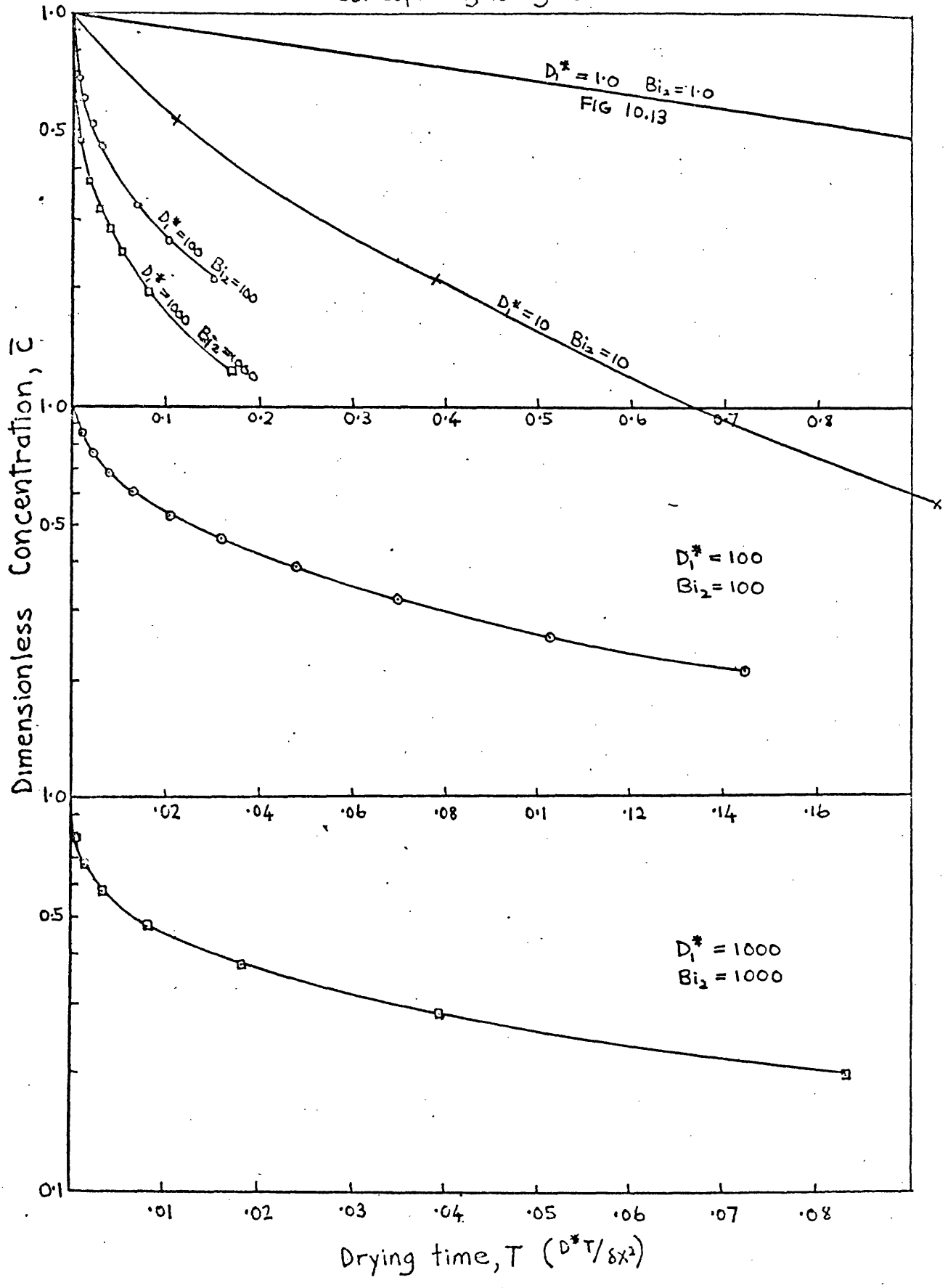

FIGURE 10.18

CHARACTERISTIC DRYING CURVES

Computer prediction - exponential diffusion coefficient

For all curves :-

(a) $Bi_1 = 1 \cdot 0$ at critical point

(b) $Bi_2 = D_l^*$

(c) $D^* \left(\frac{\partial C}{\partial x}\right)_s = Bi_2 C_s$ (equation 9.5.18)

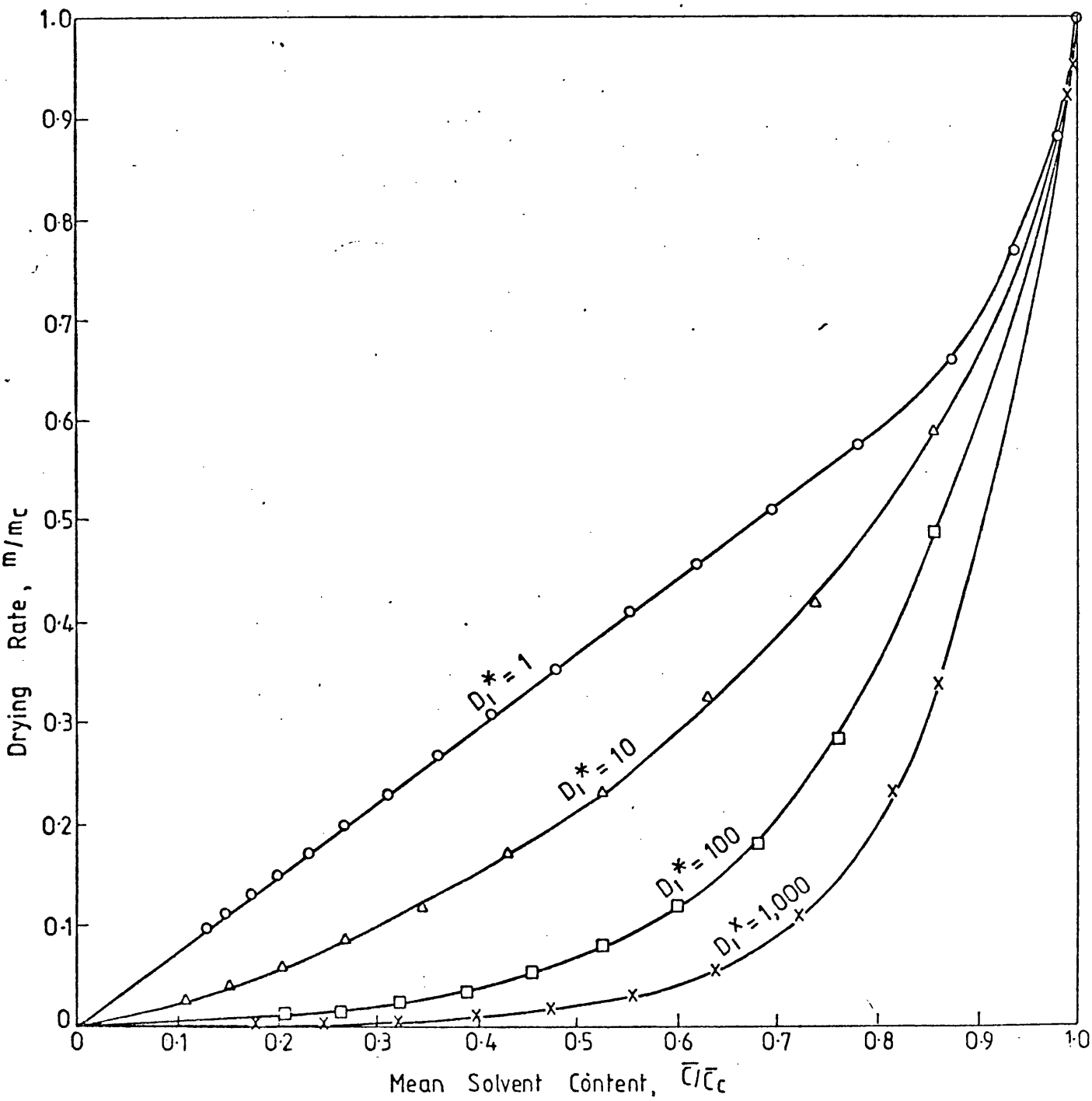

FIGURE 10.19.

CHARACTERISTIC DRYING CURVES

Computer Prediction - Experimental diffusion coefficient with case 2 behaviour

For all curves - (a) $Bi_1 = 1{\cdot}0$ at critical point
(b) $Bi_2 = D_1^*$
(c) $D^* \left(\frac{\partial C}{\partial X}\right)_2 = Bi_2$

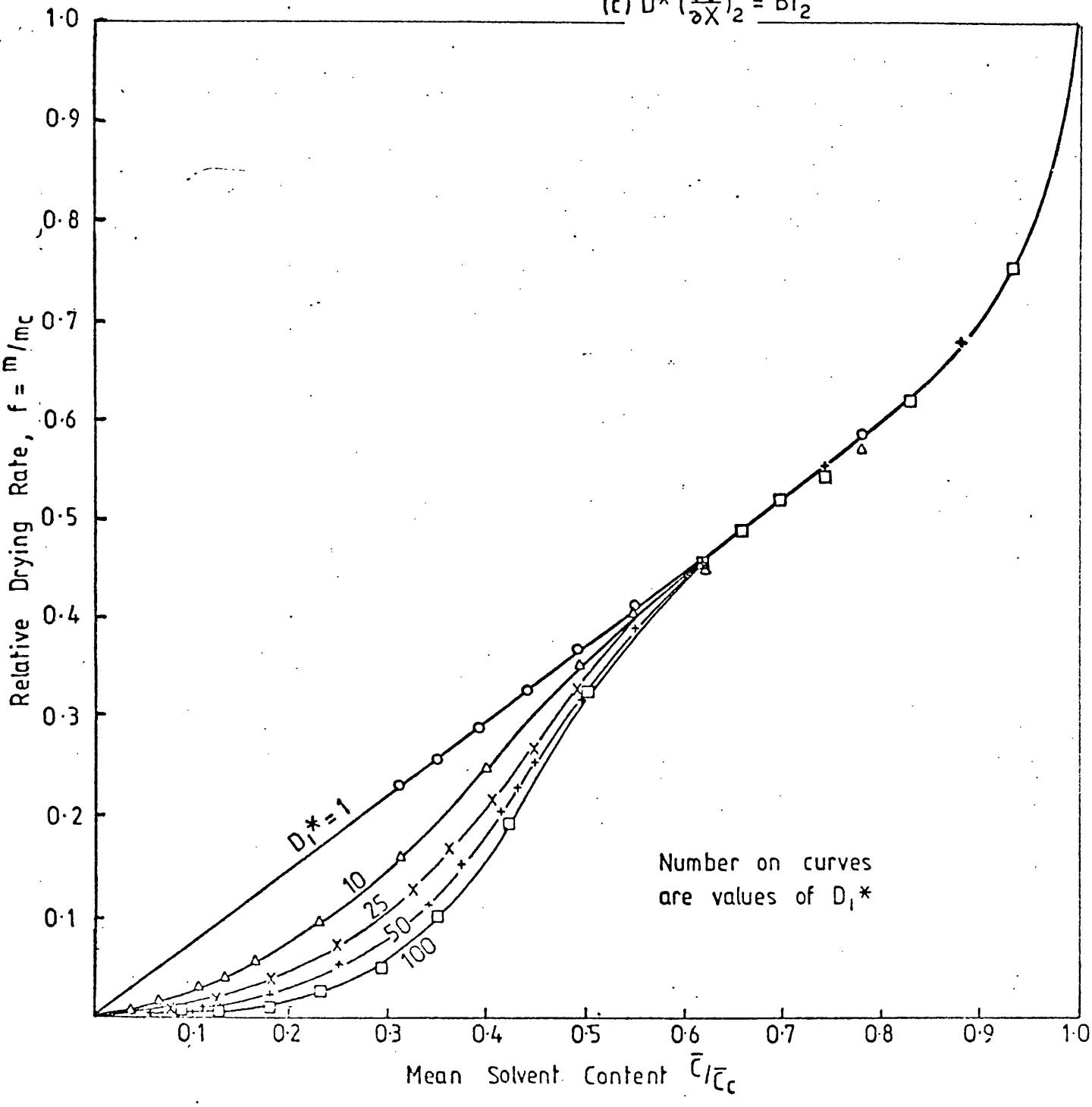

FIGURE 10.20

CHARACTERISTIC · DRYING CURVES

Computer prediction - exponential diffusion coefficient with case 2 behaviour

For all curves

(a) $Bi_1 = 0{\cdot}1$ at critical point

(b) $Bi_2 = 0{\cdot}1\ D_1^*$

(c) $D^X \left(\frac{\partial C}{\partial X}\right)_S = Bi_2$

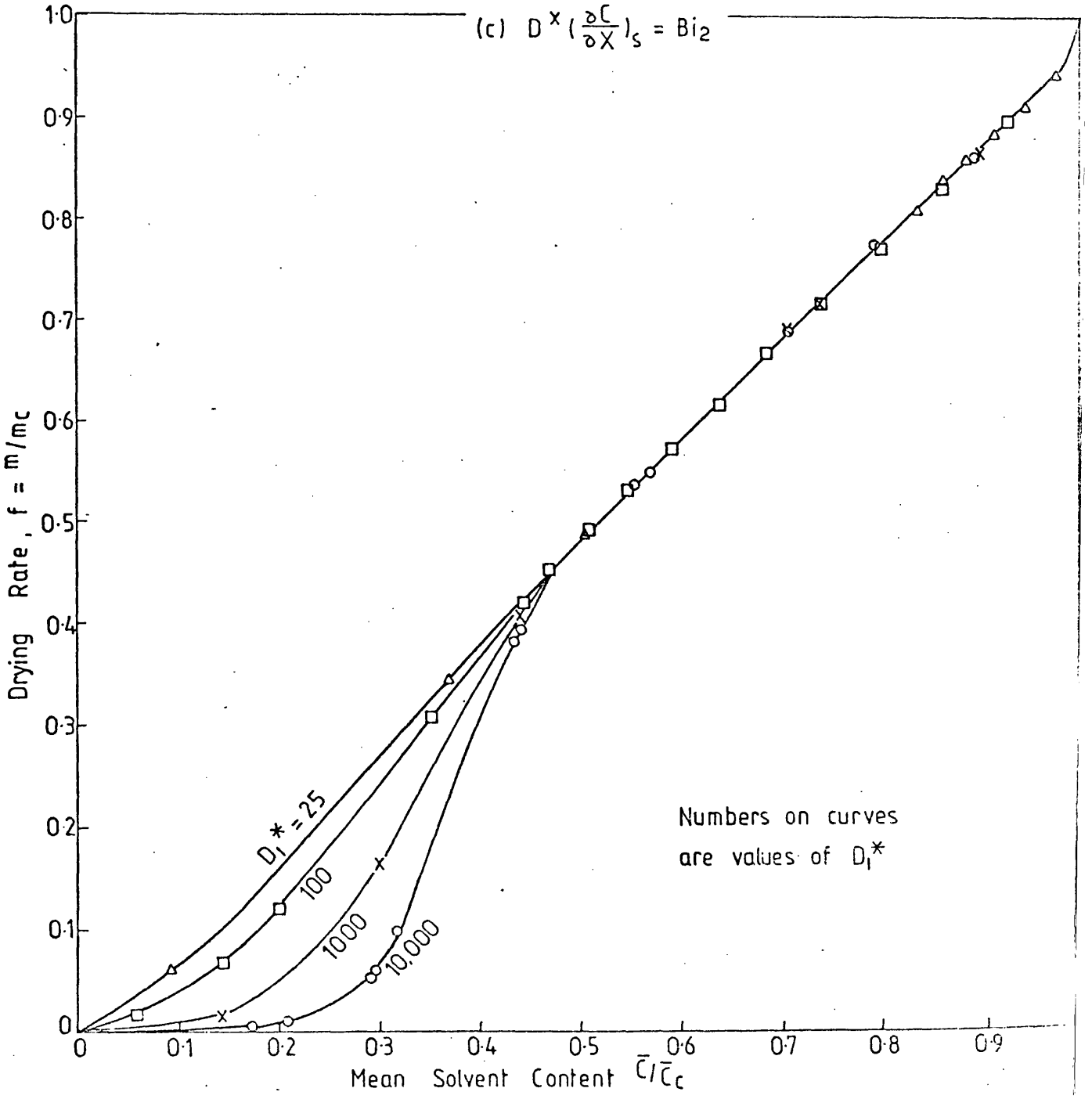

11. ANALYSIS OF IR CURVES IN THE FALLING-RATE PERIOD

11.1 Introduction

To supplement the IR drying curves already recorded, further tests were carried out in the falling-rate period. Because the quantities of solvent to be detected were minute, it was necessary to exercise particular care in setting up the Infragauge and in setting it to zero. A number of previous tests were re-run with increased amplification of the Infragauge signal, to show up the later stages of drying.

To correlate the IR drying curves for the falling-rate period, data extracted from the curves was re-plotted in various ways in an attempt to linearise it. Later the concept of the "Characteristic Drying Curve" was successfully used to normalise a group of related IR curves in a test series. All of these normalised curves were similar in shape.

Provided that drying data can be normalised in terms of a characteristic drying curve, this concept can then be used to predict the falling-rate drying time. The graphs revealed that for ink drying the normalised curve could be approximated by simple algebraic functions. Integration of these functions leads to analytic equations for the falling-rate drying time. Results from this analysis served to emphasise that long drying times were necessary to remove the final 1 or 2% of solvent from the ink. Such behaviour is consistent with the theory of an exponentially dependent diffusion coefficient developed in earlier chapters.

The falling-rate drying curve

The smooth IR drying curves, Figure 11.1a, typify plots of moisture content against drying time. Fisher (76) appears to have been the

first to point out the discontinuities which appear when the original data is re-plotted as a rate of drying curve, Figure 11.1b. Sherwood (3) also stressed that a rate of drying curve was essential for the accurate location of the critical point. As has already been pointed out, the discontinuity at the critical point arises because the nature of the resistance to solvent transfer begins to change at this point. Because of this fundamental discontinuity, the falling-rate period is most usefully analysed separately from the constant-rate period. It will be demonstrated that conditions at the critical point provide the vital link between constant-rate and falling-rate periods.

The practice of sub-dividing the falling-rate period appears to have been originated by Fisher (76). He found that in each of three sub-periods the drying rate was characteristically different, Figure 11.1b.

In the first period the drying rate was directly proportional to the moisture content

$$m = \frac{dw}{dt} = k_1 w \qquad 11.1.1$$

m = drying rate, $Kg/m^2 s$

w = moisture content of solid, Kg,m^3

k_1 = constant

In the second falling-rate period, the linear form of equation 11.1.1 remained, but the straight line no longer passes through the origin of the graph

$$m = k_2 (w - k_3) \qquad 11.1.2$$

k_2 and k_3 are constants.

In the third and final period, the moisture content fell to its equilibrium value; the relation between drying rate and moisture content was non-linear.

The critical moisture content is a parameter of fundamental importance for dryer design. There appears to be no generally accepted method of predicting the critical point and it is usually determined empirically for a particular material, Treybal (77). Some workers, such as Perry (78) regard the critical moisture content as a physical constant. Other workers, such as Fisher (76) and Sherwood (3), consider that the critical moisture content will depend upon both the previous drying rate and the thickness of the solid being dried.

It is important to note, that the characteristic shape of the drying-rate curve, Figure 11.1b, was determined for a capillary porous body. Also, physical explanations of the critical point and of falling-rate drying, such as in Keey (51), are usually given in terms of a postulated model of a capillary porous system. Because this model is not an appropriate one, concepts derived from it are not necessarily applicable to ink drying. However these concepts have provided a general framework for the present research.

Note

The following two points should be noted regarding the analysis of IR drying curves carried out later in this chapter:-

i) No attempt was made to convert the Infragauge output signal, V (volts) into a mass of solvent present on unit surface area X, (Kg/m^2). This was unnecessary as the data was later expressed

in terms of the solvent content either at the beginning of drying or at the critical point, i.e.

$$\frac{X}{X_o} \equiv \frac{V}{V_o} \quad \text{or} \quad \frac{X}{X_c} \equiv \frac{V}{V_c} \qquad 11.1.3$$

The subscripts o and c denote conditions at the beginning of drying and at the critical point respectively.

The use of normalised voltages had the additional advantage that it was unnecessary to recalibrate the Infragauge when later its amplification was increased.

ii) In the falling-rate period, the origin of the time scale is at the critical point. The term "drying time" will imply falling-rate drying time.

11.2 The Effect of Ink Thickness on Drying Time

Logarithmic Plotting

Figure 11.2 shows test results to determine the effect of ink thickness on drying time. The first attempt to correlate the IR drying curves was based on the results of classical diffusion theory outlined in section 9.3. When the diffusion coefficient is constant, the results for the drying time of a slab have the general form

$$\phi = \sum_{n=0}^{\infty} e^{-tD/L^2} \qquad 11.2.1$$

where ϕ = relative solvent content (equation 11.1.3)

t = time measured from critical point

L = thickness of ink film

In Figure 11.3a, the data of Figure 11.2 have been replotted on log/linear co-ordinates. If equation 11.2.1 is to be satisfied, then the curves of Figure 11.3a must be straight lines. Assuming that drying is diffusion controlled there appear to be two explanations for the characteristic, concave-upwards, shape of the curves:-

i) In the early part of the falling-rate period the rate of drying will still be partly controlled by external convection. The change from external to internal control will occur over a transition period. The effect of such a transition is apparent on the curves of Figure 10.1b, near the origin.

ii) The diffusion coefficient is proportional to solvent concentrations. To demonstrate the shape of a drying curve, when the diffusion coefficient is proportional to solvent concentration, a solution of equation 11.21 was obtained by trial and error. For purposes of this demonstration the following arbitrary simplying assumptions were made

$L = 1 \qquad D = \phi$

equation 11.2.1 then reduces to

$$\ln \phi = -t\phi \qquad 11.2.2$$

Table 1.1 shows solutions to this equation for various values of t

TABLE 1.1

t	0	1	5	10
D	1.0	.566	.265	.175
	1.0	.566	.265	.175

These points have been plotted on Figure 11.3a and the characteristic concave-up shape they express shows qualitative agreement with the drying curves. The numerical agreement between the arbitrary numerical solution and the points of band 1 is entirely fortuitous.

Dimensionless time-scale

Provided that the drying curves satisfy equation 11.2.1, the effect of thickness may be eliminated by using the dimensionless time scale (tD/L^2). In practice the magnitude of D is unknown and the quasi-dimensionless time scale (t/L^2) was used. Based on the ink thickness data given in chapter 4 the normalising factors were calculated as follows.

TABLE 11.2

Band No.	1	2	3	4
Ink thickness L, μm	6.6	9.4	11.3	13.8
L^2	43.6	88.4	127.7	190.5
Normalised time scale, α t/L^2	1	2.03	2.93	4.37

For each band, the drying times of Figure 11.3a were reduced by dividing by the factors given in the bottom row of Table 11.2. The data is replotted in Figure 11.3b and it can be seen that this normalising technique has been quite successful in reducing the data to a single curve.

Extraction of data from IR drying curves

Before any replotting was possible, the drying curves had first to be converted into numerical form, i.e. into a table of corresponding Infragauge voltages and times. The numerical data was in its turn transformed into non-dimensional form, and other results, such as drying rates, were derived from it. Because the numerical data was always presented as a graph, the data tables themselves were relegated to Appendix 8. Wherever necessary the location of the tabular data is given on the appropriate graph.

Comment

Replotting the drying curves in dimensionless form produced results which were consistent with a diffusion theory of drying. These dimensionless plots indicated that the diffusion coefficient was not constant, but was in some manner dependent on the solvent concentration.

11.3 The Effect of Air Velocity and Air Temperature on Drying Time

The falling-rate sections of the drying curves shown in Figure 6.10 and 6.11 were analysed in detail. The position of the critical point was difficult to locate with precision. This same problem was encountered throughout the graphical analysis of the IR drying curves. The difficulty is only partially alleviated by the construction of a rate-of-drying curve; evaluation of the gradient tends to exagerate irregularities in the IR curve.

Figure 11.4 is based on data extracted from the falling-rate region of Figure 6.10. The graphs of ϕ against drying-time, on log/linear co-ordinates, show the effect of air velocity on drying. The

following comments are relevant:-

a) At first glance, the curves in Figure 6.10 appear to approach each other as drying proceeds. In fact, a closer inspection will show that the horizontal time separation between any two curves increases with time.

b) When plotted in log/linear co-ordinates, Figure 6.10, shows that the early part of each drying curve is linear and that each straight line has a different slope. Thus, this method of plotting does not produce a single normalised drying curve.

c) The later portions of the curves have the characteristic concave-upwards shape indicitive of a concentration dependent diffusion coefficient.

Figure 11.5 is based on data extracted from the falling-rate region of Figure 6.11. The graphs of ϕ against drying time, plotted on log/linear co-ordinates, show the effect of air temperature on drying. Comments a), b) and c) immediately above apply equally to Figure 11.6.

Comment

By replotting the falling-rate data, a degree of correlation of the drying curves was achieved. However, unlike the results from classic diffusion theory, the curves showed the drying rate to be affected by both air velocity and air temperature. The drying rate appeared to be a function of the earlier drying rate at the critical point.

In an attempt to improve further, the correlation which has been achieved, the data was next normalised using the concept of the "characteristic drying curve".

11.4 The Characteristic Drying Curve

According to Keey (79), the first worker to make use of a characteristic drying curve to design a batch dryer was van Meel (80). In this paper van Meel assumed that rate of drying v moisture curves (Figure 11.1b), determined under constant conditions in a laboratory, were available. He presented his drying curve in dimensionless form by using conditions at the critical point to normalise the data, Figure 11.1c. The dimensionless co-ordinates of this curve are

$$f = \frac{m}{m_c} \qquad 11.4.1$$

f = relative drying rate

m = rate of drying, Kg/m^2 s

m_c = value of m at the critical point

$$\phi = \frac{X}{X_c} \qquad 11.4.2$$

ϕ = relative solvent content

X = mass of solvent present on unit area of web, kg/m

X_c = value of X at the critical point

Keey (79)has designated the normalised drying rate curve as a "characteristic drying curve" and has implied that it is "specific to a given material". The process of using conditions at the critical point to normalise drying data appears to be a useful one. However the hypothesis is that the characteristic curve is specific to given material required both theoretical and experimental verification. In his paper, van Meel stated that the laboratory experiments to establish the dimensionless drying rate curve should approach "as closely as possible the actual conditions in a dryer".

Keey and his co-workers have attempted to establish the validity of the characteristic drying curve concept. Its theoretical foundations were examined in Keey and Suzuki (81) for the case of a coarsely porous, non-hygroscopic solid, where the drying process was modelled by an evaporative plane slowly withdrawing into the moist material. These investigations indicated there was no single characteristic curve for a given material. However for a given dryer, it was considered that variations in drying parameters would be small enough for the characteristic drying curve to provide a basis for calculation.

Because it is based on a model of a thick porous solid, Keey's theoretical analysis is not of direct relevance to this research. However, the characteristic drying curve appeared a useful concept, which could be used on an empirical basis, to correlate ink drying data in the falling-rate region.

11.5 Correlations Using the Concept of the Characteristic Drying Curve

The effect of air velocity

Figure 11.6 shows the effect of changes in the velocity of the drying air on the drying rate in the falling-rate period. Figure 11.6 is a replot of data extracted from Figure 11.4. The rate of change of Infragauge voltage was calculated by dividing the difference between adjacent tabulated values of voltage by the corresponding time interval. Voltage derivatives, termed the "equivalent drying rate", appear on Figure 11.6a. Voltage derivatives were not converted into absolute rates of drying (kg/m^2 s), but were normalised to produce the relative drying rate f

$$f = \frac{m}{m_c} \quad \frac{(\Delta V/\Delta t)}{(\Delta V/\Delta t)_c} \qquad 11.5.1$$

Values of f and ϕ yield a characeristic drying curve, Figure 11.6b.

The following comments are pertinent to Figure 11.6a and b

a) Although plotting the data in the form of a rate of drying curve serves to emphasise the discontinuity between the constant and falling rate regions, it was still found difficult to locate the position of the critical point with precision. The data from which the drying rates were calculated was read off the IR curves by eye and small errors were unavoidable. These errors inevitably produced scatter in the derived points, and this is particularly evident in the region of the critical point, Figure 11.6b. A previous attempt to differentiate the Infragauge signal by electronic means, was unsuccessful. The signal was insufficiently smooth to allow this type of processing. Modern automatic data processing techniques were not used in this research, but it is recognised that there is scope to do so. In assessing their applicability the important question of accurately locating the critical point should be considered.

b) Making allowances for the scatter of the data on Figure 11.6b, the critical point appears to occur at a roughly constant value of (X/X_o). Thus the effect of changes in the drying rate brought about by changes in air velocity is shown to be not significant. This agrees with previous experimental evidence on the critical point already discussed in section 4.6

c) Because of the scatter of the data at the critical point, the drying rates at this point were taken from previous calculations of the constant-rate period. It should be noted that different

estimates of the location of the critical point will produce second order changes in the shape of the characteristic drying curve.

d) By means of the characteristic drying curve concept, four previously separate drying curves have been successfully reduced to a single normalised curve, Figure 11.6b.

The effect of air temperature

Figure 11.7 shows the effect of changes in the temperature of the drying air on the drying rate in the falling-rate period. The data on which Figure 11.7 is based was extracted from Figure 11.5. The remarks and comments made above about the critical point apply equally, mutatis mutandis, to Figure 11.7a. Once again, it can bee seen from Figure 11.7b that, allowing for the scatter of experimental points, the data is well correlated by the characteristic drying curve.

11.6 Experiments in the Falling-Rate Region

The characteristic drying curves illustrated in Figures 11.6a and 11.7b were derived from IR curves primarily recorded to yield test data on the constant-rate region. This replotting served to emphasise that data from the final period of drying must of the highest possible accuracy to prevent inferences drawn from it being grossly in error. To obtain more accurate data, specific to the falling-rate period, the experimental procedure was modified slightly as follows:-

a) To give a larger signal in the falling-rate period, the gain of the Infragauge amplifier was increased. The undesirable consequence of this adjustment, was that for most of the

constant-rate period the Infragauge signal was excessively large and off scale. In turn, the corresponding portion of the drying curve was meaningless. It should be noted, that it was essential to include the critical point on the meaningful section of the IR curve. This placed a practical limit on the amount of gain that could usefully be employed.

b) During these experiments it was found that driving the Infragauge signal off-scale at the beginning of a test caused the instrument output to stick in this position. When this occurred, it spoiled data from the remainder of the test. Fortunately, this difficulty was overcome, relatively easily, by incorporating a "Zenner Diode" in the electronic circuit.

c) With the increased amplifier gain, adjustment of the Infragauge zero required considerable care. Throughout the test work the instrument was set to zero with uncoated plastic in the measuring beam.

The thickness of the commercial plastic film was not constant, but varied within the tolerance of manufacture. Although the film was nominally transparent to the IR beam, at this high amplification, variations in film thickness were sufficiently large to cause slight shifts in instrumental zero (0.1/0.2 volt) To avoid these slight discepancies, the zero was frequently checked throughout a test series. However, this point should be borne in mind, when analysing data from the final stage of drying.

d) The plotting speed was reduced to allow the test period to be increased. Because of the difficulties mentioned above, it was necessary to run a number of proving tests to establish conditions and to ensure consistency.

Figures 11.8, 11.10 and 11.2 show IR drying curves recorded using the modified procedure. From them it can be seen, that at the beginning of drying the Infragauge is off-scale and registers a voltage of 10.7 volts. In the falling-rate region the curves are clearly delineated. The IR curves yielded equivalent drying rates which appear as the corresponding rate of drying and characteristic drying curves shown in Figures 11.9, 11.11 and 11.13.

The difficulty of locating the critical point already remarked upon, was exacerbated by increasing the instrumental gain. Voltages of roughly 6 - 7 volt probably represent the limit of linearity of the Infragauge. Errors in estimating the critical point will, to some degree, influence the shape of the derived rate of drying curves. Care has been taken to minimise this effect. In processing the data, scatter of the derived points is unavoidable; consequently the comments below should be taken as expressing trends.

Comments on the rate of drying curves - Figures 11.9a, 11.11a and 11.13a

a) To a first approximation the falling-rate period can be divided into two equal halves. In the first period the drying rate falls linearly with solvent content. In the second period the drying rate is a non-linear function of solvent content; the shape of the drying rate curve is concave upwards.

b) Figure 11.9a: Changes in the drying rate, brought about by variations in the air velocity, appear to have little effect on the value of (X/X_o) at the critical point. There is little separation of the curves in the second period of drying.

c) Figure 11.11a: Changes in the drying rate, brought about by variations in the air temperature, appear to have little effect on the value of (X/X_o) at the critical point. The curves retain their separation throughout.

d) Figure 11.13a: Since a considerable portion of the IR curve was recorded with the Infragauge operating in the non-linear portion of its range, the points from band 4 are of doubtful validity. If these doubtful points are neglected, the ratio (X/X_o) is roughly independent of ink thickness.

e) From all three figures it appears that for any test series the critical point remains largely unaffected by changes of the external variable. Expressed as a decimal, for most tests, the critical point lies in the range

$$0.15 < \left(\frac{X}{X_o}\right)_c < 0.2$$

The change in the value of $(X/X_o)_c$ within this range which occurs between tests separated in time requires further investigation.

f) These results are in broad agreement with the preliminary results of section 4.6.

Comments on the characteristic drying curves - Figures 11.9b, 11.11b & 11.13b

a) There is some scatter of the data points in the first period of drying, i.e. in the range $0.4 < \phi < 1$. If this qualification is accepted, then each set of curves is well correlated by this type of plot.

b) The characteristic drying curves all have approximately the same shape.

i) $0.4 < \phi < 1.0$ Linear

ii) $0 < \phi < 0.4$ Curved (concave up)

c) At the end of any test, the drying rate had diminished to an extremely low value. When the drying rate is controlled by diffusion, drying can be a protracted process. Accurate rate data for the last stage of drying is vital, because it may take up the greater proportion of the total drying time.

d) At a value of ϕ approximately equal to 0.1, the IR instrument, when used in this fairly straightforward manner, seems to have reached the limit of its accuracy.

11.7 Theoretical Predictions of Drying Time Based on the Characteristic Drying Curve

In section 11.6 it was demonstrated that test data could be successfully correlated by means of the characteristic drying curve. From the shape of these characteristic drying curves, it is evident that the empirical relation between f and ϕ can probably be represented, to sufficient

* In a parallel theoretical investigation (described in section 10.10), the empirical relation between f and ϕ was obtained by means of the computer model.

accuracy, by simple algebraic functions. It was appreciated of course that, using standard computer software, the data could more accurately be fitted by a polynomial equation. In spite of this, it was decided to derive a simple analytic formula for drying time, because of the greater physical insight which it was hoped would follow from its use.

With the drying rate expressed as an analytic function of solvent content, the drying time may be obtained from it by integration. In this section, various assumed algebraic relations between f and ϕ will be used to derive theoretical formulas for the falling-rate drying time. In the sections which follow, drying times calculated from these formulas will be checked against experimental data.

Basic Definitions

$$f(\phi) = \frac{m}{m_c} \qquad m = m_c f(\phi)$$

$$\phi = \frac{X}{X_c} \qquad X = X_c \phi$$

$$dX = X_c \, d\phi$$

$$m = \pm \frac{dX}{dt} \quad \text{or} \quad dX = -\frac{dX}{m}$$

$$t = \int_{t_1}^{t_2} dt = -\int_{x_1}^{x_2} \frac{dX}{m} = \int_{x_2}^{x_1} \frac{dX}{m}$$

$$t = \frac{X_c}{m_c} \int_{\phi_2}^{\phi_1} \frac{d\phi}{f(\phi)}$$

using the initial and final conditions

$$t_1 = 0, \quad \phi_1 = 1$$

$$t_2 = t \quad \phi_2 = \phi$$

$$t = \frac{X_c}{m_c} \int_{\phi}^{1} \frac{d\phi}{f(\phi)} \qquad 11.7.1$$

a) Basic 2 zone model

Examination of the characeristic drying curves determined from experiment, indicated that the empirical relation between f and ϕ could be modelled by the type of relationship illustrated below

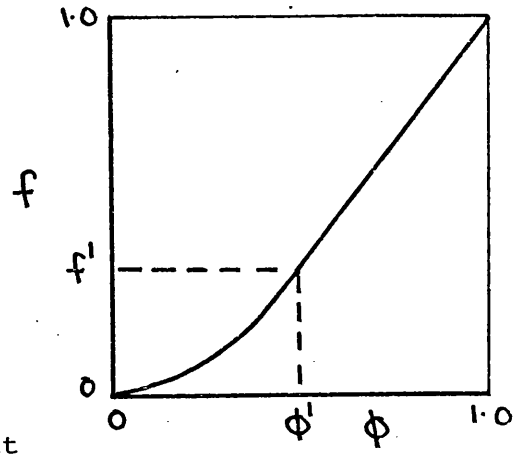

$f(\phi)$ is defined by the conditions

1) $\phi^1 < \phi < 1$, $f(\phi) = a_1 + a_2 \phi$

ii) $0 < \phi < \phi^1$, $f(\phi) = a_3 \phi^n$

from the above conditions it follows that

$$a_1 = \frac{f^1 + \phi^1}{1 - \phi^1} \qquad 11.7.2a$$

$$a_2 = \frac{1 - f^1}{1 - \phi^1} \qquad 11.7.2b$$

$$a_3 = \frac{f^1}{(\phi^1)^n} \qquad 11.7.2c$$

Consider the case when the final value of ϕ is smaller than ϕ^1, then the basic integral, equation 11.7.1 must be evaluated in two stages:-

$$t = \frac{X_c}{m_c} \int_{\phi}^{1} \frac{d\phi}{f(\phi)} = \frac{X_c}{m_c} \int_{\phi^1}^{1} \frac{d\phi}{f(\phi)} + \frac{X_c}{m_c} \int_{\phi}^{\phi^1} \frac{d\phi}{f(\phi)} \qquad 11.7.3$$

making the appropriate substitutions for $f(\phi)$

$$t = \frac{X_c}{m_c} \int_{\phi^1}^{1} \frac{d\phi}{a_1 + a_2\phi} + \frac{X_c}{m_c} \int_{\phi}^{\phi^1} \frac{d\phi}{a_3\phi^n}$$

integrating

$$t = \frac{X_c}{a_2 m_c} \ln\left(\frac{a_1 + a_2}{a_1 + a_2 \phi^1}\right) + \frac{X_c}{a_3 m_c} \cdot \frac{\left[(\phi^1)^{1-n} - \phi^{1-n}\right]}{1 - n} \qquad 11.7.4$$

It follows from this analysis that the drying time t may be expressed in the general form

$$t = \frac{X_c}{m_c} \, g(\phi) \qquad 11.7.5$$

where, for the model of $f(\phi)$ used above,

$$g(\phi) = \frac{1}{a_2} \ln\left(\frac{a_1 + a_2}{a_1 + a_2 \phi^1}\right) + \frac{1}{a_3} \left[\frac{(\phi^1)^{1-n} - \phi^{1-n}}{1 - n}\right] \qquad 11.7.6$$

It is convenient to consider the drying time t, expressed by equations 11.7.5 and 11.7.6, as the product of the two factors, (X_c/m_c) and the function $g(\phi)$. The significance of each of these factors will be discussed in turn.

i) The parameter X_c/m_c

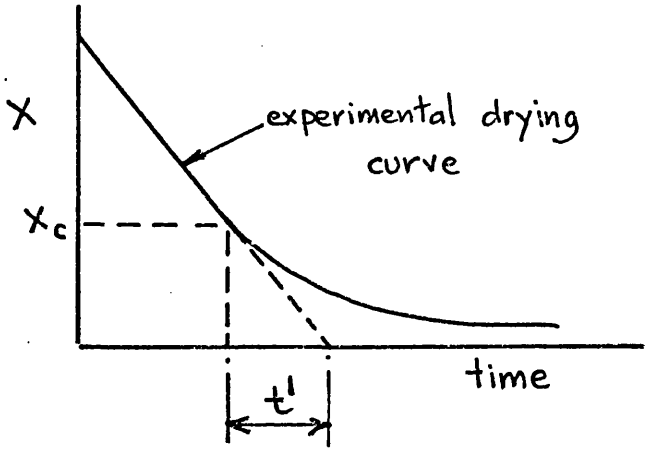

By definition

$$m_c = -\left(\frac{dx}{dt}\right)_c$$

From the drying curve

$$\left(\frac{dx}{dt}\right)_c = -\frac{X_c}{t^1}$$

Thus $$\frac{X_c}{m_c} = t^1 \qquad 11.7.7$$

The parameter (X_c/m_c) represents the hypothetical time t^1 for the solvent content to be reduced from X_c to zero, the critical drying rate being maintained constant. t^1 is analagous to a time-constant.

Analysis of the experimental drying curves in section 11.6 had indicated that the ratio $(X/X_o)_c$ remains roughly constant, and is essentially independent of drying rate. Now for all tests, the ink viscosity was maintained constant; it follows that for a particular gravure band, X_o and therefore X_c may be treated as a constant. Thus, for an ink layer of constant thickness, the parameter (X_c/m_c) is inversely proportional to m_c, the drying rate in the constant-rate period.

ii) The function $g(\phi)$

$g(\phi)$ is a dimensionless function which expresses the shape of the drying curve. It can be regarded as a dimensionless drying time with parameter (X_c/m_c) equal to unity.

By giving appropriate values to the parameters in equation 11.7.6, particular expressions for the drying time may be derived. The following special cases illustrate the method.

b) 1-zone linear

$0 \leqslant \phi \leqslant 1, \quad f(\phi) = \phi$

$$t = \frac{X_c}{m_c} \ln \frac{1}{\phi} \qquad 11.7.8$$

c) 1-zone quadratic

$0 \leqslant \phi \leqslant 1, \quad f(\phi) = \phi^2$

$$t = \frac{X_c}{m_c} \left(\frac{1}{\phi} - 1 \right) \qquad 11.7.9$$

2-zone models with $\phi^1 = 0.5$

d) 2-zone quadratic

i) $0.5 \leqslant \phi \leqslant 1$, $f(\phi) = \phi$

ii) $0 \leqslant \phi \leqslant 0.5$, $f(\phi) = 2\phi^2$

$$t = \frac{X_c}{m_c}\left[\ln\left(\frac{1}{0.5}\right) - \frac{1}{2 \cdot 0.5} + \frac{1}{2\phi}\right]$$

$$= \frac{X_c}{m_c}\left(\frac{1}{2\phi} - 0.307\right) \qquad 11.7.10$$

e) 2-zone cubic

i) $0.5 \leqslant \phi \leqslant 1$, $f(\phi) = \phi$

ii) $0 \leqslant \phi \leqslant 0.5$, $f(\phi) = 4\phi^3$

$$t = \frac{X_c}{m_c}\left[\ln\left(\frac{1}{0.5}\right) + \frac{1}{8\phi^2} - \frac{1}{8(\phi^1)^2}\right]$$

$$= \frac{X_c}{m_c}\left(\frac{1}{8\phi^2} + 0.193\right) \qquad 11.7.11$$

In endeavouring to fit the experimental data, a range of mathematical models of $f(\phi)$ was developed. Those models found most useful, together with the corresponding equations for $g(\phi)$, are illustrated in Figure 11.14. All models in this Figure are of the 2 zone type with ϕ^1 equal to 0.5.

Various expressions for the dimensionless drying time $g(\phi)$, corresponding to the mathematical models shown in Figure 11.14, are shown graphically in Figure 11.15. From this Figure it can be seen that all formulas for $g(\phi)$ are in approximate agreement down to a ϕ value of 0.5. For values of ϕ less than 0.2, the gradients of the curves become quite

small, and large differences in the value of $g(\phi)$, and hence in drying time, are possible.

Newtonian Drying

The drying rate may be expressed in a manner analagous to Newton's Law of Cooling

$$\frac{dX}{dt} = - PX \qquad 11.7.12$$

With the solution

$$t = \frac{1}{P} \ln\left(\frac{1}{\phi}\right) \qquad 11.7.13$$

Comparison of 11.7.13 with equation 11.7.8 demonstrates that the characteristic drying curve for this type of drying is a straight-line. The computer model will exhibit this type of behaviour when the diffusion coefficient is constant, see section 10.9.

Equation 11.7.13 may be rewritten

$$\phi = e^{-tP} \qquad 11.7.14$$

It is apparent that P is a dimensional parameter which depends upon the surface heat transfer coefficient k, the diffusivity D and the thickness of the ink layer Δ. It follows from dimensional analysis that

$$tP \equiv Bi\ Fo \qquad 11.7.15$$

$Bi = k\Delta/D$

$Fo = Dt/\Delta^2$

Comparing equations 11.7.13 and equation 11.7.8, it follows that

$$\frac{X_c}{m_c} = \frac{t}{Bi\ Fo}$$

11.8 Curve Fitting

It was pointed out in the previous section, that all derived equations for the drying time were similar in form (equation 11.7.5)

$$t = \frac{X_c}{m_c}\, g(\phi)$$

Data extracted from the IR drying curves may be similarly expressed

$$t = \frac{X_c}{m_c}\, h(\phi) \qquad 11.8.1$$

In this case $h(\phi)$ is an empirical function, which is implicitly contained in the ϕ, t data, tabulated in Appendix 8. This numerical relationship may be extracted from the drying data by transposing equation 11.8.1

$$h(\phi) = \frac{t}{(X_c/m_c)} \qquad 11.8.2$$

The parameter (X_c/m_c) may be evaluated directly from the tables of Infragauge voltage V, by means of the following identity

$$\frac{X_c}{m_c} \equiv \frac{V_c}{(dV/dt)_c} = t^1 \qquad 11.8.3$$

where t^1 is defined by equation 11.7.5.

Thus by comparing the various theoretical equations for $g(\phi)$ with the empirically determined function $h(\phi)$, the equation giving the best fit may be selected. To test this method, data from three drying tests was used to calculate $h(\phi)$. This allowed data from a test on each of the variables (air velocity, air temperature and ink thickness) to be assessed, but the particular tests were selected in an arbitrary manner. The data, and values of $g(\phi)$ computed from them, are set out in Table 11.1 below.

TABLE 11.1

Comparison of $h(\phi)$ and $g(\phi)$

$g(\phi)$, from model number 2, Figure 11.14

$0.5 \leq \phi \leq 1.0$; $t = \ln \frac{1}{\phi}$

$0 \leq \phi \leq 0.5$; $t = \frac{1}{4.5\ \phi^{1.5}} + 0.02$

a) Data from Figure 11.9 - Velocity 30 m/s

From graph: $V_c = 6.15$ volt; $\left(\frac{dV}{dt}\right)_c = 1.84$ volt/s; $\frac{X_c}{m_c} = \frac{6.15}{1.84} = 3.34$ s

ϕ	1.0	0.73	0.37	0.24	0.2	0.17	0.15	0.11	0.1
time, t(sec)	0	1	3	5	7	9	11	19	29
$h(\phi) = t/3.34$	0	0.3	0.9	1.5	2.1	2.7	3.3	5.7	8.7
$t = g(\phi)$	0	0.32	1.1	2.05	2.2	3.4	4.1	6.5	7.5

b) Data from Figure 11.11 - Temperature 60 C

From graph: $V_c = 4.9$ volt; $\left(\frac{dV}{dt}\right)_c = 3.0$ volt/s; $\frac{X_c}{m_c} = \frac{4.9}{3.0} = 1.63$ c

ϕ	1.0	0.29	0.16	0.13	0.11	0.1	0.09	0.07	0.066	0.06
time, t(sec)	0	2	4	6	8	10	16	26	36	46
$W(\phi) = t/1.63$	0	1.2	2.5	3.7	4.9	6.1	9.8	16.0	22.1	28.2
$t = g(\phi)$	0	1.5	3.6	5.0	6.5	7.0	8.7	12.7	13.9	16.0

c) Data from Figure 11.13 - Band 3

From graph: $V_c = 5.35$ volt; $\left(\frac{dV}{dt}\right)_c = 1.8$ volt/s; $\frac{X_c}{m_c} = \frac{5.35}{1.81} = 2.96$

ϕ	1.0	0.47	0.45	0.27	0.21	0.15	0.13	0.12	0.11
time, t(sec)	0	2.0	2.5	5.0	7.5	12.5	17.5	22.5	27.5
$h(\phi) = t/2.96$	0	0.68	0.84	1.7	2.5	4.2	5.9	7.6	9.3
$t = g(\phi)$	0	0.75	0.82	1.7	2.5	4.1	5.0	5.8	6.5

The data in Table 11.1 has been plotted in Figure 11.16. An examination of the data, in both its tabular and its graphical forms, shows that

a) $h(\phi)$ data from all three tests are reasonably consistent

b) Up to an $h(\phi)$ value of approximately 10, there is good agreement between $g(\phi)$ evaluated using model number 2 (Figure 11.14), and the empirical $h(\phi)$ data.

c) Predictions of drying may be significantly in error for values of ϕ less than 0.1.

This comparison has demonstrated that, for values of ϕ down to roughly 0.1, the falling rate data can be reasonably well correlated by means of quite a simple mathematical model of the characteristic drying curve. Indeed in the first falling-rate period, drying times predicted by the various models do not differ greatly.. This is not so for longer drying periods, when the gradient of the $h(\phi)$ curve has become quite small. For the correct prediction of drying times when the final value of ϕ is less than 0.1, it appears essential to start the modelling process by fitting accurate empirical data for this region

11.9 Correlation of Falling-Rate Data for n-Propanol

To test its range of application, the correlation technique was next tried on an ink based on a different solvent. IR curves have already been presented for n-propanol, Figures 7.2 and 7.3, as part of the constant-rate investigations. The falling-rate regions of these figures was next analysed. Rate of drying data was extracted from the curves by the same method as described in section 11.5. Voltages and rate of change of voltage were normalised by using the critical point values, to yield the relative solvent content ϕ and the relative drying rate f. Because, with n-proponal, only a small section of the constant-rate region was recorded (see section 7) a relatively small departure from the previous method was necessary. Instead of using a rate of drying curve to locate the position of the critical point, this was estimated directly from Figures 7.2 and 7.3. In addition, it is apparent from the drying curves, that the dimensionless voltage at the critical point, $(V/V_o)_c$, is largely unaffected by changes in the drying rate.

Figure 11.18a (data extracted from Figure 7.2) shows the effect on the characteristic drying curve of changing the drying rate by changing the air velocity. It can be seen that all four sets of data can be reasonably well correlated by a single curve.

Figure 11.18b (data extracted from Figure 7.3) shows the effect on the characteristic drying curve of changing the drying rate by changing the air temperature. In this case the correlation is less successful, but probably still satisfactory. There is some separation of the data in the important region where ϕ is less than 0.3.

To complete this investigation of the n-proponal ink, further tests were carried out with increased amplification of the Infragauge, to show up the falling-rate region. IR drying curves from these tests are shown in Figure 11.19. To ascertain the effect of ink thickness, curves were recorded from each of four gravure bands, while maintaining constant the conditions of the external air. To record these curves, it was necessary to take especial care to ensure correct alignment of the Infragauge after changing from one band to another. Although the IR curve from band 4 appears satisfactory, f/ϕ data calculated from it was not consistent with similar data from the other three curves. It was concluded that the reason for this significant discrepancy, was that the IR curve was inaccurate in the region of the critical point. This is the same difficulty, encountered throughout this reseach, that the early portions of IR curves recorded from band 4 are inaccurate, because the instrument is operating outside its linear range. Because of this, data from band 4 was excluded from the correlation.

Figure 11.20 shows the characteristic drying curve which has been derived from the curves of Figure 11.19. It is evidence from Figure 11.20 that the data is reasonably well correlated by a single curve.

Comparison of $h(\phi)$ and $g(\phi)$ for n-propanol

Following the procedure evolved in the previous section, the quantity (X_c/m_c) was calculated for each curve. Using equation 11.8.2

$$h(\phi) = \frac{t}{(X_c/m_c)}$$

The empirical function $h(\phi)$ was calculated for all curves appearing in Figures 11.20 and 11.21. This $h(\phi)$ data has been plotted in Figure 11.21.

It is evident from this Figure, that there is some scatter of the data but, down to a ϕ value of approximately 0.25, it could be correlated by a single line. There may be evidence of separation of the data at longer drying times. On the other hand this separation may arise from experimental discrepancies consequent upon the difficulty of making exact measurements at low solvent content.

The various models of $g(\phi)$ set out in Figure 11.15 were compared with the $h(\phi)$ data of Figure 11.21. None of the models fitted the data satisfactorily. To achieve a better fit, a slight modification was made to model 2 of Figure 11.15. From the characteristic drying curves shown in Figures 11.18 and 11.20, it is evident that the relation between f and ϕ should have the following form

i) $\quad 0.4 \leqslant \phi \leqslant 1.0, \quad f(\phi) = a_1 + a_2\phi$

ii) $\quad 0 \leqslant \phi \leqslant 0.4, \quad f(\phi) = a_3\phi^{2.5}$

The constants a_1, a_2 and a_3 can be calculated from equations 11.7.2a-c

$$a_1 = -1/3, \quad a_2 = 1\tfrac{1}{3} \qquad a_3 = 1.976$$

When these values are substituted into the general equation 11.7.6, the following equation for $g(\phi)$ are obtained

$$0.4 \leqslant \phi \leqslant 1.0, \quad g(\phi) = \frac{3}{4} \ln\left[\frac{1}{\frac{4}{3}\phi - \frac{1}{3}}\right]$$

$$0 \leqslant \phi \leqslant 0.4, \quad g(\phi) = 1.976\left[\frac{1}{1.5\phi^{1.5}} - 2.63\right] + 1.21$$

For comparison, this function has been plotted on Figure 11.21. It can be seen that it satisfactorily represents the data. For clarity numerical values of this function have also been included in Figure 11.21.

Addendum - The Characteristic Drying Curve Applied to Ink Drying

It is believed that the results described in this chapter represent the first demonstration that the concept of the characteristic drying curve can be used to normalise falling-rate, ink drying curves. The demonstration that this concept can be applied to the evaporation of organic solvents from systems such as an ink film, represents an extension of this technique.

FIGURE 11.1

TYPES OF DRYING CURVE

(a)

Moisture Content, X

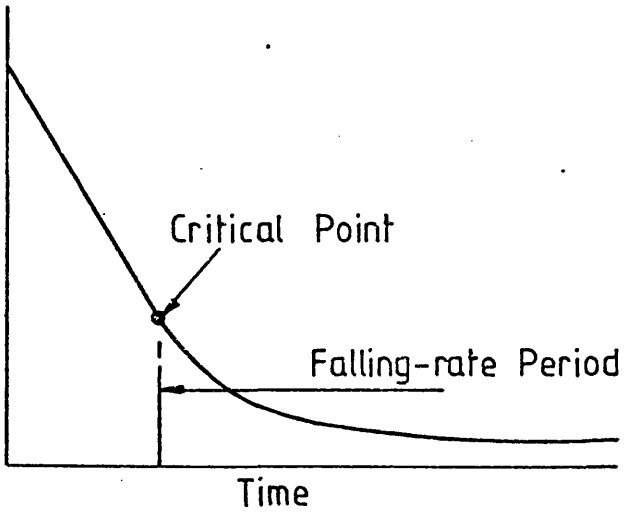

Drying Curve

(b)

Drying Rate, m

$$m = \frac{dx}{dt}$$

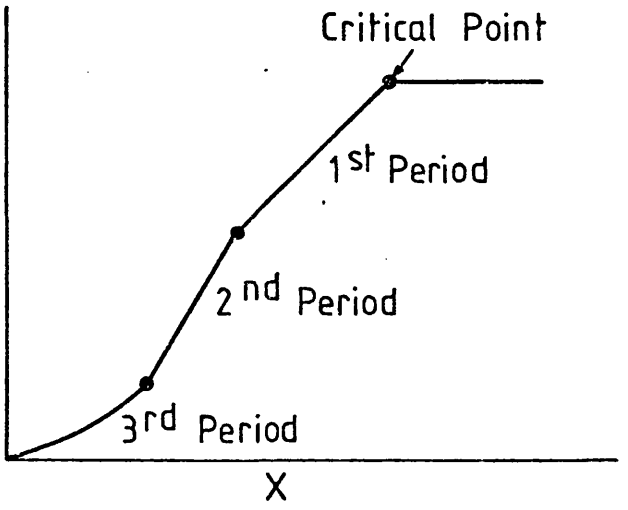

Rate of Drying Curve

(c)

Relative Drying Rate, f

$$f = \frac{m}{m_c}$$

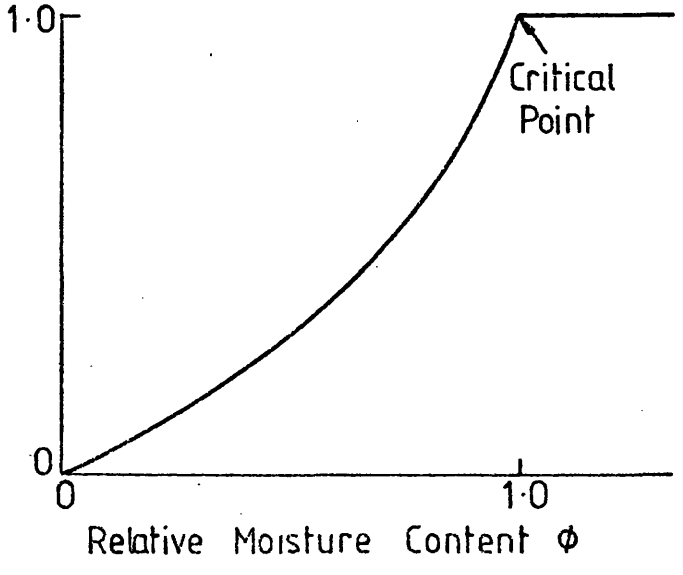

$$\Phi = \frac{X}{X_c}$$

Characteristic Drying Curve

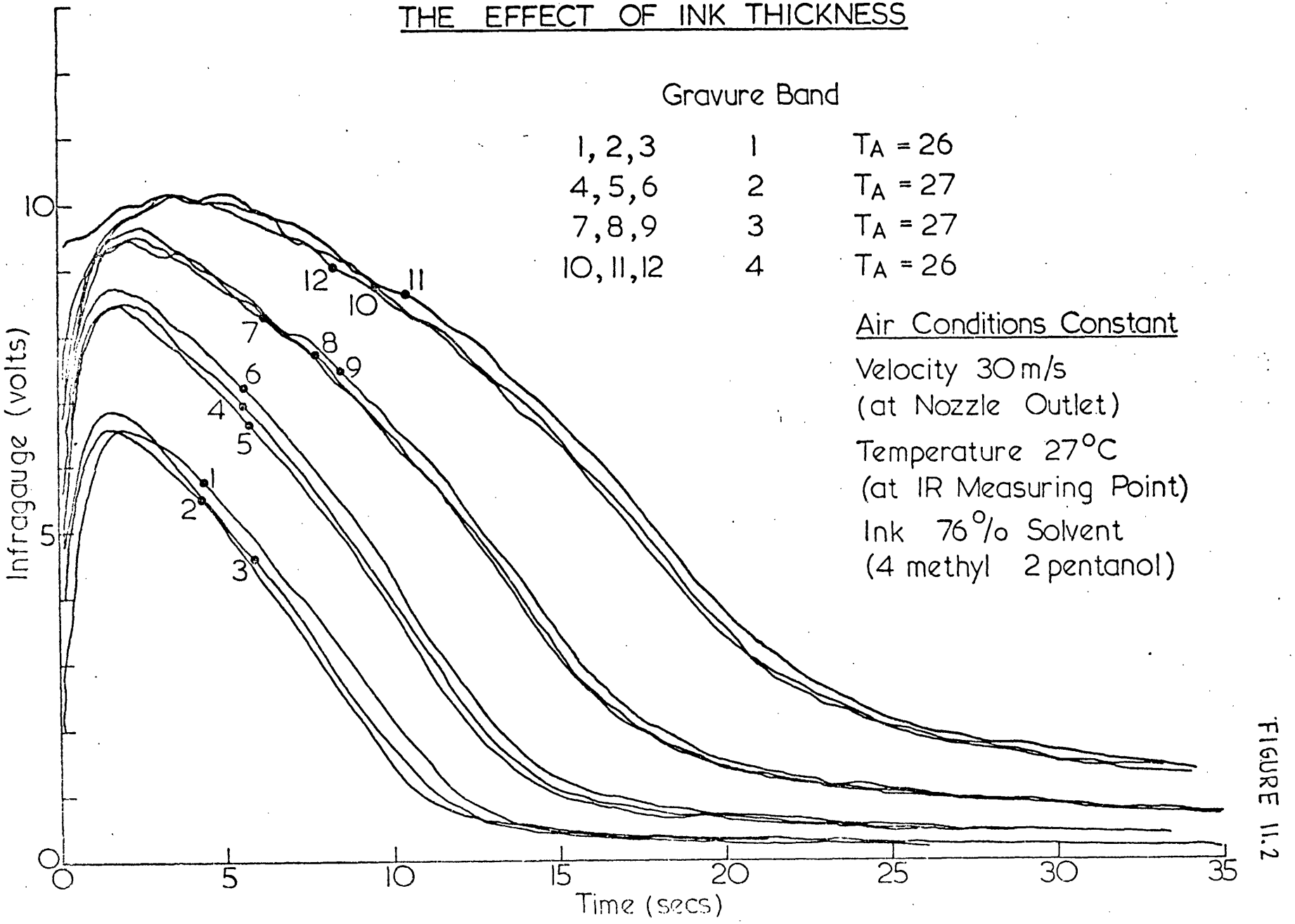
THE EFFECT OF INK THICKNESS
Gravure Band
1, 2, 3 1 TA = 26
4, 5, 6 2 TA = 27
7, 8, 9 3 TA = 27
10, 11, 12 4 TA = 26
Air Conditions Constant
Velocity 30 m/s
(at Nozzle Outlet)
Temperature 27°C
(at IR Measuring Point)
Ink 76% Solvent
(4 methyl 2 pentanol)
Infragauge (volts)
Time (secs)
0
5
10
15
20
25
30
35
1
2
3
4
5
6
7
8
9
10
11
12

FIGURE 11.2

FIGURE 11.3.

FALLING RATE DRYING

(a) DIFFERENT INK THICKNESSES – LINEAR TIME SCALE

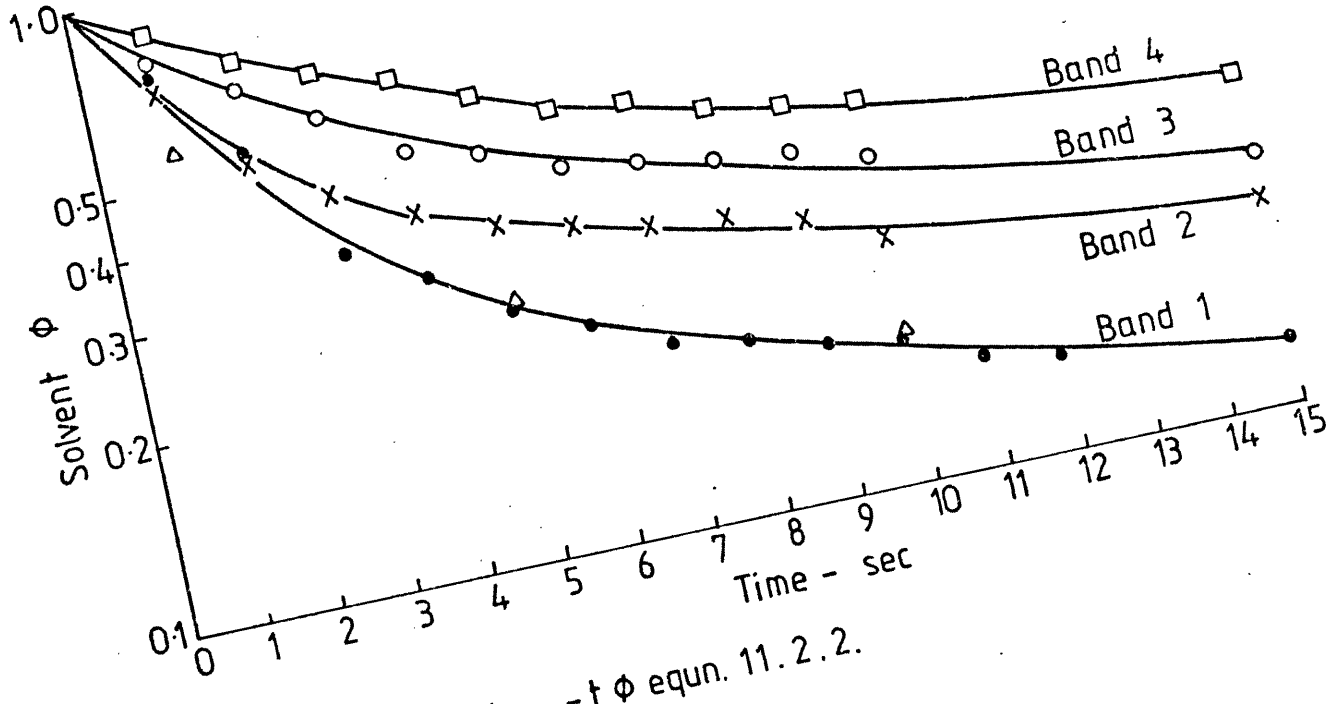

△ $\ln \Phi = -t\Phi$ equn. 11.2.2.

(b) DIFFERENT INK THICKNESSES - NORMALISED TIME SCALE

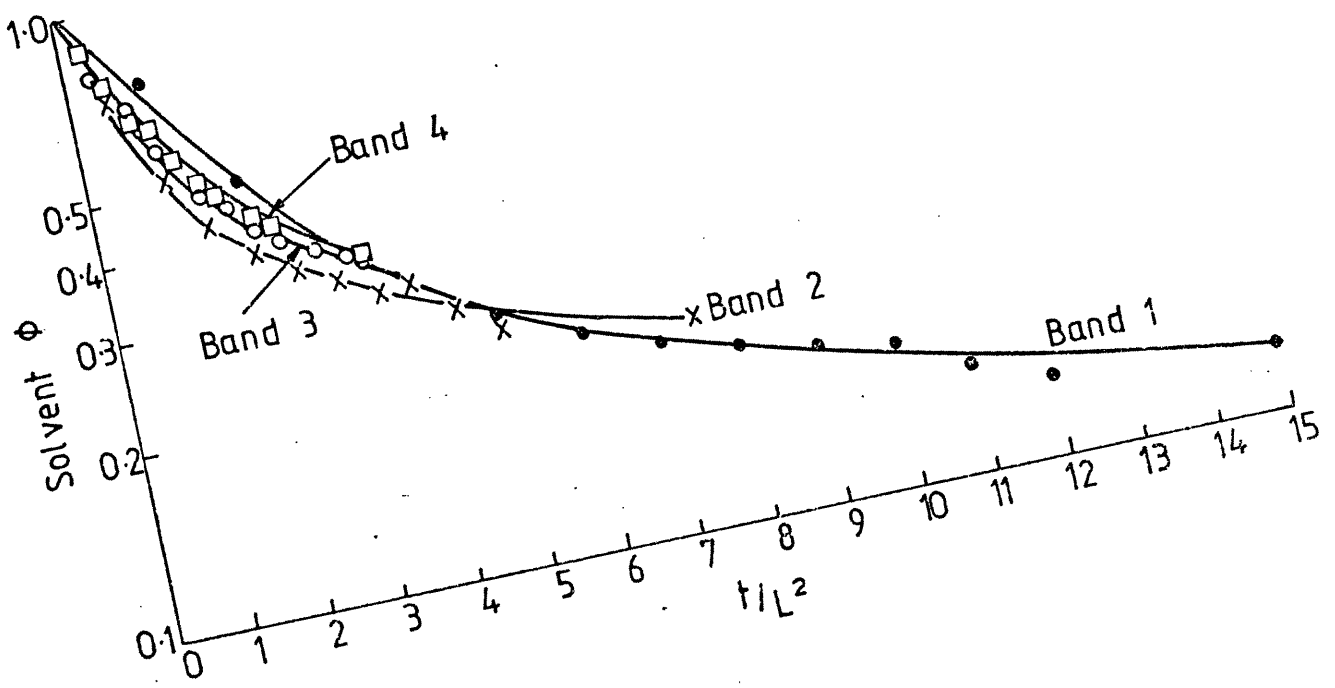

FIGURE 11.4.

EFFECT OF AIR VELOCITY ON FALLING RATE DRYING

DRYING CURVES

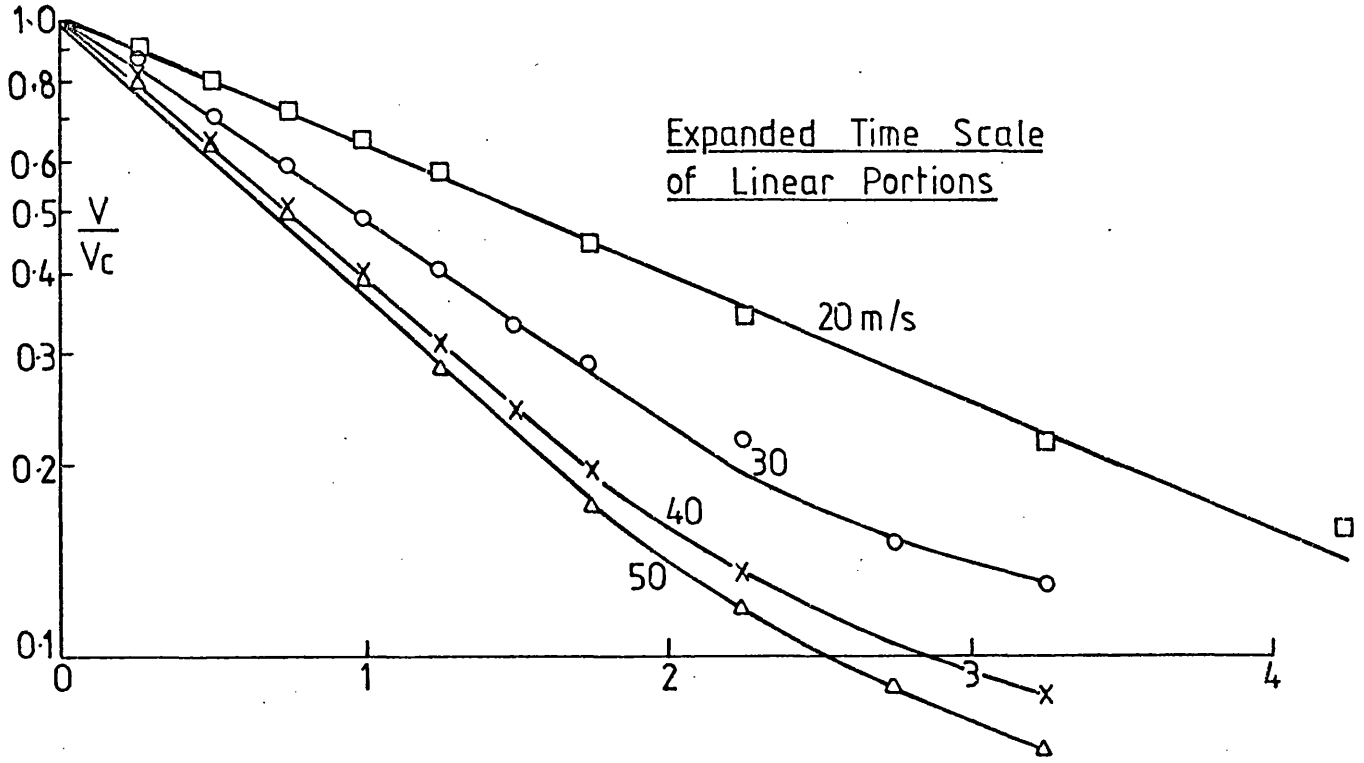

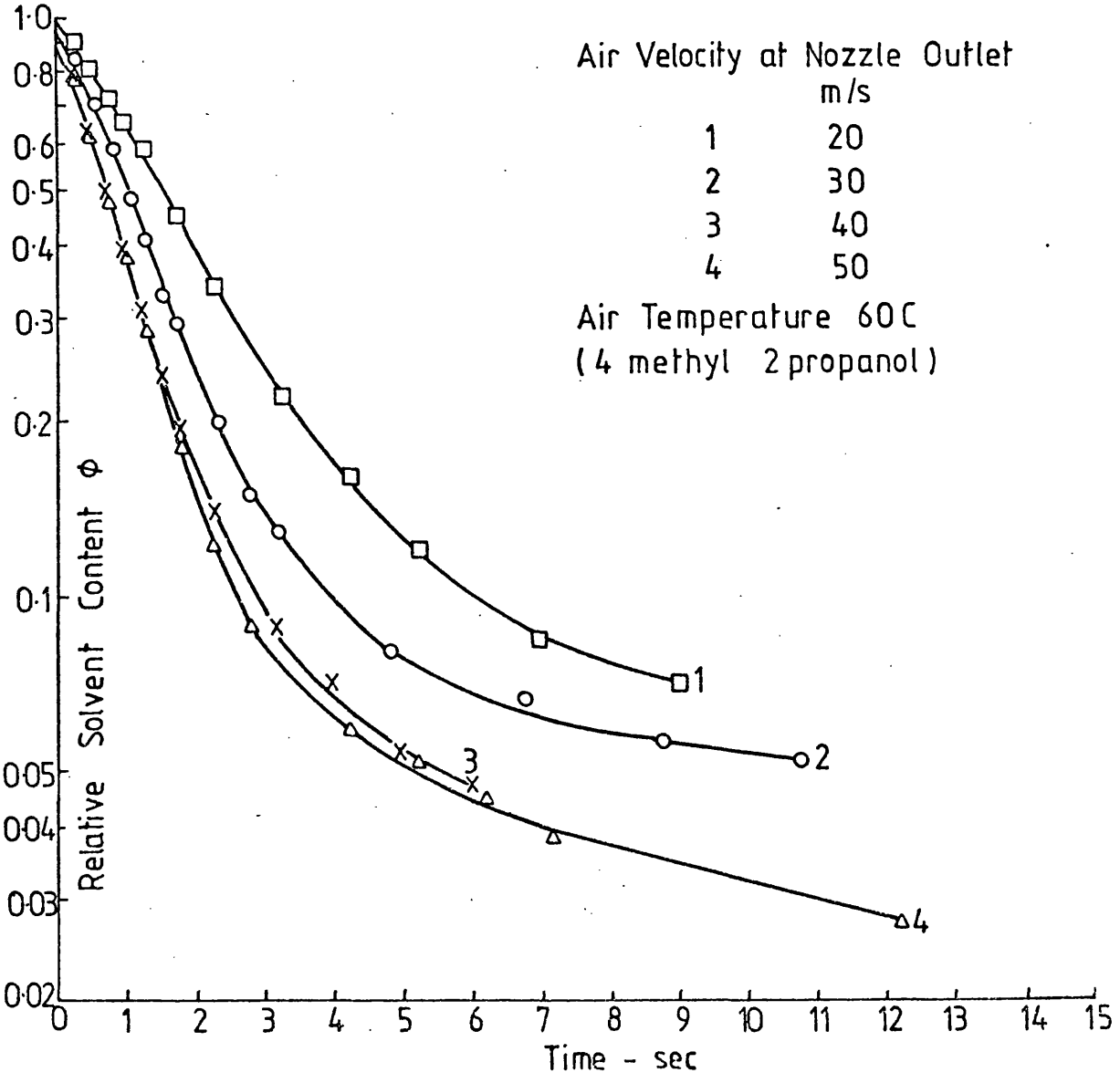

FIGURE 11.5

EFFECT OF AIR TEMPERATURE ON FALLING RATE DRYING

DRYING CURVES

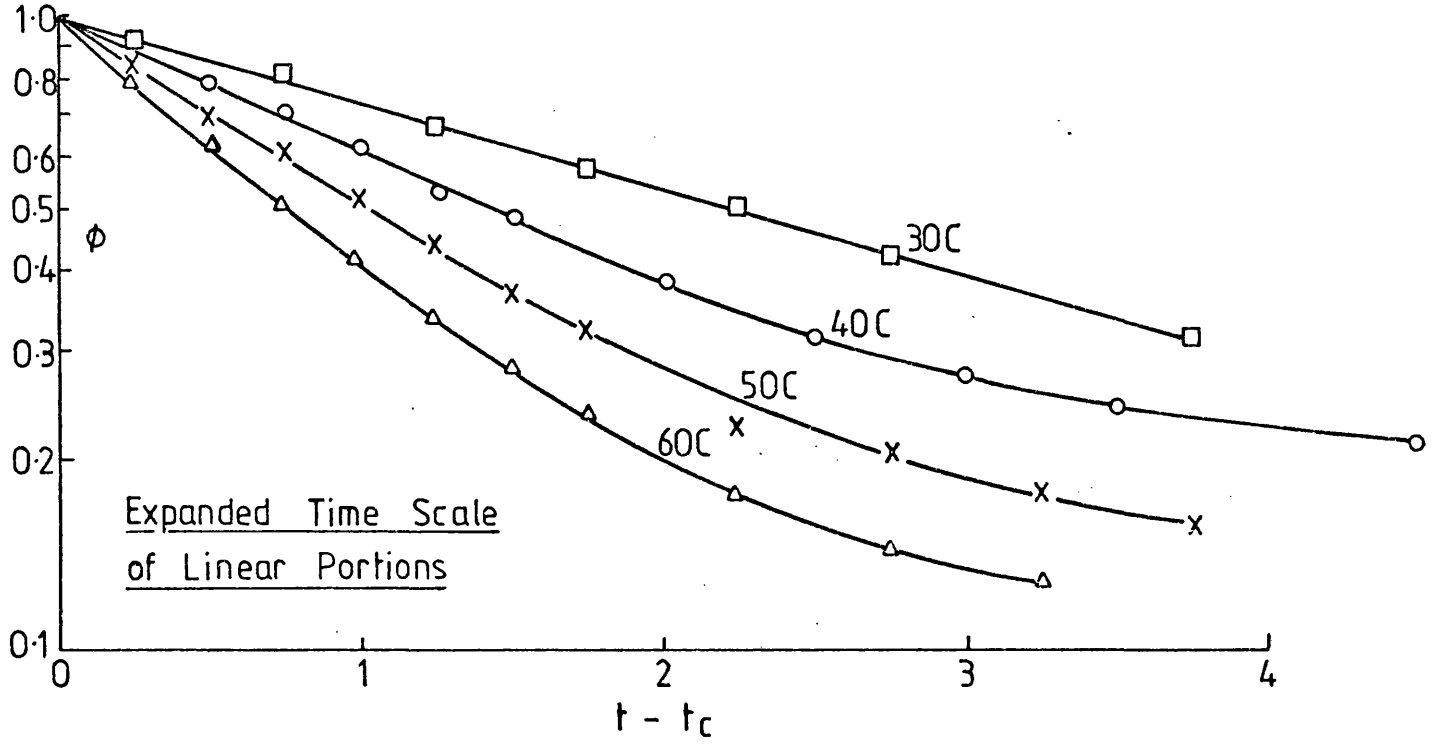

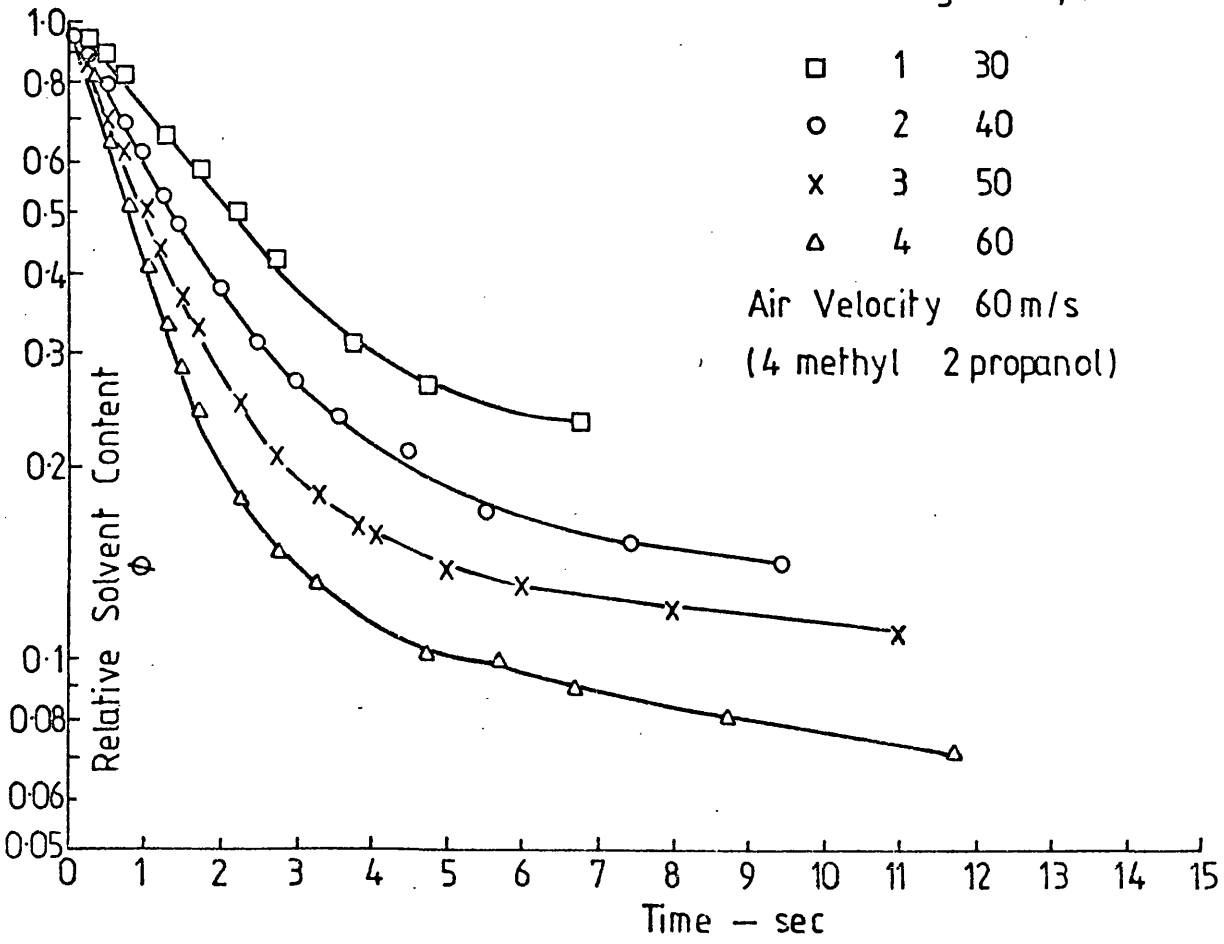

EFFECT OF AIR VELOCITY ON DRYING RATE

Temperature at IR Measuring Point 60C (Constant)
Solvent : 4 methyl 2 pentanol

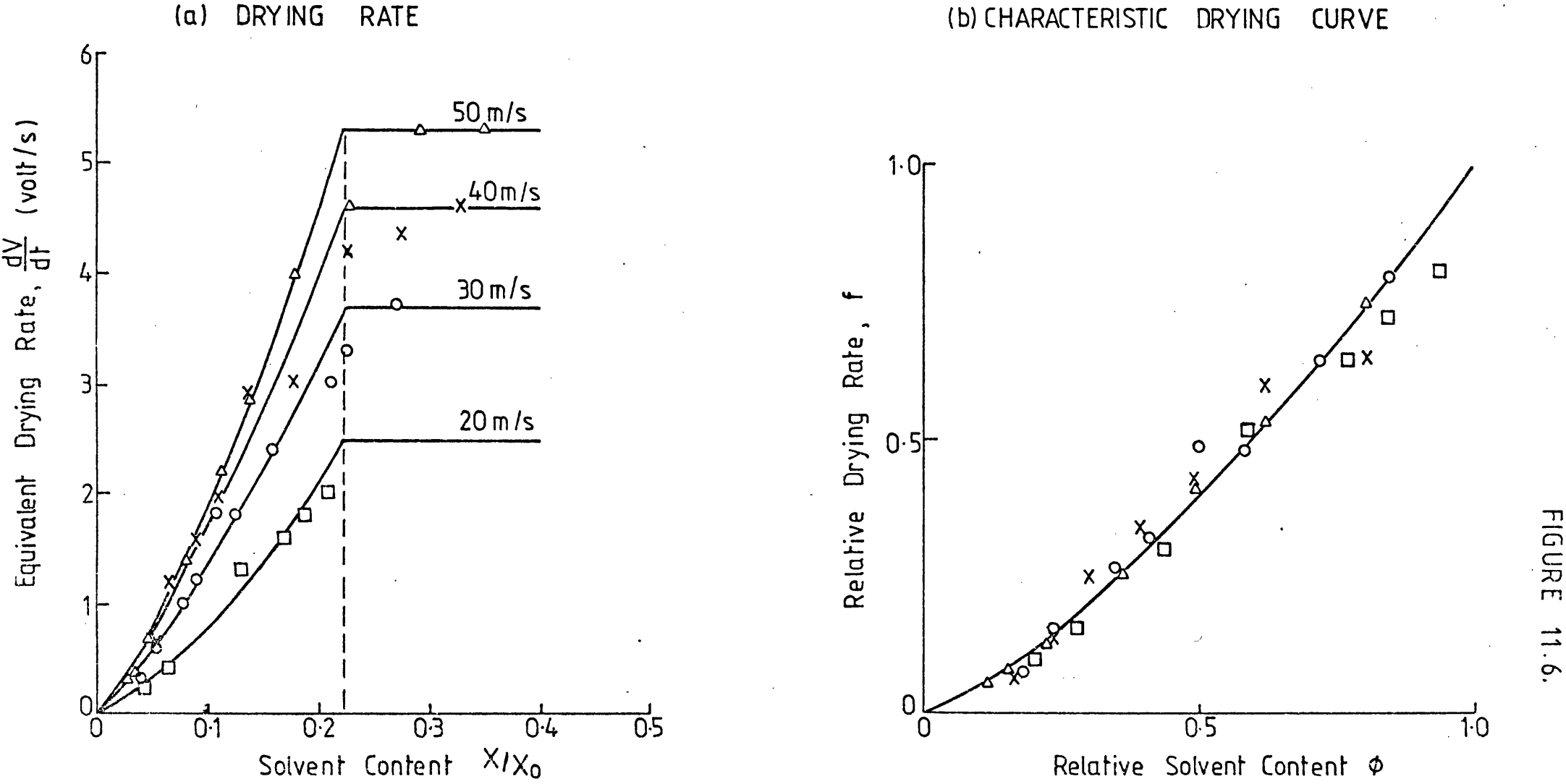

FIGURE 11.6.

EFFECT OF AIR TEMPERATURE ON DRYING RATE

Air Velocity at Nozzle Outlet 60 m/s (Constant)

Solvent : 4 methyl 2 pentanol

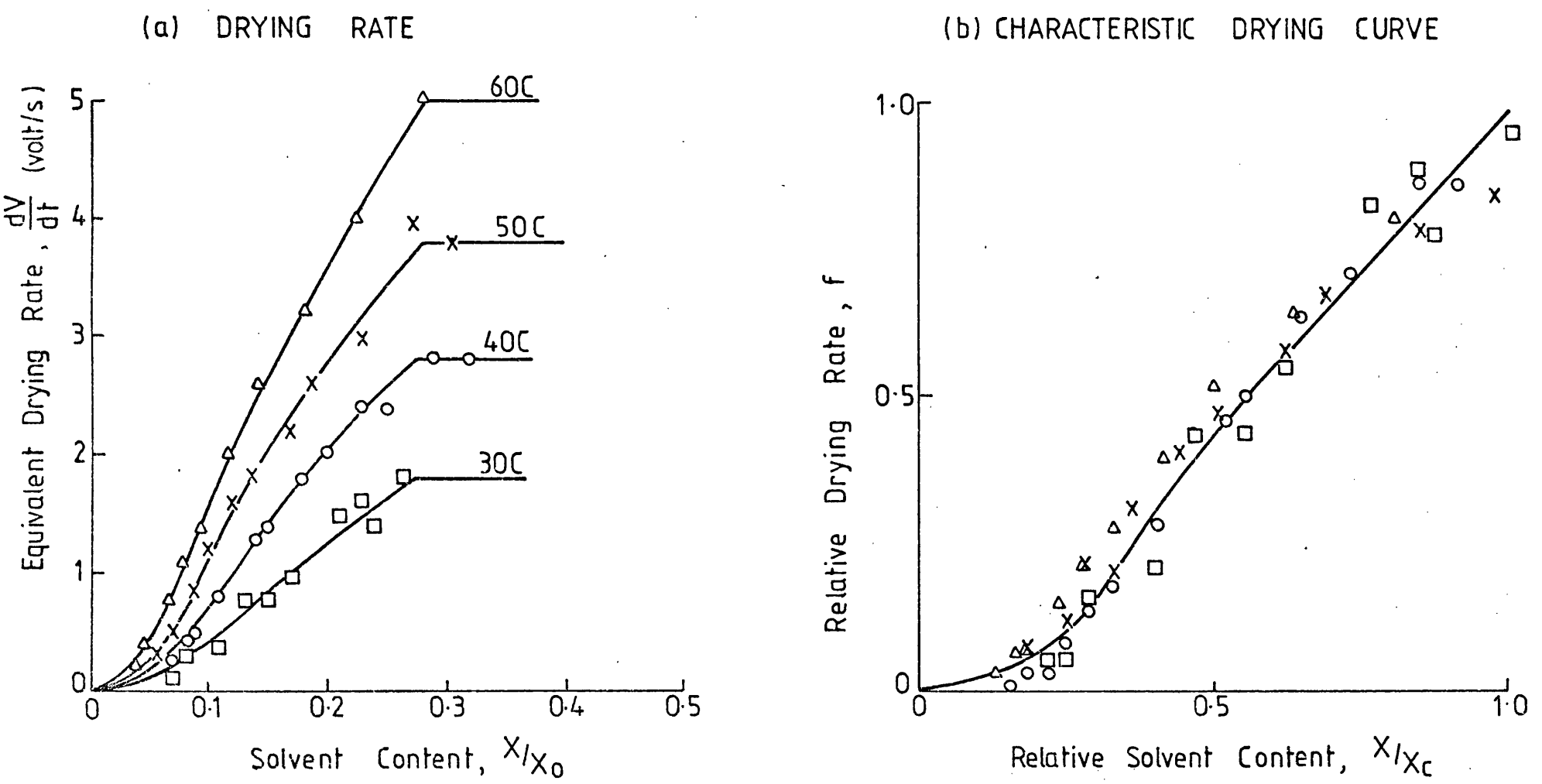

FIGURE 11.7.

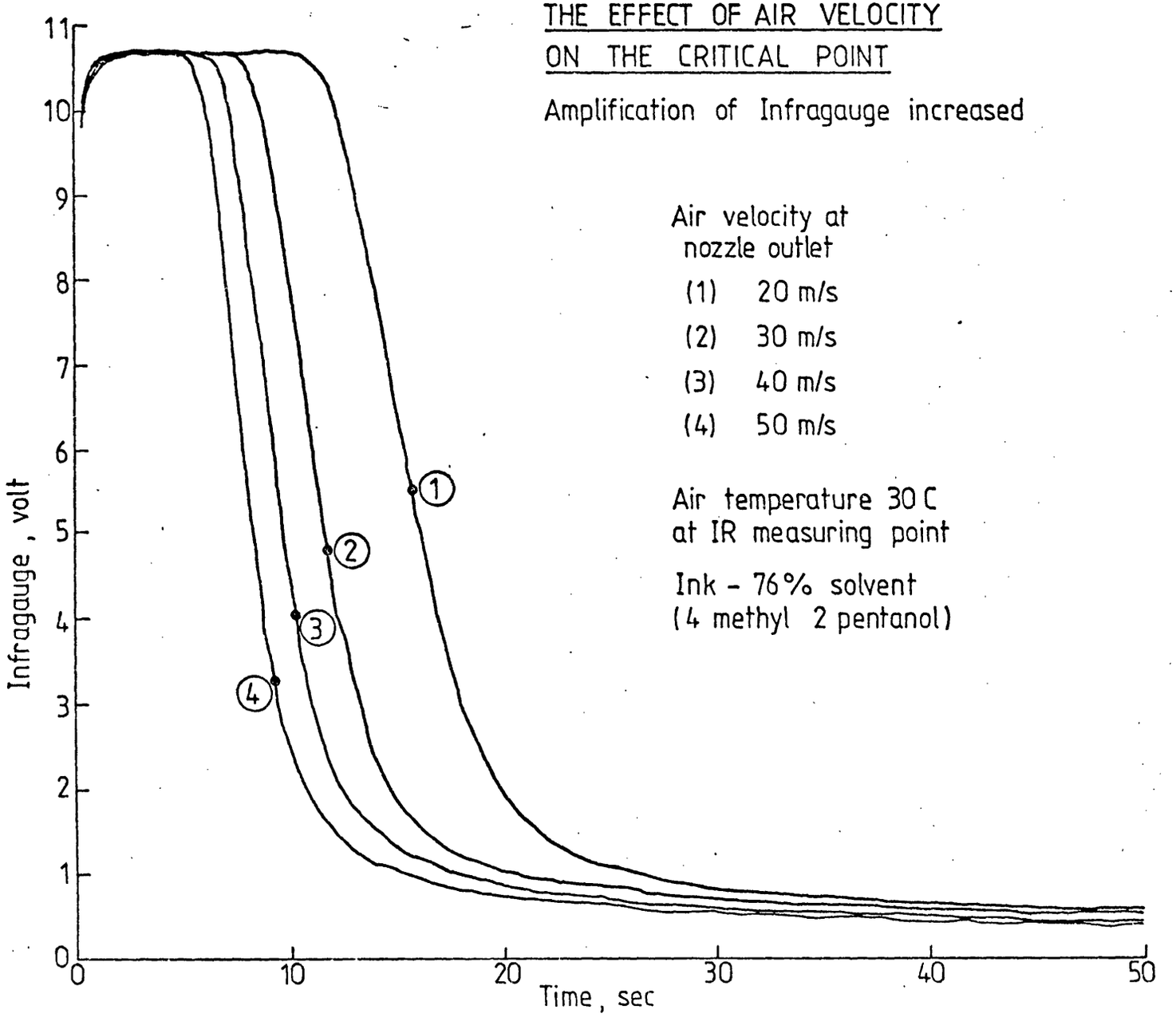
THE EFFECT OF AIR VELOCITY
ON THE CRITICAL POINT
Amplification of Infragauge increased
Air velocity at
nozzle outlet
(1) 20 m/s
(2) 30 m/s
(3) 40 m/s
(4) 50 m/s
Air temperature 30 C
at IR measuring point
Ink - 76% solvent
(4 methyl 2 pentanol)
Infragauge , volt
Time , sec
0
1
2
3
4
5
6
7
8
9
10
11
0
10
20
30
40
50

FIGURE II.8

THE EFFECT OF AIR VELOCITY

T = 30 C

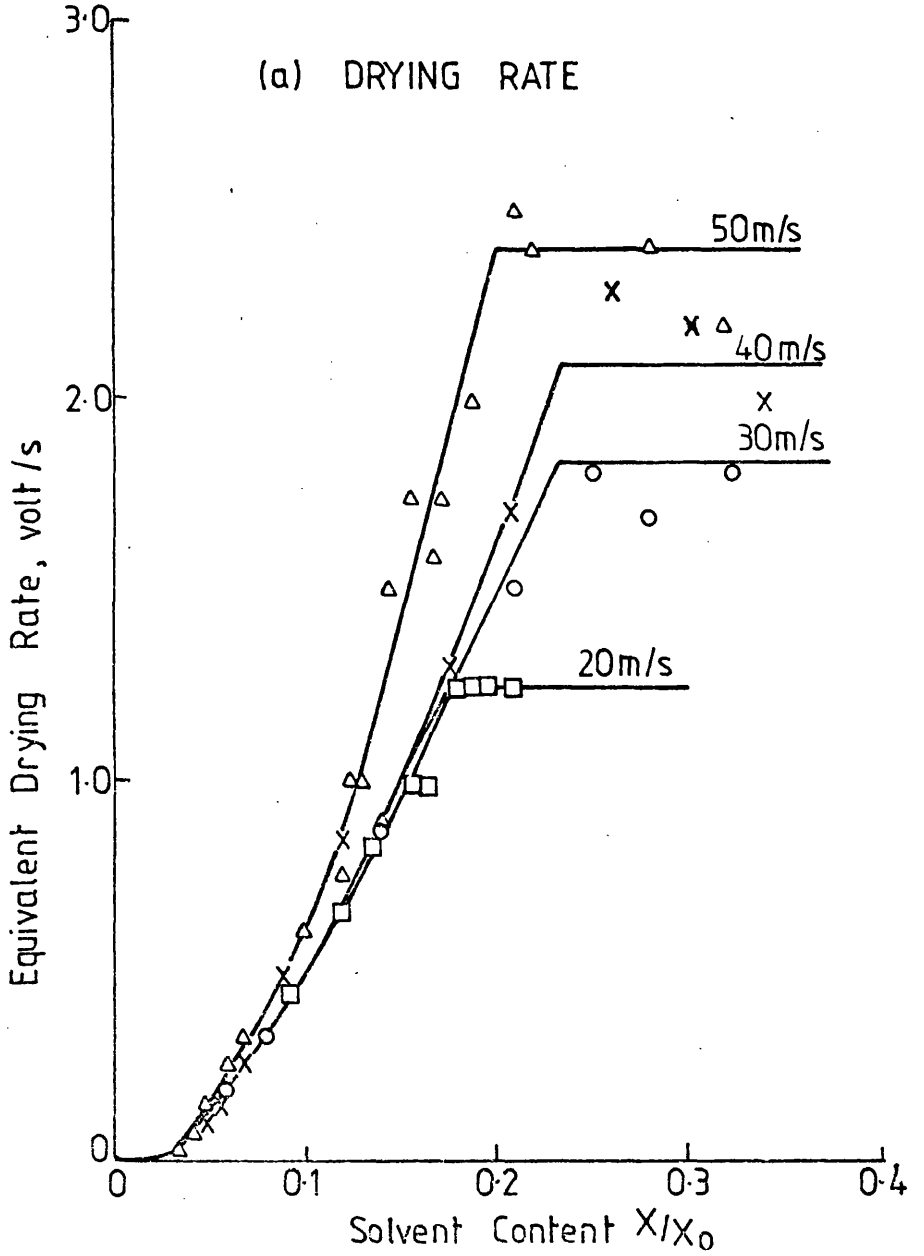

Drying Rates Corresponding to Fig. 11.8

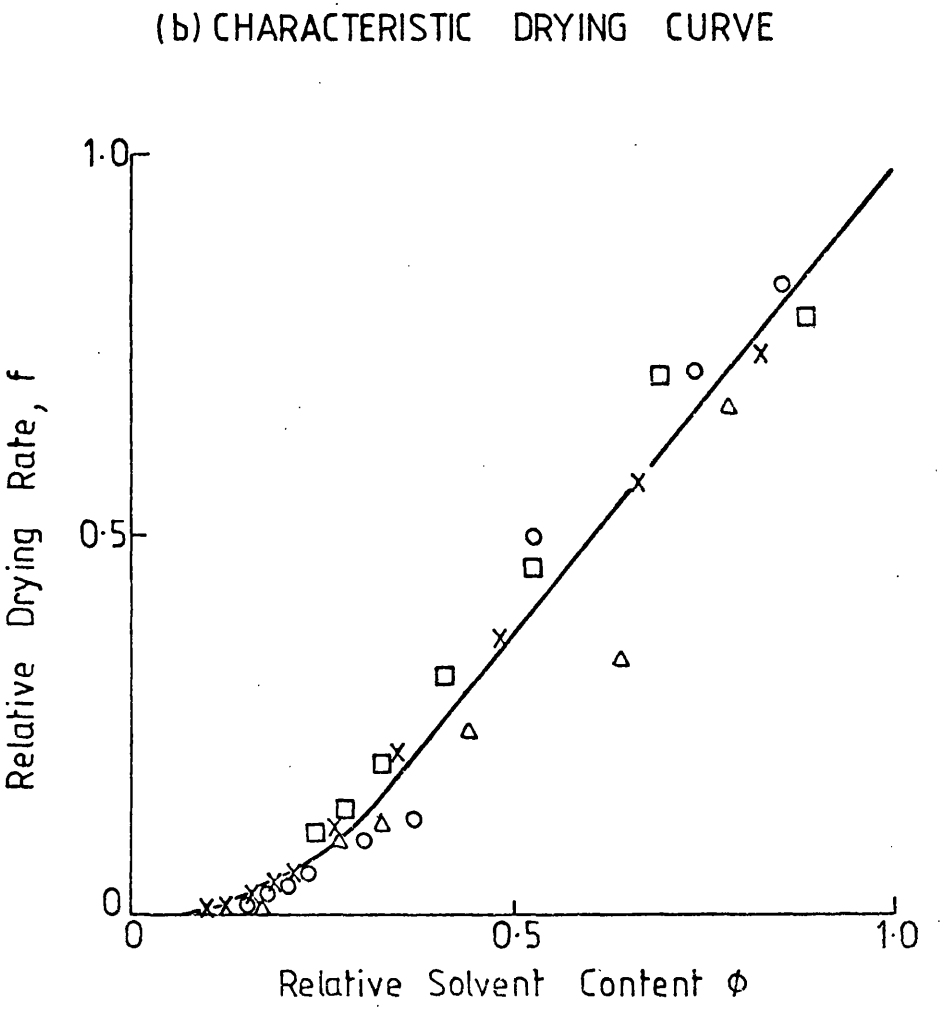

FIGURE 11.9.

FIGURE 11.10

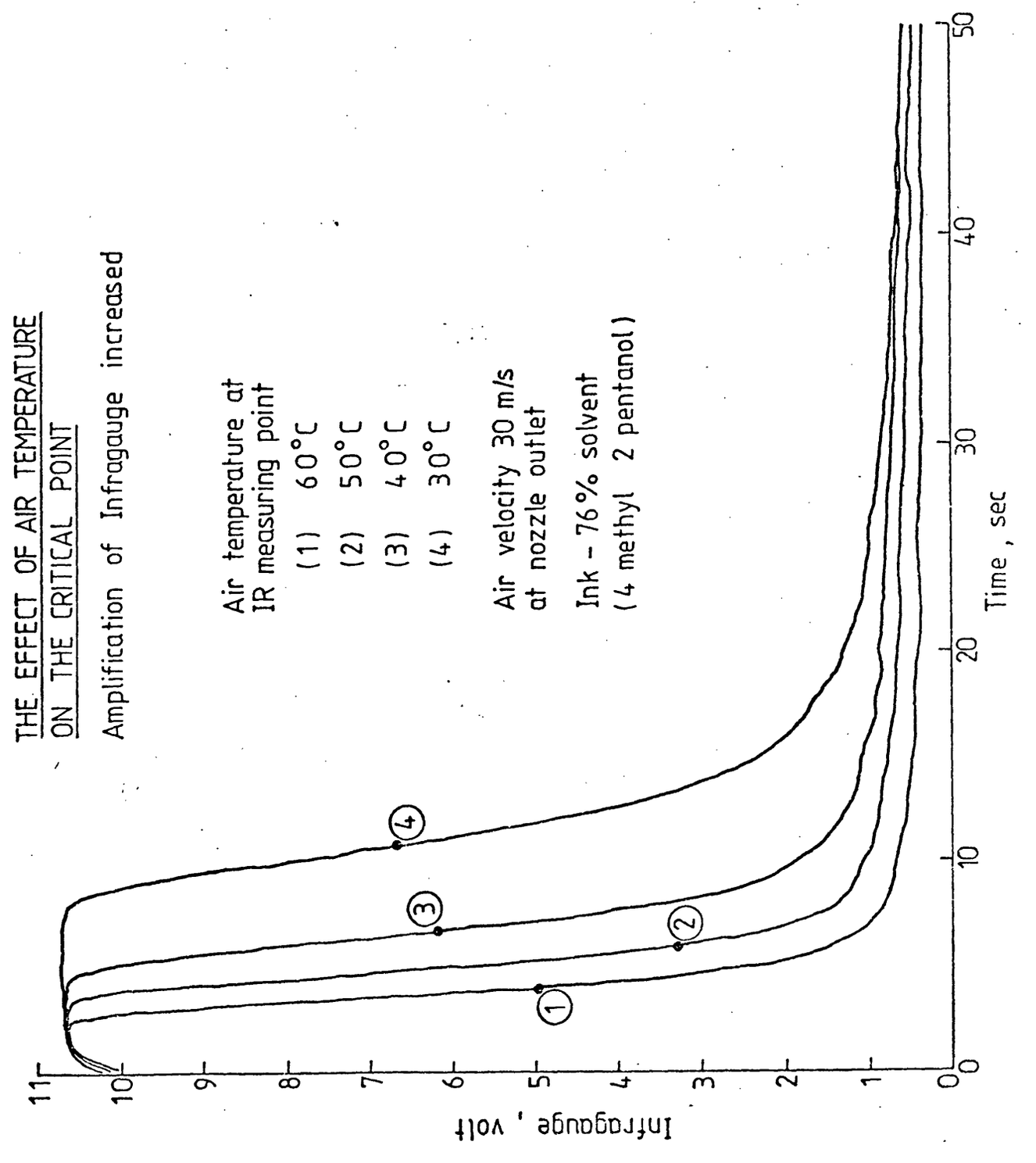
THE EFFECT OF AIR TEMPERATURE
ON THE CRITICAL POINT
Amplification of Infragauge increased
Air temperature at
IR measuring point
(1) 60°C
(2) 50°C
(3) 40°C
(4) 30°C
Air velocity 30 m/s
at nozzle outlet
Ink - 76% solvent
(4 methyl 2 pentanol)
Infragauge , volt
Time , sec
0
1
2
3
4
5
6
7
8
9
10
11
10
20
30
40
50

THE EFFECT OF TEMPERATURE

V_A = 30 m/s

Drying Rates Corresponding to Fig.11.10

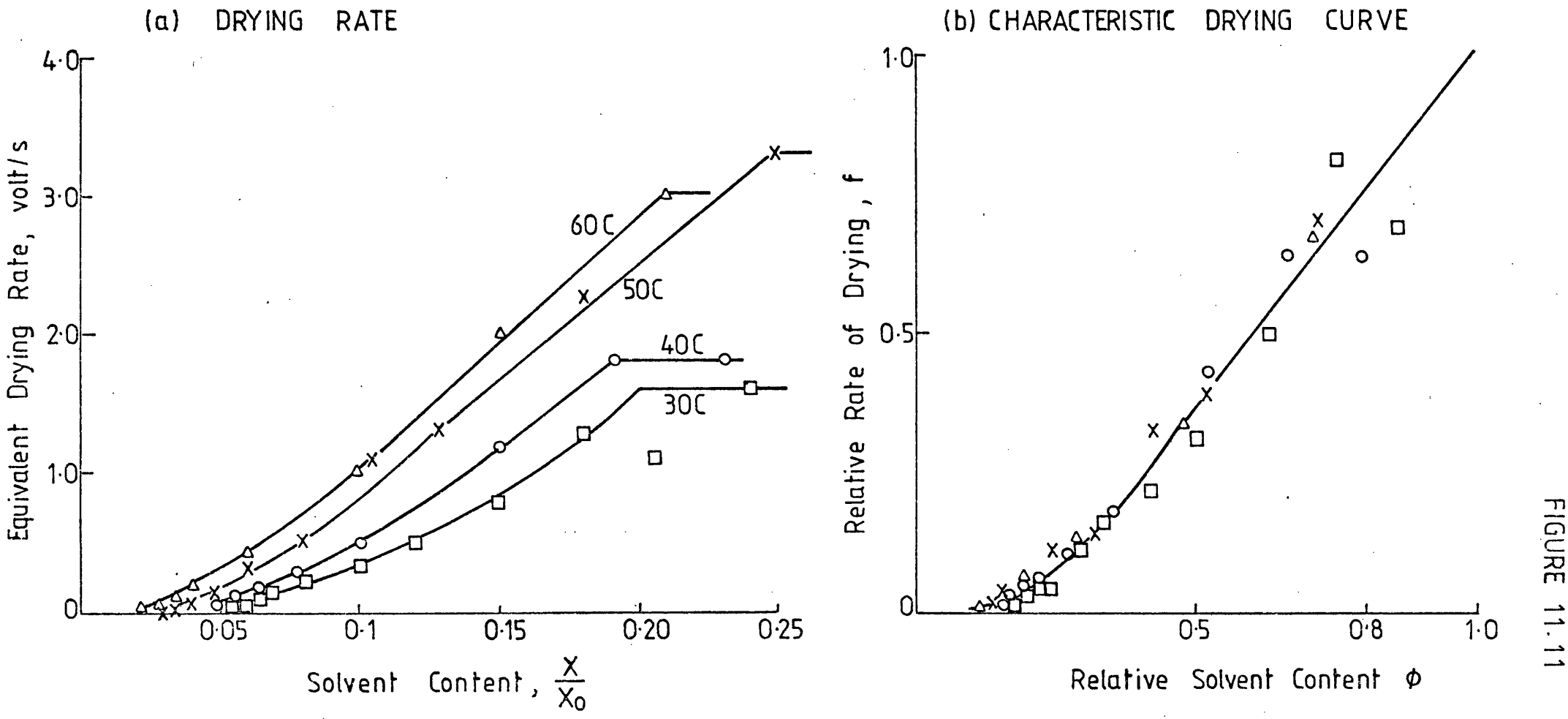

FIGURE 11.11

FIGURE 11.12

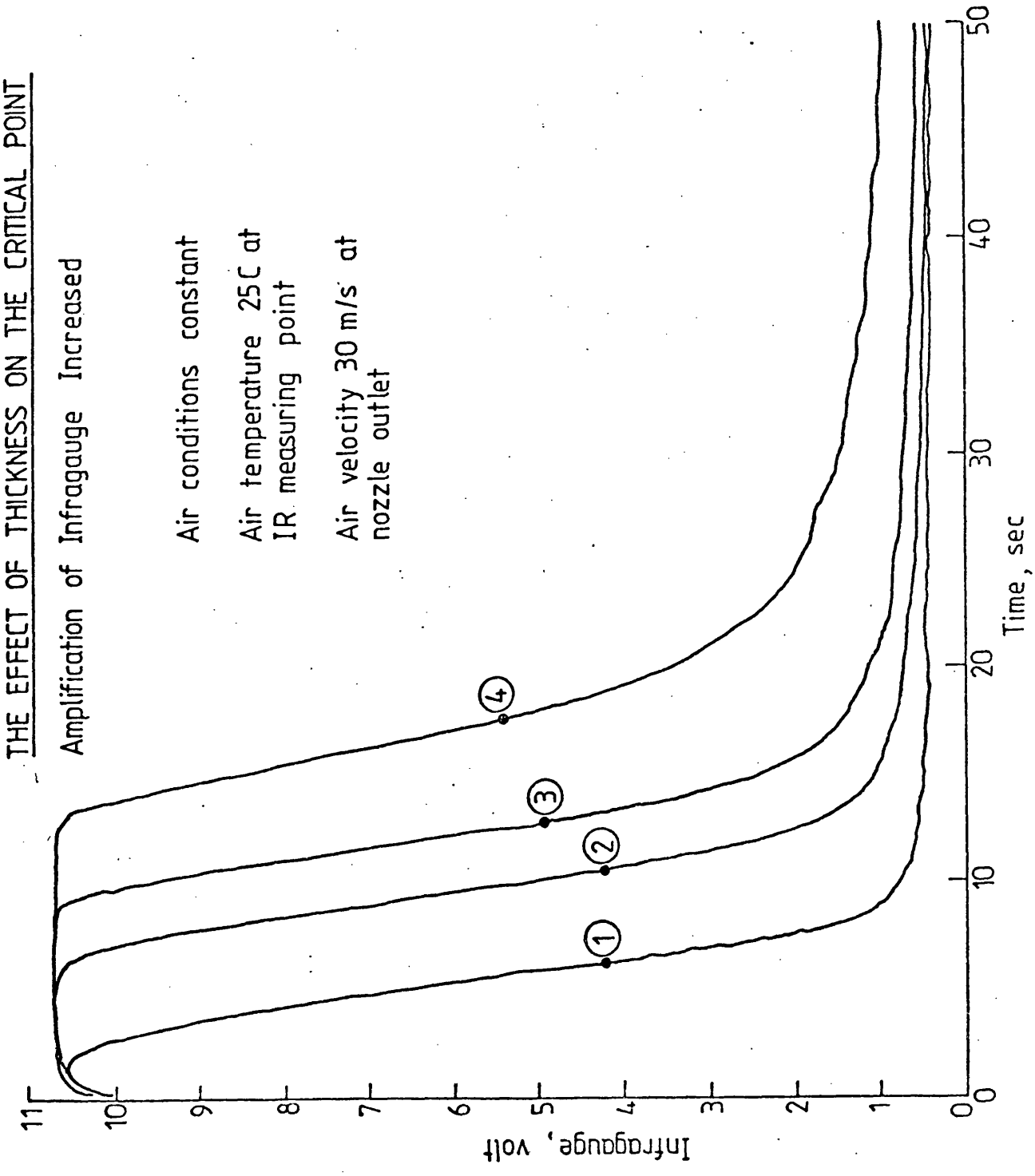
THE EFFECT OF THICKNESS ON THE CRITICAL POINT
Amplification of Infragauge Increased
Air conditions constant
Air temperature 25C at IR measuring point
Air velocity 30 m/s at nozzle outlet
Infragauge, volt
Time, sec
0
1
2
3
4
5
6
7
8
9
10
11
10
20
30
40
50
1
2
3
4

RATE OF DRYING CURVES

Drying Rates Corresponding to Fig. 11.12

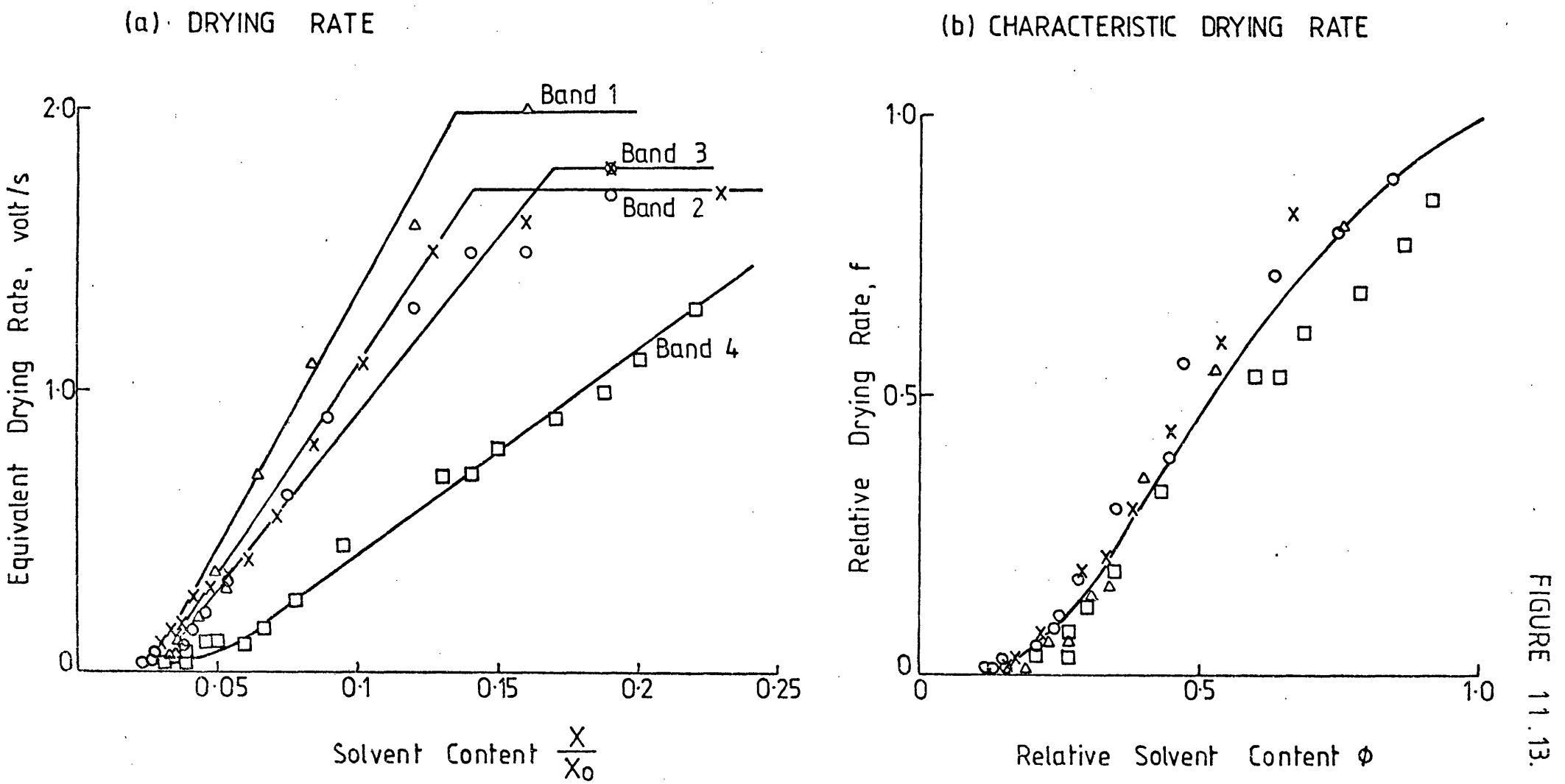

FIGURE 11.13.

FIGURE 11.14

MATHEMATICAL MODELS OF THE CHARACTERISTIC DRYING CURVE

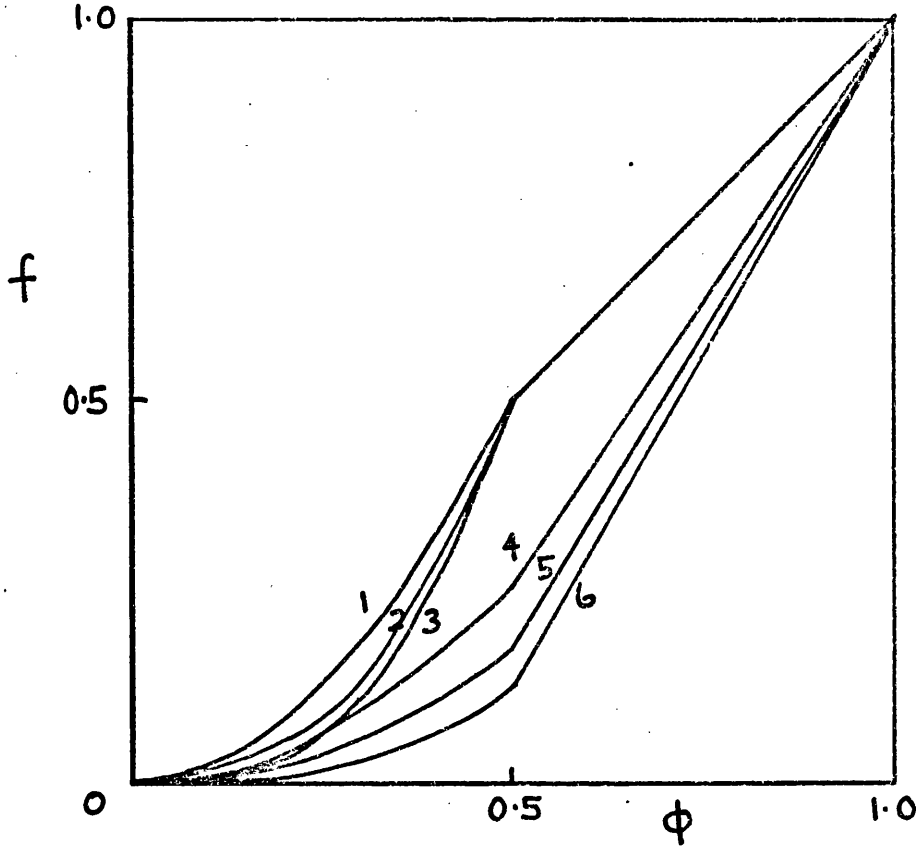

	equation for ϕ		$g(\phi)$
	$0 < \phi < 0.5$	$0.5 < \phi < 1.0$	
1	$f(\phi) = 2\phi^2$	$f(\phi) = \phi$	$\frac{1}{2\phi} - 0.307$ *
2	$f(\phi) = 2.83\phi^{2.5}$	$f(\phi) = \phi$	$\frac{1}{4.25\,\phi^{1.5}} + 0.02$ *
3	$f(\phi) = 4\phi^3$	$f(\phi) = \phi$	$\frac{1}{8\phi^2} + 0.193$ *
4	$f(\phi) = \phi^2$	$f(\phi) = 1.5\phi - 0.5$	$0.666 \ln\left(\frac{1}{1.5\phi - 0.5}\right) + \frac{1}{\phi} - 2$
5	$f(\phi) = \phi^{2.5}$	$f(\phi) = 1.64\phi - 0.64$	$0.61 \ln\left(\frac{1}{1.64\phi - 0.64}\right) + \frac{1}{1.5\phi^{1.5}} = 1.9$
6	$f(\phi) = \phi^3$	$f(\phi) = 1.75\phi - 0.75$	$0.571 \ln\left(\frac{1}{1.75\phi - 0.75}\right) + \frac{1}{2\phi^2} - 2$
7			

* Applies in the region, $0 < \phi < 0.5$.
For the region, $0.5 < \phi < 1.0$, from equn. 11.7.6, $g(\phi) = \ln\left(\frac{1}{\phi}\right)$

DRYING TIME $g(\phi)$

Numerical values of $g(\phi)$

Symbol	ϕ	·9	·8	·7	·6	·5	·4	·3	·2	·15	·1
×	1	·11	·22	·36	·51	·69	·94	1·36	2·2	3·03	4·7
+	2	·11	·22	·36	·51	·69	·95	1·45	2·7	4·1	7·5
o	3	·11	·22	·36	·51	·69	·97	1·6	3·3	5·7	12·7
□	4	·11	·24	·4	·61	·92	1·4	2·3	3·9	5·6	8·9
Δ	5	·11	·23	·41	·65	1·1	1·8	3·2	6·6	10·6	20·2
•	6	·11	·25	·43	·69	1·2	2·3	4·74	11·7	21·4	49·0

Numbers 1–6 in first column, correspond to the numbers of the mathematical models in FIGURE 11.14

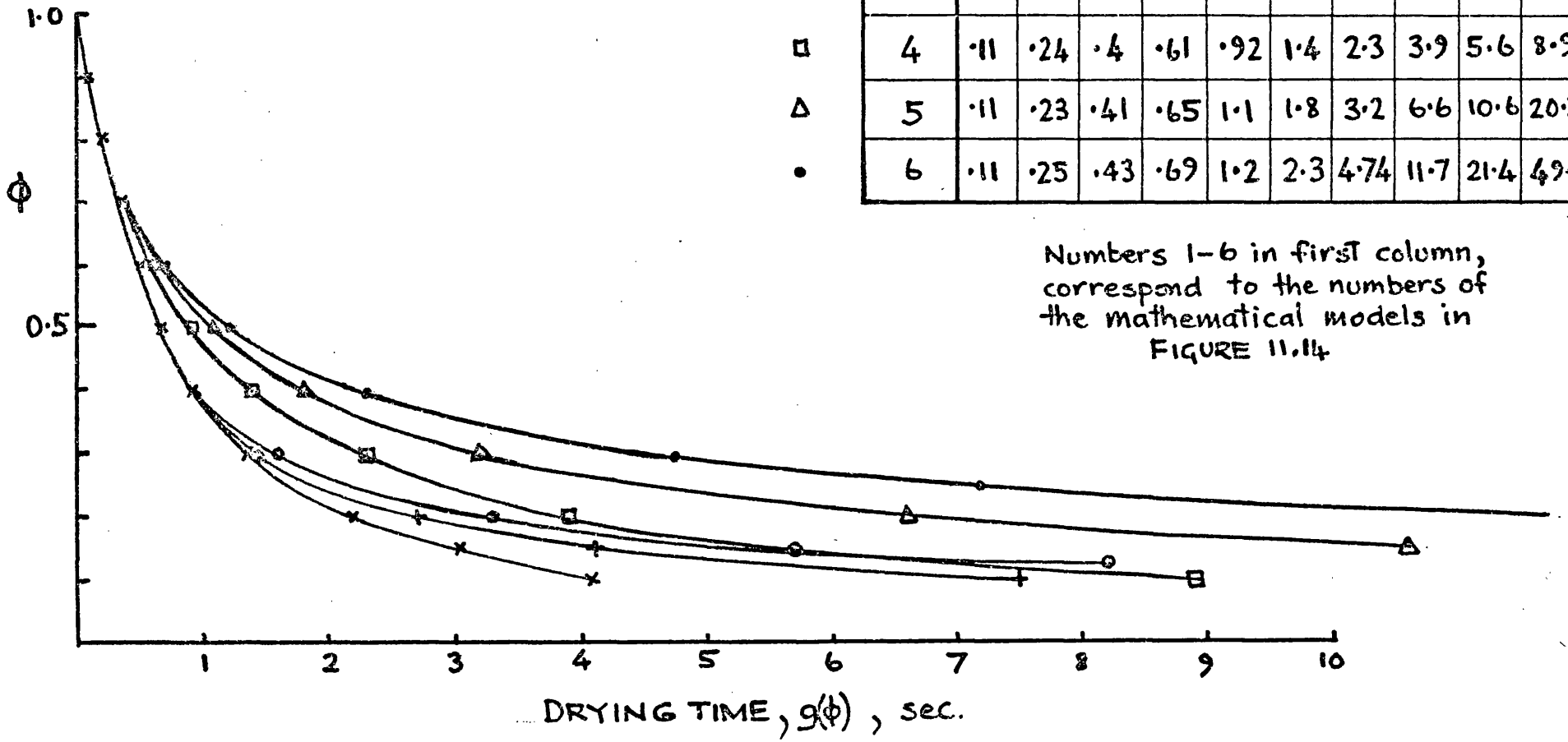

FIGURE 11.15

COMPARISON OF $h(\phi)$ AND $g(\phi)$

4 METHYL 2 PENTANOL

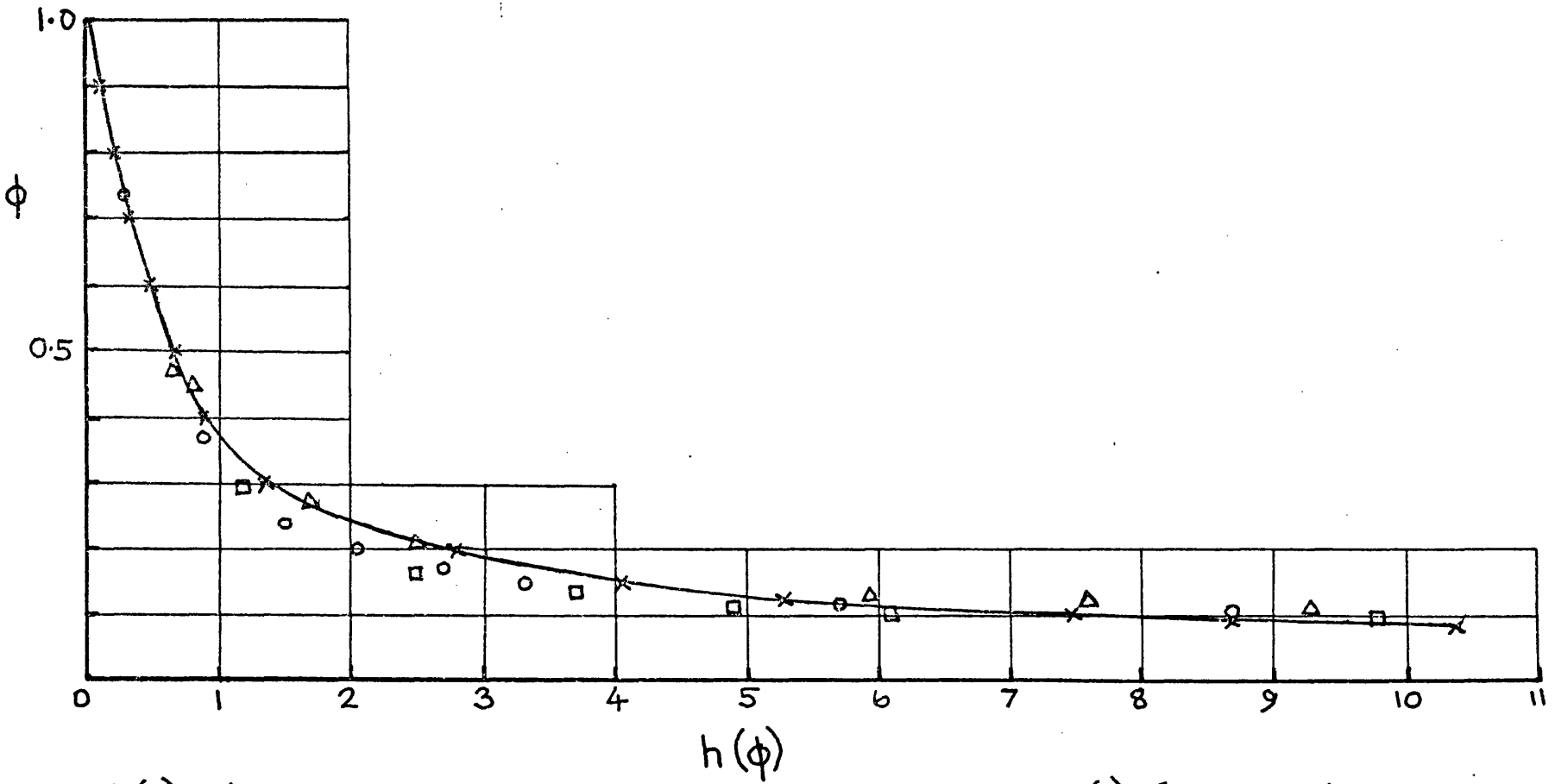

$h(\phi)$ data from

- ○ Table 11.1, item a)
- □ Table 11.1, item b)
- △ Table 11.1, item c)

$g(\phi)$ from model 2, Figure 11.14

$0.5 < \phi < 1.0$, $t = \ln\left(\frac{1}{\phi}\right)$

—×— $0 < \phi < 0.5$, $t = \frac{1}{4.25\,\phi^{1.5}} + 0.02$

FIGURE 11.16

CHARACTERISTIC DRYING CURVES n - propanol

Corresponding to Figs. 7.2 and 7.3

(a) THE EFFECT OF AIR VELOCITY

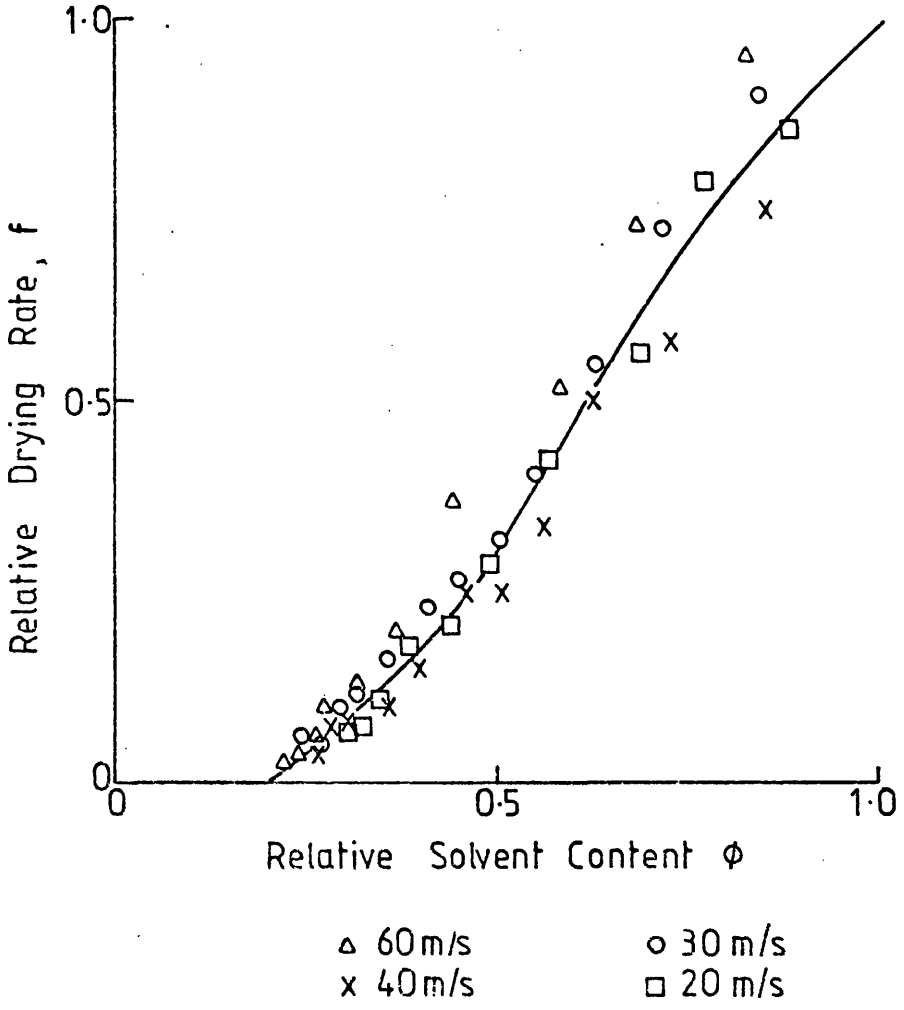

(b) THE EFFECT OF AIR TEMPERATURE

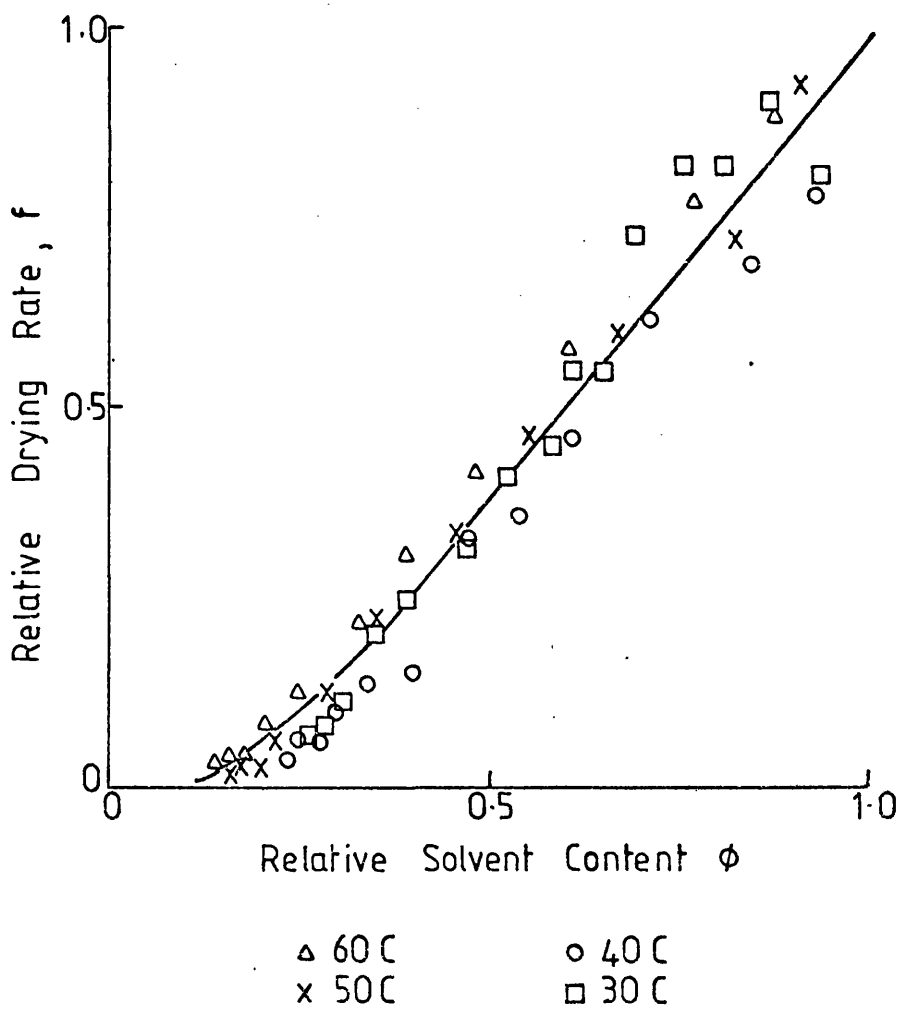

FIGURE 11.17.

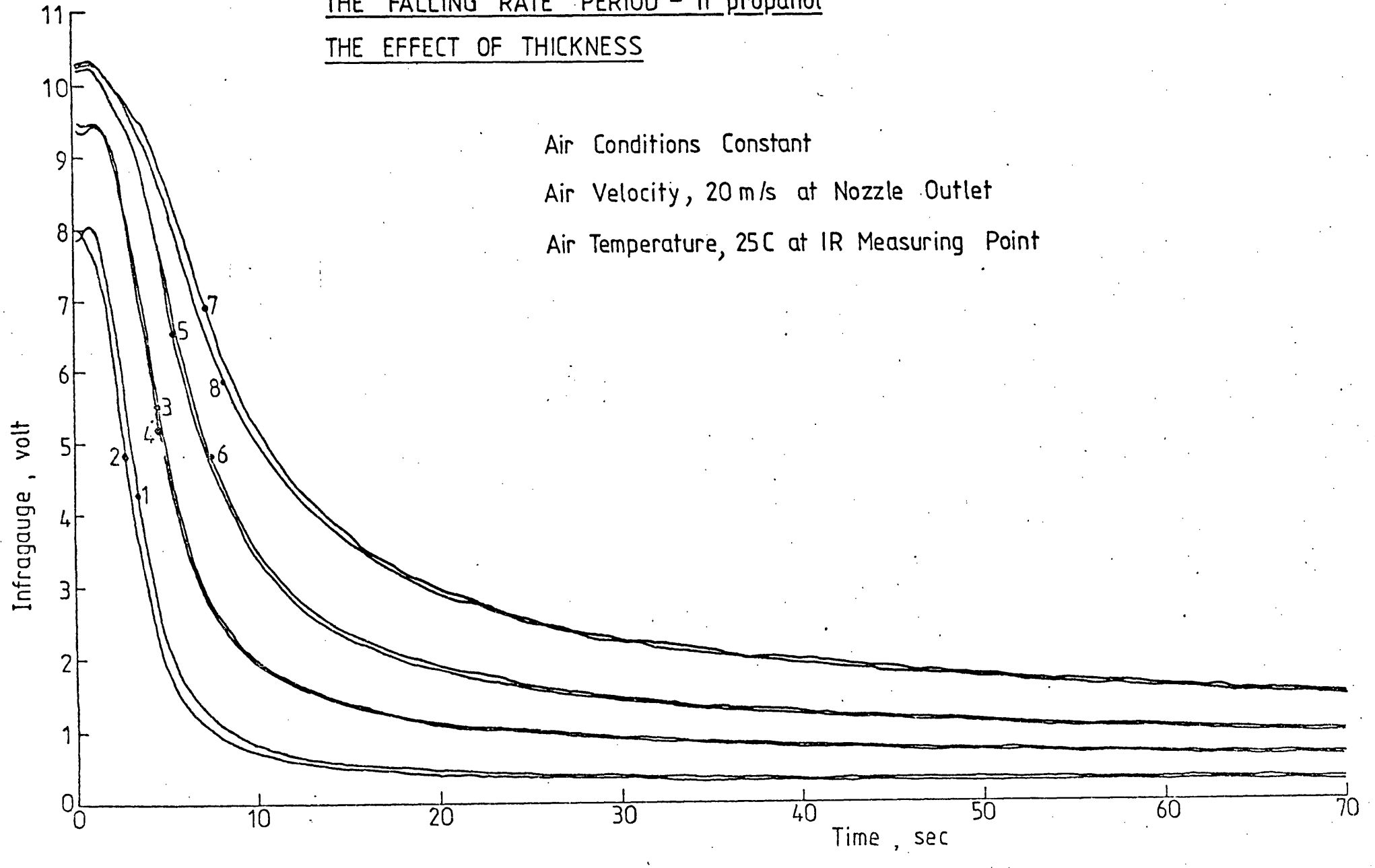
THE FALLING RATE PERIOD - n propanol
THE EFFECT OF THICKNESS
Air Conditions Constant
Air Velocity, 20 m/s at Nozzle Outlet
Air Temperature, 25C at IR Measuring Point
Infragauge, volt
Time, sec
0
1
2
3
4
5
6
7
8
0
10
20
30
40
50
60
70
0
1
2
3
4
5
6
7
8
9
10
11

FIGURE 11.18

CHARACTERISTIC DRYING CURVES n – propanol

Corresponding to Fig. 11.18

THE EFFECT OF THICKNESS

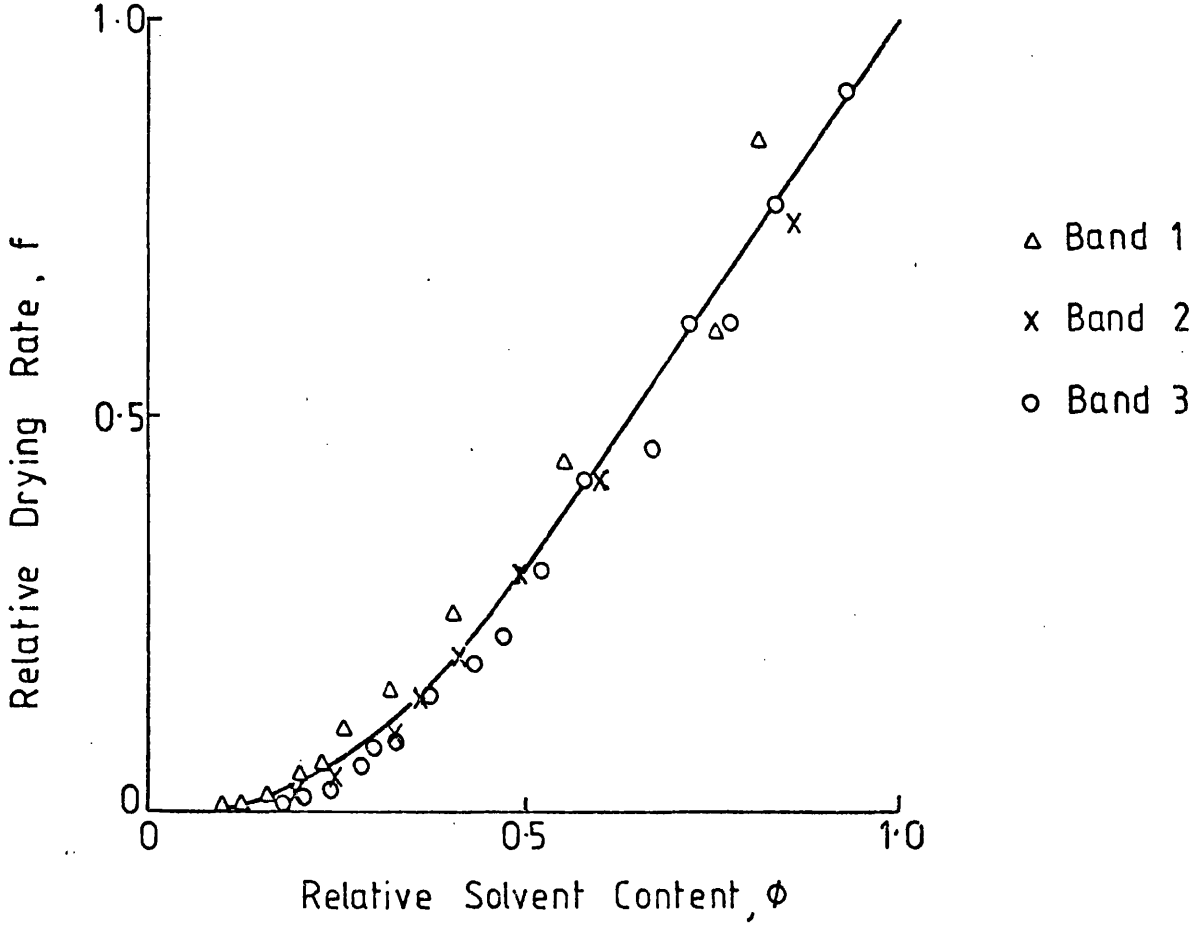

FIGURE 11.19

COMPARISON OF $h(\phi)$ AND $g(\phi)$ FOR n-PROPANOL

ϕ	1·0	·9	·8	·7	·6	·5	·4	·3	·2	·15	·1
$g(\phi)$	0	·11	·23	·38	·57	·82	1·2	1·9	3·2	4·5	7·2

$$0.4<\phi<1.0,\quad g(\phi)=\frac{3}{4}\ln\left(\frac{1}{4/3\phi-1/3}\right)$$

$$0<\phi<0.4,\quad g(\phi)=1.21+\frac{1}{1.976}\left(\frac{1}{1.5\phi^{1.5}}-2.63\right)$$

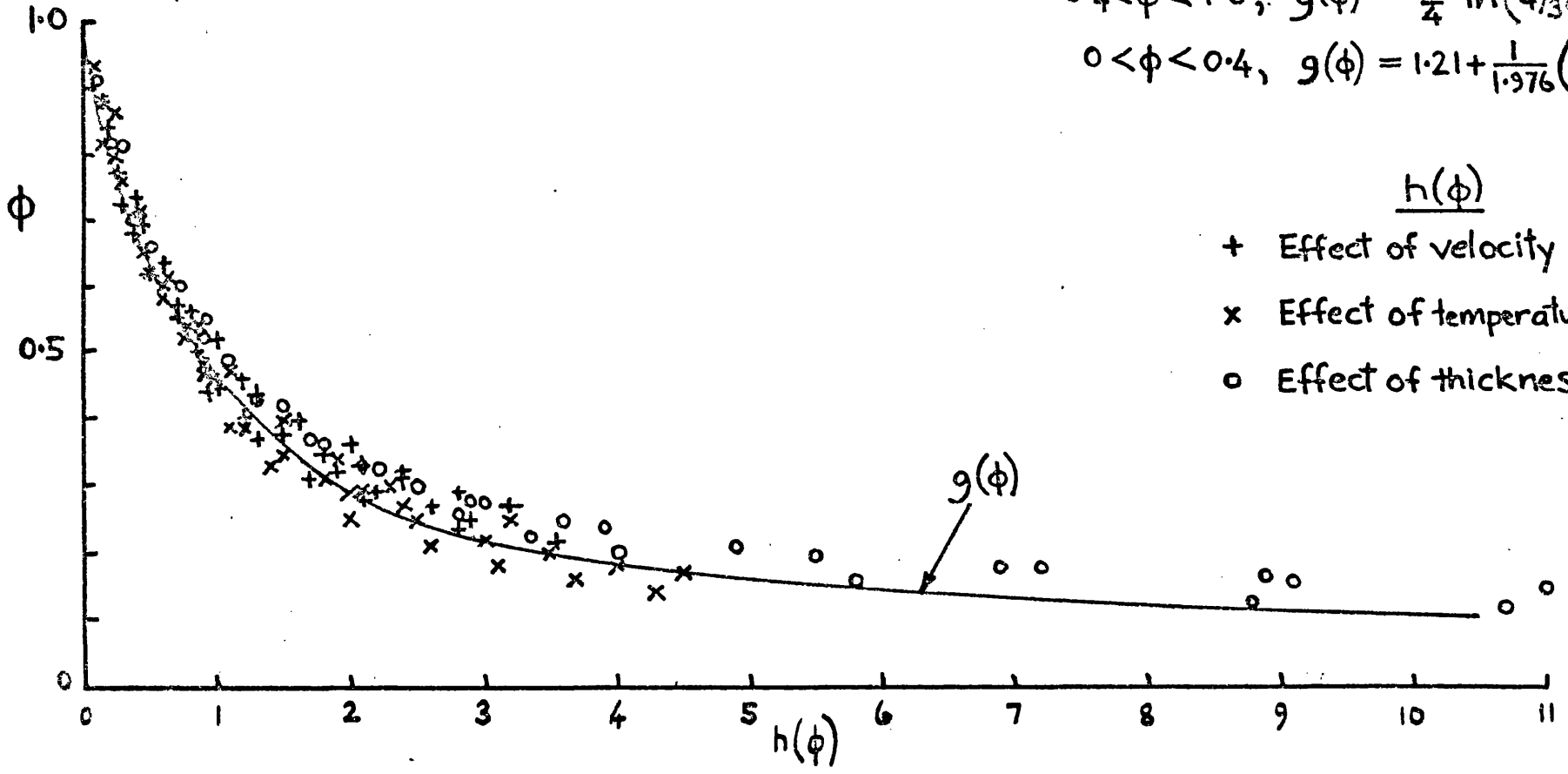

$h(\phi)$

+ Effect of velocity (FIG. 11·18a)
× Effect of temperature (FIG. 11.18b)
o Effect of thickness (FIG. 11·20)

FIGURE 11.20

12. SUMMARY, DISCUSSION AND CONCLUSIONS

12.1 Introduction

In this chapter, the results of the research will be summarised and discussed. Wherever possible the order in which the various points are dealt with, will follow the order in which these topics were originally presented in the thesis. The limitations and the achievements of the research will be assessed.

After this summing-up, an attempt is made to assess the potential of the IR instrument, not only as a tool for basic research, but more widely, as a dryness meter for use on an industrial dryer. The type of heat transfer data required by dryer designers is briefly discussed.

Finally some suggestions are made for the manner in which future ink-drying research should be carried out, to relate it to the requirements of commercial dryer design.

12.2 Summing-up

1. Ink Application

Test work has demonstrated that the adaption of the gravure press for research purposes has been quite successful. The earlier difficulties of applying an ink coating of known thickness have been overcome. The effect of uncontrollable variations in ink film thickness, which occur during a test series, have been sufficiently small for them to be neglected, in comparison with the major effects brought about by changes in air velocity, air temperature, etc.

Difficulties of matching the thickness of the ink layer to the operating characteristics of the IR instrument, have been overcome by the use of a gravure cylinder with 4 different depths of etch. The range of coating thickness produced from this cylinder, has proved to be quite adequate for research purposes. The quantity of ink deposited on the web from each gravure band, may be readily determined by sequential weighing on a sensitive chemical balance.

Experience has shown that continuous printing is neither necessary nor desirable for drying research. It has been found that the drying characteristics of a material can best be expressed in the form of a drying curve. Such a curve can be most directly arrived at, by the batch drying of a sample in a controlled environment. Of course, batch operation also offers considerable savings in cost of materials and operating time.

2. The Drying Research Rig

After overcoming some initial set backs, a drying research rig has been successfully developed which incorporates an IR absorption instrument capable of detecting solvent in ink films of quite minute thickness. A technique has been developed to record IR drying curves from stationary ink coatings drying in a closely controlled environment. During the course of the research, and within the limitations of the rig, the effect of varying the physical drying parameters has been demonstrated. Refinements carried out during the development period, both to the rig itself and to the experimental technique, have served to reduce sources of secondary error. It would appear, that in some experiments, the rig was operating at the limit of the present experimental technique.

The maximum air velocity and air temperature used in the tests, represent the practical limits of both the fan and the electrical heater. Research at the higher velocities and temperatures in use on some industrial dryers, would require replacement of the existing air supply system. More detailed measurements in the air boundary-layer require more advanced instrumentation than is presently employed.

3. The IR-Technique

The early difficulties experienced with this technique have now been largely overcome. These early difficulties arose largely from unfamiliarity with the physical principles of IR absorption and the necessity to relate the IR wavelength to the thickness or quantity of the substance being measured. Although the Infragauge is a commercial instrument, the manner in which it was employed to measure a variable solvent content, was a novel application. Once the operating characteristics of the instrument were fully understood, then, within certain limitations, it has proved to be an excellent research tool with which to measure the solvent content of extremely thin films. The initial sections of the IR drying curves are vitiated by saturation of instrument sensitivity, but the remainder of the curves constitutes an excellent record of the drying process.

4. IR Drying Curves - Constant-Rate Period

A systematic series of experiments was carried out to explore the effect of changes in the temperature of the drying air (20 - 70 C) and in the jet efflux velocity (20 - 70 m/s) on the drying rate. The change in slope of the drying curve in the constant-rate region, consequent upon these changes in the condition of the drying air, is clearly indicated on the IR curves.

After making allowance for the non-linearity of the IR instrument at the start of drying, all drying curves show that the early period of drying takes place at constant-rate. For the research ink used for most of the tests (solvent 4 methyl 2 propanol) some 80 - 90% of the total solvent content was removed during the constant-rate period.

In ink drying, because the solvent evaporates from a solution, then the experimental fact that drying takes place at constant-rate is, to some extent, an anomaly. Two possible explanations of this anomaly have been presented (in Appendix 2) but further investigation of this behaviour is required.

The Infragauge was calibrated by carrying out a series of drying tests on all four gravure bands and also varying the percentage solvent content of the ink. Solvent deposit was estimated by weighing the dry ink coating. The virtual voltage at zero time was estimated by extrapolating the constant-rate section of the IR curves. Results from this calibration were self-consistent.

5. The Critical Point

Tests showed that changes in the rate of drying in the constant-rate period, brought about by changing either air velocity or air temperature, had little effect on the occurrence of the critical point. Such behaviour is characteristically different from that occurring in solids drying. A possible explanation of this phenomenon is that the fraction of the initial solvent content which remains unevaporated at the critical point, is related to the fraction of non-volatiles in the ink. Since a detailed knowledge of the behaviour of the critical point is vital for dryer design, more research would be justified to establish the generality of this experimental finding.

6. Theory of Constant-Rate Ink Drying

A theory of constant-rate drying has been developed, in which it is assumed that the evaporating surface takes up the "wet-bulb" temperature corresponding to the temperature and humidity of the drying air. In developing this theory it was necessary to assess the various expressions of the analogy between heat transfer and mass transfer.

A theoretical criterion was developed to compare the relative evaporation rates of a range of solvents under standard external conditions. For non-volatile solvents the equation for the relative evaporation rate r, has the simple form

$$r = D^{2/3} p_o M \qquad 5.4.11$$

A theoretical expression was also derived for the correction factor F which must be applied to r, to extend the use of this concept to solvents of higher volatility. Comparison of the above theoretical criteria with published experimental measurements of relative evaporation rates, show reasonable agreement except at the more volatile end of the range.

The theory of the relative evaporation rate, under standardised external conditions, was extended to include the effects of changes in the velocity and the temperature, of the drying air. Because it was based on a linearised pressure/temperature relation for the solvent vapour, this theory was necessarily approximate. However, it served to demonstrate the effect of the physical variables on the constant-rate drying time t_c.

The energy transfer rates occurring during constant-rate drying, were also presented in a simple graphical form, which should be useful in practical design work.

7. Solvent Vapour Pressure Data

Published data on the vapour pressure of the research solvent, at conditions appropriate to the drying experiments, was found to be both sparse and contradictory. The vapour pressure/temperature relation used in the computer program is based on the manufacturers data and on confirmatory experiments carried out by the writer.

8. Heat Transfer Under Impinging Jets

Theories of heat transfer under impinging jets are presently not developed to the stage where they can be used to yield reliable data for the impingement region. This being the case, experimental heat transfer rigs and the associated heat flux meters, have been designed and constructed, to measure the required values of the heat transfer coefficients. Because of their small size, manufacture of Gardon type flux meters proved to be difficult, but these difficulties were eventually overcome. This work suffered a set back when the calibration certificate supplied with a proprietory fluxmeter was found to be erroneous. Careful test work, on a specially constructed calibration rig, was required to establish the validity of the experimentally determined heat transfer coefficients used in this thesis.

9. The Effect of Dissolved Resin on the Drying-Rate During the Constant-Rate Period

Because of the chemical complexity of the polymer-in-solvent solution, it was not practical to make a theoretical prediction of the effect of the dissolved resin on the evaporation rate of the pure solvent.

Instead, this effect was determined empirically, by comparing the slopes of the constant-rate drying curves for ink and for pure solvent. It was found that pure solvent dries more quickly than ink by a factor of approximately 1.3. Accordingly, theoretical predictions of drying time were reduced by a factor of 1.3, before comparing them with experimental results.

10. Computer Program to Predict Time of Externally Controlled Drying

Based on the theory of constant-rate drying, and incorporating the empirical data on heat transfer and on solvent vapour pressure, a computer program was written to predict constant-rate drying time. The agreement between predictions from this program and experimental drying times is reasonably good, and is consistent with the expected limitations of both theory and experimental technique.

11. Addition to Program for Practical Dryer Design

A subroutine has been written which may be incorporated into the computer program of 10 above, which allows the calculation of practical dryer designs. For given air conditions and slot geometry the subroutine calculates the average value of the heat transfer coefficient, $\bar{h}$, under an array of slot nozzles. With this facility the constant-rate drying time, may be converted into a length of a multi-nozzle dryer. By this means a number of solutions may be examined, and an economic optimum arrived at.

12. Temperature Measurement by IR Thermometer

Despite the experimental difficulties, an IR thermometer was successfully used to measure the transient temperature of the ink/substrate system during drying. These temperature traces provide valuable

corroborative evidence for the theory of constant-rate ink drying developed in this thesis. There is good agreement between the magnitude of the temperature escalation at the end of the constant-rate period and the predicted value of the wet-bulb depression. Such temperature traces could be used as an alternative means of locating the critical point.

13. Constant-Rate Drying Tests - n Propanol

To extend the range of the research, further tests were carried out on a more volatile solvent, of the type used in commercial practice. Air velocity was varied in the range, 20 - 60 m/s and air temperature in the range, 30 - 60 C. Comparisons between computer predictions of constant-rate drying time and those measured from the experimental drying curves showed good agreement.

14. Cumulative Drying Effect

To extend the experimental technique, tests were carried out to measure the total amount of drying achieved when the ink coating passes under an air jet. Drying curves from the IR measuring head located "after" the nozzle, clearly indicated the cumulative effect of an increase in the air velocity and/or the air temperature.

The computer program was modified to enable predictions to be made of the cumulative drying effect. By subdividing the total web transit into a series of discrete steps, the external conditions were adjusted to model the changing drying environment as the ink passed under the nozzle. In addition, the program was also used to predict the transient change in the ink temperature.

If allowances are made for the rather simple theoretical model on which the program for the cumulative effect of drying was based, then agreement between predictions from it and the experimental data, are encouraging.

15. The Physical Mechanism of Falling-Rate Ink Drying

The research described in this thesis, appears to indicate that in the falling-rate region, the rate at which a film of paint dries, depends upon the rate at which solvent can diffuse through the polymer residue to the surface. A literature search has established that the detailed mechanism of solvent-in-polymer diffusion processes are complex. Diffusion coefficients are not constant, but depend upon solvent concentration. To provide a basis of understanding of current research in this field, the theory of diffusion in polymers has been reviewed and is briefly outlined. The free-volume theory has been used to derive theoretical expressions for the diffusion coefficient. Experimental research on diffusion through plastics, and theoretical deductions from free-volume theory, both lead to the conclusions that the diffusion coefficient is exponentially dependent upon the solvent concentration.

16. Theoretical Solution of the Diffusion Equation

To provide background, classical solutions of the diffusion equation have been briefly described. A theoretical model of the falling-rate period of ink-drying, based on a solution of the one-dimensional diffusion equation, has been developed. For this model, it was assumed that the diffusion coefficient is exponentially dependent upon the solvent concentration. With this assumption the diffusion equation is rendered non-linear. Because of this complexity a

numerical solution on a computer was preferred over an analytical solution.

To reduce the difficulty of the solution, a subsidiary variable was used to transform the original equations to "S-form". Transformations for a "single stage" and for a "two stage" model of the diffusion coefficient have been derived. The numerical technique employed, a finite-difference method of the implicit, "Crank-Nicolson", type.

17. Computer Program to Solve the Diffusion Equation

A computer program has been developed to solve the non-dimensional form of the diffusion equation. Particular numerical values for the transport coefficients, ink thickness, etc., are not used in the program, only the non-dimensional parameters, D_1^*, Bi_2 and Fo, require specification. An iterative technique is used to solve the non-linear diffusion equation.

During the initial trials of this program, difficulties were encountered which were traced to the stability of the iterative technique. Analysis of the convergence of the iterative method, showed that it depended upon the manner in which the recursion relation had been formulated. This problem was overcome by incorporating two versions of the recurrence relation in the program.

18. Computer Solutions - The Total Drying Process

Further computational difficulties were experiences when the constant-rate boundary condition was used with a small value of Biot number. In this case, numerical analysis showed that the relatively large

number of time-steps required, cannot be reduced by making a compensating increase in the length of each time-step.

Successful computer runs were carried out with the numerical values of the program parameters D_1^* and Bi_2, set to give a Biot number equal to unity at the end of the constant-rate period. This value of Biot number was selected to combine economy of computing time with good agreement with experiment. To demonstrate the general capability of the program, further runs were carried out with the Biot number at the end of the constant-rate period not equal to unity.

19. Computer Solutions - The Falling-Rate Period Only

Results, from both the computer and the IR curves, appear to indicate that the concentration dependency of the diffusion coefficient produces its greatest effect in the falling-rate period. Accordingly, later computer runs were restricted to this period. Tests were run to demonstrate the effect of changing the value of D_1^*. It was found that results from these tests could most conveniently be presented in the form of a characteristic drying curve. The shape of these curves shows qualitative agreement with the corresponding sections of characteristic drying curves derived from experiment.

To improve the agreement between computed and experimental curves, two final adjustments were made to the program:-

a) A more complex, 2-stage, model of the diffusion coefficient was adopted.

b) The Biot number at the beginning of the falling-rate period was reduced to a value of 0.1.

With these modifications, the characteristic drying curves derived from the computer model and from experiment, are quite similar.

It should be noted, that when the computer model is constrained to produce good agreement with these particular experiments, it is not being exploited to its maximum capability. The program was written in a flexible manner, so that it can be used to model other behaviour and other conditions.

20. Analysis of the IR Curves in the Falling Rate Period - 4 methyl 2 pentanol

The falling-rate sections of IR drying curves were replotted. Both a logarithmic scale of solvent content and a non-dimensional scale of time, were used in an attempt to linearise the curves. These attempts failed, indicating the concentration dependency of the diffusion coefficient. Further experiments were performed, specifically to facilitate a more detailed analysis of the IR curves in the falling-rate region. The falling-rate data was next plotted as a series of rate of drying curves.

Conditions at the critical point were used to normalise the drying-rate data, to produce a "characteristic drying curve". This normalisation technique proved to be extremely successful in that the resultant single curve was largely independent of air velocity, air temperature and ink thickness. Results showed that, allowing for the scatter of experimental points, the normalised drying curve was truly characteristic of a particular ink/solvent system.

21. Theoretical Predictions of Falling-Rate Drying Time

The characteristic drying curve derived from experiment was found to be fairly simple in shape, and therefore it could be modelled by quite simple analytic functions. A family of theoretical models was developed. Equations for the drying time were obtained by integrating the equations for the drying rate.

A technique of curve fitting, was used to select the equation for the drying time which gave the best fit to a range of experimental data.

22. Analysis of IR Curves in the Falling Rate Region - n-Propanol

The falling-rate region of the IR curves for the faster, commercial solvent, n-propanol, were analysed in detail. It was found that drying data from this solvent was also satisfactorily correlated when plotted in the form of characteristic drying curve. This curve was similar in shape to the curve derived previously for 4 methyl 2 pentanol. However to achieve close agreement with the data, some slight adjustment of the theoretical model was required.

12.3 The Potential of the IR Technique

When assessing the future potential of the IR Technique two differing view-points are possible. These depend upon whether the instrument is to be applied to research or to commercial practice. These two applications are discussed in turn.

a) Research

The non-contact principle upon which the instrument operates, makes it ideally suited for measurements on thin, lightweight materials. For the present research, the measurements of ink solvent content were made, without any necessity to compromise or to interrupt the drying schedule. It is difficult to see how realistic measurements of the entire drying curve could have been made in any other way. Indeed, whatever the nature of the specimen, the non-contact principle has great advantages.

The principal difficulty with the type of IR absoption instrument used in the present research, is the necessity, at the design stage, to match the wavelength of the IR beam to the absorption spectrum of the substance being measured. Examination of the absorption spectrum of a particular solvent will show that a number of absorption bands exist. Relative to the band with maximum absorption, other bands with decreasing absorbance (analagous to harmonics) occur at higher frequencies. The IR designer selects a particular harmonic so that, for a given thickness of a particular solvent, the instrument will operate in a zone of optimum sensitivity. Maintaining the sensitivity of the instrument within this zone, while an entire drying curve is measured, when the quantity of solvent in the beam changes by 2 or 3 orders of magnitude, is a difficult design problem.

It must also be remembered that the present IR instrument is designed for a particular solvent/resin/substrate system. It will be recalled from section 4.1 that the IR wavelength was selected so that only the solvent absorbs IR strongly and both resin and substrate absorb IR only weakly. These conditions must be satisfied in any new system upon which research is contemplated, otherwise defective operation will result.

It is apparent that the single wavelength type of IR instrument used in this research is a powerful, but somewhat inflexible tool. Perhaps the most practical way of extending its use over a wide range of solvents, would be to select a limited number of solvents, each with a characteristic mode of behaviour. A corresponding number of optical filters could then be selected to suit the solvent systems to be investigated.

b) Use of IR instrument as a "dryness meter"

There is a great need for accurate "dryness meters" for day to day use on industrial presses. This would provide the fundamental data on dryer performance which is lacking at present. In the opinion of the writer, it is difficult to see, how the fixed wavelengths IR absorption instrument could be used for such an application in the converting industry. In this industry an "ink" is usually formulated from a blend of solvents. The ink/substrate system is changed more or less frequently during normal operation. The consequent wide variation in the absorbing properties of the material to be measured, make this an unsuitable application for the present type of instrument.

The above difficulties do not arise if only a single material, of fixed constituency, is to be measured. These conditions are satisfied in the manufacture of such important products as paper and a variety of plastic films. The technical difficulty is to distinguish the IR absorption due to the "moisture", from the absorption which arises from the other constituents of the film. Commercial IR meters appear to have been satisfactorily fitted to paper making machines in the USA and Canada.

One possible future development of the IR absorption technique will be briefly described. The limitations described above arise mainly because detection is carried out at a single wavelength. In fact this limitation can be removed, IR instruments are manufactured which scan the specimen over the entire spectrum. An IR beam of continuously varying wavelength is generated by optical systems within the instrument. After suitable calibration, such an instrument can be used to determine the analysis of a complex system consisting of a number of constituents. The rather tedious calculations necessary to produce the final analysis can be performed on a microprocessor. At present such instruments are being developed for laboratory use, but it seems feasible that the principle could also be applied to solvent detection on an industrial press.

To conclude this brief discussion, an alternative method of measuring small quantities of solvent should be briefly mentioned, this is the gas/liquid chromatograph (GLC) technique. The GLC is becoming increasingly used by convertors, to measure the degree of final dryness which has been achieved. Attempts by the writer, and a colleague, failed in attempt to use the technique to measure a drying curve. This application of the GLC technique to ink drying research merits further study.

12.4 Research on Heat Transfer Under Impinging Jets

In parallel with the drying research described in this thesis, the writer has also carried on a program of experimental research into the heat transfer characteristics of impinging air jets. Although the writer is aware of the various theoretical models of turbulent flows which can, in principle, be applied to the problem of the impinging jet, he has not attempted such a computer solution. Briefly stated, the reasons for taking this decision were:-

a) The computer solution of a practical multi-jet problem would be extremely complex.

b) It is doubtful if current turbulence models are capable of producing accurate heat transfer predictions for the complex flow field under an impinging jet. The complexities increase at the small nozzle/plate distances used in practical dryers.

c) Computer predictions must be confirmed by experimental measurements.

From discussions with designers of industrial dryers, the writer has concluded that their need is for quite basic heat transfer data. For example the effect on heat transfer of such a fundamental design variable as nozzle shape, does not appear to be available in the published literature. It is difficult for designers to apply published heat transfer data to the design of a multi-nozzle dryer of complex geometry. Designers need to relate heat transfer data to the capital and running costs not only of the dryer but to the entire plant.

Experimental research to provide such basic data is presently being pursued.

12.5 Future Ink-Drying Research

1) Within its stated limits, the research described in this thesis has successfully elucidated the physical variables which control the drying rate of thin ink films. This research should now be extended to more complex systems.

2) It is essential that future ink-drying research should be related to the needs of industry. These needs arise from two different sections of the industry - the machinery manufacturer and the press operator. If possible, further developments of theoretical models of the drying should be related to particular processes occurring in industry. If possible the models should be validated by comparison with data taken from the actual process.

3) Based on the theory and the computer programs developed in this research, sufficient information now exists to develop a practical method of dryer design. The development of such a design method should be undertaken in conjunction with an industrial designer.

4) In the constant-rate region, the manners which solvents evaporate from a blend requires investigation. Because it does not pollute the atmosphere, water is becoming increasingly used as an industrial solvent. The effect of other constituents in the blend, on the rate at which water evaporates is required.

5) Numerical values of solvent in polymer diffusion coefficients are required with which to convert the dimensionless results from the computer model of the falling-rate period into absolute values. This type of research can probably best be carried out by physical chemists.

6) Comparative heat transfer studies are required to establish the optimum nozzle shape to minimise the capital and running costs of the plant. In the face of steeply rising energy costs, efforts must be made to achieve the same evaporative load from the dryer with lower air velocities and air temperatures. Schemes for recovering energy from the dryer exhaust should be examined.

7) Because of time limitations, the full potential of the computer model of the falling rate period has not yet been fully exploited. Various drying schedules should be tried to determine the effect of such changes in the total drying time.

12.6 Conclusions

A programme of research into the evaporation of organic solvents from thin plastic coatings has been implemented and successfully carried through. By means of a novel infra-red technique, the drying process in thin films of ink has been quantified, under conditions which closely approximate those of industrial air jet dryers. The experimental drying curves clearly show the effect on the constant-rate drying time of changes in the velocity and temperature of the drying air. These experimental drying times validate the theory of constant-rate drying which has been developed. This theory could be used as the basis for air jet dryer design.

The IR technique has also provided valuable experimental data on the falling-rate period. The concept of the characteristic of the drying has been successfully used to correlate this data. After some initial difficulties, a computer model of the diffusion process in the falling-rate period has been successfully developed. Dimensionless drying curves from the computer model show good agreement with similar curves derived from experiment.

It is considered that all aspects of this research are consistent one with another, thus demonstrating that the work is soundly based. It is also considered that the research described in this, provides a rational basis for the understanding of air jet dryers. It is recommended that future drying research be carried out in close co-operation with industry.

REFERENCES

1. KEEY, R.B. Keynote Lecture. Ed. Mujumdar A.S. Proc. 1st Int. Symp. Drying. McGill University, 1978.

2. HARRISON, R.T.H. Advances in Printing Technology. Proc.I.Mech.E., 192,16, 1978.

3. SHERWOOD, T.K. The drying of solids - Parts I - VI. Ind. Eng. Chem., 21,12,1929.

4. BLACK, J. and HARDISTY, H. Heat and mass transfer in ink drying and infra-red dryness measurement. I.Mech.E. 6th Thermodynamics and Fluid Mechanics Convention, Durham, 1976.

5. HARDISTY, H. Evaporative ink drying using impinging air jets and infra-red dryness measurement. M.Sc. Thesis, University of Bath, 1977.

6. HARDISTY, H. Analysis of the constant-rate period of ink drying. J.Oil,Col.Chem,Assoc., 60,479,1977.

7. HARDISTY, H. The analysis of the drying process in thin films of ink. Proc.First International Symposium on Drying, Science Press, 1978. Princeton N.J.

8. HARDISTY, H. Drying printed ink coatings by impinging air jets. Advances in Drying.

9. VAN BRAKEL, J. Opinions about selection and design of dryers. Ed.Mujumdar A.S. Proc. 1st Int.Symp.Drying. McGill University 1978.

10. REAY, D. The place of theory and experiment in drying practice. Short Course on Industrial Drying. Dept. Chem.Eng., McGill University, 1978.

11. SHERWOOD, T.K. The curious history of the wet-bulb hygrometer, Chemistry in Canada, June 1950.

12. HOUGAN, O.A., McCAULEY, H.J. and MARSHALL, W.R.J.R. Limitations of diffusion equations in drying. Trans.Am.Inst.Chem.Eng.,36,183-206,1940.

13. LUIKOV, A.V. Heat and mass transfer in capillary-porous bodies. Pergamon, 1966.

14. HARDISTY, H. Industrial drying using imping air jets. Report No.226, School of Engineering, University of Bath, 1972.

15. BENNETT, G.W. and ANDREW WRIGHT, W. Evaporation behaviour of mixed lacquer solvents. Ind.Eng.Chem., 28,6,646,1936.

16. GRAF, E. Drying problems in rotogravure. Gravure, Nov.,Dec.,1969, Jan.,1970.

17. KRIZEK, F. and KORGER, I.M. Impinging flow drying of films. Chem. Proc.Eng, June 1967.

18. WILHOIT, D.L. Theory and practice of drying aqueous coatings with a high velocity air dryer. Tappi, 51, 1, Jan. 1968.

19. SCHEUTER, K.R. and DOSDOGRU, G.A. Factors influencing the physical drying of printing inks in drying systems. Advances in Printing Science & Technology. Vol.6. Ed.Banks W.H. Pergamon Press 1970.

20. SCHEUTER, K.R. and DOSDOGRU, G.A. Investigation of impinging air jet dryers with respect to possible automation. Proc., T.A.G.A., 1971.

21. TYRRELL, H.J.V. The origin and present status of Fick's Diffusion Law. J.Chem.Ed., 41,7,397,1964.

22. BIRD, R.B., STEWART, W.E. and LIGHTFOOT, E.N.
Transport Phenomena. Wiley, 1960.

23. PRESENT, R.D. Kinetic Theory of Gases.
McGraw-Hill, 1958.

24. FULLER, E.N., SCHETTLER, P.D. and GIDDINGS, J.C.
New method for prediction binary gas-phase diffusion coefficients. Ind.Eng.Chem. 58,5,1966.

25. SM2 Infragauge (Manufacturers Leaflet).
Infra Red Engineering, Galliford Road, The Causeway, Maldon, Essex.

26. REYNOLD, W.W. Physical Chemistry of Petroleum Solvents.
Reinhold, 1963.

27. GARDNER, G.S. Evaporate index. Ind.Eng.Chem, 32,2,226, 1940.

28. BELLMEIER, R.A. and RITTERHAUSEN, E.P.
Evaporation of petroleum thinners from protective coatings.
Official Digest, 26,283, 1954.

29. SHELL CHEMICALS. Relative evaporation rates of solvents employing the Shell Liquid Film Evaporometer
Technical Bulletin, ICS(X)/69/1.

30. TYSALL, L.A. A method of calculating composition changes of solvent mixtures during evaporation.
5th Fatipec Congress, 1959.

31. SHERWOOD, T.K. Mass, heat and momentum transfer between phases. C.E.P. Symp.Series, No.25,55,1959.

32. Von KARMAN, T. The analogy between fluid friction and heat transfer. Trans.Am.Soc.Mech.Engrs.,61,705, 1939.

33. LEWIS, J.S. A heat-mass transfer analogy and its application to finned surfaces. Ph.D. Thesis, University of Strathclyde, 1969.

34. COLBURN, A.P. A method of correlating forced convection heat transfer data and a comparison with fluid friction. Am.Inst.Chem.Eng. 29,174,1933.

35. CHILTON, T.H. and COLBURN, A.P. Mass transfer (absorption) coefficients. Ind.Eng.Chem.,26,11,1934.

36. GILLILAND. Diffusion coefficients in gaseous systems. Ind.Eng.Chem.,26,6,1934.

37. SHERWOOD, T.K. and PIGFORD, R.L. Absorption and Extraction. McGraw Hill, 2nd Edit., 1952.

38. BEDINGFIELD, C.H. and DREW, T.B. Analogy between heat transfer and mass transfer. Ind.Eng.Chem.,40,1164,1950.

39. WILKE, C.R. and WASSAN, D.T. A new correlation for the psychrometric ratio. A.I. Chem.Eng.Symp.Series,6,1965.

40. REID, R.C., PRAUSNITZ, J.M. and SHERWOOD, T.K. The Properties of Gases and Liquids. McGraw Hill, 3rd Edit., 1977.

41. CHATFIELD, H.W. The Science of Surface Coatings. Ernest Benn, 1962.

42. DURRANS, T.H. Solvents. Chapman and Hall, 1971.

43. COX, E.R. Pressure-Temperature chart for hydrocarbon vapours. Ind.Eng.Chem. 15,6,592, 1923.

44. HOVORKA, F., LANKELMA, H.P. and STANFORD, S.C. Thermodynamic properties of the hexyl alcohols. J.Am.Chem.Soc. 60,820,1938.

45. MONICK. Alcohols. Reinhold, 1968.

46. SHELL CHEMICAL CO. Technical Data Sheet.
Methyl Isobutyl Carbinol. SOL/TDS/13.

47. GARDON, R. A transducer for the measurement of heat flow rate. Trans ASME, J.Heat Transfer, 101, Feb.1966.

48. GARDON, R. and AKFIRAT, J.C.
Heat transfer characteristics of impinging two-dimensional airjets. Trans.ASME, J.Heat Transfer, 101,1966.

49. GODOY, R. and MILLER, I. Design and manufacture of a heat flux meter. University of Bath, School of Engineering, Report No. 463, Oct. 1978.

50. WHEELER, P.N.M. and MULERVY, K.F.
The temperature measurement of a thin plastic web pausing under a hot air jet. School of Engineering Report No. 465, University of Bath, 1979.

51. KEEY, R.B. Introduction to Industrial Drying Operations. Pergamon Press, 1978.

52. CRANK, J. and PARK, G.S. (eds). Diffusion in Polymers. Academic Press, 1968.

53. PARK, G.S. Transport in Polymer Films, Characterisation of Coatings, Part II. Ed Myers, R.R. and Long, J.S. Marcel Dekker, 1976.

54. ROGERS, C.E. Solubility and diffusivity.
Physics and Chemistry of the Organic State.
Vol.II, Ed.Fox,D,etal. Wiley, 1965.

55. NUNN, C.J. and NEWMAN, D.J. Solvent retention.
Studies in coatings based on single solvents and binary mixtures. XII Fatipec Congress, 1974.

56. HANSEN, C.M. The free volume interpretation of plasticizing effectiveness and the diffusion of solvents and plasticizers in high polymers. Official Digest, 37,57,1965.

57. HANSEN, C.M. A mathematical description of film drying by solvent evaporation. J. Oil. Col.Chem.Assoc,51,27,1968.

58. NUNN, C.J. and NEWMAN, D.J. Solvent release from coatings : evaporation and retention behaviour. Symposium : Advances in Chemistry, UMIST, 1974.

59. ATKINS, P.W. Physical Chemistry. Oxford University Press, 1978.

60. TYRRELL, H.J.V. Diffusion and Heat Flow in Liquids. Butterworths, 1961.

61. TREYBAL, R.E. Liquid Extraction. McGraw-Hill, 1963.

62. KISHIMOTO, A. Diffusion of vapours in organic coatings. Prog.Org.Coatings, I, 1972.

63. KUMINS, C.A. and KWEI, T.K. Diffusion in Polymers, Chapter 4. Academic Press, 1968.

64. FUJITA, H. Diffusion in polymer diluent systems. Advances in Polymer Science, Fortschritte Der Hocpolymeren Forschung, 3 Band 1 Heft, 1961.

65. DOOLITTLE, A.K. Studies in Newtonian flow II J.Appl. Phys,22,1471,1951.

66. COHEN, M.H. and TURNBULL, D. Molecular transport in liquids and gases. J.Chem. Phys 31,1164,1959.

67. RODRIGUEZ, F. Principles of Polymer Systems. McGraw-Hill, p45, 1970.

68. MACHIN, D. and ROGERS, C.E. Free volume theories for penetrant diffusion in polymers. Die Makromolekulare Chemie, 155,269,1972.

69. CRANK, J. The Mathematics of Diffusion. First Edition, Clarendon Press, Oxford, 1956.

70. NEWMAN, A.B. The drying of porous solids. Am.Inst.Chem.Eng., 27,203,1931.

71. GILLILAND, E.R. and SHERWOOD, T.K. The drying of solids VI. Ind.Eng.Chem.,25,10,1933.

72. BROUGHTON, D.B. The drying of solids. Ind.Eng.Chem., 1184,1945.

73. SMITH, G.D. Numerical Solution of Partial Differential Equations. Oxford, 1965.

74. CONTE, S.D. and de BOOR, C. Elementary Numerical Analysis. McGraw Hill, 1972.

75. SCHNEIDER, P.J. Conduction Heat Transfer. Addison-Wesley, 1955.

76. FISHER, E.A. Some moisture relations of colloids. Proc.Roy Soc (London). Series A, 103,A720, 1923.

77. TREYBAL, R.E. Mass Transfer Operations. McGraw Hill, 1968.

78. PERRY, R.H. and CHILTON, C.H. (eds) Chemical Engineers' Handbook, 20-13. Fifth Edition. McGraw Hill 1973.

79. KEEY, R.B. Process design of continuous drying equipment. A.I.Chem.E., Symposium Series, No.163,73, 1977.

80. Van MEEL, D.A. Adiabatic convection batch drying with recirculation of air. Chem.Eng.Sci, 9,36,1958.

81. KEEY, R.B. and SUZUKI, M. On the characteristic drying curve. Int.J.Heat Mass Transfer, 17,1455,1974.

APPENDIX 1 - METHOD OF CALIBRATING HEAT FLUXMETER

The paper by Gardon and Akfirat (A1.1) was the starting point for the writer's investigations into the heat transfer characteristics of impinging air jets. In Gardon's research, jets of air at ambient temperature impinged normally on an electrically heated plate. Quoting from this paper, "The plate was made of aluminium, a good thermal conductor, in order to suppress lateral temperature differences in it... Thus, steady-state convective heat transfer was obtained between an isothermal hot surface and jets of cooling air". A plot of local heat transfer coefficient (h_x) versus lateral position was recorded by traversing the fluxmeter under the flow field of the jet.

In the writer's research, and using an aluminium plate of approximately the same thickness as Gardon's, great difficulty was found in maintaining the electrically heated surface at constant temperature during the traverse. The temperature variations (±5 C) arise, because the position of the stagnation point, which is a zone of relatively low temperature, is moved across the plate by the traverse. Although this effect is probably averaged out during the traverse, because of the need for accuracy when calibrating the Medtherm probe, it was decided to remove this source of doubt.

To achieve an isothermal surface, it was decided to heat the aluminium plate from below with saturated steam at approximately atmospheric pressure. Of course this change necessitated the design and construction of a new heat transfer apparatus, which is shown diagrammatically in Figure A1. Steam is supplied from a small laboratory boiler to an inner steam chamber, the horizontal upper surface of which forms the impingement surface. The jet of relatively cold air blowing onto the impingement surface causes steam to condense. In the

steady state, the rate at which heat is transferred to the air can be calculated from an energy balance, if the rate at which condensate flows from the steam chamber is measured. The temperature of the heated plate may be taken to be equal to the saturation temperature corresponding to the barometric pressure. The value of the average heat transfer coefficient $\bar{h}$ may be calculated from the equation

$$Q = W\, h_{fg} = \bar{h}\, A_s\, (T_s - T_A) + \text{losses}$$

W = condensate flow rate, kg/s

h_{fg} = enthalpy of evaporation, J/kg

A_s = area of upper surface of cavity, m^2

T_s = surface temperature

T_A = air temperature

$$\bar{h} = \frac{W\, h_{fg}}{A_s\, (T_s - T_A)}$$

To increase the accuracy of the calibration, heat losses from all surfaces of the inner steam chamber except the upper, must be made as small as practically possible. To attain this aim, the sides and bottom of the inner chamber were enclosed by a steam jacket. Steam to this jacket was also supplied by the laboratory boiler. This jacket effectively prevents heat transfer, because the temperature difference causing it, is reduced to zero. As an additional safeguard, the lower surfaces of the inner chamber were covered with thermal insulation. By these means, heat loss from the inner chamber was reduced to a negligible figure.

When operating the steam heated plate, care is required on the following points:-

1) Water carry-over from the laboratory boiler must be avoided. To prevent this a small water separator is required.

2) Air will collect in the steam chamber and tend to blanket the lower side of the heat transfer surface. This may be removed if the chamber is periodically vented to atmosphere.

3) To prevent steam escaping with the condensate, a water lock is required in the condensate outlet pipe. The adjustment of the height of this S-bend requires care to produce a steady-condensate flow rate.

The flux meter to be calibrated is screwed from below, up into the boss provided in the centre of the heated plate. To carry out a calibration, steam is turned on to both inner and outer chambers and the apparatus is allowed to attain a steady temperature. With the flux meter output connected to the Y terminal of an XY plotter, a plot of h_x is then obtained by traversing the plate under the jet.

Typical Results From a Calibration Test

Test Conditions

Nozzle width, B = 3.175 mm

Nozzle to plate distance, Z/B = 8

Reynolds number, Re = 11,000

Air temperature, T_A = 28.5 C

Plate temperature, T_S = 100.0 C $\quad \theta = (T_S - T_A) = 71.5$ C

Heat transfer surface, A_s = 85.73 mm x 161.9 mm = 0.01388 m^2

Condensate

Flow rate W

10 cc in 1 minute 37.5 sec. (Two measurements identical)

$W = 1.026.10^{-4}$ kg/s

Enthalpy of evaporation (from tables at 1 bar) $h_{fg} = 2.258.10^{6}$ J/kg

$Q = W\ h_{fg} = 2.258.10^{6}.1.026.10^{-4} = 231.67$ W

Heat Transfer

$$\bar{h} = \frac{W\ h_{fg}}{A_s\ \theta} = \frac{231.67}{0.01388.71.5} = \underline{233.44\ W/m^2\ K}$$

The heat flux distribution obtained from the Gardon Probe is shown in Figure A2.2. The ratio of $h_o/\bar{h}$ used below is taken from that Figure.

$$h \text{ at stagnation point, } h_o = 233.44\ \frac{h_o}{\bar{h}} = 233.44\ \frac{8.9}{4.122} = 504\ W/m^2\ K$$

Comparative Checks

a) With Gardon's Figure 2, reference (A1.1)

$$\text{Nusselt number at stagnation point, } Nu_o = \frac{h_o B}{k} = 59$$

$$h_o = \frac{Nu_o\ k}{B} = \frac{59\ .\ 0.026}{0.003175} = \underline{483\ W/m^2\ C}$$

It can be seen that the value of the stagnation point heat transfer coefficient, h_o, determined using the steam heated plate, agrees, within acceptable experimental error, with Gardon's data.

Flux meter Calibration (Medtherm probe)

At stagnation point

Probe output (from Figure, A2.2) e = 2.86 mV

Heat flux, $q = h_o \theta = 504 \cdot 71.5 = 36{,}036 \text{ W/m}^2$

Probe calibration, $K = \frac{36{,}036}{2.86} = \underline{12{,}600 \text{ W/m}^2 \text{ mV}}$

This value of K is 1.99 times larger than the value given in the Medtherm test certificate, see equation 6.3.3.

References

A1.1 Gardon, R. and Akfirat, J.C., Trans ASME, J. Heat Transfer, 101, 1966.

FIGURE A1-1

STEAM HEATED PLATE

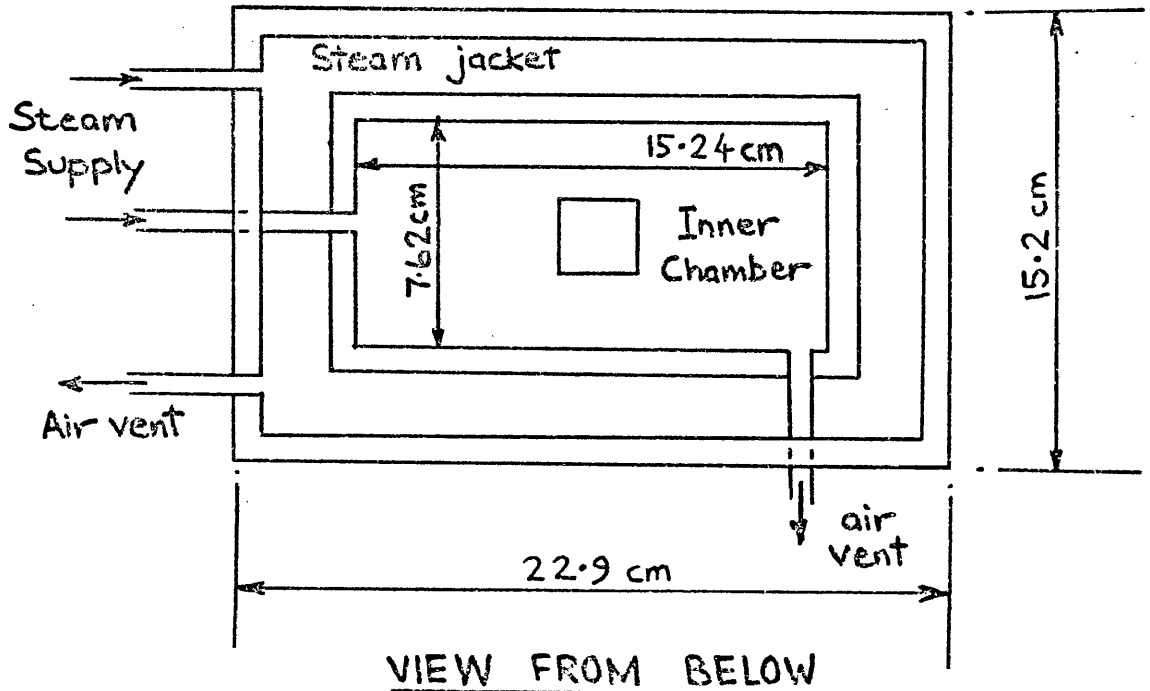

VIEW FROM BELOW

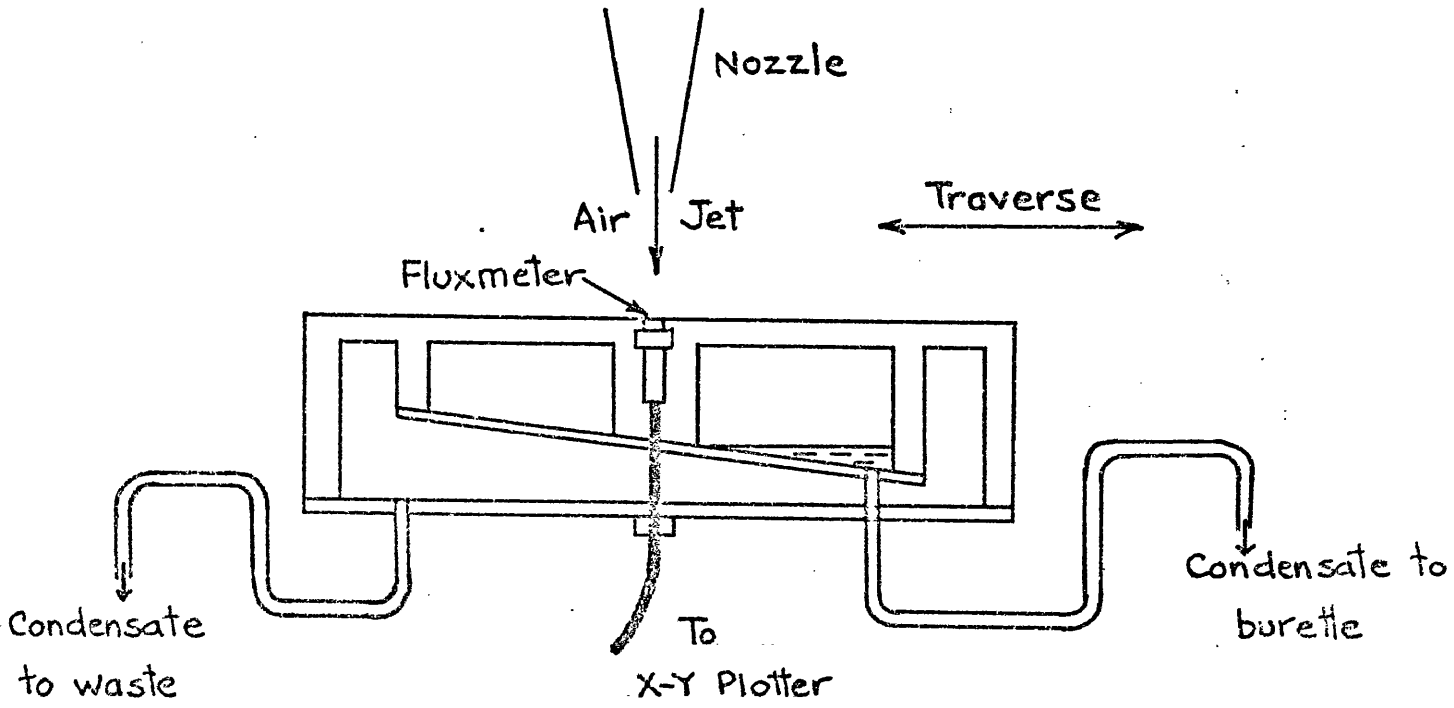

SIDE ELEVATION

FIGURE A1-2

FLUXMETER CALIBRATION IN STEAM HEATED PLATE

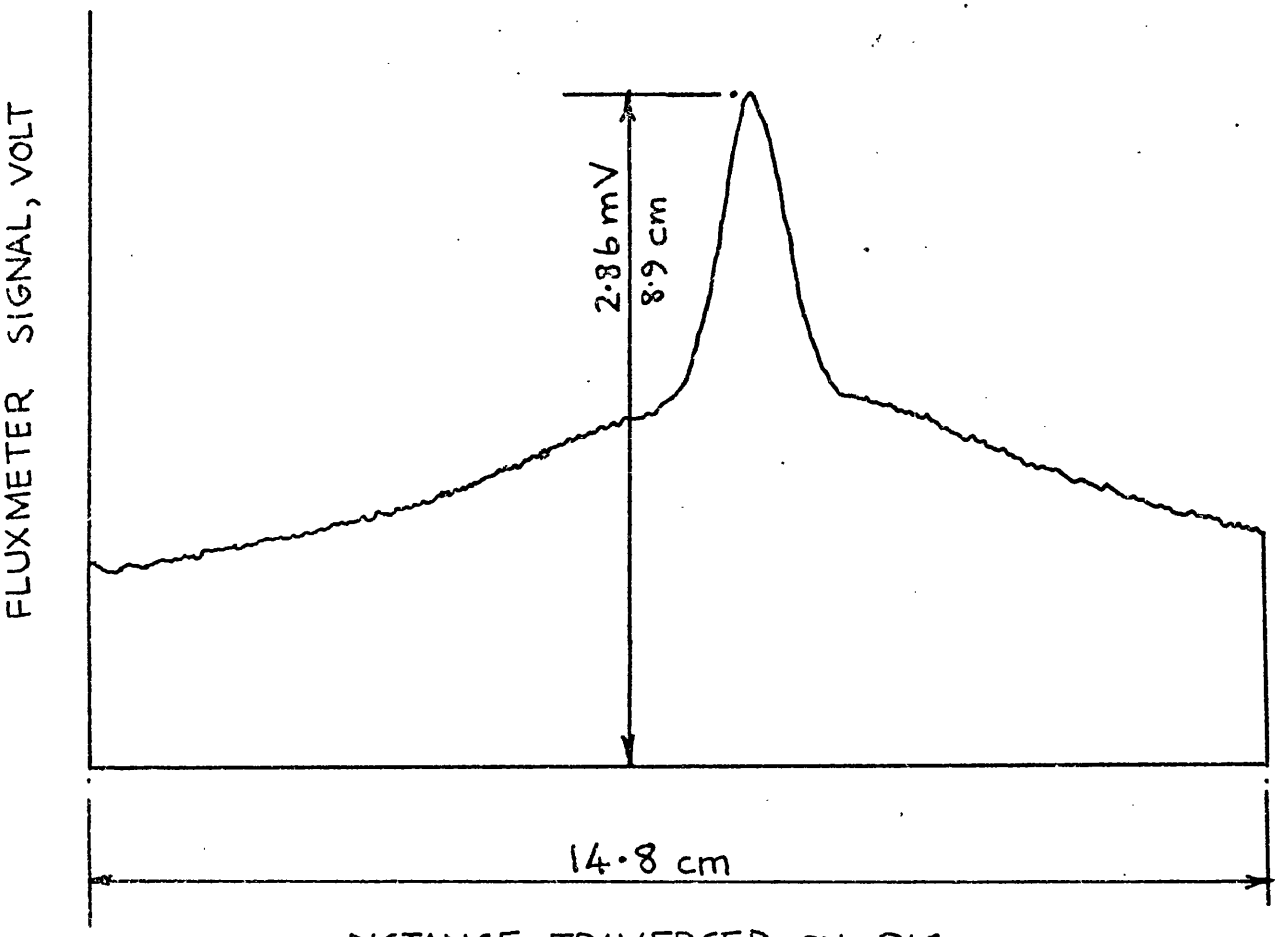

AVERAGE AREA (BY PLANIMETER) $= \frac{28.4}{3} = 9.47\ in^2 = 61.1\ cm^2$

AVERAGE HEIGHT OF GRAPH $= \frac{61.1}{14.8} = 4.12\ cm$

FROM GRAPH $\frac{h_o}{\bar{h}} = \frac{8.9}{4.12}$

APPENDIX 2 - SOLUBILITY IN CONSTANT-RATE INK DRYING

Solubility of a resin in a solvent

A resin is dissolved in a solvent to produce a solution whose viscosity is sufficiently low to allow it to be printed. According to Billmeyer (A2.1)* "Dissolving a polymer is a slow process occurring in two stages. First, the solvent is slowly imbibed into the polymer to produce a swollen gel. In the second stage, the gel gradually disintegrates into a true solution..... Solubility relations in polymer systems are more complex than those among low molecular-weight compounds".

Ideal solutions may be defined as those which obey Raoult's Law

$$\frac{p_1}{p_{o1}} = x_1 \qquad \text{A1.1}$$

p_1 = partial vapour pressure of solvent above solution

p_{o1} = saturated vapour pressure of pure solvent

x_1 = mole fraction of solvent

Unless they are extremely dilute, few solutions behave ideally, but the form of Raoult's Law may be retained

$$\frac{p_1}{p_{o1}} = a_1 = \gamma_1 x_1 \qquad \text{A1.2}$$

a_1 = activity

γ_1 = activity coefficient

* References appear at end of Appendix.

It was pointed out in section 6.6 that experimental drying curves appear to indicate that the partial pressure of the solvent vapour remains roughly constant during the early stages of evaporation. Since during this period the mole fraction of solvent, x_1, is decreasing, such behaviour is not consistent with equation A1.1. There appear to be two possible explanations:-

1) The ink, a mixture of resin and solvent, may not behave as an ideal solution. This is not surprising in view of the complex nature of the resin molecule. However in addition to any non-ideal behaviour, it is even possible that the resin is not completely dissolved. In this case, the polymer might exist as isolated particles of swollen get suspended in a liquid which is essentially pure solvent. In view of the difficulties inherent in dissolving high polymers, this hypothesis appeared to be a plausible one and accordingly it was referred to the technical department of the resin manufacturer. Their opinion was that the resin and solvent should form a true solution.

2) The mole fraction of the solvent remains approximately constant. That this does happen, in spite of significant variations in the mass fraction of the solvent, can be seen from a simple calculation set out in the table below.

Solvent Evaporated %	Mass Fraction		Moles		Mole Fraction	
	Solvent	Resin	Solvent	Resin	Solvent	Resin
0	0.80	0.20	0.00748	0.0001	0.987	0.013
25	0.75	0.25	0.00701	0.00013	0.982	0.018
50	0.67	0.33	0.00626	0.00017	0.973	0.027
75	0.50	0.50	0.00467	0.00025	0.967	0.033

Molecular weight of solvent = 107

Assume, molecular weight of polymer = 2,000

Although, to the writer, both of the above suggestions appear to offer reasonable explanations of the linear nature of the drying curves, further research is necessary before the problem can be considered to be resolved. Unfortunately, the resources necessary to devote to it have not been available. Finally, it may be noted, that other research into this topic, such as Reynolds (A2.2) and by the Shell Company (A2.3) has also shown that, in the constant-rate period, resins have virtually no effect on the solvent evaporation rate.

Solvent blends

In practice "inks" and surface coatings are formulated from a blend of solvents. The solvents are selected for their ability to dissolve the resin(s) and, by virtue of their evaporative characteristics, to produce a coating with the required physical and aesthetic properties. The rate at which individual solvents evaporate from the blend during the drying process is of significance to the ink-maker. The preferential evaporation of one solvent may upset the "solubility balance" and cause non-uniform precipitation and other undesirable effects. It is also of significance that those solvents which remain behind during the early stages of drying, may well be the solvents which give rise to retention problems in the later falling-rate period of drying.

Equations can be developed, Sarnotsky (A2.4), for the rate at which a single component evaporates from a blend, if the following assumption is made. The evaporation rate of each component in a mixture is a product of the evaporation rate of the pure component and its relative concentration. Of course the total evaporation rate is the sum of the contributions of the individual components.

In an extremely useful publication (A2.5), The Shell Company, draw attention to the marked deviations from Raoult's Law exhibited by solvent mixtures in practice. Industrial solvents are sub-divided into three characteristic groups in terms of their non-ideal behaviour in solution. Empirical graphs of activity coefficient are presented for each of the three characteristic solvents groups. This data, together with the assumptions of the previous paragraphs and the "Relative Evaporation Rate" of individual solvents from the Shell Thin Film Evaporometer allows the progressive evaporation of a solvent blend to be calculated. Because the relative concentrations of components continuously change as evaporation procedes a step-by-step calculation is required. It is apparent that the calculation method could be readily programmed for computer solution.

References

A2.1 Billmeyer, F.W., Textbook of Polymer Science, Wiley, 1962.

A2.2 Reynold, W.W., Physical Chemistry of Petroleum Solvents, Reinhold, 1963.

A2.3 Shell Chemicals, Technical Bulletin, ICS(X)/69/1.

A3.4 Sarnotsky, A.A., Evaporation of solvents from paint films, J. Paint Technology, 41,539,692, 1969.

A4.5 Shell Chemicals, Technical Bulletin, ICS(X)/70/15.

APPENDIX 3 - LISTING OF COMPUTER PROGRAM FOR EXTERNALLY CONTROLLED DRYING

Note: The flow chart for this program appears as Figure 6.8.

Meaning of Symbols in Program

The following endings to symbols denote

p - plastic vap - vapour

pig - pigment

sol - solvent

al, a2 etc	dummy variables for calculation	
alpha	thermal diffusivity, = $k/\rho C_p$	
b	width of slot nozzle	m
Cp	specific heat	
d	diffusion coefficient, solvent in air	m^2/s
denair	density of air	kg/m^3
delt 1	wet bulb depression	K
d mass	change in solvent mass	kg
d time	length of time step	s
d temp	change in temperature	K
frasol	fraction solvent in ink	
ho	heat transfer coefficient at stagnation point	w/m^2 K
hx	heat transfer coefficient at distance x from stagnation point	w/m^2 K
hxovho	hx/ho	

hdovrh	psychrometric ratio	
h_{fg}	latent heat vapourisation of solvent	J/Kg
kon	thermal conductivity air	w/m K
mdotd	mass transfer flux	kg/m^2
mdoth	mass transfer flux	kg/m^2
m	mass	kg
ms	molecular weight solvent	
msoli	mass of initial solvent deposit	kg/m^2
nuo	Nusselt no. at stagnation point (hB/k)	
pvapb	saturated vapour pressure solvent	bar
pbbar	log mean pressure of air in boundary layer (see equn 6.4.5)	
qdot	heat transfer flux	w/m^2
qd	energy equivalent of mass transfer	J
qh	heat transfer during time step	J
qsol2	energy to evaporate solvent in the constant-rate period	J
ree	Reynolds number at nozzle exit $(\frac{V_E b \rho}{\mu})$	
sg	specific gravity	
ta	air temperature	C
tl	initial drying time (see equn 6.7.6)	s
t2	constant rate drying time (see equn 6.7.9)	s

ttotal	$t_1 + t_2$ (see equn 6.7.10)	s
ts	ink surface temperature	C
ve	air velocity at nozzle exit	m/s
vis	viscosity of air	kg/m s

```
c
c  predict time of externally controlled drying
c
c  constant rate drying calculation  --12 march 1976
c   crdry0  dec 1979
c
      real ma,konc1,konc2,kon,ms,nuo,mdot,massi,massc,mdoth,mdotd ,
     &minki,mplast,msoli,msol,mp,mcpp,mcpsol,mcp,mpig,mcppig
c
c     properties of dry air
c
      ma = 28.96
      ra = 287.1
      tamb = 15.0+273.0
c
c   si  units  j and  watts  used
c
      cpc1 = 1004.9
      cpc2 = 0.086
      visc1 = 0.1846 e -4
      visc2 = 0.44   e -7
      konc1 = 0.02624
      konc2 = 0.741 e-4
c
c     properties of solvent  mibc
c
          c = 6.0
          h = 14.0
          o = 1.0
          sgsol = 0.808
          cpsol = 2730.0
          hfg = 428000.0
c
c  coating params
      frasol = 77.0
          thki = 11.3
      frasol = frasol/100.0
c
c
          frapig = 1.0-frasol
c
c
          msoli = thki*1.0 e-6*1.0 e+3*frasol*sgsol
c   pig means (pig+resin)
          sgpig = 1.1
          cppig = cpsol
          mpig = thki*1.0 e-6*1.0 e+3*frapig*sgpig
          mcppig = mpig*cppig
c
      thkp = 25.0
      sgp = 0.92
      cpp = 2350.0
c
          mp = thkp*1.0 e-6*1.0 e+3*sgp
          mcpp = mp*cpp
c
c     airjet parameters
c
      b=0.00318
      zoverb = 8.0
c
      write(0,3)
    3 format(1h1,5x,'constant rate drying',5x,'thk=11.3')
```

constants for polynomials for air properties

chemical formula of solvent

specifying ink thickness

calculating mass and c_p

```
c
      do 9 ita = 20,100,10
      ta = ita
      ta = ta+273.0
c
c
      write (0,4)
    4 format(1h0,7x,'air vel',3x,'air temp',2x,'surf temp',1x,
     &'hx',8x,'qdot',6x,'hdx',7x,'mdotd',5x,'mdoth',5x,'d',9x,'t1',8x,
     &'t2',8x,'total')
c
          do 10 ive = 10,60,10
          ve = ive
c
          msol = msoli
          time = 0.0
          dtime = 0.46-(0.006*ve)
          ts = tamb
c
c
    1 continue
c
      tf =(ta + ts)/ 2.0
c
c     vapour properties
      rmol = 8314.3
      ms = 12.0 * c +1.0 * h + 16.0 * o
      rvap = rmol / ms
          pvap = exp(27.996-(6544.0/ts))
      denvap = pvap /(rvap * ts)
c
c
c     diffusion  coefficient
c
c
      a1 =(1.0/ma + 1.0/ms) * * 0.5
      a2 = 0.001 * (tf * * 1.75) * a1
      sigmav = 16.5 *c + 1.98 * h + 5.48 * o
      a3 = 20.1 ** 0.333 + sigmav ** 0.333
      a3 = a3 ** 2.0
      d =  a2/a3
      d = d* 1.0 e-4
c
c     transport properties of air
c
      cp = cpc1 + cpc2 *(tf - 300.0)
      vis = visc1 + visc2*(tf - 300.0)
      kon= konc1 + konc2*(tf - 300.0)
      denair = (1.013 e+5 - pvap)/(ra*tf)
      alpha = kon / (denair * cp  )
      pvapb = pvap/1.013 e+5
      a1 = 1.0/(1.0-pvapb)
      pbbar = pvapb/alog(a1)
      pratio = 1.0/pbbar
c
c     wet bulb  temp ts
c
      a1 = (d /alpha) ** 0.666
      a2 = 1.0/(denair * cp)
      hdovrh =  a2*a1
      hdovrh = hdovrh * pratio
c
```

do loop on air temperature

do loop on air velocity

adjusting time interval

air "film" temperature

solvent vapour in air

see ref (24).

```
c     evaluation of ho
c
      ree = (ve * b * denair)/ vis
      a1 = (1.0/zoverb) ** 0.62
c
          nuo = 1.2*(ree**0.58)*a1
      ho  = kon * nuo / b
c
c  h at ir spot
          hxovho = 0.2
      hx = ho*hxovho
c
c  pure solvent dries 30% faster than ink
          hx = hx/1.3
c
c     transfer rates
      qdot = hx * (ta-ts)
          qh = qdot*dtime
c
c   mass transfer
          hdx = hx*hdovrh
          mdotd = hdx*denvap
          dmass = mdotd*dtime
          qd = dmass*hfg
c
          mcpsol = msol*cpsol
          mcp = mcppig+mcpp+mcpsol
c    temp change
c
          dtemp = (qh-qd)/mcp
c
          ts2 = ts+dtemp
          msol = msol-dmass
          time = time+dtime
          err = abs(ts2-ts)
          ts = ts2
c
          if(err.lt.0.1)  go  to  2
          go to 1
c
     2    continue
          t1 = time
c
          delt1 = hdovrh*denvap*hfg
          delt2 = ta-ts
          ts = ta-delt1
          qsol2 = msol*hfg
          qdot2 = hx*delt1
       mdoth = qdot2/hfg
       t2 = qsol2/qdot2
       ttotal = t1+t2
       ta = ta-273.0
       ts = ts-273.0
c
       write(0,5)ve,ta,ts,hx,qdot,hdx,mdotd,mdoth,d,t1,t2,ttotal
     5 format(1h , 5f 10.1, 3f 10.5, 1f 10.8, 3f 10.1)
       ta = ta+273.0
c
       ts = ts+273.0
c
    10 continue
c
c
     9 continue
c
       stop
```

air Reynolds no

heat transfer coefficient

δT by energy ballance

has initial transient ceased?

constant rate drying

drying times

output

APPENDIX 4 - LISTING OF A COMPUTER PROGRAM TO CAICULATE THE CUMULATIVE DRYING EFFECT OF A SINGLE NOZZLE

Note

1) This program was derived from the program listed in Appendix 3.

2) The structure of the program and the meaning of the symbols, are similar to that of Appendix 3.

Cumulative Drying Effect of a Single Nozzle

derived from program in Appendix 3

```
c
c  constant rate drying calculation  --12 march 1976
c  intdry  25 sept 79
c
c
c
      real ma,konc1,konc2,kon,ms,nuo,mdot,massi,massc,mdoth,mdotd ,
     &minki,mplast,msoli,msol,mp,mcpp,mcpsol,mcp,mpig,mcppig
c
c     properties of dry air
c
      ma = 28.96
      ra = 287.1
      tamb = 15.0
c
c   si  units  j and  watts  used
c
      cpc1 = 1004.9
      cpc2 = 0.086
      visc1 = 0.1846 e -4
      visc2 = 0.44   e -7
      konc1 = 0.02624
      konc2 = 0.741 e-4
c
c     properties of solvent  n propanol
c
         c = 6.0
         h = 14.0
         o = 1.0
         sgsol = 0.808
         cpsol = 2730.0
         hfg = 428000.0
c
c  coating params
         thki = 6.6                                  Specifying ink thickness
      frasol = 77.0
      frasol = frasol/100.0
c
c
         frapig = 1.0-frasol
c
         msoli = thki*1.0 e-6*1.0e+3*frasol*sgsol    masses and spec heats
c
         sgpig = 1.1
         cppig = cpsol
         mpig = thki*1.0 e-6*1.0 e+3*frapig*sgpig
         mcppig = mpig*cppig
c
      thkp = 25.0
      sgp = 0.92
      cpp = 2350.0
c
         mp = thkp*1.0 e-6*1.0 e+3*sgp
         mcpp = mp*cpp
c
c     airjet parameters
c
      b=0.00318
      zoverb = 8.0
c
      write(0,3)
    3 format(1h1,5x,'cumulative drying effect',5x,'thk=6.6')
```

```
c
      do 9 ita = 20,70,10
      ta = ita
      tai = ta
c
      write (0,4)
    4 format(1h0,7x,'air vel',3x,'air temp',2x,'surf temp',1x,
     &'hx',8x,'qdot',6x,'hdx',7x,'mdotd',5x,'frac1',5x,'t1',9x,'t2a',8x,
     &'t2',8x,'total')
          do 10 ive = 10,60,10
          ve = ive
c
c  calk of time step
                      time = 0.0
                      xtot = 0.2
                      spaces = 10.0
                      dx = xtot/spaces
                      wspeed = 0.3
                      dtime = dx/wspeed
          xt = xtot+(dx/10.0)
                      msol = msoli
                      ts = tamb
 c
     1 continue
c
      tf =(ta + ts)/ 2.0
c
c     vapour properties
      rmol = 8314.3
      ms = 12.0 * c +1.0 * h + 16.0 * o
      rvap = rmol / ms
          pvap = exp(27.996-6544/(ts+273))
      denvap = pvap/(rvap*(ts+273))
c     diffusion  coefficient
      a1 =(1.0/ma + 1.0/ms) * * 0.5
      a2 = 0.001 * ((tf+273) * * 1.75) * a1
      sigmav = 16.5 *c + 1.98 * h + 5.48 * o
      a3 = 20.1 ** 0.333 + sigmav ** 0.333
      a3 = a3 ** 2.0
      d =  a2/a3
      d = d* 1.0 e-4
c
c     transport properties of air
c
      cp = cpc1 + cpc2 *tf
      vis = visc1 + visc2*tf
      kon= konc1 + konc2*tf
      denair = (1.013 e+5 - pvap)/(ra*(tf+273))
      alpha = kon / (denair * cp  )
      pvapb = pvap/1.013 e+5
      a1 = 1.0/(1.0-pvapb)
      pbbar = pvapb/alog(a1)
      pratio = 1.0/pbbar
c
c     wet bulb  temp ts
c
      a1 = (d /alpha) ** 0.666
      a2 = 1.0/(denair * cp)
      hdovrh =  a2*a1
      hdovrh = hdovrh * pratio
c
c     evaluation of ho
c
      ree = (ve * b * denair)/ vis
      a1 = (1.0/zoverb) ** 0.62
      nuo = 1.2*(ree**0.58)*a1
      ho  = kon * nuo / b
```

do loop on air temperature

do loop on air velocity

```
c
          x = time*wspeed
          if(x.lt.xt)  go  to  66
          dtime = 0.46-(0.006*ve)
          go to 64
c
66        continue
c
c  hxovho  ta  change  with  x
c
          if(x.gt.0.0875)  go  to  61
          hxovho=0.2 +4.857*x
          go  to  60
61        if(x.gt.0.1)  go  to  62
          hxovho=0.625+(30.0*(x-0.0875))
          go  to  60
62        if(x.gt.0.1125) go  to  63
          hxovho=1.0-(30.0*(x-0.1))
          go  to  60
63        if(x.gt.xt) go  to  60
          hxovho=0.625-(4.875*(x-0.1125))
c
60        continue
c
          if(x.gt.0.1)  go  to  65
          ta = tai*(1.0+5.0*x)
          go  to  64
c
65        continue
          ta = 2.0*tai-(5.0*x*tai)
c
c
          t1 = time
          frac1 = (msoli-msol)/msoli
64        continue
c  h at ir spot
      hx = ho*hxovho
c
c  pure solvent dries 30% faster than ink
          hx = hx/1.3
```

distance moved

heat transfer coefficient changes with x

air temperature changes with x

```
c
c     transfer rates
      qdot = hx * (ta-ts)
          qh = qdot*dtime
c
c   mass transfer
          hdx = hx*hdovrh
          mdotd = hdx*denvap
          dmass = mdotd*dtime
          qd = dmass*hfg
c
          mcpsol = msol*cpsol
          mcp = mcppig+mcpp+mcpsol
c   temp change
c
          dtemp = (qh-qd)/mcp
c
c
          fracs = (msoli-msol)/msoli
          ttotal = time-t1
          if(fracs.gt.0.999)  go  to  8
          ts2 = ts+dtemp
          msol = msol-dmass
          time = time+dtime
          err = abs(ts2-ts)
          ts = ts2
          if(x.lt.xt) go to 1
c
          if(time.lt.t1)  go  to  1
c
          if(err.lt.0.1)  go  to  2
          go  to 1
c
     2    continue
c
          delt1 = hdovrh*denvap*hfg
          delt2 = ta-ts
          ts = ta-delt1
          qsol2 = msol*hfg
          qdot2 = hx*delt1
      mdoth = qdot2/hfg
          t2 = qsol2/qdot2
c
          go to 11
   8      continue
          t2 = 0
  11      continue
          t2a = time-t1
          ttotal = t2+t2a
c
c
      write(0,5)ve,ta,ts,hx,qdot,hdx,mdotd,frac1,t1,t2a,t2,ttotal
   5      format(1h ,5f 10.1,2f 10.5,1f 10.3,4f 10.2)
c
c
c
  10 continue
c
c
     9 continue
c
      stop
          end
```

energy balance to determine transient temperature change

is transit distance complete?

is transient complete?

constant rate drying

drying times

output

APPENDIX 5 - EARLY LISTING OF COMPUTER PROGRAM TO SOLVE DIFFUSION EQUATION

Note

1) The flow chart for this program appears as Figure 10.1.

2) Comments on program operation appear on the later version listed in Appendix 6.

3) The meaning of the symbols used in the program are listed in Appendix 6.

```
      C SOLVES DIMENSIONLESS DIFFUSION EQUATION (CRANK P208)
      C USES EXPONENTIAL D ,  D1 = DO EXP(KC)
      C THE ABOVE IS TERMED  THE CSIMPLE CASE C
      C
 1          REAL K
 2          DIMENSION D(10),DP(10),DG(10),S(10),SP(10),SG(10),X(10),C(10),
           1  ERROR(10)
      C
      C
      C
      C       SPECIFYING FD PARAMETERS
      C
 3          INTSX=8
 4          FO=1.0
 5          BI=1.0 E+4
 6          PARAM1=0.5
 7          TOL=0.1
      C
      C   SPECIFYING DIFFUSION COEFFICIENT
      C
 8          DC1=1.0 E+6
 9          K=ALOG(DC1)
10          EK=EXP(K)
11          EK1=EK-1
      C
      C   INITIAL    CONDITIONS
      C
12          J=0
13          T=0.0
14          CI=0.75
15          L=INTSX+1
16          L1=L+1
17          XINTS=INTSX
18          DELX=1/XINTS
      C
19          X(1)=0.0
20          DO 1 I=2,L
21        1 X(I)=X(I-1)+DELX
      C
22          DI=EXP(K*CI)
23          SI=(DI-1)/EK1
24          DO 2 I=1,L1
25          D(I)=DI
26        2 S(I)=SI
27          WRITE(6,101)DI,SI
28      101 FORMAT(1H1,5X,2E15.6)
      C
29          WRITE(6,3)
30        3 FORMAT(1H0,5X,'X=0',8X,'X=0.125',8X,'X=0.25',8X,'X=0.375',8X,
           1              'X=0.5',8X,'X=0.625',8X,'X=0.75',8X,'X=0.865',8X,
           2              'X=1.0')
      C
      C   FIRST GUESS AT D AND S FOR ITERATIVE SOLN OF FIN DIFF EQUATNS
31        4 DO 5 I=1,L
32          DG(I)=D(I)
33        5 SG(I)=S(I)
34          DG(L+1)=D(L-1)
35          SG(L+1)=S(L-1)
36          DLLT=FO*(DELX**2)/D(L)
37          ITER=0
      C
      C   FINITE DIFFERENCE EQUATIONS
      C
```

```
C
C  FINITE DIFFERENCE EQUATIONS
C
C
C     CONVECTIVE BOUNDARY   I=1
C
C
      6 A=ALOG((S(1)*EK1)+1)
        IF(J.GT.0) GO TO 22
        A=0.0
     22 CONTINUE
        PRINT,A
        SO=S(2)-(BI*2*DELX*A)/EK1
        PRINT,SO
C
        A1=ALOG((SG(1)*EK1)+1)
        PRINT,A1
        SPO=SG(2)-(BI*2*DELX*A1)/EK1
        PRINT,SPO
C
        A=S(2)-2*S(1)+SO
        PRINT,A
        A1=SG(2)-2*SG(1)+SPO
        PRINT,A1
        A2=DELT/(4*(DELX**2))
        PRINT,A2
C
        SP(1)= S(1)+A2 *(DG(1)+D(1)) *(A1+A)
        PRINT,SP(1)
C
C
C     GENERAL INTERNAL POINT
        DO 7 I= 2,L
        A=DELT/(4 * (DELX ** 2))
        PRINT,A
        A=A * (DG (I)+ D(I))
        PRINT,A
        A1= SG(I+1) - 2 *SG(I)+ SG(I-1)
        PRINT,A1
        A1= A1 + S(I+1) -2* S(I)+ S(I-1)
        PRINT,A1
        SP(I)=S(I)+(A*A1)
        PRINT,SP(I)
      7 CONTINUE
C
C     SUBSTRATE BOUNDARY
        SP(L+1)=SP(L-1)
C
C
C     FINDING  LARGEST ERROR
C  ALSO  BETTER  GUESS  FOR  SGS
        ERROR(1)= SG(1)- SP(1)
        SG(1)=SP(1) +PARAM1 *ERROR(1)
        ERROR(1)=ERROR(1)/SP(9)
        ERROR1=ABS(ERROR(1))
        DO 8 I= 2,L
        ERROR(I)=SG(I) -SP(I)
        SG(I)=SP(I) +PARAM1 *ERROR(I)
        ERROR(I)=ERROR(I)/SP(9)
        ERROR2=ABS(ERROR(I))
        IF (ERROR1.GT.ERROR2) GO TO 8
        ERROR1 =ERROR2
      8 CONTINUE
C
C
```

```
82          IF (ERROR1.LT.TOL) GO TO 11
      C
      C  CALC  OF  NEW  DGS
83          DO 9 I =1,L
84          DG(I)=(SG(I) * EK1)+1
85          PRINT,SG(I),ERROR(I)
      C
86        9 CONTINUE
87          SG(L+1)=SG(L-1)
88          DG(L+1)=DG(L-1)
89          ITER=ITER+1
90          WRITE(6,102)ITER
91      102 FORMAT(1H1,5X,'ITER= ',I3)
92          GO TO 6
      C
      C     RECOVERING CONCENTRATIONS
93       11 CBAR=0.0
94          DO 12 I = 1,L
95          D(I)=(S(I)*EK1)+1
96          C(I)=ALOG(D(I))/K
97       12 CBAR=CBAR+C(I)
98          RL=L
99          CBAR = CBAR/RL
      C
100         WRITE(6,15)J,T
101      15 FORMAT(1H1,5X,'J= ',I4,5X,'T= ',F14.8)
      C
102         WRITE(6,16) ( D(I) , I=1,L)
103      16 FORMAT(1H0,9 E 14.6)
      C
104         WRITE(6,17) (S(I)  ,I=1,L)
105      17 FORMAT(1H0,9 E 14.6)
      C
106         WRITE(6,18) (C(I) ,I=1,L)
107      18 FORMAT(1H0, 9 F 14.5)
      C
108         T=T+DELT
109         J=J+1
110         DO 20  I=1,L
111         DP(I)=(SP(I)*EK1)+1
112         S(I)=SP(I)
113      20 D(I)=DP(I)
      C
114         IF(J.GT.100) GO TO 21
115         GO TO 4
116      21 STOP
117         END

      $ENTRY
```

APPENDIX 6 - LATEST LISTING OF COMPUTER PROGRAM TO SOLVE DIFFUSION EQUATION

Note

1) The flow chart for this program appears as Figure 10.1.

2) Comments on program operation appear on the listing.

Meaning of symbols used in the program

al, a2 etc	Dummy variables used for calculating
bi	Biot number (Bi_2)
c(i)	Concentration at grid point i, j
cp(i)	Concentration at grid point i, j + 1
cbar	Mean concentration
cdcrit	D_c^*
ci	Initial concentration
cscrit	Surface concentration at critical point
cr	Constant rate surface condition
d(i)	D* at grid point i, j
dp(i)	D* at grid point i, j + 1
dg(i)	Guessed value of dp(i)
di	Initial value of D*
dcl	D* when C = 1 (D_1^*)
dcdt	Drying rate
deld(i)	Change in D*
delc(i)	Change in C
dels(i)	Change in S

dscrit	D* corresponding to cscrit
delx	X interval
delt	T interval
ek	exp (k)
ekl	(ek - 1)
error(i)	Error in guessed value of s(i)
fo	Fourier number
intsx	Number of X intervals
icrit	An index, either 1 or 2. Selects either constant-rate or falling-rate boundary condition
iform	An index, either 1 or 2. Selects the form of the recursion relation which will converge
j	Number of time-steps
k	Exponential index of diffusion coefficient
k2	Number of steps between printing
L	Value of I at substrate boundary
m	Index to control printing
paraml	Parameter in recursion relation
r	Ratio of liquid to vapour concentration
s(i)	S at grid point i, j
sp(i)	S at grid point i, j + 1
sg(i)	Guessed value of sp(i)
si	Initial value of s
so	Hypothetical value of s at surface, j

spo	Hypothetical value of s at surface, j + 1
sgo	Guessed value of spo
t	Time
tol	Tolerance on error(i)
x(i)	X dimension at grid point i
xints	Number of X intervals

```
      c
      c   numerical  model  of  ink  drying
      c     h.hardisty july 1978
      c
      c  constant rate boundary condition
      c
      c  solves the dimensionless diffusion equation (crank p208)
      c uses exponential d ,  d1 = do exp(kc)
      c
      c the above is termed  the  simple case c
      c
            real k
            dimension d(10),dp(10),ds(10),s(10),sp(10),ss(10),x(10),c(10)
           &error(10),cp(10),x1(11),u1(11),
           &  x2(9),u2(9,11),deld(10),dels(10),delc(10),u2i(11),
           &  deld10(10),dels10(10)
                external plot_$setup(descriptors),plot_(descriptors)
      c
      c  specifying  f d grid  x coodinate
      c
            intsx=8
            l=intsx+1
            l1=l+1
            xints=intsx
            delx=1/xints
            x(1)= 0.0
            do 1 i=2,l
          1 x(i) = x(i-1) + delx
      c
      c  specifying diffusion coefficient
      c
            cderit = 1.0
            dc1 = 1.001
            k=alog(dc1)
            k = k/cderit
            ek = dc1
            ek1=ek-1
      c
      c  initial    conditions
      c
            j = 1
            t=0.0
            ci = 1.0
            cbar = 1.0
            k2 = 5
            k3 = 5
            jmax = 50
      c
            k4 = k2
            m = 2
      c
      c
      c  specifying convective bc ,i=1
      c
            bi = 0.1
      c
```

```
c    ratio rhos/es
       r = 1.0
c
c conditions at critical point
c  icrit = 1  constant rate
c   icrit = 2  falling rate
c
       icrit = 2
       cscrit = 1.0
       dscrit = exp(k*cscrit)
       sscrit = (dscrit-1.0)/ek1
c constant rate criteria
       cr = alog((sscrit*ek1) + 1.0)
       cr = (2.0*delx*r*bi*cr)/ek1
c
c
c
c  setting coods  for  drying  curve
       x1(1) = 0.0
       y1(1) = 1.0
c
       do 3  i = 1,1
       y2(i,1) = ci
     3 continue
c
c
c  setting initial values  d  s  c
c
       di=exp(k*ci)
       si=(di-1)/ek1
       do 2 i=1,11
       d(i)=di
       c(i) = ci
       deld(i) = 0.0
       dels(i) = 0.0
     2 s(i)=si
c
       so = s(1)
c
c  setting f d params
c
       fo = 0.5
       tol = 0.01
c
       param1 = 0.5
c    iform = 1  oris  formn
c   iform = 2  exponl  formn
       iform = 1
c
       write(6,101)j,t,bi
  101 format(1h0,5x,'j= ',i4,5x,'t= ',f14.8,5x,'bi= ',f10.1)
c
       go to 29
c
```

icrit controls boundary condition

graphics

```
c
c
 4 continue                    <-- Main iterative loop begins here
c
      j=j+1
c
c
c  setting time step
      delt = fo * (delx ** 2.0)/ d(1)
      iter = 1
c
      t=t+delt
c
c  first guess at d and s for iterative soln of fin diff equatns
c
      do 5 i=1,l
      ds(i) = d(i)+deld(i)
      ss(i) = s(i)+dels(i)
 5 continue
      ds(l+1) = ds(l-1)
      ss(l+1) = ss(l-1)
c
c
c  finite difference equations
c
c
c  convective boundary  i=1
 6 continue
c  constant  rate
c
      if  (icrit.eq.2)  go  to  53
      if (j.eq.2) go to 23
      so = s(2)-cr
c
 23 continue
c  original  formn
c
      if (iform.eq.2)  go  to  70
c
      sso = ss(2)-cr
      a1 = (ds(1)+d(1)) * delt
      a1 = a1/(4.0*(delx**2.0))
      a2 = ss(2)-2.0*ss(1)+sso
      a3 = s(2)-2.0*s(1)+so
      sp(1) = s(1)+a1*(a2+a3)
c
      go  to 71
c
 70 continue
c
c  hish  fo  formn
c
      sso = ss(2)-cr
      a1 = (ds(1)+d(1))*delt
      a2 = 4.0*(delx**2.0)*(ss(1)-s(1))
      a1 = a2/a1
      a2 = ss(2)+sso
      a3 = s(2)-2.0*s(1)+so
      sp(1) = (a2+a3-a1)/2.0
c
 71 continue
c
      go to 54
c
 53 continue
c
```

equations for constant-rate boundary condition

alternative formulation of equation to suit convergence of iterative loop

```
c   falling rate
c
      if (iform.eq.2) go to 55
c   original formulation
c
c
      a5 = (r*bi*2.0*delx) / ek1
      so = s(2)-(a5*alog((s(1)*ek1)+1))
      sso = ss(2)-(a5*alog((ss(1)*ek1)+1))
      a6 = s(2)-2.0*s(1)+so
      a7 = ss(2)-2.0*ss(1)+sso
      a8 = (ds(1)+d(1))*delt
      a8 = a8/(4.0*(delx**2.0))
      sp(1) = s(1)+a8*(a6+a7)
c
      go to 54
c
   55 continue
c
c
c   exponl formn
      a5 = alog((s(1) * ek1)+1)
      so = s(2)-(r*bi*2.0*delx*a5)/ek1
      a6 = -ek1/(r*bi*2.0*delx)
      a7 = (4.0*(delx**2.0))/((ds(1)+d(1))*delt)
      a8 = (ss(1)-s(1))*a7
      a9 = -s(2)+2.0*s(1)-so-2.0*ss(2)
      a10 = a8+a9+2.0*ss(1)
      a11 = a6*a10
      a12 = exp(a11)
c
      sp(1) = (a12-1.0)/ek1
c
      write(6,40)a5,so,a6,a7,a8,a9,a10,a11,a12,sp(1)
   40 format(1h0,5x, 10f10.5)
c
   54 continue
c
c
c   general internal point
c original formational
c
      if (iform.eq.2) go to 61
   60 continue
      a1 = delt/(4 * (delx * * 2.0 ))
      do 7 i = 2,1
c
      a2 = a1 * (ds(i) + d(i))
      a3 = ss(i+1) - 2 * ss(i) + ss(i-1)
      a4 = a3 + s(i+1) -2* s(i) + s(i-1)
      sp(i) = s(i) + a2 * a4
c
    7 continue
c
      go to 62
c
c   high fo formn
   61 continue
c
      a15 = (4.0*(delx**2.0))/delt
c
      do 63 i = 2,1
      a16 = (ss(i)-s(i))/(ds(i)+d(i))
      a16 = a16*a15
      a17 = a16-s(i+1)+2.0*s(i)-s(i-1)-ss(i+1)-ss(i-1)
      sp(i) = -a17/2.0
c
   63 continue
```

equations for falling-rate boundary condition.

alternative formulations

internal points within the ink layer.

alternative formulations

```
c
   62 continue
c  substrate boundery    i = 1 = 9
      sp(1+1) = sp(1-1)
c
c
c  calc of errors
c
      do 8 i = 1,1
      error(i)=ss(i) -sp(i)
      error1 = abs(error(i))
      error3 = error(i)/ss(i)
c
c
c  better guess at  ss(i)
c
      ss(i) = sp(i) + param1 * error(i)
c
c     finding  largest error
c
      error(i) = error1/ss(i)
      if  (i.eq.1)  go  to  8
      if  (error(i).ge.error(i-1)  )  go  to  8
      error(i) = error(i-1)
    8 continue
c
c
c  calc  of  new  dss
c
      do 9 i =1,1
      ds(i)=(ss(i) * ek1)+1
c
    9 continue
      ss(1+1)=ss(1-1)
      ds(1+1)=ds(1-1)
c
c  test for iteration
c
      if  (error(1) . lt . tol )  go  to  11
      iter=iter+1
c
c
      if(iter . gt . 20 ) go to 31
c
      go to 6
c
c   recovering  concentrations
c
   11 continue
      cbar = 0.0
      do 12 i = 1,1
      dp(i)=(sp(i)*ek1)+1
      cp(i) = alog(dp(i))/k
      cbar = cbar+cp(i)
   12 continue
      cbar = cbar/9.0
c
c  drying rates
c
      dc = cbar1-cbar
      cbar1 = cbar
      dcdt = dc/delt
      alogc = alog(cbar)
      lncr = alog(cbar)
```

finite-difference calculations completed

Assessing the error in the "guessed" value of S

estimating next guess of S in the iterative loop.

next guess for D

calculating concentrations at the completion of iteration.

calculating drying rate

```
c  reset of s and d for start of next time step
c
          write(6,120)j,t,cbar,dc,delt,dcdt
  120     format(1h0,5x,i4,5x,5f10.8)
c
        do 20  i=1,l
        deld(i) = dp(i)-d(i)
        dels(i) = sp(i)-s(i)
        delc(i) = cp(i)-c(i)
        d(i) = dp(i)
        s(i)=sp(i)
        c(i) = cp(i)
   20 continue
c
        s(l+1) = sp(l-1)
        d(l+1) = dp(l-1)
c
        if (s(1).gt.sscrit) go to 29
        icrit = 2
c
   29 continue
c
c  storing conc distributions
c
c
   25 if (j.eq.k4) go to 26
      if(j.eq.2)  go  to  26
      go to 27
c
   26 do 14 i = 1,l
   14 y2(i,m) = c(i)
c
        x1(m) = t
        y1(m) = cbar
c
        m = m + 1
            if  (j.eq.2)  go  to  150
            k4=k4+k3
  150       continue
c
c
        write(6,15) j,t,bi
   15 format(1h0,5x,'j= ',i4,5x,'t= ',f14.8,5x,'bi= ',f10.1)
c
        write(6,28)
   28 format(1h0,5x,'x=0',8x,'x=0.125',8x,'x=0.25',8x,'x=0.375',8x,
     &           'x=0.5',8x,'x=0.625',8x,'x=0.75',8x,'x=0.865',8x,
     &           'x=1.0')
        write(6,16) ( d(i) , i=1,l)
   16 format(1h0,9 e 14.6)
c
        write(6,17) (s(i)  ,i=1,l)
   17 format(1h0,9 e 14.6)
c
        write(6,18) (c(i) ,i=1,l)
   18 format(1h0, 9 f 14.5)
c
        write(6,24)cbar,dcdt,alosc
   24 format(1h0,5x,'cbar = ',f 10.5,5x,'dcdt= ',f 10.5,5x,
     &'alosc= ',f 10.5)
c
   27 continue
```

changes in the values of D, S and C

control of printing

graphics

Print out

```
370     c
371           if  (j.eq.jmax)  go  to  21
372     c
373           go to 4
374     c
375        21 continue
376     c
377     c
378     c    setting co-ords for conc/dist curves
379     c
380           x2(1) = 0.0
381           do 22  i = 2,1
382        22 x2(i) = x2(i-1) + delx
383              call plot_$setup('concentration profiles','distance  x/l',
384           &     conc  c/co',1, base,1,0)
385              do 110  j=1,11
386              do  100  i=1,9
387      100     y2i(i)=y2(i,j)
388      110     call plot_(x2,y2i,11,2,'+')
389     c
390     c
391        19 continue
392     c
393     c
394        31 continue
395     c
396     c
397           stop
398           end
```

graphics

Amendments to Program to Produce 2 stages of Falling Rate Drying

Remove lines 32-37 and insert

```
      cdash = 0.5
      dcl = 10.0 (say)
      k = alog (dcl)/cdash
      ek = dcl
      ekl = ek - 1

      hl = ekl - (k * dcl * cdash)
      h2 = ekl + (k * dcl) * (1 - cdash)
```

Remove lines 85 and 86, and insert

```
      di = exp(k * cdash)
      si = 1.0
```

Remove lines 182 to 184, and insert

```
      if (c(1). lt.cdash) to to 200

      a5 = (r * bi * 2.0 * delx)/dcl
      so = s/2) - a5 * (s(1) - (hl/h2))
      spo = sg(2) - a5 * (sg(1) - (hl/h2))
      go to 201
200   continue

      a5 = (r * bi * 2.0 * delx)/h2
      so = s(2) - (a(5) * alog((s(1) * h2) + 1))
      spo = sg(2) - (a(5) * alog((sg(1) * h2) + 1))
201   continue
```

Remove line 274 and insert

```
      if(c(i).lt.cdash) go to 210
      dg(i) = dcl
      to to 211

210   continue
      dg(i) = (sg(i) * h2) + 1

211   continue
```

Remove lines 295 and 296, and insert

```
      if(c(i).lt.cdash) go to 220
      dp(i) = dcl
      cp(i) = ((sp(i) * h2) - h1)/(k * dcl)
      go to 221

220   continue
      dp(i) = (sp(i) * h2) + 1
      cp(i) = alog (dp(i))/k
211   continue
```

APPENDIX 7 - AN ATTEMPT TO REDUCE COMPUTING TIME IN THE CONSTANT-RATE PERIOD WHEN D_1^* IS LARGE AND $Bi_2 = 1$

Under these conditions, the concentration gradients are small and concentrations change little during a single time-step. It therefore appeared possible to compute only a small number of steps, and then to use this computed data to predict future S-values by means of an extrapolation process. At each grid point, the change in S-value for 10 time-steps of normal computation was used to evaluate the average time derivative of S over the 10 steps. Using this gradient, linear extrapolation was used to predict the S values a further 90 time-steps in the future. Computation started again from the predicted values and the sequence of computation followed by extrapolation could, in principle, be repeated indefinitely. In practice, operation was not satisfactory. The profiles predicted by the extrapolation technique contained slight irregularities, which became further exaggerated as the sequence continued. Eventually instability occurred and failure ensued. After making a number of attempts to remedy the difficulties further work on this method was discontinued.

APPENDIX 8 - DRYING RATE DATA EXTRACTED FROM IR DRYING CURVES

t = Drying time, s

$t - t_c$ = Drying time measured from critical point, s

V = Infragauge voltage

$\Delta V/\Delta t$ = Drying rate (by differencing), V/s

V_o = Virtual voltage at zero time

f = Relative drying rate, m/m_c

ϕ = Relative solvent content, X/X_c

DATA FOR FIGURE 11.3 Falling Rate Drying

Data extracted from FIG 11.2

L=1 Band 1 $t/L^2 \propto 1$						L = 9·4 Band 2 $t/L^2 \propto 1/2.03$					
$t-t_c$	V	$\Delta V/\Delta t$		f	ϕ	$t-t_c$	V	$\Delta V/\Delta t$	$t-t_c/L^2$	f	ϕ
0·0	2·0	·63		1·0	1·0	0	2·25		0		1·0
1	1·45	·55		·87	·75	1	1·6		0·5		·71
2	1·0	·45		·71	·5	2	1·2		1·0		·53
3	0·7	·3		·48	·35	3	1·0		1·5		·44
4	0·6	·1		·95	·3	4	·85		2·0		·38
5	0·5	·1		·95	·25	5	·78		2·5		·35
6	0·45	·05		·08	·225	6	·75		3·0		·33
7	0·4	·05		·08	·2	7	·7		3·5		·31
8	0·38	·02		·03	·19	8	·68		4·0		·30
9	0·35	·03		·05	·18	9	·6		4·5		·27
10	0·33	·02		·03	·17	10	·55		5		·24
15	0·26	·01		·01	·13	15	·5		7·5		·22
20	0·2	·004		·008	·1	20	·4		10		·18

L = 11·3 Band 3 $t/L^2 \propto 1/2.93$						L = 13·8 Band 4 $t/L^2 \propto 1/4.37$					
$t-t_c$	V	$\Delta V/\Delta t$	$t-t_c/L^2$	f	ϕ	$t-t_c$	V	$\Delta V/\Delta t$	$t-t_c/L^2$	f	ϕ
0	3·2		0·0		1·0	0	4·0		0·0		1·0
1	2·5		·34		·78	1	3·5		·23		·88
2	2·2		·68		·69	2	3·0		·46		·75
3	1·85		1·02		·58	3	2·7		·69		·68
4	1·55		1·36		·48	4	2·5		·9		·63
5	1·45		1·71		·45	5	2·25		1·15		·56
6	1·3		2·04		·4	6	2·0		1·38		·5
7	1·25		2·4		·39	7	1·9		1·6		·48
8	1·18		2·7		·37	8	1·8		1·8		·45
9	1·15		3·1		·36	9	1·7		2·1		·43
10	1·05		3·4		·33	10	1·65		2·3		·41
15	·8		10		·25	15	1·35		3·4		·34
20	·7				·22	20	1·25				·31

DATA FOR FIGURE 11.6 Effect of Air Velocity on Drying Rate

Data extracted from FIG 11.4

V_0 = 21·8 50 m/s $(V/V_0)_c$ = ·225

t	V	$\Delta V/\Delta t$	V/V_0	f	ϕ
2·5	7·9		·35		
2·75	6·5	5·3	·29	1·0	
3·0	5·25	5·3	·23	1·0	
3·25	4·1	4·6	·18	·86	·8
3·5	3·1	4·0	·14	·75	·62
3·75	2·4	2·8	·11	·53	·49
4·0	1·85	2·2	·08	·42	·36
4·5	1·15	1·4	·05	·26	·22
5·0	0·8	·7	·035	·13	·16
5·5	0·6	·4	·027	·08	·12
6·0	0·45	·3	·02	·06	·09

V_0 = 21·8 40 m/s $(V/V_0)_c$ = ·225

t	V	$\Delta V/\Delta t$	V/V_0	f	ϕ
2·75	8·25		·38		
3·0	7·15	4·8	·33		
3·25	6·0	4·6	·28	1·0	
3·5	4·9	4·4	·23	·96	
3·75	3·85	4·2	·18	·91	·8
4·0	3·1	3·0	·14	·65	·62
4·25	2·4	2·8	·11	·61	·49
4·5	1·9	2·0	·087	·43	·39
4·75	1·5	1·6	·067	·35	·3
5·0	1·2	1·2	·055	·26	·24
5·5	0·85	·7	·039	·15	·17
6·5	·55	·3	·086	·07	·38
7·25	·45		·071		·32
8·25	·35		·053		·24

V_0 = 21·8 30 m/s $(V/V_0)_c$ = ·225

t	V	$\Delta V/\Delta t$	V/V_0	f	ϕ
3·75	7·75				
4·0	6·9	3·6			
4·25	5·9	4·0	·27		
4·5	5·1	3·6	·23	·97	
4·75	4·25	3·3	·19	·89	·84
5·0	3·5	3·0	·16	·81	·71
5·25	2·9	2·4	·13	·65	·58
5·5	2·45	1·8	·11	·49	·49
5·75	2·0	1·8	·092	·49	·41
6·0	1·7	1·2	·078	·32	·35
6·5	1·2	1·0	·055	·27	·24
7·0	0·9	0·6	·041	·16	·18
7·5	0·75	0·3	·034	·08	·15

V_0 = 21·8 20 m/s $(V/V_0)_c$ = ·225

t	V	$\Delta V/\Delta t$	V/V_0	f	ϕ
5·0	8·15				
5·25	7·5				
5·5	6·9				
5·75	6·3				
6·0	5·65	2·5		1·0	
6·25	5·08	2·3		·92	
6·5	4·55	2·2	·21	·88	·93
6·75	4·05	2·0	·19	·8	·84
7·0	3·6	1·8	·17	·72	·76
7·5	2·8	1·6	·13	·64	·58
8·0	2·15	1·3	·01	·52	·44
9·0	1·4	·75	·064	·3	·28
10·0	1·0	·4	·046	·16	·2
11·0	·75	·25	·034	·1	·15

DATA FOR FIGURE 11.7 Effect of Air Temperature on Drying Rate

Data extracted from Fig. 11.5

V_o = 22·5			60 C		$(V/V_o)_c$ = ·275						
$t-t_c$	V	$\Delta V/\Delta t$	V/V_o	f	ϕ	$t-t_c$	V	$\Delta V/\Delta t$	V/V_o	f	ϕ
0·0	6·3		·34	1·0		0·0	5·8	3·8	·275	1·0	1·0
0·25	5·05	5·0	·28	1·0	1·0	0·25	5·0	4·0	·23	·84	·98
0·5	4·05	4·0	·275	·8	·8	0·5	4·25	3·0	·19	·79	·84
0·75	3·25	3·2	·18	·64	·64	0·75	3·6	2·6	·17	·68	·69
1·0	2·6	2·6	·14	·52	·51	1·0	3·05	2·2	·14	·58	·62
1·25	2·1	2·0	·115	·4	·42	1·25	2·6	1·8	·12	·47	·51
1·5	1·75	1·4	·093	·28	·33	1·5	2·2	1·6	·1	·42	·44
1·75	1·48	1·08	·078	·22	·28	1·75	1·9	1·2	·09	·32	·36
2·25	1·1	·76	·066	·152	·236	2·25	1·5	0·8	·07	·21	·33
2·75	0·9	·4	·049	·08	·175	2·75	1·25	0·5	·057	·13	·25
3·25	0·8	·2	·04	·04	·143	3·25	1·1	0·3	·05	·078	·21
3·75	0·7	·2	·036	·04	·129	3·75	·95	0·3	·044	·078	·18
6·75	·55	·05		·01	·09	8·0	·72	0·04		·01	·12
11·75	0·42	·02		·004	·07	11·0	·65	0·02		·005	·11
V_o = 21·4			40 C		$(V/V_o)_c$ = ·275						
$t-t_c$	V	$\Delta V/\Delta t$	V/V_o	f	ϕ	$t-t_c$	V	$\Delta V/\Delta t$	V/V_o	f	ϕ
0·0	6·15	2·8	·29	1·0		0·0	5·45	1·8	·26	1·0	1·0
0·25	5·45	2·8	·25	1·0	1·0	0·25	5·0	1·4	·24	·78	·87
0·5	4·85	2·4	·23	·86	·91	0·5	4·65	1·6	·23	·89	·84
0·75	4·25	2·4	·2	·86	·84	0·75	4·25	1·5	·21	·83	·76
1·0	3·75	2·0	·18	·71	·73	1·25	3·55	1·0	·17	·55	·62
1·25	3·3	1·8	·15	·64	·65	1·75	3·0	·8	·15	·44	·55
1·5	2·95	1·4	·14	·5	·55	2·25	2·6	·8	·13	·44	·47
2·0	2·3	1·3	·11	·46	·51	2·75	2·2	·4	·11	·22	·4
2·5	1·9	·8	·09	·29	·4	3·75	1·8	·3	·08	·17	·29
3·0	1·65	·5	·08	·18	·33	4·75	1·5	·1	·07	·06	·25
3·5	1·45	·4	·07	·14	·29	5·75	1·4	·1	·07	·06	·25
4·5	1·2	·25	·06	·08	·25	6·75	1·3		·06		
5·5	1·1	·1	·05	·036	·22						
9·5	0·9	·025	·042	·009	·15						

DATA FOR FIGURE 11.9 The Effect of Aiw Velocity on the Critical Point

Data extracted from 11.8

V_o = 25 50 m/s

t	V	$\Delta V/\Delta t$	V/V_o	f	ϕ
8·0	5·5		·22	1·0	1·0
8·5	4·3	2·4	·17	·67	·78
9·0	3·5	1·6	·14	·38	·64
10·0	2·4	·9	·1	·25	·44
11·0	1·8	·6	·07	·13	·33
12·0	1·5	·3	·06	·104	·27
13·0	1·25	·25	·05	·063	·23
14·0	1·1	·15	·044	·03	·2
16·0	·95	·075	·038	·01	·17
18·0	·8	·025	·032		·145
20·0	·75	·025	·030		·136
22·0	·7		·028		·127
24·0	·65		·026		·118
26·0	·6		·024		·109

V_o = 25 40 m/s

t	V	$\Delta V/\Delta t$	V/V_o	f	ϕ
8·0	8·5		·34	1·0	
8·5	7·5		·30		
9·0	6·4	2·3	·26	1·0	1·0
9·5	5·25	1·7	·21	·74	·82
10·0	4·4	1·3	·18	·57	·67
11·0	3·1	·85	·12	·37	·48
12·0	2·25	·5	·09	·22	·35
13·0	1·75	·25	·07	·11	·27
14·0	1·5	·15	·06	·065	·23
16·0	1·2	·1	·05	·043	·19
18·0	1·0	·08	·04	·035	·16
20·0	·85	·03	·034	·013	·13
22·0	·8	·04	·032	·017	·125
30·0	·6	·01	·024	·004	·097

V_o = 25 30 m/s

t	V	$\Delta V/\Delta t$	V/V_o	f	ϕ
10·0	7·9		·32	1·0	
11·0	6·15	1·8	·25	1·0	1·0
11·5	5·25	1·5	·21	·83	·85
12·0	4·5	1·3	·18	·72	·73
13·0	3·2	·9	·13	·5	·52
14·0	2·3	·45	·09	·25	·37
15·0	1·85	·35	·08	·19	·3
16·0	1·5	·2	·06	·11	·24
17·0	1·3	·1	·052	·06	·21
18·0	1·2	·08	·048	·04	·2
20·0	1·05	·06	·042	·03	·17
22·0	·93	·03	·037	·016	·15
24·0	·87	·03	·035		·14
40·0	·6	·01	·024	·0055	·098

V_o = 25

t	V	$\Delta V/\Delta t$	V/V_o	f	ϕ
15·5	5·8	1·4	·24	1·0	1·0
16·0	5·1	1·1	·2	·79	·88
17·0	4·0	1·0	·16	·71	·69
18·0	3·0	·65	·12	·46	·52
19·0	2·35	·45	·09	·32	·41
20·0	1·9	·3	·08	·21	·33
21·0	1·6	·2	·062	·14	·28
22·0	1·4	·15	·056	·11	·24
23·0	1·25	·12	·05	·086	·22
24·0	1·13	·06	·044	·043	·195
26·0	1·0	·05	·04	·036	·17
28·0	·9	·04	·036	·029	·16
30·0	·82	·02	·033	·014	·14
32·0	·78		·032		

DATA FOR FIGURE 11.11 The Effect of Temperature

Data extracted from FIG 11.10

$V_0 = 23{\cdot}4$ 60 C					
t	V	$\Delta V/\Delta t$	V/V_0	f	ϕ
4·0	4·9		·21		
4·5	3·4	3·0	·15	1·0	1·0
5·0	2·4	2·0	·1	·67	·71
6·0	1·4	1·0	·06	·33	·48
7·0	1·0	·4	·04	·13	·29
8·0	·8	·2	·034	·07	·19
10·0	·65	·08	·027	·027	·16
12·0	·55	·05	·023	·017	·13
14·0	·5	·025	·021	·008	·11
16·0	·45	·025	·019	·008	·1
20·0	·4	·013	·017	·004	·09
30·0	·35	·005	·015	·0017	·08
40·0	·32	·003	·014	·001	·07
50·0	·30	·002	·013	·0007	·066

$V_0 = 23{\cdot}4$ 50 C					
t	V	$\Delta V/\Delta t$	V/V_0	f	ϕ
5·5	4·25	3·3	·18	1·0	1·0
6·0	3·1	2·3	·13	·7	·72
6·5	2·45	1·3	·105	·39	·52
7·0	1·9	1·1	·081	·33	·42
8·0	1·4	·5	·06	·15	·32
9·0	1·15	·35	·05	·11	·24
10·0	1·0	·15	·04	·05	·2
12·0	·86	·07	·036	·02	·16
14·0	·8	·03	·034	·01	·14
16·0	·75	·025	·032	·008	·14
20·0	·65	·025	·027	·008	·13
25·0	·6	·01	·026	·003	·12
30·0	·54	·01	·023	·003	·1

$V_0 = 23{\cdot}4$ 40 C					
t	V	$\Delta V/\Delta t$	V/V_0	f	ϕ
6·5	6·7		·286		
7·0	5·3	2·8	·23	1·0	1·0
7·5	4·4	1·8	·19	·64	·8
8·0	3·5	1·8	·15	·64	·66
9·0	2·3	1·2	·1	·43	·52
10·0	1·8	·5	·077	·18	·35
11·0	1·5	·3	·064	·11	·27
12·0	1·32	·18	·056	·06	·196
13·0	1·18	·14	·05	·05	·17
14·0	1·1	·08	·047	·029	·16
15·0	1·05	·05		·018	
16·0	1·0	·05		·018	
18·0	·9	·05			
30·0	·7	·013	·03	·011	·10

$V_0 = 23{\cdot}4$ 30C					
t	V	$\Delta V/\Delta t$	V/V_0	f	ϕ
11·5	5·6	1·4	·239	1·0	1·0
12·0	4·8	1·6	·205	·69	·86
12·5	4·25	1·1	·18	·81	·75
13·0	3·6	1·3	·15	·5	·63
14·0	2·8	·8	·12	·31	·50
15·0	2·3	·5	·10	·22	·42
16·0	1·95	·35	·08	·16	·33
17·0	1·7	·25	·07	·11	·29
18·0	1·52	·18	·065	·1	·27
19·0	1·36	·16	·058	·05	·24
20·0	1·28	·08	·055	·05	·23
22·0	1·13	·08	·048	·03	·2
24·0	1·03	·05	·044	·02	·18
40·0	0·65	·01	·028		·12

DATA FOR FIGURE 11.13 Rate of Drying Curves — The Effect of Thickness
Data extracted from FIG 11.12

V_0 (Estd) = 36·33 Band 4

t	V	$\Delta V/\Delta t$	V/V_0	f	ϕ
17·0	6·05	1·3	·22	1·0	1·0
17·5	5·5	1·1	·2	·85	·91
18·0	5·0	1·0	·19	·77	·86
18·5	4·55	·9	·17	·69	·77
19·0	4·15	·8	·15	·62	·68
19·5	3·8	·7	·14	·54	·64
20·0	3·45	·7	·13	·54	·59
22·0	2·6	·43	·095	·33	·43
24·0	2·1	·25	·078	·19	·35
26·0	1·8	·15	·067	·12	·30
28·0	1·6	·1	·06	·08	·27
30·0	1·5	·05	·06	·04	·27
35·0	1·25	·05	·046	·04	·21
50·0	0·95	·01	·035	·01	·16

V_0 = 28 Band 3

t	V	$\Delta V/\Delta t$	V/V_0	f	ϕ
12·5	5·35	1·8	·19	1·0	1·0
13·0	4·6	1·5	·16	·89	·84
13·5	3·85	1·5	·14	·78	·74
14·0	3·25	1·3	·12	·72	·63
14·5	2·8	·9	·09	·56	·47
15·0	2·4	·7	·086	·39	·45
16·0	1·87	·54	·066	·3	·35
17·0	1·55	·31	·055	·172	·29
18·0	1·35	·2	·048	·11	·25
19·0	1·2	·15	·043	·08	·23
20·0	1·1	·1	·039	·06	·21
25·0	·8	·06	·028	·03	·15
30·0	·7	·02	·025	·01	·13
0	·62	·015	·022	·008	·12

V_0 = 22·33 Band 2

t	V	$\Delta V/\Delta t$	V/V_0	f	ϕ
10·5	4·3	1·8	·19	1·0	1·0
11·0	3·6	1·6	·16	·89	·84
11·5	2·85	1·5	·127	·83	·67
12·0	2·3	1·1	·103	·61	·54
12·5	1·9	·8	·085	·44	·45
13·0	1·62	·56	·073	·31	·38
13·5	1·42	·4	·064	·22	·34
14·0	1·25	·34	·056	·19	·29
15·0	1·1	·15	·049	·083	·26
16·0	·96	·14	·042	·077	·22
17·0	·88	·08	·039	·044	·21
18·0	·8	·08	·035	·044	·18
19·0	·75	·05	·033	·027	·17
20·0	·72	·03	·031	·016	·163

V_0 = 17·3 Band 1

t	V	$\Delta V/\Delta t$	V/V_0	f	ϕ
7·0	2·8	2·0	·16	1·0	1·0
7·5	2·0	1·6	·12	·8	·75
8·0	1·45	1·1	·084	·55	·53
8·5	1·1	·7	·064	·35	·4
9·0	·95	·3	·055	·15	·34
9·5	·83	·24	·05	·12	·31
10·0	·74	·18	·043	·06	·27
11·0	·63	·11	·036	·055	·23
12·0	·59	·04	·034	·02	·21
13·0	·55	·04	·032	·02	·2
14·0	·52	·03	·03	·015	·19
15·0	·5	·02	·029	·01	·18
16·0	·48	·02	·028	·01	·18

DATA FOR FIGURE 11.18a n-propanol – The effect of air velocity

Data extracted from FIG 7.2.

$t_c = 2.5$	60 m/s				$\frac{X_c}{m_c} = \frac{7.2}{2.7} = 2.66$
$t - t_c$	V	$\Delta V/\Delta t$	$h(\phi)$	f	ϕ
0.0	7.2	2.7	0	1.0	1.0
0.5	5.9	2.6	.19	.96	.82
1.0	4.9	2.0	.38	.74	.68
1.5	4.2	1.4	.56	.52	.58
2.5	3.2	1.0	.94	.37	.44
3.5	2.7	.55	1.3	.20	.37
4.5	2.3	.35	1.7	.13	.32
5.5	2.05	.25	2.1	.09	.28
6.5	1.85	.2	2.4	.07	.26
7.5	1.75	.1	2.8	.04	.24
9.5	1.55	.05	3.6	.02	.22

$t_c = 4.0$	40 m/s				$\frac{X_c}{m_c} = \frac{5.9}{2.4} = 2.46$
$t - t_c$	V	$\Delta V/\Delta t$	$h(\phi)$	f	ϕ
0.0	5.9	2.4	0.0	1.0	1.0
0.5	5.0	1.8	.2	.75	.85
1.0	4.3	1.4	.4	.58	.73
1.5	3.7	1.2	.6	.5	.63
2.0	3.3	.8	.8	.33	.56
2.5	3.0	.6	1.0	.25	.51
3.0	2.7	.6	1.2	.25	.46
4.0	2.35	.35	1.6	.15	.40
5.0	2.1	.25	2.0	.10	.36
6.0	1.9	.2	2.4	.08	.32
7.0	1.7	.2	2.8	.08	.29
8.0	1.6	.1	3.2	.04	.27

$t_c = 4.5$	30 m/s				$\frac{X_c}{m_c} = \frac{6.4}{2.2} = 2.91$
$t - t_c$	V	$\Delta V/\Delta t$	$h(\phi)$	f	ϕ
0.0	6.4	2.2	0	1.0	1.0
.5	5.4	2.0	.17	.91	.84
1.0	4.6	1.6	.3	.73	.72
1.5	4.0	1.2	.5	.55	.63
2.0	3.55	.9	.7	.41	.55
2.5	3.22	.7	.86	.32	.5
3.0	2.99	.6	1.0	.27	.45
3.5	2.65	.5	1.2	.23	.41
4.5	2.3	.35	1.5	.16	.36
5.5	2.05	.25	1.9	.11	.32
6.5	1.85	.2	2.2	.09	.29
7.5	1.75	.12	2.6	.05	.27
8.5	1.6	.13	2.9	.06	.25

$t_c = 6.5$	20 m/s				$\frac{X_c}{m_c} = \frac{5.0}{1.4} = 3.57$
$t - t_c$	V	$\Delta V/\Delta t$	$h(\phi)$	f	ϕ
0.0	5.0	1.4	0	1.0	1.0
.5	4.4	1.2	.14	.86	.88
1.0	3.85	1.1	.28	.79	.77
1.5	3.45	0.8	.42	.59	.69
2.5	2.85	0.6	.7	.43	.57
3.5	2.45	0.4	1.0	.29	.49
4.5	2.15	0.3	1.3	.21	.43
5.5	1.9	0.25	1.5	.18	.38
6.5	1.75	0.15	1.8	.11	.35
7.5	1.65	0.1	2.1	.07	.33
8.5	1.55	0.1	2.4	.07	.31

DATA FOR FIGURE 11.18b n-propanol The effect of air temperature

Data extracted from FIG 7·3

t_c = 2·5 60 C					$\frac{X_c}{m_c} = \frac{6·3}{3·6} = 1·75$
$t-t_c$	V	$\Delta V/\Delta t$	$h(\phi)$	f	ϕ
0·0	6·3	3·6	0·0	1·0	1·0
·25	5·5	3·2	·14	·89	·87
·5	4·8	2·8	·28	·78	·76
1·0	3·75	2·1	·6	·58	·60
1·5	3·0	1·5	·9	·42	·48
2·0	2·45	1·1	1·1	·31	·39
2·5	2·05	0·8	1·4	·22	·33
3·5	1·6	·45	2·0	·13	·25
4·5	1·3	·3	2·6	·08	·21
5·5	1·15	·15	3·1	·04	·18
6·5	1·0	·15	3·7	·04	·16
7·5	0·9	·1	4·3	·03	·14

t_c = 3·0 50 C					$\frac{X_c}{m_c} = \frac{6·0}{3·0} = 2·0$
$t-t_c$	V	$\Delta V/\Delta t$	$h(\phi)$	f	ϕ
0·0	6·0	3·0	0·0	1·0	1·0
·25	5·4	2·8	·13	·93	·9
·5	4·85	2·2	·25	·73	·81
1·0	3·95	1·8	·5	·6	·66
1·5	3·25	1·4	·8	·47	·54
2·0	2·75	1·0	1·0	·33	·46
3·0	2·1	·65	1·5	·22	·35
4·0	1·75	·35	2·0	·12	·29
5·0	1·5	·2	2·5	·07	·25
6·0	1·3	·2	3·0	·07	·22
7·0	1·2	·1	3·5	·03	·2
8·0	1·1	·1	4·0	·03	·18
9·0	1·03	·07	4·5	·02	·17

t_c = 3·5 40 C					$\frac{X_c}{m_c} = \frac{6·1}{2·6} = 2·35$
$t-t_c$	V	$\Delta V/\Delta t$	$h(\phi)$	f	ϕ
0·0	6·1	2·6		1·0	1·0
·25	5·6	2·0		·77	·92
·5	5·15	1·8		·69	·84
1·0	4·35	1·6		·62	·71
1·5	3·75	1·2		·46	·61
2·0	3·28	·94		·36	·54
2·5	2·85	·86		·33	·47
3·5	2·45	·4		·15	·40
4·5	2·1	·35		·14	·34
5·5	1·85	·25		·1	·30
6·5	1·7	·15		·06	·28
7·5	1·55	·15		·06	·25
8·5	1·45	·1		·04	·24

t_c = 4·0 30 C					$\frac{X_c}{m_c} = \frac{7·35}{2·2} = 3·34$
$t-t_c$	V	$\Delta V/\Delta t$	$h(\phi)$	f	ϕ
0·0	7·35	2·2	0·0	1·0	1·0
·25	6·85	2·0	0·08	·91	·93
·5	6·35	2·0	·15	·91	·86
·75	5·9	1·8	·23	·82	·8
1·0	5·5	1·8	·3	·82	·75
1·25	5·1	1·6	·4	·73	·69
1·5	4·8	1·2	·45	·55	·65
2·0	4·25	1·0	·6	·45	·58
3·0	3·45	·7	·9	·32	·47
4·0	2·9	·55	1·2	·25	·39
5·0	2·55	·45	1·5	·2	·35
6·0	2·3	·25	1·8	·11	·31
7·0	2·1	·2	2·1	·09	·29
8·0	1·95	·15	2·4	·07	·27

DATA FOR FIGURE 11.19 n-propanol The effect of thickness

Data extracted from FIG. 11.18

$t_c = 3.5$ Band 1				$\frac{X_c}{mc} = \frac{3.45}{2.1} = 1.64$		$t_c = 4.5$ Band 2				$\frac{X_c}{mc} = \frac{5.5}{2.0} = 2.75$	
$t-t_c$	V	$\Delta V/\Delta t$	$h(\phi)$	f	ϕ	$t-t_c$	V	$\Delta V/\Delta t$	$n(\phi)$	f	ϕ
0·0	3·45	2·1	0·0	1·0	1·0	0·0	5·5	2·0	0·0	1·0	1·0
·5	2·8	1·7	·3	·85	·81	·5	4·75	1·5	·18	·75	·86
1·5	1·9	·9	·91	·45	·55	1·0	4·15	1·2	·36	·6	·75
2·5	1·4	·5	1·52	·25	·405	2·0	3·3	·85	·73	·42	·6
3·5	1·1	·3	2·1	·15	·32	3·0	2·7	·6	1·09	·3	·49
4·5	·9	·2	2·74	·1	·26	5·0	2·0	·3	1·8	·15	·36
5·5	·78	·12	2·35	·06	·226	10·0	1·8	·1	3·6	·05	·25
6·5	·7	·08	4·0	·04	·2	15·0	1·1	·05	5·5	·025	·2
9·5	·55	·05	5·8	·025	·16	20·0	1·0	·02	7·2	·01	·18
14·5	·45	·025	8·8	·013	·13	25·0	·9	·02	9·1	·01	·16
17·5	·4	·01	10·7	·05	·12	30·0	·85	·01	11·0	·005	·15
21·5	·35	·01	13·1	·05	·1	35·0	·8	·01	12·7	·005	·15
25·5			15·5			40·0	·78	·004	14·2	·002	·14
29·5	·33	·0025	10·4	·0012	·09	45·0	·75	·005	16·4	·002	·14

$t_c = 5.5$ Band 3				$\frac{X_c}{mc} = \frac{6.5}{1.3} = 5$							
$t-t_c$	V	$\Delta V/\Delta t$	$h(\phi)$	f	ϕ	$t-t_c$	V	$\Delta V/\Delta t$	$h(\phi)$	f	ϕ
0·0	6·5	1·3	0·0	1·0	1·0						
·5	5·9	1·2	·1	·92	·91						
1·0	5·4	1·0	·2	·77	·83						
1·5	5·0	·8	·3	·62	·77						
2·0	4·6	·8	·4	·62	·71						
2·5	4·3	·6	·5	·46	·66						
3·5	3·75	·55	·7	·42	·58						
4·5	3·35	·4	·9	·31	·52						
5·5	3·05	·3	1·1	·23	·47						
6·5	2·8	·25	1·3	·19	·43						
8·5	2·4	·2	1·7	·15	·37						
10·5	2·15	·12	2·1	·09	·3						
12·5	1·95	·1	2·5	·08	·3						
44·5	1·1	·01	8·9	·008	·17						